Shielded Hydrogen Plasma: A Novel Hydrogenation Method for Silicon Solar Cells



Gabrielle A. Bourret-Sicotte

Oriel College

The University of Oxford

A thesis submitted for the degree of

Doctor of Philosophy

Trinity Term 2019

"The secret of change is to focus all of your energy, not on fighting the old, but on building the new."

Socrates

Acknowledgments

I'd first like to thank the EPSRC for funding my DPhil, the Department of Materials, and UNSW for allowing me use of their expertise and eCV. The Semicon Group has been a family to me for the last 4 years, I couldn't imagine my DPhil story without you. Seb, thank you for building countless equipment, making all of our work possible and for supporting my growth into a true scientist. Phill, you truly have been an amazing supervisor and friend, reading my work every week, organising Skype meetings in the middle of the Australian night, all the while juggling with baby Tristan! Radka and Jono, thank you for saving me from very painful experiences in the clean-room. Katie, thank you for being my conference buddy, room-mate, pizza-sharer, conference slide looker-over, thesis proof-reader, house-mate and number one lab partner. Lastly thank you Katherine for your endless stonking advice and mentoring. I'd also like to mention Peter, who forced me to believe in and stand up for myself.

My Oxford life would not have been complete without the amazing people I have met along the way. Lena, thank you for always joining me in whatever adventure we dreamt up and whichever acrobatics trick we mistakenly thought was easy. I cannot wait to collect a lifetime of memories with you. Tops, thank you for the laughs, the back-garden pools, the late night chats and for always keeping me grounded, see you in Cali for CocoHut part two! Chazza, you have been by my side through all of my biggest achievements and all of my craziest craft ideas in the last 7 years, thank you for being my rock and for letting me poke holes in your tea towels. Henry, thank you for all your design expertise, having a bit of you in the lab everyday always made me smile.

This year would not have been the same without all the OUWPC Ladies, thank you for keeping sane and for unknowingly letting me wrestle all of my stress out onto you. Dom, thank you from the bottom of my heart for supporting me through all of this year, for listening to me, for laughing with me, for loving me and for enduring my hyphen-disliking self. You make my bad days good and my good days better.

Finally, a huge thank you to my parents and my family. Dad, you made me believe as a little girl that anything I wanted to do was possible and you allowed me to follow all of my dreams along the way. Mom, you made me into the woman that I am today, thank you for encouraging me to be inquisitive and for doing everything you could to make this a reality. I hope this makes you both proud. Linda, Seb and Kuky thank you for bringing sunshine into my life and for always making me laugh. Vanessa thank you for being my loudest cheerleader! Xavier, thank you for fuelling my motivation through competition, I probably would not have done this without you, see you on the other side of the pond!

Abstract

Shielded Hydrogen Plasma: A Novel Hydrogenation Method to Improve the Efficiency of Solar Cells

Gabrielle Bourret-Sicotte
Oriel College, Oxford

Improving the efficiency of solar cells will play a key role in ensuring that solar generated power reaches grid-parity across the globe. One of the main challenges in achieving high-efficiency silicon cells is the recombination of minority carriers at defects, both at the silicon surface and throughout the bulk. Introducing hydrogen into silicon is a well-recognised method to achieve excellent chemical passivation of surface and bulk defects.

In this thesis, a novel method for the introduction of hydrogen into silicon is demonstrated, called Shielded Hydrogen Plasma (SHP). SHP is shown to effectively introduce neutral atomic hydrogen into silicon without the drawbacks of other hydrogenation techniques such as plasma damage or high-temperature steps. A palladium membrane is placed between the silicon and the PECVD-generated plasma to avoid plasma-related damage whilst still allowing the release of atomic hydrogen. The potential of converting SHP from a batch process to an in-line process by using cheaper and more resistant metallic shields is also considered, to encourage industry uptake. Palladium-silver and aluminium foils were shown to be effective alternatives to palladium leaf shields.

SHP passivates silicon-oxide/silicon interfaces extremely well, as demonstrated using thermally-oxidised 1Ω-cm 200 μm n-type silicon where the effective lifetime was found to increase from 12 μs to 1.05 ms after SHP processing and to 6.3 ms upon application of corona charge. This corresponded to a surface recombination velocity of ≤ 0.17 cm/s.

SHP is also shown to be a useful tool for the study of hydrogen-related defects in silicon. These defects are shown to be introduced into n-type silicon in the form of a damaged region with or without a dielectric layer. A new hydrogen-transport model across the silicon-oxide silicon interface is presented, showing that the interface is the main barrier to hydrogen incorporation into silicon. It is observed that the introduction of charged ions at the interface generates a strong field which enables an increased incorporation flux of hydrogen into bulk silicon. This higher concentration of hydrogen in the near-surface silicon is observed to be responsible for the damage layer.

TABLE OF CONTENTS

PREFACE ..... **VIII**

LIST OF FIGURES ..... **X**

LIST OF TABLES ..... **XVI**

CHAPTER 1 INTRODUCTION **1**

1.1 GLOBAL CLIMATE CHANGE 1

1.2 SOLAR POWER AND SILICON PHOTOVOLTAICS 3

1.3 SILICON SOLAR CELLS 7

1.3.1 Carrier recombination in crystalline silicon *8*

1.3.2 Surface recombination *16*

1.3.3 Summary of recombination processes *17*

1.4 AIM OF THIS WORK 18

1.5 STRUCTURE OF THIS THESIS 18

CHAPTER 2 LITERATURE ON HYDROGENATION AND THE MOVEMENT OF H IN SI AND PD **20**

2.1 IMPROVING BULK AND SURFACE LIFETIME OF SI 20

2.1.1 Chemical Passivation *20*

2.1.2 Field Effect Passivation *23*

2.1.3 Observing hydrogen *26*

2.1.4 Hydrogen passivation methods *27*

2.1.5 Summary of Hydrogen Passivation Techniques *33*

2.2 HYDROGEN-RELATED DEFECTS IN SI 33

2.3 BEHAVIOUR OF HYDROGEN IN PALLADIUM 36

CHAPTER 3 EXPERIMENTAL METHODS **39**

3.1 BASE SILICON 39

3.1.1 Substrates *39*

3.1.2 Surface Finish *39*

3.2 DIELECTRICS 40

3.2.1 Thermal Oxide Growth *40*

3.2.2 Silicon Nitride Deposition *41*

3.2.3 Thin Film Characterisation *41*

3.3 CORONA DISCHARGE 42

3.4 ION DEPOSITION 43

3.4.1 Spin coating *43*

3.4.2 Ion Migration *44*
3.5 Shielded Hydrogen Passivation 44
3.5.1 Hydrogen Passivation Method *45*
3.5.2 Shield Preparation *46*
3.5.3 Shield Sulphur Poisoning *46*
3.6 Characterisation Methods 47
3.6.1 Photoconductance Decay Lifetime *47*
3.6.2 Capacitance-Voltage *49*
3.6.3 Electrochemical Capacitance Voltage *53*
3.6.4 Kelvin Probe *58*
3.6.5 Light and Elevated Temperature Induced Degradation (LeTID) *61*
3.6.6 PEDOT:PSS *61*

CHAPTER 4 PASSIVATION USING SHIELDED HYDROGEN PLASMA 63

4.1 SHP Principle 63
4.1.1 Motivation *63*
4.1.2 SHP Requirements *64*
4.2 Detailed Methodology 65
4.3 Results 68
4.3.1 Background Experiments *68*
4.3.2 Atomic Hydrogen Release *71*
4.3.3 Damage-Free Passivation *74*
4.3.4 Temperature Dependence *77*
4.3.5 Time, Plasma Power and Chamber pressure Dependence *78*
4.3.6 Variability in SHP Efficiency *84*
4.4 Discussion 91

CHAPTER 5 SHP APPLICATION TO STRUCTURES 97

5.1 SHP Applications 97
5.1.1 Thick Oxide Passivation *97*
5.1.2 P-type Si *99*
5.2 Investigating Different Metallic Shields 100
5.2.1 Motivation *100*
5.2.2 Metallic Shields *106*
5.2.3 Pd-Ag *106*
5.2.4 Using Pd-Ag for SHP *109*
5.2.5 Aluminium Leaf *111*
5.2.6 Aluminium Foil *112*

5.2.7 Nickel Foil *114*
5.2.8 Platinum Leaf *116*
5.2.9 Summary of Different Metallic Shields *117*
5.3 SHP Compared to Common Hydrogenation techniques 119
5.3.1 Direct Plasma *119*
5.3.2 H_2 Anneal *121*
5.3.3 HF Dip *122*
5.3.4 Remote Plasma *123*
5.3.5 Fired Silicon Nitride For Hydrogen Release *126*
5.4 Discussion 128

CHAPTER 6 THE USE OF SHP TO STUDY H-RELATED DEFECTS 135

6.1 Effect of SHP on Bare and Ionic FEP Si 135
6.1.1 Hydrogen Related Defects in Bare Si *135*
6.1.2 Effects on Bare Si *137*
6.1.3 Effects on SiO_2 with Ionic FEP *140*
6.1.4 Discussion on the Effect of SHP on Bare and Ionic FEP Samples *146*
6.1.5 Investigation of the cause of SHP-induced lifetime reduction in n-type Si. *155*
6.2 Transport of H in Si through an Oxide layer: Discussion and Conclusions 170
6.2.1 Further Work *174*

CHAPTER 7 SUMMARY & FURTHER WORK 176

7.1 Shielded Hydrogen Plasma – A novel Hydrogenation Technique 177
7.2 SHP: Applications and Metallic Shield Investigation 179
7.3 SHP to Study H-Related Defects 181
7.4 Conclusions and Further Work 182

REFERENCES 184

Preface

This thesis is an account of the work I have carried out as a doctoral student at The University of Oxford and the Department of Materials. I confirm that I have not submitted any part of this thesis for another degree at this University or elsewhere. I hereby confirm that the work presented is my own, unless otherwise stated and duly acknowledged in the text as well as separately referenced.

Gabrielle Bourret-Sicotte

During the course of this doctorate, I have written and contributed towards the following publications:

Bourret-Sicotte, G., P.G. Hamer, D.Tweddle, R. S. Bonilla, and P. R. Wilshaw. "Hydrogen Related Defects in Float Zone Silicon Investigated Using a Shielded Hydrogen Plasma." *IEEE 7th World Conference on Photovoltaic Energy Conversion, WCPEC 2018 - A Joint Conference of 45th IEEE PVSC, 28th PVSEC and 34th EU PVSEC (pp. 298–302),* proceedings, 2018.

Bourret-Sicotte, G., P.G. Hamer, R.S. Bonilla, K. Collett, A. Ciesla, J. Colwell, and P.R. Wilshaw. "Shielded Hydrogen Passivation − A Potential In-Line Passivation Process." *Physica Status Solidi (A) Applications and Materials Science*. vol. *214,* no.7, 2017.

Bourret-Sicotte, G., P. Hamer, R. S. Bonilla, K. Collett, and P. R. Wilshaw. "Shielded Hydrogen Passivation - A Novel Method for Introducing Hydrogen into Silicon." In *Energy Procedia*. Silicon PV Conference proceedings, 2017.

Chan, Ca. P. Hamer, **G.Bourret-Sicotte**, R. Chen, Al. Ciesla, B. Hallam, D. Payne, R.S. Bonilla, and S. Wenham. "Instability of Increased Contact Resistance in Silicon Solar Cells Following Post-Firing Thermal Processes." *Solar RRL*. Sol. RRL vol.1, pp. 1700129 ,2017.

Chen, D., P.G Hamer, M. Kim, T.H Fung, **G. Bourret-Sicotte**, S. Liu, C.E Chan, et al. "Hydrogen Induced Degradation: A Possible Mechanism for Light- and Elevated Temperature-Induced Degradation in n-Type Silicon." *Solar Energy Materials and Solar Cells*. vol.185, pp. 174–182, 2017.

Collett, K.A., R.S. Bonilla, P. Hamer, **G. Bourret-Sicotte**, R.Lobo, T.Kho, and P. R. Wilshaw. "An Enhanced Alneal Process to Produce SRV < 1 Cm/s in 1 Ω Cm n-Type Si." *Solar Energy Materials and Solar Cells*. vol. *173*, pp. 50–58, 2017.

Collett, K. A., S. Du, **G.Bourret-Sicotte**, Z. Luo, P. Hamer, B. Hallam, R.S. Bonilla, and Peter R. Wilshaw. "Scalable Techniques for Producing Field-Effect Passivation in High-Efficiency Silicon Solar Cells." *IEEE Journal of Photovoltaics*. vol. *9,* no. 1, pp. 26–33, 2019.

Hamer, P., **G. Bourret-Sicotte**, G. Martins, A. Wenham, R.S. Bonilla, and P. Wilshaw. "A Novel Source of Atomic Hydrogen for Passivation of Defects in Silicon." *Physica Status Solidi - Rapid Research Letters*, vol. *11,* no. 5, 2017.

Hamer, P., C. Chan, R.S. Bonilla, B. Hallam, **G. Bourret-Sicotte**, K.A. Collett, S.Wenham, and P.R. Wilshaw. "Hydrogen Induced Contact Resistance in PERC Solar Cells." *Solar Energy Materials and Solar Cells*. vol. *184*, pp. 91–97, 2018.

Wenham, A.Ciesla , S.Wenham, R. Chen, C. Chan, D. Chen, B. Hallam, **G.Bourret-Sicotte**, D. Payne, et al. "Hydrogen-Induced Degradation." Joint Conference of 45th IEEE PVSC, 28th PVSEC and 34th EU PVSEC, proceedings, 2018.

List of Figures

Figure 1 Energy resources of the world. Renewable resources potential as a proportion of the total present day global energy consumption [10] 3

Figure 2 Exponential growthcurve on a semi-log scale of worldwide installed photovoltaics in gigawatts since 1992. (Figures for cumulative capacity in watt DC, watt-peak). Public Domain, after [8], [12], [13] 4

Figure 3 Primary Energy Use - Long Term Prediction by Shell in [14] 4

Figure 4 PV learning curve: the average PV module price against cumulative shipments from 1976 to 2018 and the associated learning rate (LR). Labelled by Dr. Brett Hallam [15]. 5

Figure 5 NREL 2017. Modelled Commercial in US PV markets. [17] 6

Figure 6 Comparison of the proportion of the price attributable to different module cost elements between 2017 and 2019 [15]. 6

Figure 7 Schematic of a conventional PERC (passivated emitter rear contact) Si solar cell [20]. 7

Figure 8 Schematic of PECVD equipment used for Direct Plasma Hydrogenation 30

Figure 9 Remote Plasma CVD System 32

Figure 10 Schematic representation of the diffusion of H through Pd as per [136] 36

Figure 11 Schematic of Corona discharge apparatus, after [79]. 42

Figure 12 Schematic of SHP apparatus used in this work. 100 nm Pd leaf held in place by two aluminium grids, 10 cm by 10 cm with 5 mm lattice and 2 mm thickness. 45

Figure 13 Equivalent circuit used in CV analysis 50

Figure 14 Schematic of eCV apparatus after [156] 54

Figure 15 (a) Schematic of Kelvin Probe apparatus (b) Associated band diagram with charge at SiO_x interface 58

Figure 16 Schematic of measurement set up including a semi-transparent PEDOT:PSS gated symmetrical specimen. By courtesy of [161]. 62

Figure 17 Engineering drawing of a) (left) grid plate of SHP rig b) (right) hole plate of SHP rig 66

Figure 18 Schematic of SHP rig.....66

Figure 19 Schematic representation of SHP apparatus used in this work. 67

Figure 20 Active B concentration versus etch depth measured using eCV. Bare Si sample annealed in pure H_2 at 200 °C for 20 mins in tube furnace at 1 atm. Background doping concentration 1.17 x $10^{17}/cm^3$ (red dashed line).....69

Figure 21 Active B concentration versus etch depth measured using eCV. Bare Si sample exposed to direct NH_3 plasma in PECVD at 200 °C for 20 mins. Background doping concentration 1.17 x $10^{17}/cm^3$ (red dotted line) 70

Figure 22 Effective minority carrier lifetimes as a function of minority carrier density for 1 Ωcm 200 μm n-type FZ Si sample with a 10 nm SiO_2 (red) or 100 nm SiO_2 (blue). Lifetime tested prior and post direct plasma exposure for 30 mins at 380 °C.....70

Figure 23 Active B concentration versus etch depth measured using eCV. Bare Si samples exposed to SHP (blue triangles), direct plasma (black squares), and shielded nitrogen plasma (SNP) (pink circles) all at 200 °C for 20 mins. H_2 annealed samples at 200 °C for 20 mins included for comparison as well as background B doping (red dashed line) 72

Figure 24 A)Maximum effective lifetime of n-type Si with 100 nm SiO_2 after corona charging as a function of minority carrier density for wafers processed for 40 min on each side, with direct plasma exposure (No leaf), SHP and thermal annealing (leaf in place, no plasma) at temperatures of 473 and 623 K. B) Extracted J_0 as a function of surface potential for each set of conditions. 75

Figure 25 Effective minority carrier lifetimes as a function of minority carrier density for a 1 Ωcm 200 μm n-type FZ Si sample with a 10 nm thermal oxide. The SHP exposure was performed at 380 ˚C for 45 minutes each side. The J_0 values were extracted using the Kane-Swanson method [150] 76

Figure 26 Depth profile of active B concentration as measured using ECV after exposure to SHP at temperatures between 150 °C and 250 °C. Inset: table with integrated [H-B] and corresponding penetration depth.....78

Figure 27 Minority carrier lifetime at 10^{15} / cm^3 injection level for varying exposure times. Filled in icons represent the SHP samples, empty icons the control annealed sample (no H). 80

Figure 28 Minority carrier lifetime at 10^{15} / cm^3 injection level for varying exposure times after corona charging. Filled in icons represent the SHP samples, empty icons the control annealed sample (no H).....80

Figure 29 Minority carrier lifetime at 10^{15} / cm^3 injection level for varying RF plasma power before corona charge, and after corona charging (dashed).....82

Figure 30 Minority carrier lifetime at 10^{15} / cm^3 injection level for varying chamber pressure power before corona charge, and after corona charging (dashed). 83

Figure 31 Active B-Concentration /cm^3 using three different conditions. Direct plasma (no leaf), untreated leaf (new leaf), prepared leaf for 30mins 250 ˚C. Samples exposed to plasma for 5, 10 and 20 mins all at 200 °C.....85

Figure 32 Measured minimum active B concentration in the first 1 μm of Si samples with a uniform doping concentration of 1.17×10^{17} cm^{-3} after exposure to an NH_3 plasma for 20 minutes at 200 °C. Smaller values of active B indicate a larger concentration of atomic H in the Si. Samples were exposed under the following Pd leaf conditions: as received, prepared, re-oxidised, poisoned and under direct plasma without a leaf. 87

Figure 33 B concentration cm^{-3} versus depth measured using ECV. Samples exposed to NH_3 plasma for 20 mins at 200 ˚C, plasma power of 100 W. Samples were processed using a prepared Pd leaf (red squares) and a prepared and poisoned Pd leaf (blue circles) Background doping concentration is ˜ 1.1 x 10^{17} cm^{-3}.....90

Figure 34 Schematic representation of H transport through Pd with an atomic H source 92

Figure 35 Minority carrier lifetime versus minority carrier density. Initial lifetime shown as black dots. SHP performed using a prepared, poisoned Pd leaf for 45 mins at 380 °C on both sides (blue squares). Corona charging was used to achieve maximum lifetime (green triangles). The Richter intrinsic lifetime limit is shown as a red dashed line for comparison [34]. 98

Figure 36 Minority carrier lifetime versus minority carrier density. Initial lifetime (black squares) and after corona charging (green squares). SHP with prepared, poisoned Pd leaf for 45 mins at 350 °C on p-type FZ Si (brown circles) and after corona (red circles).....99

Figure 37 Schematic representation of SHP apparatus adapted for in line processing.....101

Figure 38 Permeability of H in different metals as a function of temperature [174] 105

Figure 39 Phase diagram showing typical absorption relationship in Pd-H system. The $\alpha\rightarrow\beta$ transformation occurs below 300 °C and below 20 atm pressure, causing lattice distortion. Figure from Bruning and Sieverts [206].....107

Figure 40 Photograph of SHP set-up in Oxford. Seen is the Pd leaf having been exposed to a few cycles of hydrogenation. The part of the leaf exposed to the H-containing plasma appears less reflective. 108

Figure 41 Ionised B concentration as a function of depth measured using eCV. Samples were exposed to NH_3 plasma under SHP shield for 30 mins at 200 ℃, with a plasma power of 100W. Pd leaf shield is shown as empty black squares. Pd-Ag foil shield is shown as red dots. 110

Figure 42 Active B concentration against etch depth measured with eCV. Four samples exposed to shielded H containing plasma at 200 °C for varying times and using different shields. Standard prepared Pd leaf for 30 mins and 5 mins shown as purple squares and half black squares. Al leaf for 20 and 50 mins shown as blue squares and green circles. 111

Figure 43 Active B concentration against etch depth measured with eCV. Five samples exposed to shielded H containing plasma at 200 °C for varying times and using different shields. Standard prepared Pd leaf for 30 mins and 5 mins shown as purple squares and half black squares. Al foil for 30 min 1h20 and 2h20 blue squares, green circles and half red circles.....113

Figure 44 Active B concentration against etch depth measured with eCV. Five samples exposed to shielded H-containing plasma at 200 °C for varying times and using different shields. Standard prepared Pd leaf for 30 mins and 5 mins shown as purple squares and half black squares. Ni foil for 30 mins not prep, prep and S poisoned shown as blue squares, green circles and half red circles. 115

Figure 45 Active B concentration against etch depth measured with eCV. Samples exposed to shielded H-containing plasma at 200 °C for varying times and using different shields. Standard prepared Pd leaf for 30 mins and 5 mins shown as purple squares and half black squares. Pt leaf for 30 mins not prep, prep and S poisoned shown as blue squares, green circles and half red hexagons respectively 116

Figure 46 Minority carrier lifetime at $10^{15}/cm^3$ injection level for 10 nm and 100 nm SiO_2.....120

Figure 47 Minority carrier lifetime versus injection level for n-type 1 Ω.cm Fz Si with 100 nm SiO_2. Sample exposed to SHP at 350 °C for 45 minutes under prepared Pd-Ag foil is shown as red squares. Sample exposed to direct plasma at 350 °C for 45 minutes is shown as black squares. Both samples were corona charged for 60 s at 30 kV.....121

Figure 48 Extracted minority carrier lifetime at 10^{15} cm^{-3} injection level for three sample batches. As received (no H exposure) shown as black square and empty black square post corona charging (CC). SHP for 30 mins at 380 °C with prepared Pd leaf (green circles) and after corona charging (half green circle). Remote plasma 30 mins at 380 °C (red triangle) and after corona charging (half red triangle). 124

Figure 49 Surface passivation metrics for dielectric coatings developed over the past two decades, for n-type (closed symbols) and p-type (open symbols) Si surfaces. (a) effective.....128

Figure 50 Schematic of H transport through Pd shield using atomic H source 133

Figure 51 Process flow chart for both n- and p-type FZ Si. 137

Figure 52 Minority carrier lifetime in μs versus injection level for n-type FZ Si with 50 nm SiN_x coating. As received (black diamonds) is HF dipped with SiN_x. SNP (empty red circles) is HF dipped, SNP 30 mins 350 °C with SiN_x. SHP (green triangles) is HF dipped, SHP 30 mins 350 °C with SiN_x. All samples are corona charged as per [143]. 138

Figure 53 Minority Carrier Lifetime in μs over injection level for p-type FZ Si with a 50 nm SiN_x coating. As-received (black half-filled squares.). As-received with SiN_x and corona charge (CC) (green half-filled squares). SHP 30 mins 350 °C with SiN_x (dark red circles). SHP 30 mins 350 °C with SiN_x and corona charge (red circles). All samples are corona charged (CC) [143]. 139

Figure 54 Effective minority carrier lifetime for each sample batch. Control (black), SHP prior to K FEP (red), K FEP prior to SHP at 100, 150, 200 °C (blue, green, orange), K FEP prior to SNP at 200 °C (pink). SHP and SNP were processed under PECVD plasmas for 40 minutes on either side. 142

Figure 55 Ionic FEP introduction followed by SHP showing (a) the effective lifetimes at an injection level of 10^{15} cm^{-3} after each processing step along with the final interface charge concentration and (b) the injection dependent effective lifetime curves after each step [26]. 144

Figure 56 Minority carrier lifetime in μs over injection level for p-type FZ Si with 100 nm SiO_2 coating. As-received (black diamond). KCl spin coated (red rhombus). KCl + corona charge (blue rhombus). KCl spin-coated + drifted through with corona and 450 °C anneal (green rhombus). KCl spin-coated and drift with SHP exposure under Pd-Ag foil, 350 °C 30 minutes with corona. All samples are corona charged as per [143]. 145

Figure 57 Compilation of experimental data, diffusivities of H in Si, together with lines representing the Van Wieringen and Warmoltz and Ichimiya and Furuichi data. (After ref.[231].) 148

Figure 58 Schematic of atomic H transport at 200 °C and 800 °C in n-type Si 149

Figure 59 Schematic of atomic H transport at 200 °C (SHP) and 800 °C (theoretical) in 100 nm SiO_2-Si n-type Si 150

Figure 60 Schematic of atomic H transport at 380 °C with K ions deposited on 100 nm SiO_2-Si n-type Si. No drift 151

Figure 61 Schematic of atomic H transport at 380 °C with K^+ ions drifted using CC and 450 °C anneal. K^+ ions at the interface between 100 nm SiO_2 and n-type Si. 152

Figure 62 Process flow chart for both n- and p-type FZ Si, with added batch (4) which receives a TMAH etch 156

Figure 63 Minority carrier lifetime in μs versus injection level for 200 μm n-type FZ Si with 50 nm SiN_x coating. As-received (bare Si + SiN_x) (black diamonds). SNP (empty red circles) (bare Si + SiN_x). SHP (green filled triangles), HF+ SHP 30 mins 350 °C + SiN_x. TMAH samples (empty green triangles) are the SHP sample + TMAH for 3 mins each time. All samples are corona charged as per [143]. 157

Figure 64 Minority Carrier Lifetime (μs) against Applied Voltage (V) (from SMU) for different injection levels in cm^{-3}. Sample received K^+ ion, drifted using CC and hot plate, SHP exposure for 30 mins at 350 °C. PEDOT PSS applied on front surface. 159

Figure 65 Effective lifetime as a function of gate bias on the surface of the dielectric for n-type 1 Ωcm FZ Si passivated with SiO_2, SiO_2/SiN_x and SiO_2 with an FGA treatment. 160

Figure 66 Minority carrier lifetime (μs) versus injection level (cm^{-3}) for negative applied V on n-type Si with K^+ driften at interface and exposed to SHP at 350 °C for 30 mins. 161

Figure 67 Minority carrier lifetime (μs) versus injection level (cm^{-3}) for positive applied V on n-type Si with K^+ drifted at interface and exposed to SHP at 350 °C for 30 mins. 161

Figure 68 Normalised Lifetime Reduction (NLR) vs hot illumination time (97 °C ± 2 °C at 0.6 W/ cm^2). N-type SHP with SiN_x passivation with TMAH etch (0 mins, 6 mins, 12 mins and 18 mins) and control (oxide strip and SiN_x passivation) 163

Figure 69 Minority carrier lifetime vs minority carrier density. n-type SHP for 350 °C for 30 mins both sides and SiN_x passivation. Degradation time 0.33 h (black squares), 18 h (red circles) and 280 h (blue empty triangles). 164

Figure 70 Active B concentration versus depth characterised using C-V technique on 1 Ωcm p-type Si. Red dot sample was exposed to SHP for 30 mins at 200 °C. Black square sample has had K^+ ions drifted to interface followed by SHP for 30 mins at 200 °C.....166

Figure 71 Minority carrier lifetime vs minority carrier density for n-type FZ Si 100 nm SiO_2. a) Control sample (black), KCl spin-coated (blue) K drift with corona and hot plate (green), SHP - Al foil at 380 °C for 40 mins both sides (pink). b) As received sample (black), KCl spin-coated and corona (red) K^+ drift with corona and hot plate (blue), SHP with Pd-Ag foil at 380 °C for 2.5 mins both sides (green).....169

List of Tables

Table I Summary of intrinsic charge for dielectric films 24

Table II Summary of silicon substrates used in this thesis 39

Table III Summary of SiO_2 growth processes of samples used in this thesis 40

Table IV Summary of deposited SiN_x processes for samples used in this thesis 41

Table V Summary of standard SHP process used throughout this thesis 46

Table VI Summary of constants used for H-B concentration calculations 57

Table VII Summary of calculated H-B pairs 73

Table VIII Summary of calculated H-B pairs 87

Table IX List of metals tested for usage as SHP shields 106

Table X Total level of H-deactivating B with Pd leaf and Al leaf 112

Table XI Total level of H deactivating B with Pd leaf and Al foil..... 113

Table XII Total level of H deactivating B with Pd leaf and Ni foil 115

Table XIII Total level of H-deactivating B with Pd leaf and Pt leaf 117

Table XIV Summary of total level of H deactivating B 118

Table XV Total level of H deactivating B using SHP Pd leaf and H2 anneal 122

Table XVI Total level of H deactivating B using SHP Pd leaf and HF dip.... 123

Table XVII Summary of Process Steps..... 142

Table XVIII Minority carrier lifetimes for samples exposed to H-containing plasma using SHP and Al foil or Pd-Ag foil. 169

CHAPTER 1 INTRODUCTION

1.1 GLOBAL CLIMATE CHANGE

Scientific evidence for the warming of the climate system is unequivocal. Although the Earth's climate has changed throughout history, going through seven cycles of glacial advance and retreat in the past 650,000 years, the carbon dioxide level in the atmosphere has never been measured to be as high as it is today [1]. The previous glacial cycles are likely to have been caused by slight shifts in the earth's orbit changing the amount of solar energy our planet receives [2]. The current warming trend of our climate cannot be attributed to that and is extremely likely the result of human activity since the mid-19th century [3].

Emission of greenhouse gases, primarily caused by the increased usage and burning of fossil fuels, has disrupted the climate system of our planet. Carbon dioxide (CO_2) is the most produced greenhouse gas, and its atmospheric concentration has increased by 40% over the last two centuries, as recently reported by the latest IPCC report [1]. Greenhouse gases present in the atmosphere reflect infrared radiation emitted by the earth back towards the earth's surface. This reflection effectively stops the earth from completing a full cooling cycle by trapping the heat it releases, causing global warming.

Global warming describes the consequences of climate change based on accumulated scientific data. The planet's average surface temperature has risen by more than 1.1 °C since the late 19th century [2], the oceans have absorbed most of that heat with a measurable temperature increase in the top 700 m of water. This temperature increase, albeit small, has had devastating consequences on the Antarctic and Greenland ice sheets. Papers have reported that Greenland has lost up to 250 km^3 of ice per year between 2002 and 2006 and similar figures

have been reported for Antarctica [4]–[6]. The melting of ice sheets is only one of the evidence of global warming, others include decreased snow cover, sea level rise, ocean acidification and the increase in extreme weather event occurrence. Additionally, WWF have reported that the size of wildlife has decreased by 60% globally between 1970 and 2014, partly caused by changing natural habitats because of global warming [7].

In order to stop and potentially reverse this climate trend, the world's energy demand must be met by solutions other than fossil fuels. The world's annual energy demand is around 157 PWh [8], and is expected to grow at a rate of 3% per year. Developing countries are expected to make up most of that growth, especially those known as BRICS (Brazil, Russia, India, China) countries, which opens a world of opportunities for the implementation of renewable energy sources.

Making solar power, as well as other renewables, commercially viable energy sources, and switching the transport and heating fuel source from fossil fuels to electricity, will be essential to mitigate the effects of climate change [9]. Renewable resources as a whole amount to over 3000 times the global energy consumption of today, with solar energy having the biggest potential as displayed in Figure 1.

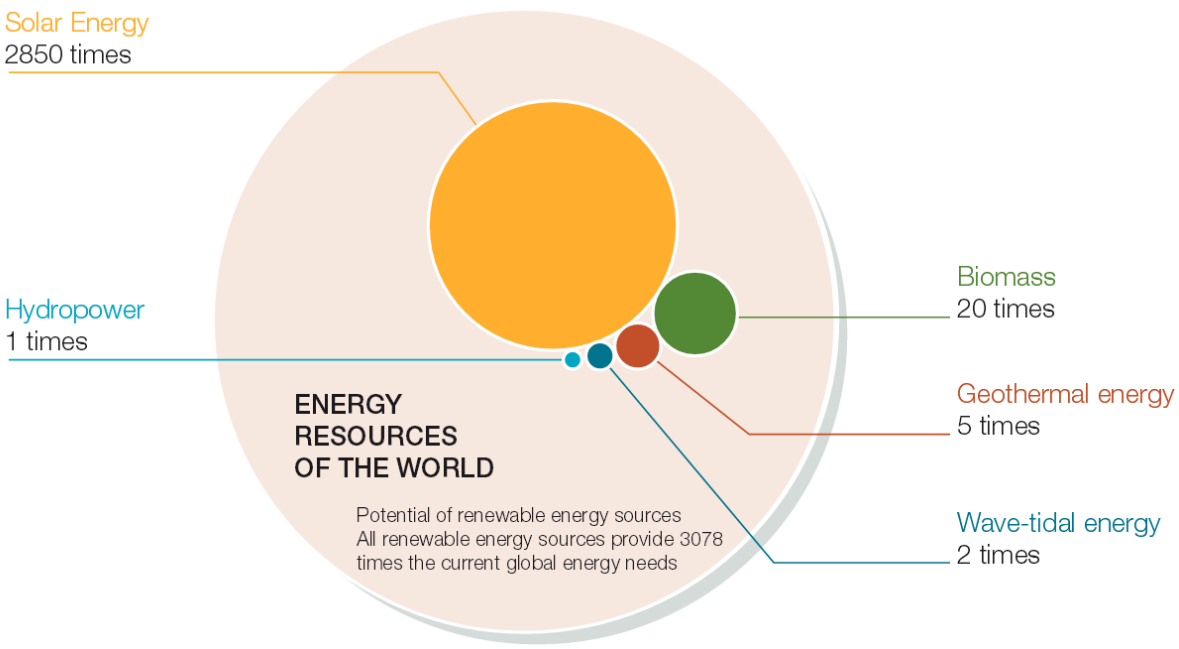


Figure 1 Energy resources of the world. Renewable resources potential as a proportion of the total present day global energy consumption [10]

1.2 Solar Power and Silicon Photovoltaics

In the past decade, the Photovoltaics (PV) industry has transformed from a cottage industry centred around Germany and fuelled by government subsidies to a $100 billion global economy [11]. Government subsidies contributed to the initial growth, but the recent boom was largely fuelled by new entrants in production and constant innovation. This has driven the price of installed units down, encouraging growth, and by 2018, installed solar PV surpasses 500 GW; demonstrating a steady exponential growth since 1992, with 2019 cumulative forecasts at around 650 GW [12]. This goes to show that the solar industry in not only growing at an amazing rate, it has sustained this exponential growth for the past decade and was virtually unaffected by the global financial crisis. This growth is represented in Figure 2.

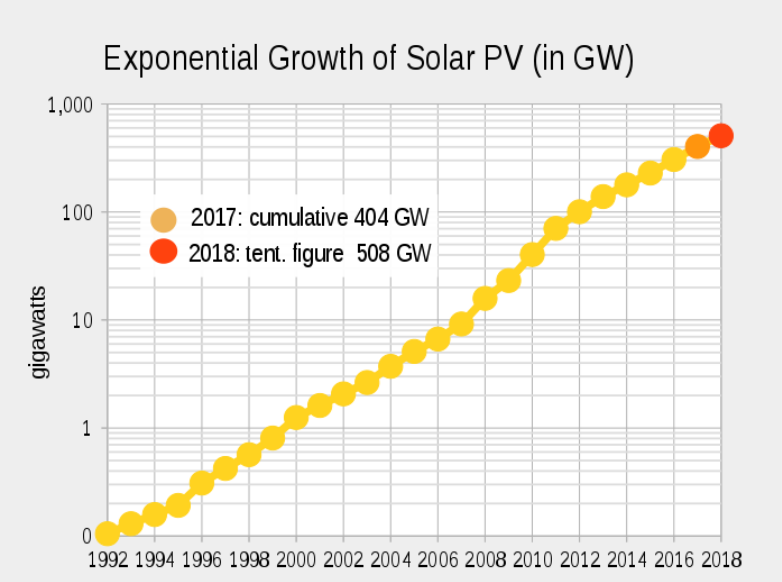


Figure 2 Exponential growthcurve on a semi-log scale of worldwide installed photovoltaics in gigawatts since 1992. (Figures for cumulative capacity in watt DC, watt-peak). Public Domain, after [8], [12], [13]

It is unlikely that solar power will meet total global electricity demand in the near future, as even 500 GW only accounts for 4% of global demand [10]. However, corporate entities such as Shell are considering Solar PV as the main source of electricity in their long-term scenarios as shown in Figure 3, which is extremely promising for the PV sector.

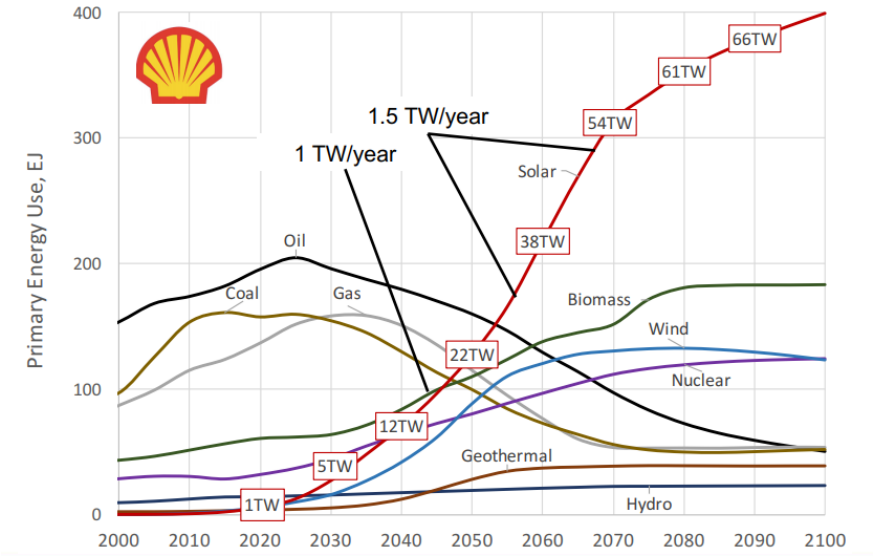


Figure 3 Primary Energy Use - Long Term Prediction by Shell in [14]

Solar PV is not viable in all regions of the world due to different solar irradiance levels. It is forecasted, however, that non-OECD (Organisation for Economic

Cooperation and Development) countries will represent two-thirds of the global energy consumption by 2050 [12]. Many of these countries are located in non-OECD Asia and Africa and receive on average over 2MWh/m²/year of solar energy, this makes them ideal candidates for economically viable PV installations even at today's rates (2019) [13]. Solar power has the biggest potential out of all known renewable sources and is the most applicable technology to the largest potential consumers of energy. For these reasons, solar PV is an important research area to explore.

Despite the sustained exponential growth in installed solar capacity, there is still a drive to improve the financial appeal of solar PV globally. In parallel to improvements in the power conversion efficiency, production volumes have increased leading to a reduction in the cost of modules (0.30US$/$W_p$), which has allowed utility-scale solar PV to reach grid parity in many countries [15]. This cost reduction follows the predicted PV learning curve of average module sales price (2018 US$/Wp) as a function of cumulative module shipment from 1976 to 2018 as shown in Figure 4.

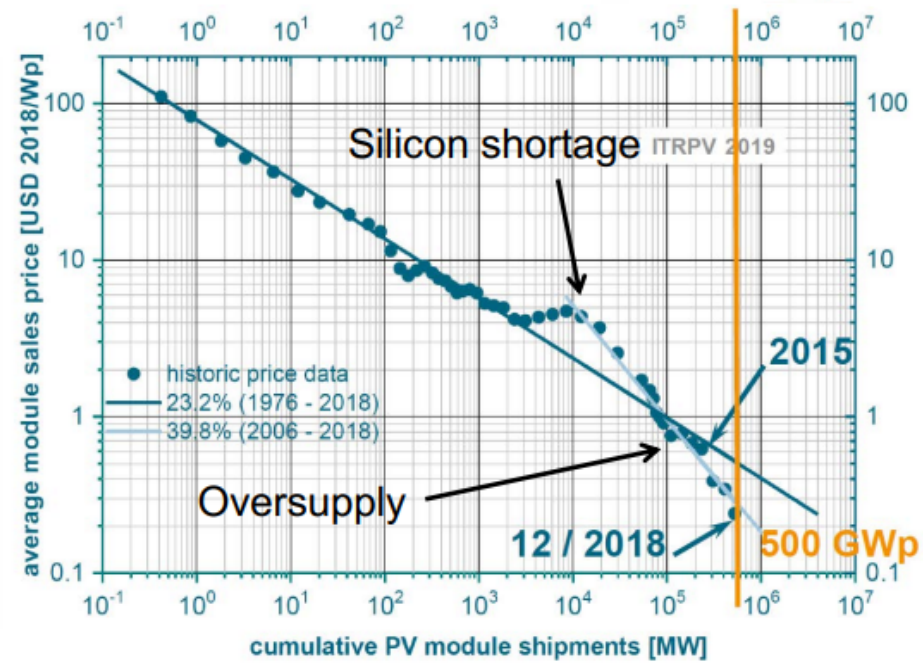


Figure 4 PV learning curve: the average PV module price against cumulative shipments from 1976 to 2018 and the associated learning rate (LR). Labelled by Dr. Brett Hallam [15].

It is important to note that the costs associated with the Si makes up only 28% of the total module cost and only 7.5% of the cost at system level [16] as shown in Figure 5 and Figure 6. Since the cost of the Si used in PV installations is a relatively small fraction of the total cost, it is much more effective to improve the efficiency of the Si rather than reduce production costs. Indeed, reducing module cost would only affect the small fraction of overall cost. By improving the efficiency of the module instead, the entire system benefits from the improvement as more electricity is generated from the same cost, thus reduce the price per watt.

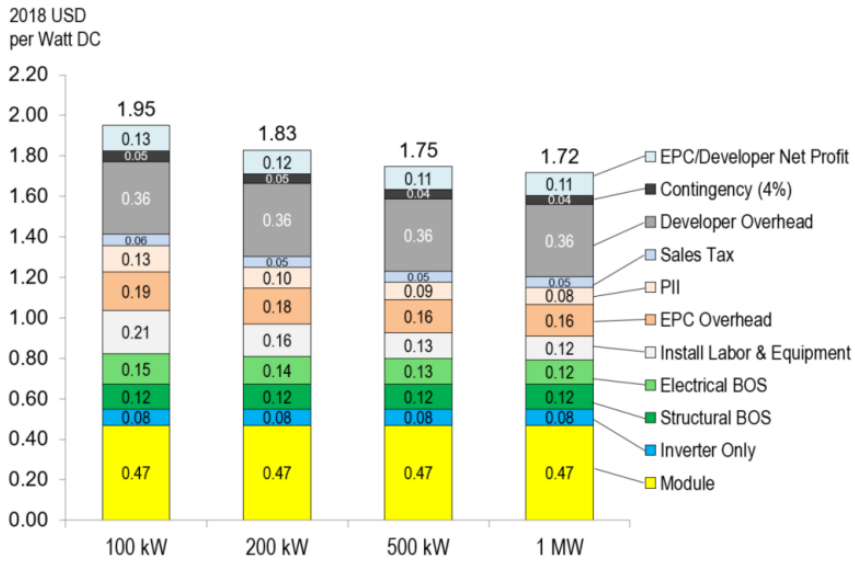


Figure 5 NREL 2017. Modelled Commercial in US PV markets. [17]

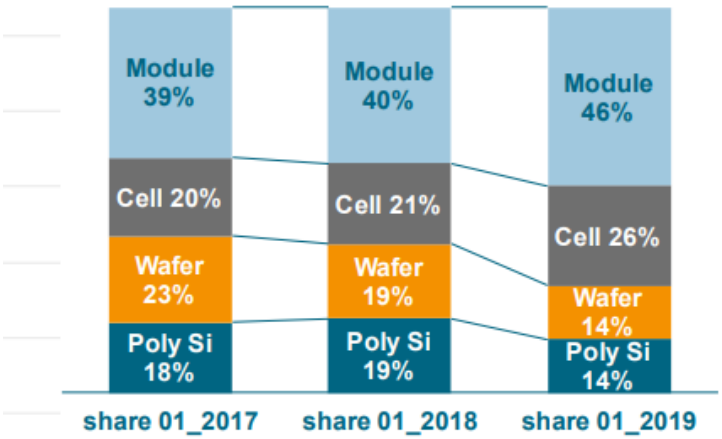


Figure 6 Comparison of the proportion of the price attributable to different module cost elements between 2017 and 2019 [15].

1.3 Silicon Solar Cells

Solar cells are devices that convert photons into electricity using the electronic properties of materials known as semiconductors. Silicon is a non-toxic, stable semiconductor and is the second most abundant element in the Earth's crust. It also has a well-established manufacturing process and a bandgap of 1.12 eV which is close to the ideal value of 1.34eV to convert electromagnetic waves into electrical energy [18]. This bandgap, however, is indirect, which limits the minimum thickness of Si required to form an efficient solar cell [19]. Despite this, Si remains the most widely used material for solar cells today, making up for 95% of all solar cell production [15] .

Si converts solar energy into electrical energy through a process known as the photovoltaic effect. This is a direct process that involves no other polluting steps or mechanical movement [19]. A typical solar cell will consist of a p-n^+ junction, an anti-reflection coating, a front contact and a metal back contact as shown in Figure 7.

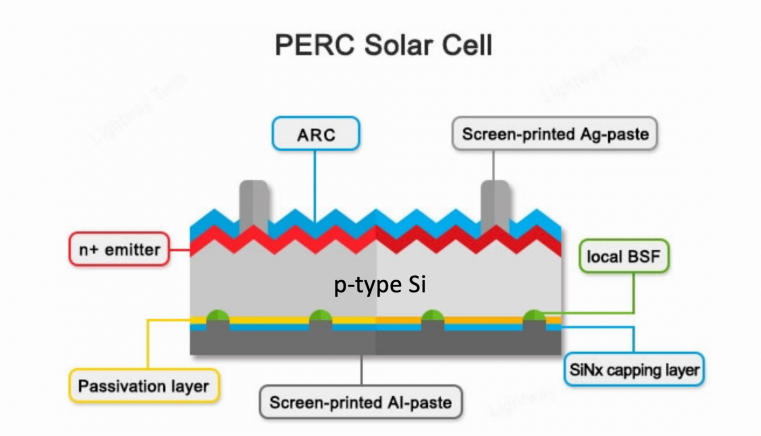


Figure 7 Schematic of a conventional PERC (passivated emitter rear contact) Si solar cell [20].

Another less common type of solar cell but one that is relevant to the application of the hydrogenation technique presented in this thesis, is a heterojunction solar cell. This cell architecture contains a n-type base wafer which is textured and passivated using a sacrificial SiN_x layer. An amorphous Si layer is then added to

both sides of the texture and H-passivated n-type Si, followed by an antireflective transparent conductive oxide and metal contacts [21].

The p-n^+ junction theory, developed by Shockley, states that photons absorbed on a cell generate electron-hole pairs (EHP) in the few microns closest to the surface of a device which will be spatially separated by the n- and p-type Si [22]. An EHP will only be created when a photon of light with energy greater than that of the bandgap (E_{BG}) strikes the cell. The photon may then be absorbed resulting in an electron being excited to the conduction band (CB) and a hole to the valence band (VB), thus generating an EHP. After generation, the electron in the CB is in a metastable state and may fall back down to a lower energy state in the VB, stabilising and annihilating a hole, thus recombining. This process also occurs in the opposite direction if holes are minority carriers. If the process of recombination occurs before the minority carrier crosses the p-n junction, no photocurrent will be added and thus the power conversion efficiency (PCE) of the cell will decrease [18]. A high recombination rate will also affect the open circuit voltage of the cell. The open-circuit voltage, V_{oc}, is the maximum voltage available from a solar cell. It is when the forward bias diffusion current is exactly equal to the short circuit current. The forward bias diffusion current, I_0, is affected by levels of recombination. If the recombination is high, the value of I_0 increases which in turn decreases V_{oc} which reduces the PCE of the cell.

EHPs can recombine via intermediate bandgap energy levels or due to crystallographic defect and impurities creating steps in the forbidden band gap [23]. The way in which recombination rates affect efficiency and ways to reduce them are discussed in the next Section 1.3.1.

1.3.1 Carrier recombination in crystalline silicon

When Si is under steady state conditions, i.e. when applied light or voltage remains constant with time, the generation rate, G, of EHPs is equal to the

recombination rate, R, of EHPs. The electron or hole carrier concentration, depending on n- or p-type, is denoted by n_0 or p_0. At thermal equilibrium it is assumed that all donor atoms are ionised so that $n_0 = N_D$ where N_D represents the donor concentration and $p_0 = N_A$ where N_A represents the acceptor concentration. As such, the carrier concentration can be defined as:

n-type:
$$n_0 = N_D \, , p_0 = \frac{n_i^2}{n_0} \tag{1.1}$$

p-type:
$$p_0 = N_A \, , n_0 = \frac{n_i^2}{p_0} \tag{1.2}$$

When light of sufficient energy is incident, additional carriers are injected from the VB to the CB so that $G \neq R$. Equilibrium is restored by means of recombination which causes the excess carriers concentration $\Delta n = n_b - n_0$ and $\Delta p = p_b - p_0$ to be reduced and the net recombination rate is then $U = R - G$. Here n_b and p_b denote the bulk carrier concentration in steady state [24]. However, in the case where there is charge neutrality and trapping centres are negligible, $\Delta n = \Delta p$.

For ease of calculations we assume charge neutrality so that the excess injected carriers are equal, with $\Delta n \approx \Delta p$. Since the minority charge carriers are in a metastable state they will recombine. The average time they will exist in that state before recombination is defined as carrier lifetime (τ) and follows:

$$\tau \equiv \frac{\Delta p}{U} \tag{1.3}$$

Carrier lifetime is related to the average distance travelled prior to recombination according to:

$$L = \sqrt{D\tau} \tag{1.4}$$

Where L is the minority carrier diffusion length and D the minority carrier diffusion coefficient.

In the case of solar cells, it is of interest to maximize the diffusion length L in order to increase the likelihood of the minority carrier reaching the depletion region and thus contributing to the photocurrent generated.

Although the low injection assumption is not usually valid for solar cell applications, the definition for lifetime, τ, remains widely used. It holds true for multi-exponential decays and allows for the comparison of different mechanisms that affect total carrier recombination.

The lifetime of a minority carrier is dependent on both the bulk and the surface recombination rates of a semiconductor which differ, thus the effective lifetime τ_{eff} is given by:

$$\frac{1}{\tau_{eff}} = \frac{1}{\tau_s} + \frac{1}{\tau_b} \tag{1.5}$$

Here the subscripts 's' and 'b' denote surface and bulk processes. The processes will be discussed in more detail in the following sections.

1.3.1.1 Bulk recombination

Bulk recombination comprises of intrinsic processes, present in all semiconductors, and of extrinsic processes which are due to impurities and defects in the crystal structure. Intrinsic processes are divided into Auger recombination and radiative recombination. Extrinsic recombination is due to energy states in the band-gap. These are defined using Shockley-Read-Hall statistics, and therefore extrinsic recombination is commonly called Shockley-Read-Hall

recombination (SRH) [25]. The total bulk recombination is the sum of the three independent recombination rates and the bulk lifetime is the reciprocal sum:

$$\frac{1}{\tau_B} = \frac{1}{\tau_{Rad}} + \frac{1}{\tau_{Aug}} + \frac{1}{\tau_{SRH}} \tag{1.6}$$

Each mechanism is discussed in more details in the following Sections.

1.3.1.2 RADIATIVE RECOMBINATION

Radiative recombination is a mechanism that dominates in direct bandgap semiconductors, but is of minor importance for an indirect bandgap material such as Si. Radiative recombination occurs when an electron from the CB directly combines with a hole in the VB and releases a photon. In indirect bandgap Si this process requires the additional participation of a phonon since the electron has to make a change in both momentum and energy to transfer from the CB to VB [24], [26]. This is because in indirect bandgap materials the CB minimum energy and the VB maximum energy are offset in k-space and thus the electron is required to change its own momentum as well as energy level.

The net radiative recombination rate depends on the concentration of both holes and electrons according to:

$$U_{rad} = B(n_b p_b - n_i^2) \tag{1.7}$$

Resulting in a carrier lifetime of:

$$\tau_{rad} = \frac{1}{B(n_0 + p_0 + \Delta p)} \tag{1.8}$$

Here B is defined as the band-to-band recombination coefficient and can be calculated from the semiconductor's absorption coefficient [18].

Many values for B have been found throughout the years, the first one for Si was by Gerlach et al. [27] as $B = 1.1 \times 10^{-14}\ cm^3/s$ in 1970 followed by Pankove [14]

in 1972 with $B = 2 \times 10^{-15}\ cm^3/s$. Comparing B for Si to a direct band gap semiconductor like GaAs we obtain $B = 7.2 \times 10^{-10}\ cm^3/s$ [28], a difference of almost 4 orders of magnitude. Radiative recombination forms the basis of commercial semiconductor lasers and LEDs and as such is of great importance for direct bandgap semiconductor research. For Si solar cells other recombination mechanisms are of far greater importance, as discussed below.

1.3.1.3 AUGER RECOMBINATION

Auger recombination is a three-particle process started by the energy released from the transition of an electron in the CB to the VB. This energy is then transferred to either another electron in the CB or a neighbouring hole in the VB instead of giving off a photon [24]. In turn, the third particle is excited into its respective band to relax back to its original energy by emitting phonons. Auger recombination is the inverse of the more commonly known impact ionization effect, whereby a high-energy electron collides with an atom, breaking a bond and creating an EHP. For Auger recombination to occur, two carriers of the same type need to be available, which is more common in highly doped material or material under high injection level conditions [29].

When the energy released from the electron transiting from the VB to the CB is transferred to another electron, two electrons and one hole (eeh) are needed so that the recombination rate is proportional to n^2p. When the energy is transferred to a neighbouring hole, two holes and one electron (ehh) are needed, making the recombination proportional to p^2n. The net Auger recombination, U_A, is defined by the weighted sum of both processes:

$$U_A = C_n(n_b^2 p_b - n_0^2 p_0) + C_p(n_b p_b^2 - n_0 p_0^2) \tag{1.9}$$

where C_n and C_p represent the Auger coefficients for eeh and ehh processes.

At first these coefficients were assumed to be constant values, but it was later shown that carrier concentration needs to be included in the model [30]. In 1990 when Hangleiter and Hacker conducted experiments at low carrier concentrations ($10^{18}\,cm^{-3}$), they realized that the experimental results did not correspond to the theoretical results obtained by extrapolating Auger recombination using the constant coefficient values [31]. It was then concluded that Coulomb interactions between carriers needed to be included in the Auger model [31]. This was done by adding enhancement factors g_{eeh} and g_{ehh}, to account for the probability of the three required particles existing at a given location. This is now widely accepted as the Coulomb-enhanced (CE) Auger recombination model for low level injection (LLI) conditions, as shown in equation 1.10.

$$U_A = g_{eeh}C_n(n_b^2 p_b - n_0^2 p_0) + g_{ehh}C_p(n_b p_b^2 - n_0 p_0^2) \tag{1.10}$$

Since then, a complete model to accommodate for all injection levels was proposed by Glunz et al [32] where Auger coefficients are defined as functions of the other parameters in equation 1.10. They used Altermatt's [33] parameterisation of the enhancement factors for LLI. Building on this model, Richter et al [34] used data collected from wafers subjected to different doping and passivation methods to propose a combined Auger and radiative lifetime depending on dopant and injection level. They were able to improve on Glunz's [32] model by using wafers that had higher-quality dielectrics to measure the limiting bulk lifetime more precisely. The presented model is shown in equations 1.11 to 1.14.

$$\tau_{int} = \frac{\Delta p}{(np - n_{i,eff}^2)(2.5 \times 10^{-31} g_{eeh} n_0 + 8.5 \times 10^{-32} g_{ehh} p_0 + 3.0x \times \Delta n^{0.92})} \tag{1.11}$$

$$g_{eeh} = 1 + 13\left\{1 - tanh\left[\left(\frac{n_0}{N_{0,eeh}}\right)^{0.66}\right]\right\} \tag{1.12}$$

$$g_{ehh} = 1 + 7.5\left\{1 - tanh\left[\left(\frac{p_0}{N_{0,ehh}}\right)^{0.63}\right]\right\} \tag{1.13}$$

where $N_{0,eeh}$=3.3 x 10^{17} cm^{-3} and $N_{0,ehh}$=7.0 x 10^{17} cm^{-3}.

This model is known as Richter's parametrisation and is used in the present work. The next section will cover the final type of bulk recombination: Shockley Read Hall, or defect mediated, recombination.

1.3.1.4 SHOCKLEY-READ-HALL

Dislocations, impurities and vacancies are all crystallographic defects that place energy levels in the otherwise forbidden band-gap in Si. These defects create an efficient two-step recombination process whereby electrons can relax from the conduction band to the valence band via this defect, annihilating a hole and as such, these defects are referred to as recombination centres. The recombination rate of this process was first modelled by Shockley and Read [25] and completed by Hall [35]. The model is a statistical analysis predicting the net recombination rate, U_{SRH}, associated with defects as a function of the recombination centre density, N_t, the capture cross section for holes or electrons $\sigma_{n,p}$, and the energy level of a specific recombination centre E_t. The capture cross section is defined as the area surrounding a trap in which a carrier has a high probability of being captured, the net recombination rate is:

$$U_{SRH} = \frac{n_b p_b - n_i^2}{\tau_{h0}(n + n_1) + \tau_{e0}(p + p_1)} \tag{1.14}$$

where τ_{h0} and τ_{e0} are lifetime parameters for electrons and holes. Their values vary as:

$$\tau_{h0} = \frac{1}{N_t \sigma_p \nu_{th}} \tag{1.15}$$

$$\tau_{e0} = \frac{1}{N_t \sigma_n \nu_{th}} \tag{1.16}$$

where $\nu_{th}$is the thermal velocity of carriers so that they sweep a volume equal to $\nu_{th}\sigma_{n,p}$. Lastly the carrier concentrations in the traps, n_1 and p_1 are given by:

$$n_1 = n_i e^{\frac{E_t - E_i}{kT}} \tag{1.17}$$

$$p_1 = n_i e^{\frac{E_i - E_t}{kT}} \tag{1.18}$$

Using the original lifetime equation (1.3) and the equation for SRH recombination rate (1.14), the SRH lifetime, τ_{SRH}, can be found:

$$\tau_{SRH} = \frac{\tau_{h0}(n_0 + n_1 + \Delta p) + \tau_{e0}(p_0 + p_1 + \Delta p)}{p_0 + n_0 + \Delta p} \tag{1.19}$$

The Si used in this work is single crystal Si, but multicrystalline Si (mc-Si) is commonly used in the industry. Single crystal Si is classified by its method of production as either float zone (FZ) Si or Czochralski (CZ) Si. Since its creation FZ Si was always thought to be very pure, with a virtually defect-free bulk as it is devoid of grain boundaries [18]. This means that SRH recombination is negligible compared to the less pure CZ Si. However, recent studies by Grant have shown that grown-in defect can exist in p-type FZ Si which would limit the bulk [36]. This recent information will have to be accounted for when testing for record efficiencies.

Mc-Si has a defect filled bulk due to the presence of numerous grain boundaries and dislocations. Mc-Si is, however, a very interesting material to work with as it makes up 69% of the world's market share of Si-PV due to its much lower price and has scope for efficiency improvements [37]–[39].

The model for SHR presented assumes defects only produce single energy level traps in the bandgap. However, defects such as grain boundaries and surfaces will produce an array of traps at different energy levels throughout the bandgap. For

these circumstances an extension to the SRH model will be necessary which can sometimes be achieved by integrating the recombination at every energy level across the bandgap.

1.3.2 SURFACE RECOMBINATION

The surface of Si is considered a large defect area as it is an abrupt lattice discontinuity leaving unbonded dangling Si bonds. These create intermediate bandgap energy levels, or surface states, which are easily accessible for the near surface generated minority carriers leading to increased recombination rates. The effectiveness of a surface as a recombination site is expressed as the surface recombination velocity (SRV) and defined by:

$$S_0 = \frac{U_s}{\Delta p} \tag{1.20}$$

where S_0 is SRV in cm/s, U_s is the surface recombination rate in $cm^{-2}s^{-1}$, and Δp is the excess carrier concentration. With an increased SRV, there will be an increased surface recombination rate. SRV is dependent on injection level, doping concentration and doping type as they affect the energy level of the introduced intermediate bandgap state. Thus, to calculate the surface recombination rate, U_s, SRH statistics are used to integrate the recombination at the approximate continuum formed of discrete energy level states across the bandgap (E_v to E_c):

$$U_S = (n_s p_s - n_i^2)\nu_{th} \int_{E_v}^{E_c} \frac{D_{it}(E)}{\frac{n_s + n_1(E)}{\sigma_p(E)} + \frac{p_s + p_1(E)}{\sigma_n(E)}} dE \tag{1.21}$$

where n_s and p_s are the electron and hole surface concentration, D_{it} is the density of interface traps at the different energy levels E.

It is important to note the difference between bulk and surface recombination and more specifically at what depth surface recombination becomes bulk

recombination. When in thermal equilibrium the CB and VB in Si are flat throughout the semiconductor due to uniform defect density and doping. In practical semiconductors, however, a space charge region (SCR) will be present at the surface due to traps or charge at the interface. The SCR will cause the CB and VB to bend. Recombination due to surface induced defects occurring in the band-bent region is defined as surface recombination whilst recombination occurring deeper, where bands remain flat, is considered bulk recombination. As such, a more generalized equation for surface recombination velocity taking into account the SCR depth SRV, $S_{d_{scr}}$, can be written as:

$$S_{eff} = \frac{U_{z<d_{scr}}}{\Delta p_{d_{scr}}} = S_0 + S_{d_{scr}} \tag{1.22}$$

where z is normal to the Si surface down to the SCR depth d_{scr} and where S_0 is the recombination at the very surface. The S_0 term is extremely relevant for this work, as some of the experiments investigate near-surface defects caused by H.

1.3.3 Summary of recombination processes

In sections 1.3.1.1 and 1.3.2, different types of recombination processes were outlined as well as their effect on the effective minority carrier lifetime. This reduction in lifetime will also reduce the overall cell efficiency which is why it is important that recombination is limited.

Ensuring active impurity concentrations remain below a critical limit and reducing the effect of defects at surfaces and in the bulk are essential in improving minority carrier lifetime. Chapter 2 discusses methods for limiting recombination processes in Si, including hydrogen passivation which is central to this thesis.

1.4 Aim of this work

The first Chapter of this Doctoral Thesis has given context for the work that will be presented. It was shown that solar photovoltaic energy is predicted to be the main electricity source in the coming decades, contributing to mending our current climate crisis. It was also highlighted that the Si material only contributes to 7.5 % of the total PV system cost. This makes improving the efficiency of the Si material more effective than reducing its processing cost, which is the aim of this doctorate.

In this thesis, a novel technique for damage-free, direct H passivation, developed during the course of this doctorate and dubbed Shielded Hydrogen Plasma, is used to introduce atomic H into Si wafers. This technique allows for the excellent interface and surface passivation of both n- and p-type Si wafers. This method also allows for the investigation of purely H-induced defects without the need for a high-temperature dielectric firing step. The aims of this thesis are as follows:

1. Demonstrate that neutral atomic H is released from Pd
2. Establish SHP as a damage free, low temperature, effective hydrogenation technique
3. Observe the efficacy of SHP on different structures
4. Explore the possibility of converting SHP to an in-line process with the use of different metallic shields
5. Introduce SHP as a tool to study movement of H in SiO_2 and Si
6. Attempt to understand H-related damage in n-type FZ Si.

1.5 Structure of this Thesis

An introduction to the need for alternative sources of energy, specifically solar power through Si PV devices has been given in Chapter 1. Background knowledge to general recombination theories was also shown in Chapter 1. Chapter 2 describes methods for mitigating recombination in Si, specifically via H-passivation. Common hydrogenation techniques are described, as is the

movement of H in Si and Pd. The experimental methods used throughout this thesis are presented in Chapter 3. Chapter 4 introduces the novel hydrogenation technique: Shielded Hydrogen Plasma (SHP), developed as part of this doctorate and presents proof of principle results. Chapter 5 focuses on the application of SHP to more complex Si structures, and compares SHP to other known hydrogenation techniques. Chapter 5 also investigates the possibility of converting the current PECVD based batch SHP to an in-line process, by investigating different metals to use as SHP shields. Chapter 6 presents a different application for SHP: as a tool to investigate H-related defects in Si at low temperature and without the need for a dielectric layer. In Chapter 6, H-related defects are seen in n-type FZ Si even with the presence of a 100 nm dielectric layer. This leads to the investigation of H transport across SiO_2-Si at low temperatures, and new models are proposed. Lastly, Chapter 7 summarizes the findings presented and discusses possible avenues for the future of SHP and the work required to achieve these.

CHAPTER 2 Literature on Hydrogenation and the movement of H in Si and Pd

Chapter 1 introduced climate change and the need for solar PV cells. Initial solar cell concepts and mechanisms were discussed as were the effect of different types of minority carrier recombination on the efficiency of a Si solar cell. In this literature review common methods for mitigating recombination processes are discussed, particularly through H passivation. The movement of H through Si as well as metals. and more specifically palladium is also discussed.

2.1 Improving bulk and surface lifetime of Si

The methods currently employed to reduce the concentration of defects and impurities in the bulk fall into two broad categories. The first one is gettering, which encourages the diffusion of impurities to locations where their electrical activity is less detrimental to the electrical performance of the cell. Although gettering is an interesting and effective technique, it is not relevant to the work presented in this thesis. The second category is passivation, which can be classified into field effect passivation (FEP) and chemical passivation. Chemical passivation is the technique more frequently used in this thesis. Specifically, H-passivation is used, which involves diffusing H into Si, to bond to a defect or an impurity which reduces or nullifies its electrical activity.

2.1.1 Chemical Passivation

There are currently two main methods to achieve excellent chemical surface passivation of Si solar cells. The first method uses a capping dielectric layer and the second uses H. Typically both methods are used in conjunction with one

another to achieve the best results. The chemical passivation principle of Si surfaces uses chemical bonding to the unsatisfied Si bonds found at the surface. This bond removes the electrical activity of unsatisfied Si bonds from the Si bandgap, thereby removing them as defect states and reducing total number of recombination centres.

2.1.1.1 Dielectric Coatings

Even without a dielectric coating, Si wafers will be coated with a native SiO_2 layer that is a few nm thick. This layer, however, does not provide a high-quality chemical passivation and as such is often removed. It does not provide effective passivation as it is grown at room temperature which does not favour the satisfaction of most Si dangling bonds. Instead, a dielectric layer is added. This is often SiO_2, SiNx or Al_2O_3. These layers have two purposes. The first is to act as an antireflective coating. Si is extremely reflective when polished, with a reflectance of over 30 % [40], whilst an optimised anti-reflective coating (ARC) can reduce this to well below 5 % [41]. The ARC is of a chosen thickness to purposefully create interference waves which are out of phase with the reflected waves from the Si. These out-of-phase waves destructively interfere, resulting in zero reflected energy and 100 % transmitted.

The second purpose of dielectric layers is for chemical passivation, used both for the upper and lower surface of the Si wafer. Different dielectrics are used for different purposes and on different types of Si. SiO_2 is generally used on both surfaces, for it has a superior chemical passivation ability [42], but it does not provide good anti-reflection properties on its own. SiN_x is usually used on the top surface as it combines good ARC, chemical passivation, H-passivation and also introduces an intrinsic positive charge which creates FEP. It is common to see a combination of SiO_2 and SiN_x layers to optimise all these properties.

Most solar cells today have some form of dielectric coating for chemical passivation, but due to the optimisation of the other properties dielectrics provide, some surface states remain unsatisfied. As such, it is common for solar

cells to receive an additional H-passivation treatment in order to further passivate surface defects.

2.1.1.2 HYDROGEN PASSIVATION

Hydrogen is the most abundant element on earth and is easily incorporated in materials due to its small size. H shows a range of complex reactions when it is introduced into a semiconductor. The study of H in semiconductors began more than 50 years ago by Mollwo [43], when he noticed that exposing ZnO to H increased the conductivity of the material. In the 1980s H research exploded after Haller *et al* [44] demonstrated that H can passivate electrically active impurities in Ge. This was reproduced in Si by Sah et al. [45] when they observed Boron impurities being passivated by H originating from the Al gate of a metal-oxide-semiconductor (MOS). Pankove et al. [46] confirmed the role of H in this, via vibrational spectroscopy of H-B bonds. Up until that point, all research showed that H acted as a donor by passivating B which is an acceptor. Johnson *et al.* [47] however, showed that H could also be an acceptor as it was able to passivate P in n-type Si. By the end of the 1980s it was confirmed that H is amphoteric by acting both as a donor (H^+) in p-type Si and as an acceptor (H^-) in n-type material, always counteracting the prevailing conductivity [48]. Since then, many research papers [49]–[52] and books [9], [19], have been devoted to the study of H in Si as a passivation technique. H is so widely used that almost all Si solar cells today will have had some form of H passivation performed during their production.

H passivation is a technique used to passivate bulk defects and terminate surface bonds in Si [49] by the introduction of H in its atomic form. Atomic H is widely accepted to be a rapid diffuser capable of cancelling the electrical activity caused by dangling bonds and by some transition metals at surfaces and grain boundaries. This results in large increases in surface and bulk lifetimes [53]. Recent investigations into the passivation of donor impurities in Si, have also shown that the passivating ability of interstitial H is affected by its differing

charge states [54], [55]. Lastly, the passivation abilities of H with respect to the B-O defect has recently come into the light, as illumination was reported to play a role in the recovery and permanent deactivation of these defects with H [56]. What this finding also demonstrate with respect to H, is that it remains mobile and active at low temperatures, (70 °C), in solar cells. This low temperature mobility of H in Si is relevant for the H-passivation work presented in this thesis.

Over the years, techniques for introducing atomic H have been discovered and optimized. Hydrogenation techniques amongst others include ion implantation [57] and plasma exposures [58]. However, the most commercially used technique remains the release of H from a dielectric layer such as SiN_x as it doubles as an antireflection coating and surface passivating layer [59]. Regardless of which technique is used, researchers have faced the same problem, which is to quantify how much H is being introduced into the Si wafer. Ways of observing H are discussed in Section 2.1.3 followed by more details on H-passivating techniques in Section 2.1.4.

2.1.2 Field Effect Passivation

FEP is a technique routinely used to reduce surface minority carrier recombination in Si and is often employed in conjunction with chemical passivation [60]–[63]. There are two main techniques employed to apply FEP. Both aim to control the carrier concentration at the surface of the Si via charge, thereby limiting the access of one type of carrier to the recombination active region that is the surface. One effective method is the diffusion of a doping profile in the near-surface region which creates an internal electric field [64]. This method is not used in this thesis and as such will not be explained in further detail. A second method is adding charge to a capping dielectric layer. These charges repel charged carriers of the same sign from the near-surface Si region [65], [66]. More details on the dielectric charging as well as methods to add this charge are given in Section 2.1.2.1.

2.1.2.1 CHARGED DIELECTRICS

Adding charge in or on the dielectric, as well as at the interface between the dielectric and the Si is a method to effectively field effect passivate Si. The charge reduces the carrier access to the surface, which is an area of high recombination, by repelling carriers of like charge. SiO_2 and SiN_x films are intrinsically positively charged, and therefore are commonly used on n-type Si [67], [68]. The minority carriers in n-type Si are positively charged holes, and are therefore repelled by the film's charge [67], [68]. Al_2O_3, which is negatively charged, is commonly used on p-type Si [69], [70]. The charge of these dielectrics is usually measured in q/cm^2. Where q is the magnitude of the elementary charge of an electron, $q = 1.6 \times 10^{-19}$ C. The typical intrinsic film charge is summarised in Table I below.

Table I Summary of intrinsic charge for dielectric films

Film	Charge concentration
Thermally grown SiO_2 [71]	10^{11} q/cm^2
PECVD deposited SiN_x [68]	2×10^{12} q/cm^2
Al_2O_3 REF [72]	-10^{13} q/cm^2

The added benefit of these dielectric films is their chemical passivation ability. They chemically bond to the dangling Si bond at the Si surface, reducing the concentration of recombination sites [73], [74].

A method to further improve the efficacy of these dielectric films is through adding additional charge via extrinsic processes. This allows for the charge concentration present in the dielectric to be decoupled from the deposition/growth parameters. This decoupling permits for the optimisation of the dielectric's chemical passivation capabilities as well as their anti-reflection coating properties, whilst the field-effect passivation is added extrinsically. The methods by which extrinsic charge is added to the dielectrics used in this thesis is explained in Sections 2.1.2.1.1 and 2.1.2.1.2

2.1.2.1.1 Corona Discharge

Throughout this work corona discharge was used as a method to introduce extrinsic FEP through surface charge. For this technique a corona is produced through the application of a high voltage to a metal pin. The voltage is of the order of tens of kV. The pin acts as an electrode which ionises molecules near it, forming a corona-shaped plasma. Ionised atoms slowly scatter and drift towards the sample which is placed on a grounded plate [75], [76]. The medium between the electrodes is usually air, oxygen or inert gas [76].

The ionised atoms deposited on the surface of the dielectric coated Si sample cause the surface to be charged. This technique has been used for decades [75], [76], but has not been viewed as an adequate FEP technique for solar cells as the corona charge usually decays [77]–[79]. Bonilla *et al* published work however, that showed that a hydrophobic layer, hexamethyldisilazane (HMDS) can be used for stabilising the corona charge [79]–[81]. This extremely hydrophobic layer prevents water access to the oxide surface, reducing lateral surface conduction. Bonilla *et al* obtained the low surface recombination velocities (SRV) of 1.6 cm/s on 1Ωcm n-type FZ Si using this technique [79].

Corona discharge without the use of HMDS is used throughout this thesis to achieve excellent surface passivation in order to investigate potential bulk-lifetime limiting defects.

2.1.2.1.2 Ionic Charge

Another method to add extrinsic charge to a dielectric without the stability issue of corona discharge is ionic charge introduction. Bonilla and Collett have reported that the introduction of Na^+ and K^+ into SiO_2 films provide sufficient charge to cause effective FEP [26], [82], [83]. The charge concentration they obtained was of the order of 5 x 10^{12} q/cm^2, and has been reported stable for at least 4 years. Collett *et al* also investigated [65], methods for making ionic FEP appropriate for

large scale solar cell manufacturing. It is reported that spin-coating can be used to deposit the ions on the surface of the dielectric which makes the process much faster and cost-effective. This technique is used in this thesis in combination with the investigated Shielded Hydrogen Plama passivation. More details are given in Section 3.5 .

2.1.3 Observing hydrogen

The investigation and optimisation of different H passivation processes has been the subject of intensive research efforts over the years [39], [47], [53], [84]–[86]. There is, however, a great deal of controversy on this topic in the literature. Most of the discrepancies arise from the difficulty of detecting H in Si. A direct method of H detection such as Secondary Ion Mass Spectroscopy (SIMS) exists but has detection limits that are well above the H concentration within most Si solar cells [52], [87]. The detection limit of these instruments is high because vacuum systems cannot effectively purge H as its small size allows it to effectively diffuse back into the chamber. As such, the presence of H within Si is almost always observed indirectly through its interaction with other impurities or by changes in the minority carrier lifetime. This problem can sometimes be remedied by using a deuterium, D, source for hydrogenation which improves the detection limit in systems using a vacuum.

Another cause of disagreement in the literature is the fact that H release from dielectrics is highly dependent upon the deposition parameters of a given dielectric. These deposition parameters are sometimes equipment dependent causing many different dielectric recipes to be published. Gas flows and small concentrations of O_2 have been shown to heavily alter the concentrations of H present within a dielectric such as SiN_x [88]–[90]. These variations are also known to affect the quality of the nitride and its ability to act as an anti-reflection coating. Furthermore, H released from a dielectric can either diffuse into Si or effuse back into the atmosphere. Quantifying the fraction of H released from Si

has been shown to present challenges [87]. All of these parameters are hard to monitor and make observing the effect of H in Si difficult.

B-doped crystalline Si has been used as a model substance for experimental and theoretical investigations of the H passivation mechanisms for at least 30 years [91]. Wafers containing high enough concentrations of B are used such that H being diffused through is effectively trapped through the formation of H-B complexes. The H passivation of B increases the resistivity of the passivated region which affects the C-V curve measured using a capacitance-voltage meter resulting in a calculation of the total amount of H present. These calculations are shown in Chapter 3 Section 3.6.3.1.

2.1.4 Hydrogen passivation methods

Atomic H readily diffuses into Si and can be introduced by a variety of techniques. These processes can generally be split into four categories: (1) electro-chemical hydrogenation, (2) molecular gas systems, (3) ionic implantation and (4) plasma based systems. [46], [92].

2.1.4.1 electro-chemical Hydrogenation

This process, sometimes referred to as wet hydrogenation, is the simplest method of introducing atomic H into Si but has limited efficacy [93]. It involves dipping the Si sample into boiling water, into dilute HF or exposing the sample to any other H containing liquid. These processes are usually done at low temperatures ($\leqslant$100 °C) and as such the density of atomic H present is minimal as atomic H will not readily dissociate and diffuse into Si at these low temperatures. The presence of any H introduced into Si using these processes is usually limited to less than a micron [93].

2.1.4.2 Molecular Gas System

Forming gas annealing (FGA) is a common method to introduce H into Si. FGA is typically a mixture of N_2 and H_2 gas in a ratio of 94:6, which is heated to

≥ 450 °C during the anneal. It is a popular method as it requires no complicated machinery, only a furnace, and causes no damage to Si surfaces. FGA has been demonstrated to be capable of significantly improving surface passivation of Si/SiO2 interfaces [59], [94]. In order to perform FGA however, the samples need to be annealed at temperatures above 450 °C to allow for the dissociation of H_2 into H. The dissociation mechanism of H_2 into H at those temperatures remains disputed. FGAs have been used for decades in the MOS industry, and it is believed that the H_2 dissociation occurs in that case because of the metal present [95]. It has been shown that FGA passivation of MOS does not occur without a metal present [96]. As such for Si devices that do not have a metal component, the proposed mechanism is one of surface damage. The dissociation of H_2 occurs by the vacancies associated with surface damage[97], [98]. These theoretical studies have suggested that H_2 molecules can spontaneously dissociate in order to passivate the surface dangling bond [51]. Although this is an interesting mechanism, the presence of surface damage is not common to all Si solar cells. As such, forming gas anneals have a relatively low efficacy of introducing H into non-damaged Si cell structures.

2.1.4.3 Ionic Implantation

Ionic implantation of atomic H involves direct exposure to a H ion beam at high energies, between 50 keV and 100 keV. The atomic H concentration implanted is usually of the order of 1 x 10^{16} cm^{-2}, which is depth intergrated. Although this technique has a high throughput of H introduction it has the drawback of considerable surface damage caused by impingement [99].

Energetic particle impingement caused by ion bombardment can severely damage the surface of Si or SiO_2. The first extensive study of this problem was conducted by Mazey *et al* in 1968 [100]. The authors observe that point defects are created when there is a passage of energetic ions through a solid. This is due to atoms being displaced during atomic collisions. These create point defects, modify the electrical properties of the Si and reduce its carrier lifetime by increasing

recombination rates. Jeng, Oehrlein and Scilla conducted experiments exposing Si directly to a H plasma and observed substantial damage in the top 15nm of the samples [101]. They concluded that the "heavily damaged regions (top 15 nm layer) in the H_2, RIE exposed Si are caused by the energetic ion bombardment". Interestingly, they observed a different type of defect in the [111] plane which appeared to be caused by the condensation of supersaturated H in Si. A similar effect is also discussed in the present work and is described in Chapter 6.

2.1.4.4 Plasma Based Systems

2.1.4.4.1 Dielectric layer deposition

The most common method used to introduce H into Si solar cells is through its release from dielectric layers either before or during cell metallisation. Silicon nitride coatings (SiN_x) to release H are preferred as they simultaneously saturate a majority of surface dangling bonds and act as anti-reflection coatings (ARCs) present in almost all current Si solar cell technologies [59]. These films are commonly deposited using a plasma enhanced chemical vapour depositor (PECVD) with H-containing reactants, such as ammonia, NH_3, resulting in a non-stoichiometric SiN_x:H film with up to 40% of H [102].

H is released from SiNx during high temperature annealing. In the case of screen printed solar cells, the high temperature process is made more cost- and time-effective by combining H release with the firing of metal contacts and the Al back surface field (Al-BSF). Because all processes are achieved with a single high-temperature anneal, the temperature is within the 973K to 1173K range in order to optimise the BSF properties. There is also significant debate as to how much atomic H is introduced to the bulk Si during these firing steps [103], [104], as there is a sharp trade-off between the surface passivation quality and the release of atomic H into Si [105]. Another trade-off present in the H release from SiN_x is that the high temperatures required for this release also allow for significant effusion of H from Si surfaces. Indeed, a significant portion of it will diffuse through the bulk Si and either exit the back surface or get stored in the Al back

surface region. Hallam *et al* have recently published work which advises a lower firing temperature of 620 °C to 700 °C in order to retain more of the released H [39].

Whilst H containing dielectrics, such as SiN_x or AlO_x, have proven to be excellent sources of atomic H through a post-deposition anneal at temperatures ranging from 400 to 900 °C [106]–[108], not all cell structures incorporate such dielectrics or high temperature processing such as heterojunction solar cells [21], [109]. For these devices it would be preferable to have a direct source of atomic H. In the absence of a dielectric source typical sources of H include direct and remote hydrogen plasma exposure.

2.1.4.4.2 Direct Hydrogen plasma

A plasma enhanced chemical vapour depositor (PECVD) equipment can be used as a dissociative plasma source to perform direct plasma H passivation of Si with atomic H.

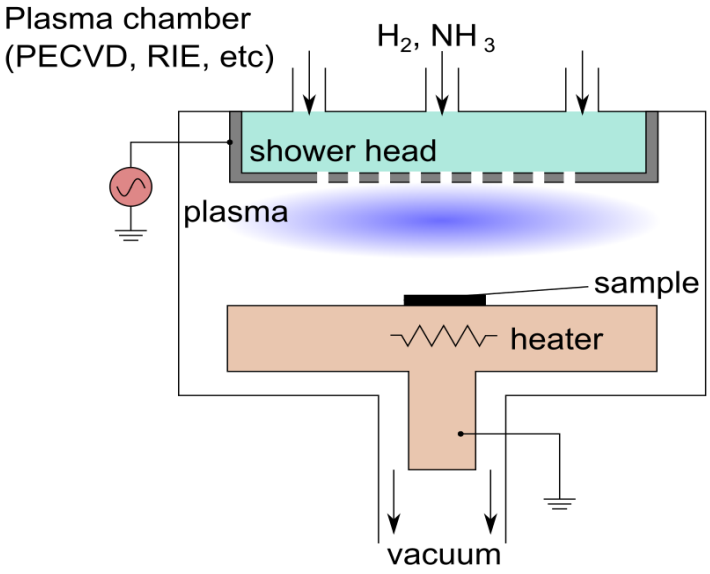


Figure 8 Schematic of PECVD equipment used for Direct Plasma Hydrogenation

The plasma is generated by RF power from NH_3 or H_2 gas which dissociates into H. Atomic H diffuses to the sample placed on the lower heated electrode as shown

in Figure 8. However, this technique produces highly energetic H ions (100-500 eV) and hard UV (short wavelength photons with high energy), which leads to surface damage of the Si sample [58].

The primary sources of damage from plasmas are a) hard UV radiation, b) impingement of energetic particles and c) charge deposition on and subsequent electrostatic breakdown of dielectric layers. The effect of each of these will vary based on the structure of the sample being exposed and the temperature of the exposure. Radiation damage caused by energetic particles such as ions, electrons and UV photons generated in the PECVD plasma has been a serious problem for direct plasma hydrogenation techniques [110]–[113]. Experiments by Mizutani et al, in which SiO_2-Si samples were independently irradiated, showed that most of the damage is induced by UV photons and ions and that the damage caused by electrons is relatively small. Radiation damage can be caused by UV photons released from PECVD plasma. These have short wavelengths ranging from 10 nm to 200 nm and penetrate dielectrics and generate electron-hole pairs, causing a positive charge exceeding breakdown limits. Dielectric breakdown is an issue as it reduces passivation quality by increasing recombination velocity. This decreases the overall efficiency of the sample.

Ionic impingement caused by highly charged particles was an issue seen in ionic implantation systems as they can cause physical lattice damage. These often take the shape of physical pits on the surface of the sample which increases surface defect density and therefore the overall recombination rate in the sample.

The third type of direct plasma related damage is charge deposition on a dielectric. Similar to UV photon damage, charged ions can also cause electrical damage, as opposed to lattice damage caused via bombardment. When charged ions are deposited onto the surface of a dielectric, a build-up of charge occurs [114], [115]. If this charge generates a field that is greater than the breakdown field of the dielectric, as is sometimes the case for thin SiO_2 films, the dielectric will break down, causing a reduction in the passivation quality. Ephrath *et al*

conducted experiments in 1981 to analyse this effect, by exposing SiO_2 films to RIE plasmas and noted that a trapping layer close to the exposed oxide was created because of the implantation of low energy ions (less than 400 eV)[116].

2.1.4.4.3 Remote Plasma Hydrogenation

The second and less damaging class of plasma-based hydrogenation is the remote plasma system. This technique is similar in apparatus to the direct plasma approach but is characterised by the placement of the Si sample outside of the plasma region by means of a remote chamber [117]–[119]. This prevents the sample from being exposed to UV radiation and allows for atomic H to lose some of its energy before incidence at the sample. The H-containing plasma is generated in a tubular vacuum chamber by PECVD RF power and NH_3 or H_2 gas. A schematic of the apparatus is depicted in Figure 9.

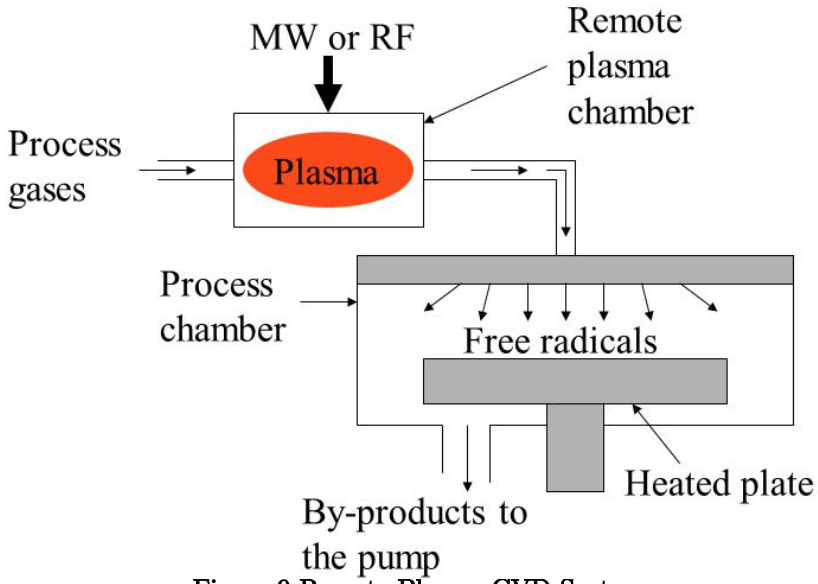


Figure 9 Remote Plasma CVD System

However, this method is not easily accessible for research laboratories as it requires specialist equipment. The distance between the remote plasma source and the sample is much greater in this system than in direct plasma hydrogenation, leading to potentially more H recombining to form H_2 along the way. However, it is unclear how much concentration of atomic H reaches the surface of Si in remote plasma CV, and as such wether there is more than enough

H, which could have negative effects in Si or not enough, thus not optimising the passivation quality [120].

2.1.5 Summary of Hydrogen Passivation Techniques

The aim of H passivation is to deactivate electrically active impurities and defects by encouraging a reaction with atomic H. Direct plasmas and ion beam implantation both cause a lot of damage to the Si surface, which is a major drawback. Remote plasmas are a way to avoid causing surface damage but are often expensive and potentially less effective than direct plasmas due to the decreased concentration of atomic H reaching the wafer.

2.2 Hydrogen-Related Defects in Si

H in semiconductors has been extensively researched for the past 30 years, primarily due to its ability to passivate both deep-level defects and shallow-level dopants [48], [51], [121]. As such, the introduction of H into Si is commonly perceived as a performance-enhancing process and is standard in the vast majority of commercial Si solar cells.

It has been observed however, that H can sometimes cause negative effects when introduced into Si. There are multiple reports that H plays a major role in the activation of light and elevated temperature induced degradation in p-type mc-Si Si (LeTID) [122], [123]. The degradation of p-type mc-Si was first seen through a decrease in lifetime and electronic characteristics, and is particularly noticeable in fabricated cells that have high efficiencies such as passivated emitter and rear contact (PERC) cells [124]. H was identified as a possible cause for LeTID partly through the work of Chan *et al* and Bredemeier *et al* [122], [125]. They observed that the extent of LeTID activation in fired samples could be increased when firing temperatures were increased and, conversely, unfired samples showed an

absence of degradation. Bredemeier's work also showed evidence that the lifetime recovery after degradation could be caused by the diffusion of species to or from the wafer surface [125], [126]. Based on the required diffusivity for this effect to occur, they suggested that these species could be metal impurities or H.

Although the bulk of LeTID work has been done on p-type mc-Si, recent papers have reported the effect on p-type Czochralski Si, which suggests that at least part of this effect is unlikely to be related to crystallographic defects. Following this, p-type Float Zone (FZ) Si has been investigated for LeTID and work by Niewelt *et al* [127] followed by Sperber *et al* [128] confirmed its occurrence by observing an initial degradation in bulk lifetimes. They subsequently observed a second decrease in lifetimes which they speculated to be due to a decrease in surface passivation quality.

The presence of LeTID in n-type Si is a disputed finding as authors report varying results. Niewelt *et al* investigated LeTID in n-type FZ Si and did not observe any bulk degradation, concluding that the defect was either not present or not recombination active in this material [127]. Conversely, Renevier *et al* observed some instability in the lifetime of B-diffused n-type when first passivated with a H rich dielectric and subsequently fired [129]. The LeTID type defect only arose when the wafers were illuminated annealed or dark annealed. Renevier also observed that a P-diffusion stopped the occurrence of any bulk degradation and this was also the case for wafers with a H-lean dielectric. More recently Chen *et al* [130] observed n-type FZ degradation which only occurred when diffused layers were present.

There are other H-related defects discussed in the literature, mostly from direct or remote plasma sources. Indeed, it has been reported that in high concentration and at low temperatures the introduction of H from a plasma into Si can form recombination active defects [131]. These defects have been reported by a number of authors, [131]–[133], to be in the form of molecular stabilized platelets or microcracks. These defects are also only seen in the first 100 nm of the exposed

Si surface, and all of the published work introduced H on a bare n- or p-type Si surface. The authors have also observed that a 60 minute, 350 °C anneal was enough to dissociate the platelets observed using TEM, transmission electron microscopy [131], and to recover the minority carrier lifetime which had been degraded by these H-related recombination active centres.

The majority of published work reporting Si degradation attributed to H-related defects has used a deposited SiN_X:H layer as the H source which involves a high-temperature step. This increases the diffusivity of H which raises the probability of H diffusion out of the upper surface of SiN_x, or across the bulk of Si and out from the other surface. As such, it is not widely known what quantity of H is released from SiN_x into bulk Si, and it would be interesting to study the effect of H-introduction at temperatures much lower than the SiN_x firing temperatures (less than 600 °C). As such, a damage free hydrogenation technique effective at a wide range of temperatures is desirable to study H induced bulk defects in greater detail.

In this work, a novel method that enables the use of a direct plasma without the associated Si surface damage is proposed. This method has the potential to allow laboratories worldwide to achieve extremely effective H-passivation without the need for a dielectric or a remote plasma system. A grounded metal film is placed between the plasma and the sample to stop hard UV and highly charged ions from degrading the Si surface while allowing the unimpeded diffusion of H. The most suitable metal for this appears to be Pd due to its extensive use in the H industry, as explained further in the following section.

2.3 Behaviour of hydrogen in palladium

Pd is unique amongst metals in having the ability to absorb large quantities of H compared to other Group VIII elements [134]. Pd has been the subject of H-related research for at least 50 years when Pd membranes started being widely used for the separation and purification of H gas [135].

The diffusion mechanism of H through Pd have previously been published and is thought to occur in 7 distinct steps, as described by Pick *et al* [136] and illustrated in Figure 10.

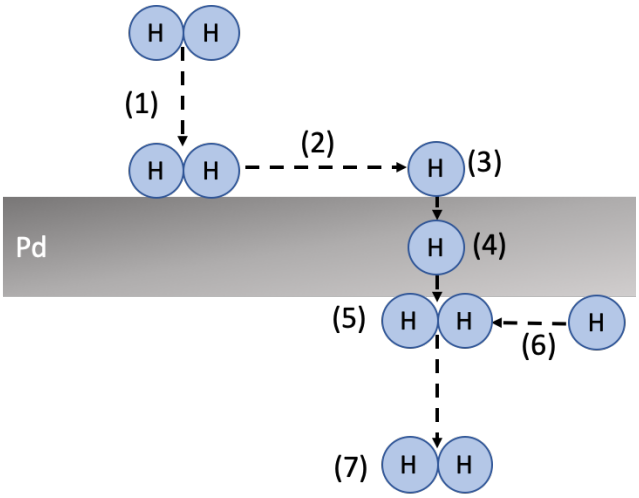


Figure 10 Schematic representation of the diffusion of H through Pd as per [136]

Figure 10 shows the seven steps of H transport through Pd as reported by Pick *et al*. The first step (1) is the diffusion of H_2 to the surface of the Pd membrane, (2) is the dissociative adsorption of H_2 into atomic H on the surface of Pd, (3) is the transition of atomic H from the surface into the bulk of Pd, (4) is the diffusion of atomic H through the Pd bulk, (5) is the transition of atomic H from the bulk to the surface, where it (6) combines with a nearby atomic H to form H_2 and finally (7) is the exit of H_2 from the surface of Pd, being transported via gas transport mechanisms. Steps (6) and (7) represent the "recombinative desorption" mechanism.

This is the most widely accepted theory for the transport of H through Pd. It is interesting to question whether the rate limiting steps of this mechanism are the recombinative desorption or the rate at which atomic H can diffuse through bulk Pd. This is investigated in Chapter 5 Section 5.2 when thicker Pd membranes are used as well as different metals. [137]

As shown in Figure 10, the accepted literature on H diffusion through Pd involves the release of H_2 from the Pd surface after transport. H_2 would not passivate Si effectively as it is much less reactive than atomic H [49], [91], [121]. As such, if H-passivation is seen in a Si sample which has received H from the surface of a Pd membrane, atomic H must be present somewhere in the overall system. Atomic H could be released from external Pd to generate an atomic H source for passivation, or H_2 could have dissociated on the surface of the Si sample before introduction into Si for H-passivation.

There are only a handful of published works that demonstrate atomic H released from Pd, and all them have specific Pd-H conditions. Lisowski et al. have reported that H_2 dissociates when in contact with Pd, but only during Pd-H decomposition [138]. Their work focused on increasing the volume fraction of H in Pd, using a plasma source, in order to form a Pd-H film and to then decompose this film by increasing its temperature. When the film decomposed, they observed a release of atomic H, measured via gold film and TMDS [91]. A second published paper on atomic-H release from Pd was by Tyurin *et al,* [139], who raised the energy level of the H on the surface of Pd via ion bombardment. The ionic bombardment of the Pd containing H is said to have excited the H atoms enough to stimulate non-equilibrium emissions of atomic H.

Most of the H literature related to release from Pd disagrees however, and still state that only H_2 is released via recombinative desorption. This work aims to clarify this discrepancy and determine if the disagreement is due to most studies simply not looking for atomic H and therefore not making the distinction between

the two forms of released H from Pd. This work will use atomic H as a source compared to the H_2 gas mostly used in the literature.

CHAPTER 3 EXPERIMENTAL METHODS

This chapter lists the material used throughout this work. It also outlines the experimental methods and the analysis techniques used.

3.1 BASE SILICON

3.1.1 SUBSTRATES

Both n- and p-type mono-crystalline Si was used in this project as summarized in Table II. The majority of experiments were conducted on high purity, Float Zone (FZ) n-type Si doped with a P concentration of 5 x 10^{15} cm^{-3} obtaining a wafer resistivity of 1 Ωcm. Experiments using the deactivation of B were done on Czochralski (Cz) p-type B-doped Si of 0.17-0.22 Ωcm with a doping concentration of 1.17 x 10^{17} cm^{-3} .

Table II Summary of Si substrates used in this thesis

Ref.	Type	Dopant	Resistivity	Thickness	Supplier
UnOx	n-type FZ	P	1 Ωcm	200 μm	Fraunhofer ISE
UnOx	p-type FZ	B	1 Ωcm	200 μm	Fraunhofer ISE
7NK	p-type CZ	B	0.17-0.22 Ωcm	700 μm	MEMC Electronic Materials

3.1.2 SURFACE FINISH

The best solar cell efficiencies in commercial installations are achieved by texturing the surface of Si in order to increase photon absorption. In this project however, the Si has a planar finish to facilitate characterization and lifetime

measurements. The n- and p-type monocrystalline samples were double side SEMI (international standard) flat polished.

It would be interesting to apply the hydrogenation technique presented in this thesis to textured surfaces in future projects.

3.2 Dielectrics

In this work either SiO_2 or SiN_x or a combination of both were used as dielectrics.

3.2.1 Thermal Oxide Growth

All samples coated in a SiO_2 dielectric used in this thesis were dry thermally oxidised in a quartz tube furnace either at Fraunhofer ISE or in the Oxford Cleanroom. Dichloroethylene (DCE) was used to enhance oxide growth at Fraunhofer. This is summarised in Table III.

Table III Summary of SiO_2 growth processes of samples used in this thesis

Ref.	Gas Conditions	Temperature	Laboratory	Oxide Thickness
UnOx	DCE/O_2	1050 °C Dry	Fraunhofer ISE	100 nm ± 5 nm
UnOx	O_2 ramp down in N_2	1050 °C Dry	Oxford Cleanroom (Begbroke)	100 nm ± 10 nm

One of the aims of this thesis was to obtain excellent surface passivation between the SiO_2 dielectric and the Si sample. As such, excellent oxidisation processes were insured by sourcing samples from Fraunhofer ISE. It is important to note that these oxides are considered thick by industry standard which usually process cells with less than 10 nm thick oxides. However, testing processes on thicker oxides allows for the use of more characterisation tools which was deemed valuable for this work. Additionally, although the oxides are grown to the highest standard, variations in quality remain. Lucy Rands has reported in her MEng thesis that these sample to sample variations can represent differences of up to

20 μs of the effective minority carrier lifetime at 10^{15} cm^{-3} injection level, even on the same wafer [140].

3.2.2 Silicon Nitride Deposition

Silicon nitride (SiN_x) dielectrics were deposited in the Oxford Department of Materials Cleanroom at the Begbroke Science Park. SiN_x was deposited using the Oxford Instruments (OI) PlasmaLab 80+ plasma enhanced chemical vapour depositor (PECVD). Different recipes were used to obtain varying thicknesses of SiN_x as summarised in Table IV. Specimens were placed on the heated lower electrode at different temperatures depending on the recipe. The chamber pressure was 400 mTorr. A 20 W radio-frequency (RF) source was used at 13.56 MHz to generate and maintain the plasma. The recipes were optimised for passivation quality and their thicknesses were measured using an elipsometer. Once again, the effective minority carrier lifetimes observed using these nitrides have been found to differ by up to 20 μs at 10^{15} cm^{-3} injection level [140].

Table IV Summary of deposited SiN_x processes for samples used in this thesis

Ref.	Gasses	Temp	Chamber Pressure	Time	Nitride Thickness
UnOx	400sccm SiH_4, 20sccm NH_3, 600sccm N_2	380 °C	600 mTorr	10 mins	80 nm ± 5 nm
UnOx	400sccm SiH_4, 20sccm NH_3, 600sccm N_2	400 °C	400 mTorr	8 mins	70 nm ± 5 nm

3.2.3 Thin Film Characterisation

The optical characterisation of both the oxide and nitride dielectrics was conducted using a Film Sense FS1 elipsometer. The accuracy of the tool was reported to be 0.18 nm on a 100 nm SiO_2/SiN_x film, with a precision of ± 0.002 nm [141]. The refractive index used for SiO_2 was 1.7 and 2.46 for SiN_x.

3.3 Corona Discharge

Corona discharge is a technique that was utilised throughout this work to add extrinsic surface charge to dielectric surfaces. The surface charge provides field effect passivation and thus increases minority carrier lifetime. Corona discharge is achieved through the ionisation of air molecules via the application of a large voltage. 30 kV is applied to a metallic pin which is suspended above the sample as shown in Figure 11. The polarity of the applied voltage affects which ions are deposited on the surface of the sample. Positive voltage deposits H_3O^+ molecules and negative voltage deposits CO_3^- molecules [77], [79], [142].

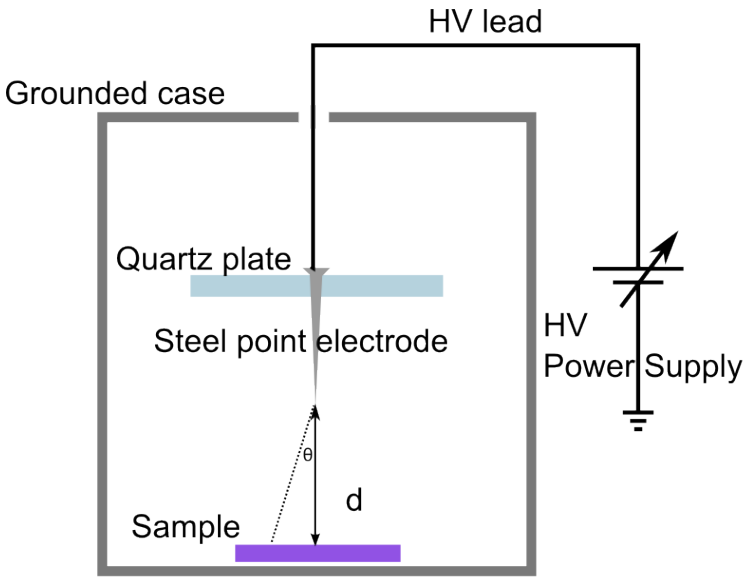


Figure 11 Schematic of Corona discharge apparatus, after [79].

The ionisation of the air molecules occurs near the electrode and forms a plasma in a corona-like shape, which gave its name to the technique. The corona-like shape of the plasma is responsible for the uniformity of the charge distribution as reported by Woodcock and Bonilla [66]. In this work, the surface potential was measured using a Kelvin Probe, the experiment was conducted using a pin height of 15 cm, they observed a charge distribution difference of 5% across the sample surface compared to the measured sample. The corona discharge apparatus used in this thesis has a pin height of 20 cm which was seen to provide even better

uniformity [143]. The standard corona charging of samples with 100 nm SiO_2 layers throughout this thesis is 30 kV, 0.03 mA, 20 cm pin height, for 60 s on each side of the sample. This results in a surface potential between 16 and 18 V on SiO_2 depending on the quality of the oxide and ambient conditions.

3.4 Ion Deposition

Another method by which to apply field effect passivation to Si samples is ionic deposition and migration. The effect of introducing positive ions to the SiO_2 has been researched by Bonilla and Collett [82], [144]. They investigated different techniques by which to introduce ions including thermal evaporation, spin coating and spray pyrolysis. The technique used in this work in conjunction with H-passivation was spin coating.

3.4.1 Spin coating

Uniform layers of liquids are routinely deposited using spin coating in the industry. For the deposition of ions on Si substrates, it is important to avoid the formation of droplets upon drying as this would facilitate the formation of salt crystals which would not in-diffuse effectively. Spin coating avoids this problem though the use of a solvent which wets the surface. The experiments in this thesis use a solution of 75% IPA and 25% de-ionized (DI) water for the solvent. Water is used to obtain an adequate salt solubility, whilst IPA is used as it evaporates quickly at room temperature, and wets the surface.

The sample was secured on a clean glass wafer using double sided tape, this wafer was then vacuum suctioned onto the spin coater chuck. Using a pipette 2 ml of solution was deposited onto the sample surface as the spin coater reached a steady speed of 2000 rpm. The sample is then spun for 2 minutes and this process is repeated on the other side of the sample. This spin coating process was optimised by Siyao Du as per her M.Eng thesis [145].

In the present work a solution of 3 x 10^{-4} mol/L of KCl is dissolved in the solvent in order to obtain a surface ionic concentration of 10^{14} ions/cm^2. More information on the ionic concentration calculations can be found in [26], [145].

3.4.2 Ion Migration

The ions deposited as per Section 3.4.1 are then driven into the oxide using field-assisted thermal annealing. The corona discharge apparatus described in Section 3.3 is used to deposit between 10 and 20 V of surface voltage, depending on the oxide thickness. The surface voltage is measured using KP. The sample is then annealed on a hot-plate to assist migration. The samples are annealed at 450 °C as this was shown to cause less risk of contamination whilst still migrating the ions in a short time (15 s) [65]. To reduce the risk of contamination further, the samples are placed on the hot-plate inside a clean borosilicate glass petri-dish with a lid placed on top. This permits the temperature of the atmosphere inside the petri dish to be 450 °C ± 10 °C. The temperature inside the dish is measured using a thermocouple. When the annealing time is over, the whole petri dish is removed from the hotplate and the sample is quickly removed from the hot atmosphere into room temperature atmosphere, quickly stopping migration assistance. The surface voltage is then measured to check that the corona charge deposited had dissipated.

3.5 Shielded Hydrogen Passivation

This section describes the technique in which Shielded Hydrogen Passivation (SHP) is conducted in this thesis. More details are included in Chapter 4 Section 4.2 .

3.5.1 Hydrogen Passivation Method

The setup shown in Figure 12 is used to introduce atomic H into samples from a PECVD generated H-containing plasma.

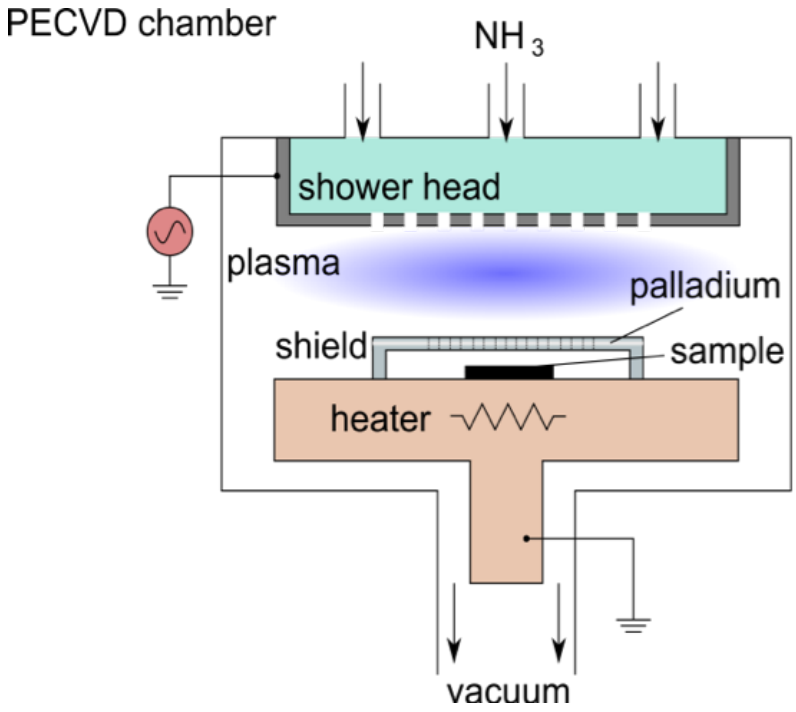


Figure 12 Schematic of SHP apparatus used in this work. 100 nm Pd leaf held in place by two aluminium grids, 10 cm by 10 cm with 5 mm lattice and 2 mm thickness.

An Al holder encases a metallic membrane, labelled as palladium in Figure 12, and is positioned between the sample and the shower head in the PECVD chamber. This apparatus acts as the shield between the plasma and the sample; it is placed on the heated grounded stage of the PECVD. The sample to be passivated is placed under the shield and on top of a clean Si substrate to prevent contamination from the stage. The standard parameters for SHP applied to Si substrates are: 100W RF power, 13.56 MHz, 650 mTorr chamber pressure, 100 sccm (standard cm^3/min) NH_3 gas, with various base plate temperature and times, depending on experimental purpose. The NH_3 gas is used as the source of atomic H. Before the metallic membrane, in this case a leaf, is appropriate for use it must be "prepared". This involves the removal of any native oxide and, where appropriate, S poisoning which is outlined further in Section 3.5.2. All

samples are processed using either a "prepared" 99.9% pure, 10 cm x 10 cm, 100 nm Pd leaf, or a 99.9% pure 10 μm Pd-Ag foil (with a ratio of 75:25) of the same dimensions. The standard recipe for SHP is summarised in Table V.

Table V Summary of standard SHP process used throughout this thesis

	Gasses	Temp	Shield	Time	Chamber pressure	HF Plasma power
Standard SHP process	100 sccm NH_3	350 °C	Pd-Ag foil prepared: 30 mins, 350 °C	45 mins	650 mTorr	100 W

3.5.2 Shield Preparation

The Pd leaf and Pd-Ag foil used in this work are both prepared in order to remove any native oxide present. The standard method for removing the native oxide is a prolonged exposure to H-containing plasma. The atomic H etches off the native oxide on the side exposed to the plasma first. Subsequently atomic H diffuses through the Pd bulk and exits from the underside of the leaf/foil. Upon its exit the atomic H etches off the native oxide present. The standard recipe in the PECVD for shield preparation is: 100W HF power, 650 mTorr chamber pressure, 100 sccm ammonia gas, 350 °C, 30 mins. When the Pd leaf is used (100 nm thick), it is routinely checked for pinholes prior to SHP usage, if a pin hole is spotted the leaf is either replaced or the hole is fixed with additional Pd leaf. The Pd-Ag foil (10 μm), being thicker, is less prone to pin holes.

3.5.3 Shield Sulphur Poisoning

In Chapter 4 Section 4.3.6.2, the efficacy of S poisoning the surface of the Pd shield, to suppress the catalytic property of Pd, is reported. The poisoning of the shield was achieved exposure to H_2S gas using the following method. First, an enclosed space was created in a fume hood by using a large trough that could be covered by another, larger, upturned trough. A 50 ml beaker containing ≤1 mm^3

of FeS mixed with 20 ml of 10% concentrated HCl acid was placed within the trough. The Pd leaf was kept in the Al holder to minimize the risk of ripping, and both the leaf and holder were placed inside the enclosed space formed by the two troughs. The reaction of FeS with HCl releases H_2S, most of which is confined around the holder and leaf. The leaf and holder are left to be poisoned in the H_2S gas for 10 minutes which results in some coverage of the Pd with S atoms.

3.6 Characterisation Methods

Multiple characterisation methods were used throughout this thesis. This section focuses on methods for photoconductance decay lifetime measurements, Kelvin Probe (KP), capacitance-voltage (CV) and enhanced capacitance-voltage (eCV).

3.6.1 Photoconductance Decay Lifetime

Effective minority carrier lifetime was measured using a Sinton WCT-120 photo-conductance instrument. It is measured as a function of excess minority carrier concentration (Δp), and using both quasi-state and transient modes [146].

The Sinton instrument measures a sample's conductivity using a bridge circuit and a coil which is in close proximity to the sample. The coil's impedance varies as the conductivity of the sample changes due to photo-injected carriers. The change in conductivity ($\Delta\sigma$), which is measured with Sinton, of a semiconductor can be expressed as:

$$\Delta\sigma = \frac{\Delta \mathrm{p}}{q(\mu_n + \mu_p)} \tag{3.1}$$

Where μ_n and μ_p, is the mobility of electrons and holes in the semiconductor respectively, and q is electron charge at 1.6 x 10^{-19} coulomb.

In QSS mode, the photo generation $G(t)$ is measured and calibrated using a photo sensor near the sample. In transient mode $G(t) = 0$ which obeys the relationship with minority carrier concentration over time:

$$\frac{\partial \Delta p}{\partial \mathrm{t}} = G(t) - R = G(t) - \frac{\Delta p}{\tau_{eff}} \tag{3.2}$$

$$\tau_{eff}(\Delta p) = \frac{\Delta p(t)}{G(t) - d\Delta p/dt} \tag{3.3}$$

Where τ_{eff} is the effective lifetime and R is the recombination.

The samples to be lifetime tested using the Sinton tool are required to be at least 3 cm x 3 cm in order to minimise the negative impact of edge effects [147]. Measurements are taken over a range of injection levels, but it is common practice in the literature to quote effective minority carrier lifetime values at 10^{15} cm^{-3} minority carrier injection level. The error of the Sinton tool has been determined through a collaborative study by 24 different laboratories on the same sample and was established to differ ± 8 % between the laboratories [148].

3.6.1.1 Recombination Current Density

A common metric to characterise recombination in Si is the recombination current density J_0 which is sometimes called dark current density. It measures the current loss due to recombination at the surface. McIntosh and Black [149], recently reported that in most solar cell application J_0 was independent of doping concentration. As such J_0 can be defined by the formula published by Kane and Swanson [150]:

$$J_0 = \frac{1}{2} qWn^2 \frac{d}{d\Delta n}\left(\frac{1}{\tau_{Aug}}\right) \tag{3.4}$$

Where W is width of the wafer, n is the doping density and τ_{Aug} is the Auger corrected effective lifetime defined in [150].

This calculation is implemented in the Sinton WCT-120 software and can be extracted after each minority carrier lifetime measurement [151]. Throughout this work J_0 was extracted at an injection level of 2 x 10^{15} cm^{-3}. This injection level was reported in [152] to avoid J_0 deviation due to asymmetric SRH recombination and shunting effects usually seen at lower injection levels.

3.6.2 Capacitance-Voltage

Charge concentration at the interface of a dielectric-Si structure can be measured by the well-established Capacitance-Voltage (CV) technique. CV uses a metal-oxide-semiconductor (MOS) structure, the metal and semiconductor materials act as the two electrodes between which a voltage can be applied. The applied voltage is varied, which modifies the surface band bending. This subsequently changes the space charge region at the Si surface. This region now acts as a capacitor C_{scr} which is in series with the oxide also acting as the capacitor C_{ox}. The interface trap states denoted by C_{it} are represented by a capacitor in parallel to the space charge region, as depicted in Figure 13 below.

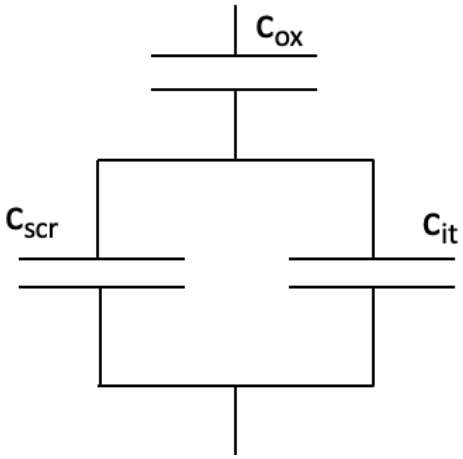


Figure 13 Equivalent circuit used in CV analysis

The oxide capacitance, C_{ox}, is defined as:

$$C_{ox} = \varepsilon_{ox}\varepsilon_0 \frac{t_{ox}}{A} \tag{3.5}$$

Where t_{ox} is the oxide thickness which can be accurately measured using an elipsometer, A is the area of the MOS capacitor, and ε_{ox} is the permittivity of the oxide and ε_0 is the permittivity of free space.

The oxide layers used in this thesis are of very high quality and it is therefore possible to neglect the contribution of interface capacitance, C_{it}, from the total measured capacitance, $C_{meas.}$

$$C_{meas} = \frac{C_{scr}C_{ox}}{C_{scr} + C_{ox}} \tag{3.6}$$

Where C_{scr} is the capacitance of the space charge region. However, measuring the area accurately is experimentally difficult and as such the area is defined by putting the sample in accumulation whereby $C_{ox} = C_{meas}$.

When the junction is placed in reverse bias the measured capacitance is defined by

$$C_{meas} - C_{ox} = \frac{\varepsilon_{ox}\varepsilon_0 A}{W} \tag{3.7}$$

And as such the width of the SCR, W, is calculated using equation 3.4 and 3.6 to obtain:

$$\mathrm{W} = \varepsilon_{ox}\varepsilon_0 A\left(\frac{1}{C_{meas}} - \frac{1}{C_{ox}}\right) \tag{3.8}$$

The flat band voltage (V_{FB}) is the voltage at which there is no charge on the plates of the capacitor and hence there is no electric field across the oxide. V_{FB} is the value at which the Si sample is not in depletion or accumulation, the bands are flat. V_{FB} depends on the doping of the semiconductor and on any residual interface charge that may exist at the interface between the semiconductor and the insulator.

The flat band capacitance is governed by the Debye Length (L_D). It is the distance over which a charge imbalance is neutralised by majority carriers. This occurs under steady-state or equilibrium conditions [153]. It is defined by equation 3.8.

$$L_D = \sqrt{\frac{kT\varepsilon_s\varepsilon_0}{q^2(p+n)}} \tag{3.9}$$

Where k is the Boltzman constand, T the temperature in kelvin, ε_s the permittivity of Si and p and n are the number of electrons and holes.

As such the flatband capacitance, C_{fb}, is defined by the permittivity of Si, ε_s, over the Debye length:

$$C_{fb} = \frac{\varepsilon_s}{L_D} = \frac{\varepsilon_s}{\sqrt{\frac{kT\varepsilon_s\varepsilon_0}{q^2(p+n)}}} \tag{3.10}$$

The flatband voltage V_{fb} can be calculated from the total measured capacitance at flatband conditions. Equation 3.9 is used to calculate C_{fb} which is then used to replace C_{scr} in equation 3.5. The total theoretical capacitance required to achieve flatband is thus calculated. The voltage needed to achieve this capacitance is the experimental V_{fb}.

The interface charge density can be calculated using V_{fb} . When CV measurements are taken, the sample is considered an MOS structure and as such the V_{MOS} equation is:

$$V_{MOS} = V_{\Delta wf} - V_{scr} - V_{interface} - V_{ox} \tag{3.11}$$

From which we can substitute in equations for $V_{\Delta wf}$ and $V_{interface}$. During flatband conditions $V_{scr} = \Phi_{scr} = 0$.

$$V_{MOS} = \frac{\Phi_{ms}}{q} - \frac{Q_{it}(\phi_{scr})t_{ox}}{\varepsilon_{ox}\varepsilon_0} - V_{ox} \tag{3.12}$$

where Φ_{ms} is the metal to semiconductor work-function difference, V_{ox} is the potential difference lost across the oxide, and Q_{it} is the interface trapped charge. Q_{it} develops at the interface due to ionized acceptor and donor states and thus depends on the surface potential Φ_{scr}. By substituting the definition of V_{ox} in 3.11 we obtain the known expression for V_{fb} as reported in [154].

$$V_{fb} = \frac{\Phi_{ms}}{q} - \frac{1}{\varepsilon_{ox}\varepsilon_0}\int_0^{t_{ox}} x\rho_{ox}(x)dx \tag{3.13}$$

where $\rho_{ox}(x)$ is the volumetric charge distribution through the oxide.

The interface trap charge is neglected throughout this thesis as it only accounts for ~0.5 V. Indeed, in the SiO_2-Si interface the mid bandgap state density was found the be below 10^{12} $eV^{-1}cm^{-2}$ [32]. The charged states most likely to contribute to Q_{it} are ones between the intrinsic Fermi level (E_i) and the Fermi level (E_F). In this work $E_F - E_i = 0.34\ eV$ and as such the number of states contributing to Q_{it} is ~3.4 x 10^{11} cm^{-2}. Estimating that only 10^{11} of these states are charged, the potential charged states would only contribute ~0.5 V. The instrumental error was characterised by Masters student Lucy Rands, who reported in her MEng thesis that the instrument reports to an accuracy of ± 0.1 x 10^{12} q/cm^2 which is generally less than 10 %, as such error bars are not included in graphs [140].

3.6.3 Electrochemical Capacitance Voltage

Electrochemical Capacitance Voltage (eCV) is an elegant method to determine the near surface dopant concentration of semiconductors whilst etching the sample surface to provide a depth profiling capability [154], [155]. This profiling technique is based on the capacitance depletion region created by a semiconductor-electrolyte Schottky contact at a constant DC bias voltage. The electrochemical etching is performed at the same time as the measurement and has no depth limit. It is a destructive technique however, as it etches a hole in the sample. The schematic of the eCV apparatus used at the University of New South Wales (UNSW) is shown in Figure 14.

To take measurements, a small DC reverse bias is applied between the electrolyte-cathode and the working electrode (the sample). Two low-voltage signals of different frequencies are applied to the electrolyte so that there is a modulation in voltage ΔV. The carrier density measurement, p, can be defined and thus

calculated using the following equation which is derived from C-V characterization methodology:

$$p(W) = \frac{2\varepsilon_s \varepsilon_{ox}}{q} \frac{\Delta V}{\Delta(W)^2} \tag{3.14}$$

Where ε_s is the permittivity of the Si, ε_{ox} the permittivity of the oxide. The width of the space charge region (scr), as shown in 3.6.2 is defined as W and ΔW is the change in width with a change in applied voltage. W is measured in the eCV apparatus. As such, the relation between W and capacitance C can be used to find the doping density N_A.

$$W = \frac{K_s \varepsilon_o A}{C} \tag{3.15}$$

$$N_A(W) = -\frac{C^3}{qK_s \varepsilon_o A^2 dC/dV} = \frac{2}{qK_s \varepsilon_o A^2 d(1/C^2)/dV} \tag{3.16}$$

The importance of the area measurement should be noted here as the term A^2 will have a big impact on the error of the measurement.

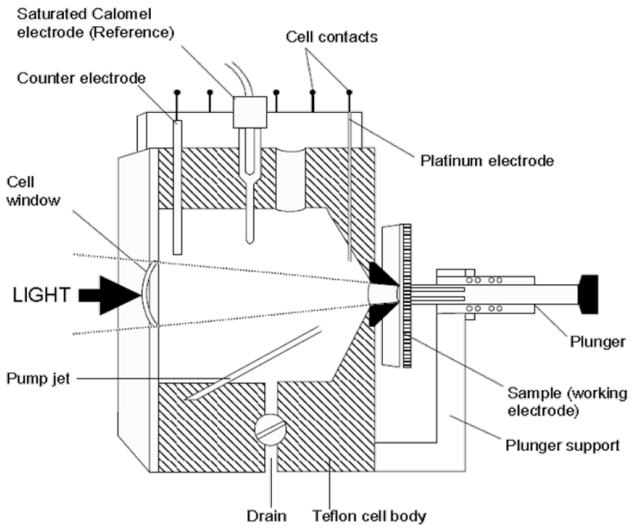


Figure 14 Schematic of eCV apparatus after [156]

The semiconductor sample is pressed against a sealing ring in the electrochemical cell which contains the electrolyte. The opening of the ring is constant and therefore a defined area. A DC current is passed between the counter (carbon) electrode and the sample (working) electrode, this controls the etching rate. The DC current is set so as to maintain a constant overpotential with respect to the saturated calomel electrode. The AC voltage is measured by a Pt electrode located near the sample in order to reduce series resistance.

The depth profiling is achieved by dissolving the semiconductor using the electrolyte. For p-type material this is straight forward as holes are plentiful due to the B doping, the dissolution of the material is achieved by forward biasing the junction between the semiconductor and the electrolyte. For n-type material holes are generated through illumination and a reverse bias at the junction. The etching depth W_R can be expressed by the following expression [155]:

$$W_R = \frac{M}{zF\rho A}\int_0^t I_{dis}dt \tag{3.17}$$

Where M is the semiconductor sample's molecular weight, z the dissolution valency (which is defined as the number of charge carriers required to dissolve one atom of the semiconductor), F is the Faraday constant (taken as 9.64 x 10^4 C), ρ is the density of the semiconductor and finally A remains the contact area. The etching depth W_R can be calculated by integrating the dissolution current electronically through measurements in the eCV. This gives the total measurement depth as:

$$x = W + W_R \tag{3.18}$$

For Si, the HF containing electrolyte used was 0.1 mol/kg of $NH_4F{\bullet}HF$ in an aqueous solution which corresponds to 0.57 weight percent of the HF solution in distilled water [157].

3.6.3.1 Boron Deactivation Method to Measure Hydrogen

As mentioned in Chapter 2 Section 2.1.3, atomic H is notoriously difficult to observe and quantify directly. Instead, it is measured through its interaction with other atoms. B is well known to be an extremely effective trap for atomic H. Herrero *et al* have experimentally derived that the degree of acceptor (B) passivation is ~ 99% for B dopant concentrations of 1.5 x 10^{19} cm^{-3} below 200 °C [158], [159]. For temperatures above 200 °C the effect of H trapping at B atoms quickly becomes negligible and D_{eff} for H transport through Si increases, as it no longer becomes trap limited.

At low temperatures therefore, the dopant passivation quality of H introduction into p-type Si can be used to measure the level of H-B pairs. The level of H-B recorded provides a lower level for the total H introduced into the Si sample.

When H pairs with B the resistivity of the p-type Si sample will change. As shown in section 3.6.2, capacitance is related to the space charge region width, W by:

$$\mathrm{W} = \varepsilon_s \varepsilon_0 A \left(\frac{1}{C}\right) \tag{3.19}$$

where $C = C_{scr} - C_{ox}$. The oxide capacitance, however, is either zero (in the absence of an oxide when using eCV which etches any native oxide) or constant for CV measurements. It is also known that for a change in a semiconductor charge (Q_s) the space charge region (scr) will change with respect to changing width (W) as defined by:

$$\mathrm{C} = \frac{\varepsilon_s \varepsilon_0 A}{W} \tag{3.20}$$

$$C = qA \frac{d}{dV} \int_0^W N_A dx = qAN_A(W) \frac{dW}{dV} \tag{3.21}$$

Where N_A is the B doping density and A the capacitor area (in this case the eCV etching area).

As such it is possible to differentiate 3.19 by dC/dV to obtain:

$$W\frac{dC}{dV} = -\frac{\varepsilon_s \varepsilon_0 A}{C^2}\frac{dV}{dC} \tag{3.22}$$

And combining 3.20 and 3.21 to obtain:

$$N_A(W) = -\frac{C^3}{qA^2\varepsilon_s\varepsilon_0\frac{dC}{dV}} \tag{3.23}$$

Using the identity: $d(1/x^2)/dy = -(2/x^3)dx/dy$ to obtain:

$$N_A(W) = -\frac{2}{qA^2\varepsilon_s\varepsilon_0\frac{d\left[1/C^2\right]}{dV}} \tag{3.24}$$

Finally, the two equations needed to calculate the doping profile from a CV measurement and as such estimate a lower limit for the atomic H introduced are (3.18) and (3.23).

Throughout this thesis the constant values used are shown in Table VI.

Table VI Summary of constants used for H-B concentration calculations

Constant	Symbol	Value
Relative permittivity of Si	$\boldsymbol{\varepsilon_s}$	11.9
Elementary charge	$\boldsymbol{q}$	1.62 x 10^{-19} C
Area of capacitor plate / Al dot / eCV etching circle	$\boldsymbol{A}$	1.36 x 10^{-7} m^2 for Al dot
Permittivity of free space	$\boldsymbol{\varepsilon_0}$	8.85 x 10^{-12} Fm^{-1}

3.6.4 KELVIN PROBE

Surface charge calculations were obtained through the Kelvin Probe (KP) method throughout this thesis. KP is a non-contact method which measures the dielectric surface charge as depicted in Figure 15.

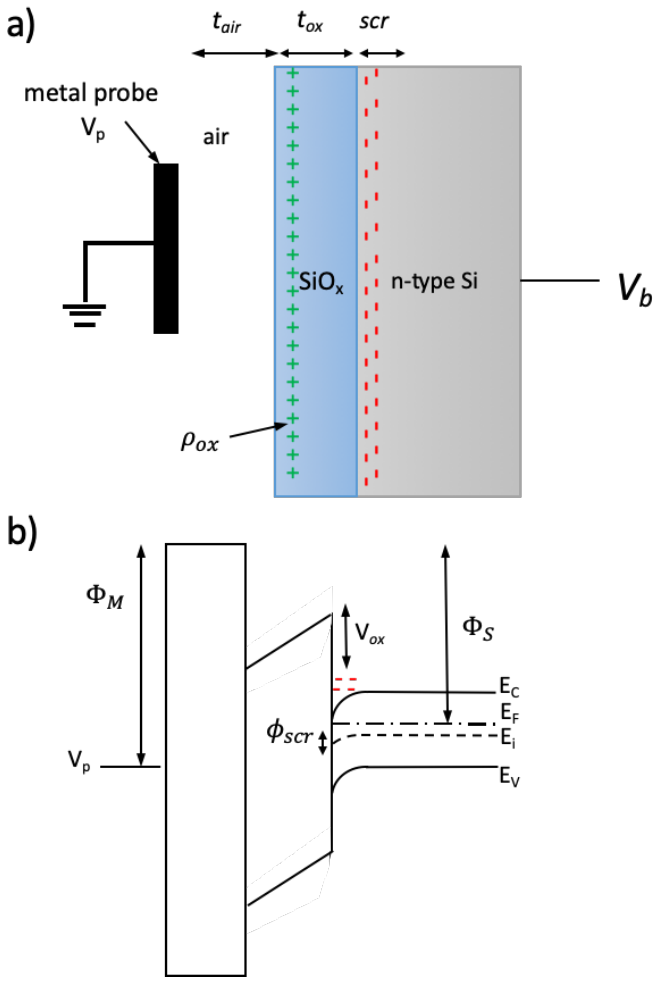


Figure 15 (a) Schematic of Kelvin Probe apparatus (b) Associated band diagram with charge at SiO_x interface

The probe is typically a small plate or pin which acts as the electrode and is held 0.1-1 mm above the sample. The Kelvin Probe electrode is made to vibrate, changing the distance between the sample and the electrode, hence causing a change in capacitance. A capacitor is created where the Si substrate act as one electrode and the metal pin the other. The dielectric and air act as insulators. From this the charge can be defined by:

$$Q = VC = \frac{V\varepsilon_{ox}\varepsilon_s}{d} \tag{3.25}$$

Where the internal voltage between the electrodes is V, the capacitance C, d is the spacing between the plates and ε_o remains the permittivity of free space. When the probe vibrates, the distance (d) changes to (d_2), since the internal voltage is constant as the electrodes are grounded, the charge must decrease and thus the electric field is also reduced. The current, I, flowing between the probe and the semiconductor as the capacitance varies with time is described by:

$$I = \frac{dQ}{dt} = V\frac{dC}{dt} = -V\frac{\varepsilon_o}{d^2}\frac{dd}{dt} \tag{3.26}$$

The difference between the probe voltage V_b and the voltage across the substrate V_s can be calculated as:

$$V_b - V_s = \frac{\Phi_{ms}}{q} + \phi_{scr} + V_i \tag{3.27}$$

In order to calculate the voltage caused by the oxide surface charge after a process such as Corona, the *zero current method* is used [155]. This entails applying a negative backing voltage to the semiconductor substrate so that the charge between the electrodes is now zero, thereby reducing the current flow to zero. As the probe vibrates and the distance increases the voltage is adjusted so that the current remains zero. The applied backing KP voltage is denoted by V_{bKP} and equal to:

$$V_{bKP} = V_s = \frac{\Phi_{sm}}{q} - \phi_{scr} - V_i \tag{3.28}$$

Where Φ_{sm} is the semiconductor to metal work function difference, ϕ_{scr} is the semiconductor SCR potential and V_i is the voltage across the insulator, in this case the oxide and air. When charge is present in the metal probe, as is the case

in Figure 15, part of the potential is dropped inside the semiconductor as ϕ_{scr}. Calculating ϕ_{scr} is notoriously difficult and was first done iteratively by Girisch et al [160]. It has been found in previous theses [24], [26] that when positive charge is measured on the oxide, the contribution from ϕ_{scr} amounts to less than 0.25 V when the surface charge concentration is below 10^{13} q/cm^3 using Boltzmann statistics. The accuracy of the KP instrument used in this work is ≈ 0.4 V [140], thus ϕ_{scr} can be neglected from the calculation in equation (3.27).

By isolating the KP sufficiently it is appropriate to assume that there is no charge concentration in the air gap. The voltage across the oxide with uniform charge density ρ_{ox} is described by:

$$V_i = \frac{1}{\varepsilon_{ox}\varepsilon_0}\int_0^{t_{ox}} x\rho_{ox}(x)dx \tag{3.29}$$

It follows that the backing potential at the KP surface, using (3.27) and neglecting ϕ_{scr} and the air contribution is:

$$V_{bKP} = \frac{\Phi_{sm}}{q} - \frac{1}{\varepsilon_{ox}\varepsilon_0}\int_0^{t_{ox}} x\rho_{ox}(x)dx \tag{3.30}$$

It is assumed, after [154], that all the charge in the insulator resides on a plane that is a distance x_c away from the surface and has concentration Q_{ox}. The uniform charge density ρ_{ox} can therefore be written as $\rho_{ox} = Q_{ox}\,\delta(x - x_c)$ where x is the distance between the probe surface and the interface. This definition can be substituted into equation (3.29) to obtain:

$$V_{bKP} = \frac{\Phi_{sm}}{q} - \frac{x_c Q_{ox}}{\varepsilon_{ox}\varepsilon_0} \tag{3.31}$$

As such the surface charge concentration can be found as:

$$Q_{ox} = \frac{\varepsilon_{ox}\varepsilon_0}{x_c}\left(\frac{\Phi_{sm}}{q} - V_{bKP}\right) \tag{3.32}$$

The error for this equipment was characterised by Rands [140] and found to be ± 0.2 x 10^{12} q/cm^2. Since the samples measured in this thesis have a significantly higher surface charge, this error is less than 10 % and error bars are generally not included.

3.6.5 Light and Elevated Temperature Induced Degradation (LeTID)

Some of the experiments in this thesis used Light and elevated Temperature Induced Degradation (LeTID) set-ups in order to investigate the nature of defects observed. LeTID is commonly used in researching H-related defects, as H has a recognizable behaviour under LeTID. The set-up used was as follows.

Si samples were placed on a hot plate at 97 °C ± 2 °C, the temperature was recorded using a thermocouple which measured the temperature of the sample rather than the hotplate. A halogen lamp was placed 40 cm ± 1 cm away from the sample using a stand. The lamp provided 0.6 W/cm^2 which was measured using a light meter directly next to the sample. The time was recorded using a stop watch. The samples were measured at given time intervals using Sinton lifetime tool.

3.6.6 PEDOT:PSS

Poly(3,4-ethylenedioxythiophene)-poly(styrene sulfonate), or thankfully abbreviated to PEDOT:PSS has recently been used by Bonilla to control the surface carrier population of Si during photo-conductance decay (Sinton lifetime) measurements. PEDOT:PSS acts as a semi-transparent gate which allows for the direct measurement of measurements of surface recombination as a function of

surface carrier population [161]. This technique mimics the effect of corona charging but without the added complication of charge stability and leakage. A schematic of the set-up can be seen in Figure 16.

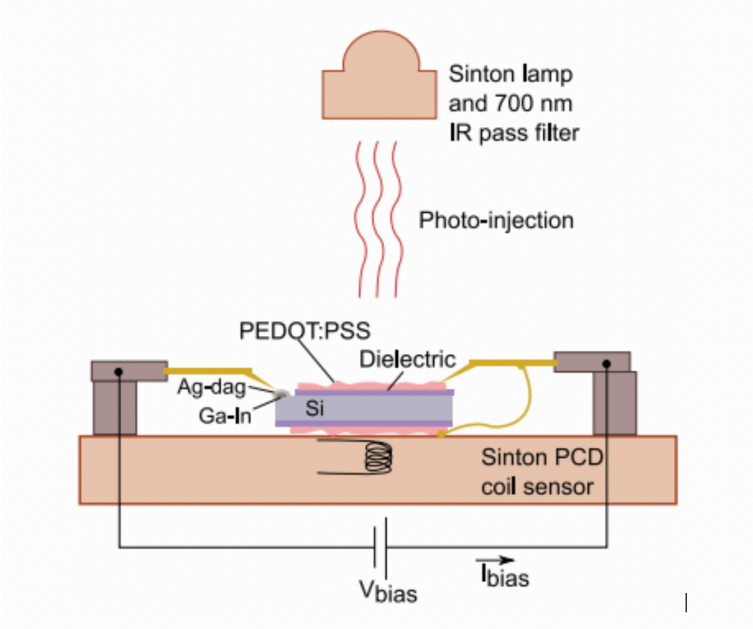


Figure 16 Schematic of measurement set up including a semi-transparent PEDOT:PSS gated symmetrical specimen. By courtesy of [161].

In Figure 16, the set-up comprises two spring-loaded probes connected to a source measurement unit and to a gate electrode at both the front and rear of the specimen. The sample is placed on Sinton WCT 120 lifetime tester to record measurements. The SMU used was an Agilent B2901A. The voltage is applied using the SMU and changed incrementally; the lifetime is recorded each time as well as the voltage and current.

The PEDOT solution used was Sigma–Aldrich 3.0–4.0 wt% in H_2O which was painted on in two thin layers on both sides of the sample. The painted sample was cured each time by being placed on a hot plate at 70 °C ± 5 °C for 2 min, under an extractor hood.

CHAPTER 4 Passivation using Shielded Hydrogen Plasma

In this chapter, a novel H-passivation methodology is introduced, and passivation quality from this technique is demonstrated. The process is called Shielded Hydrogen Plasma (SHP).

4.1 SHP Principle

The experimental set up for SHP was outlined in Chapter 3 Section 3.5.1, the section below gives further details on the process.

4.1.1 Motivation

The use of atomic H to passivate impurities and defects in Si has been widely reported in the literature with the broad consensus being that the effectiveness of this process is heavily reliant upon the quantity of H introduced into the Si [51], [107]. In particular, recent work on thin oxides for passivated contacts has shown significant reductions in recombination at Si interfaces after exposure to H [162], [163].

As discussed in Chapter 2 Section 2.1.4 there are a number of ways of introducing H into Si. However, some of the most standard hydrogenation techniques have major drawbacks when it comes to operating temperatures, surface damage or concentration of atomic H. Indeed forming gas anneal (FGA) causes no damage to Si surfaces, and has been demonstrated to be capable of significantly improving surface passivation of Si/SiO_2 interfaces [59], [94]. However because H in FGA is in its molecular form, it is less effective in the absence of surface damage or a layer to split the H_2 [51]. In contrast, direct exposure to a H containing plasma introduces vastly greater concentrations of atomic H, unfortunately, a

consequence of the plasma exposure is significant damage to the Si surface [51]. This damage can be greatly reduced through the use of a remote hydrogen plasma system [50], [117], where the plasma is confined, such that there is no direct line of sight between the plasma and the samples. Such systems have been successfully used in high-efficiency passivated contact cell architectures [164], but have limitations in application as the method is a batch process.

This work presents an alternative method of introducing atomic H into Si, at a wide range of temperatures, in high concentrations without any plasma induced surface damage and with a potential in-line process design. The following sections presents the results obtained with this technique, named Shielded Hydrogen Plasma (SHP).

4.1.2 SHP Requirements

The novel technique of Shielded Hydrogen Plasma (SHP) was developed as part of this doctorate and is as an alternative approach to avoid damage, whilst still exposing samples to atomic H. This was achieved through the insertion of an appropriate "shield" between the H-containing plasma and the Si samples. In order to be effective, this shield should possess the following properties:

1. It should not transmit UV radiation
2. It must be chemically stable such that it is not itself damaged through plasma exposure
3. It should be electrically conductive such that it can be grounded to stop a charge build-up on the surface of the shield. Such charge build-up, and hence potential, would repel charged species from reaching its surface and being absorbed.
4. It should be highly permeable to H

The materials most likely to fill all these requirements are metals. There are numerous studies on the interaction of H with Pd [134], [137], [172], [138], [165]–

[171], suggesting that this material has a high permeability for atomic H even at room temperature and thus may be useful as a shield for SHP.

4.2 Detailed Methodology

Throughout this doctoral work, two versions of the SHP rig were developed. This chapter presents the first version using a palladium leaf, the next chapters use version two which accommodates bigger wafers and uses Pd-Ag foil as the shield.

Version 1 of the SHP rig uses a 100 nm thick layer of 99% pure Pd, referred to as Pd leaf. It is placed between a H generating NH_3 plasma and the sample, as shown in Figure 17. As introduced in Section 4.1.2, the Pd leaf is intended to absorb UV photons, neutralise and thermalise energetic ions, stop charge build-up on the surface of the sample, whilst being permeable to H.

When the proof of principle experiment for SHP was designed using the Pd leaf as a shield, the cost of materials was a big concern. The £ 1000 Pd foil supplied by Fischer Scientific was deemed too expensive, and an alternative was found. Art suppliers routinely stock Pd leaf, 100 nm in thickness, for gilding purposes as it does not tarnish like Ag. The art supplier guaranteed 99% purity, which was deemed appropriate and was $1/500^{th}$ of the price of scientific suppliers. The Al rig was designed as shown in the engineering drawings in Figure 17 to hold the Pd leaf in place.

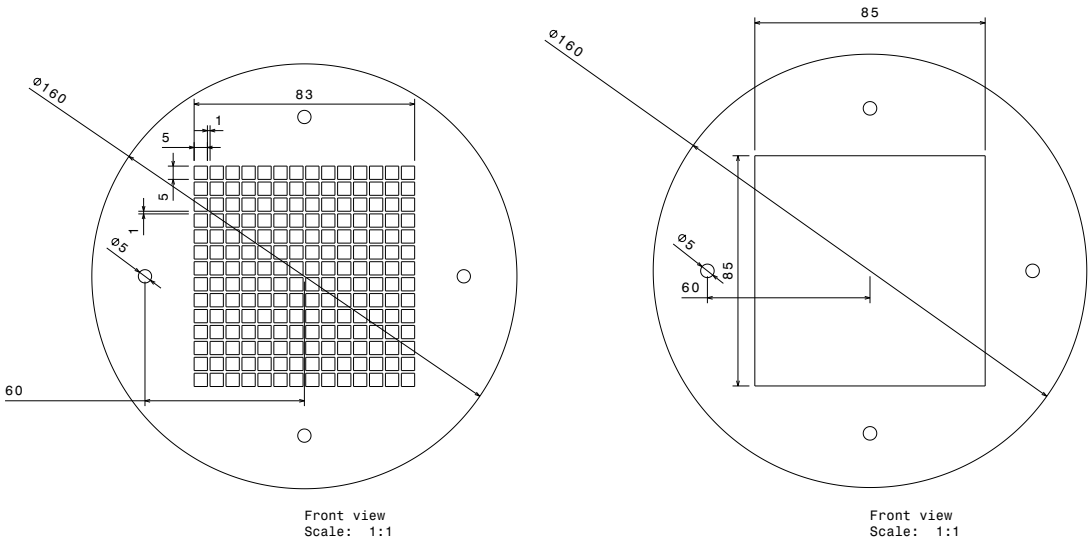


Figure 17 Engineering drawing of a) (left) grid plate of SHP rig b) (right) hole plate of SHP rig

The rig is made up of two grid plates to securely hold the Pd leaf in place between them. A hole plate is placed on top of the grids to ensure the structure is flat as the laser cut grid plates were often warped. This is then screwed into the lower disk which creates the final rig. The lower disk is slightly thicker than the other parts, in order to allow for samples of up to 1.5 cm in height to fit under the rig. This is depicted in Figure 18.

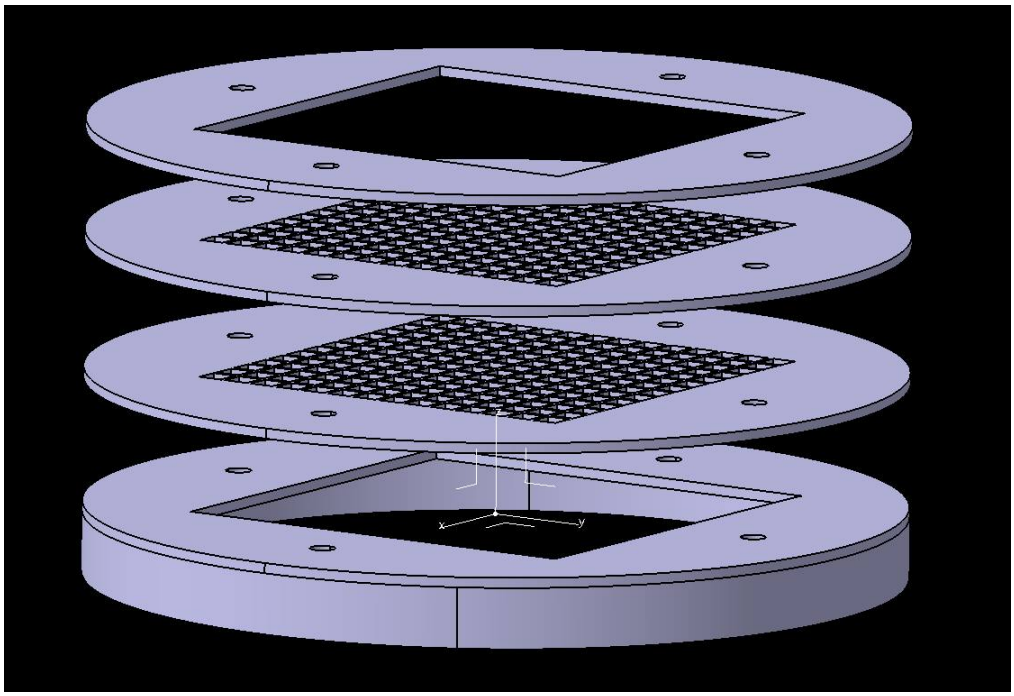


Figure 18 Schematic of SHP rig

The screws used to secure the structure are stainless steel vacuum screws, supplied by Fischer Scientific. These have a vent through their centre, to prevent gas from being trapped in the screw thread and leaking out slowly in the chamber, compromising the vacuum.

The sample to be passivated is placed on a Si 'dummy' wafer in order to prevent contamination from the lower electrode of the PECVD equipment. The Si sample, as well as the dummy wafer, are cleaned with a standard RCA1 and RCA2 treatment [173]. The rig is placed on top of the sample which itself is placed on top of the clean wafer, as shown in Figure 19. The PECVD system used throughout this thesis is an Oxford Instruments Plasmalab Plus 80. Throughout the experiments the system is set at a range of flowrates and plasma powers. The specimen temperature is adjusted by controlling the temperature of the lower electrode on which the dummy wafer sits. However, the standard recipe for SHP was optimised to be 40 mins of exposure to a 100 W plasma power, with a gas flow of 100 sccm (cm^3/min) of NH_3 and a chamber pressure of 650 mTorr.

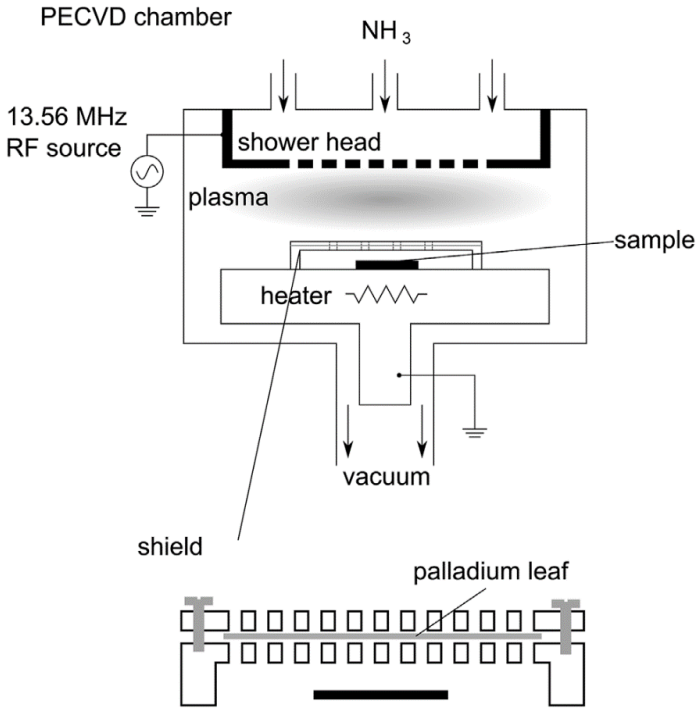


Figure 19 Schematic representation of SHP apparatus used in this work.

The PECVD lower electrode is set to a chosen temperature and once it is reached, the sample and rig is loaded, the PECVD chamber is then evacuated. NH_3 gas is released into the chamber and the RF source is switched on to create a plasma. When atomic H is generated in the NH_3 plasma, it diffuses to the surface of Pd leaf, then through the Pd leaf. As discussed in Chapter 2 Section 2.3 , literature suggests that the atomic H, upon reaching the lower surface of the Pd leaf, would undergo recombinative desorption and leave the leaf as H_2 [137], [174]. If this was the case, no passivation improvement would be seen in the Si samples, as it has been shown that below 400 °C H_2 rarely splits into H on the surface of Si [175]. H_2 does not improve interface passivation or bulk passivation, because it is a lot less reactive than atomic H [97]. Similarly, if H_2 was released from the underside of the Pd leaf, the B deactivation method explained in Chapter 3 Section 3.6.3.1 would not show any B deactivated as B reacts with H not H_2.

The results presented in the rest of this chapter aim to demonstrate that atomic H was released from the underside of the Pd leaf, thus contradicting the literature. Results reported in Section 4.3 aim to assess the ability of SHP to improve SiO_2-Si interfaces. The potential of not only for use in a research environment but as an industrially relevant technique is discussed.

4.3 Results

4.3.1 Background Experiments

Background experiments are presented in this section, to give context to the results obtained using SHP. If atomic H is detected in Si it is crucial to rule out the possibility of it being introduced from H_2 dissociating on the surface of Si rather than being released as atomic H from the Pd leaf. To test this, a highly B-doped Si sample was exposed to pure H_2 gas in a tube furnace at 1 atm and

200 °C. eCV characterization was used to measure active B concentration against depth. This is shown in Figure 20.

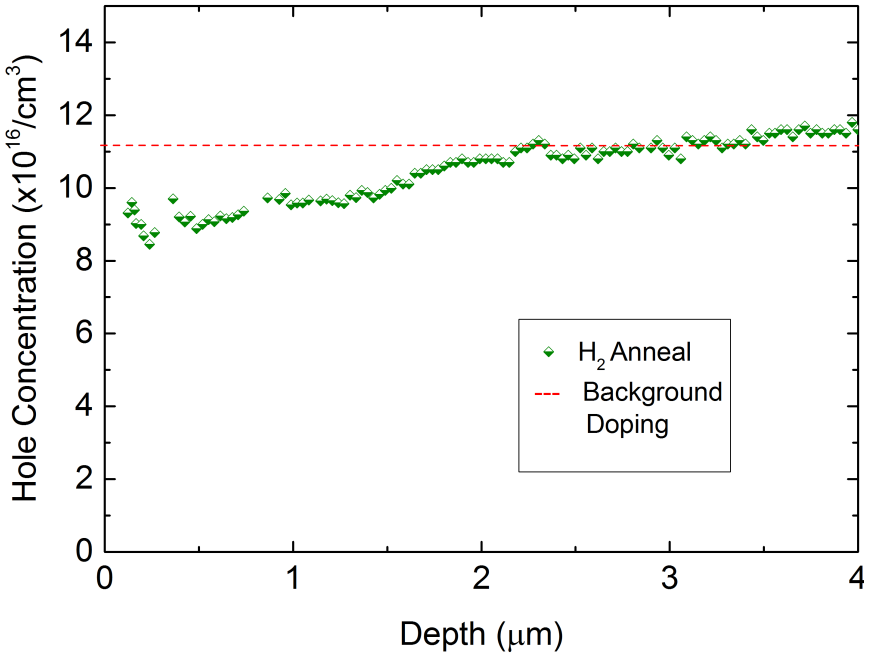


Figure 20 Active B concentration versus etch depth measured using eCV. Bare Si sample annealed in pure H_2 at 200 °C for 20 mins in tube furnace at 1 atm. Background doping concentration 1.17 x 10^{17}/cm³ (red dashed line)

The background doping concentration, reported from the wafer supplier, is 1.17 x 10^{17} B atoms/cm³. This level is represented by the red dotted line in Figure 20. It is evident that the level of B deactivated by atomic H is negligible. This is strong evidence that H_2 does not dissociate and enter Si as H at 200 °C.

The next experiment to run in order to provide context for SHP results was a direct plasma exposure, to observe any sample damage caused by the plasma. In this case two methods were used. A B-doped wafer was directly exposed to the NH_3 plasma in the PECVD at 200 °C for 20 minutes. The level of active B atoms was then measured using eCV. This is shown in Figure 21. The second experiment was to test the effect of a direct plasma exposure on minority carrier lifetime. 1 Ω.cm n-type FZ-Si samples with either 10 nm or 100 nm thermal SiO_2, standard

oxide, were directly exposed to the NH_3 plasma at 380 °C for 30 minutes. The minority carrier lifetime before and after direct plasma exposure was measured using Sinton Lifetime [176], and is shown in Figure 22.

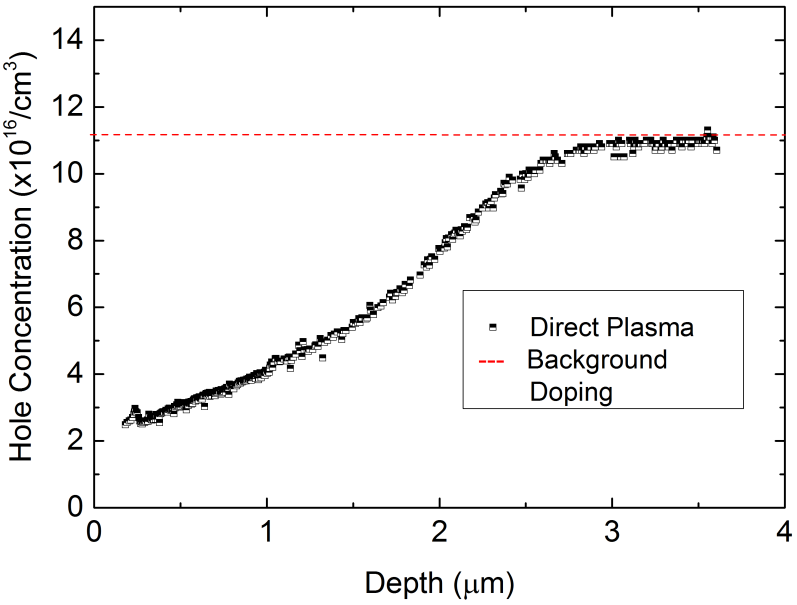


Figure 21 Active B concentration versus etch depth measured using eCV. Bare Si sample exposed to direct NH_3 plasma in PECVD at 200 °C for 20 mins. Background doping concentration 1.17 x 10^{17}/cm³ (red dotted line)

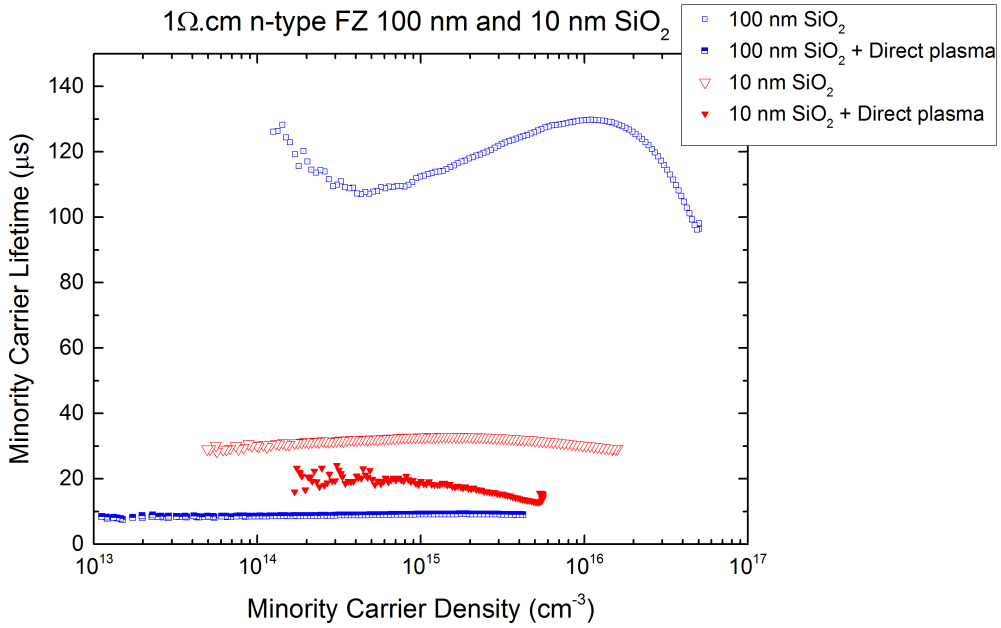


Figure 22 Effective minority carrier lifetimes as a function of minority carrier density for 1 Ωcm 200 μm n-type FZ Si sample with a 10 nm SiO_2 (red) or 100 nm SiO_2 (blue). Lifetime tested prior and post direct plasma exposure for 30 mins at 380 °C.

From Figure 22, it is clear that direct plasma exposure causes considerable surface damage on both the 10 nm and 100 nm SiO_2 oxides, as expected from the literature in Chapter 2 Section 2.1.4.4.2. The lifetime of the 100 nm SiO_2 prior to plasma exposure is 150 μs at 10^{15} cm^{-3} injection level. However, once it is exposed to the unshielded plasma, the lifetime falls to 9 μs at 10^{15} cm^{-3} injection level. Similarly, the minority carriers in the 10 nm SiO_2 oxide sample had an original lifetime of 32 μs at 10^{15} cm^{-3} injection level, which falls to 19 μs at 10^{15} cm^{-3} injection level after being exposed directly to the plasma.

The eCV results shown in Figure 21 present the total level of B atoms deactivated by H, and therefore a lower level the quantity of H introduced. The shape of the curve clearly indicates a concentration gradient of H-B pairs, which is higher nearer the surface and decreases until a depth of 3 μm where there appears to be a negligible amount of H trapped by B. By calculating the area between the profile depth of the direct plasma exposed sample and the background doping level, the level of H-B pairs is found to be 1.28 ± 0.2 x $10^{13}/cm^3$.

Now that the results obtained with traditional hydrogenation techniques have been shown, results showing atomic H in Si using SHP can be discuss with appropriate context in Section 4.3.2.

4.3.2 Atomic Hydrogen Release

The first test to judge the efficacy of SHP as a H-passivation technique, is to determine if atomic H is being released from the underside of the Pd shield.

Atomic H is notoriously difficult to measure, and is usually observed through its interactions with other elements [45]. The experiment presented here uses a highly B-doped Si sample in the version 1 SHP set-up. H_2 would not deactivate B donors, and as such if a change in dopant concentration is measured, atomic

H must be present in the Si [45]. Figure 23 shows results obtained using eCV on B doped Si samples.

The first sample was exposed to the NH_3 plasma, containing H, in the PECVD using Pd leaf as a shield. The plasma was generated by 100 sccm of NH_3 at 650 mTorr and 100 W RF, 13.56 MHz power. The second sample was exposed to a N_2 plasma under the same conditions, but with 100 sccm of N_2 gas instead. This is dubbed SNP (Shielded Nitrogen Plasma) as it contains no atomic H. The third sample is exposed to a direct plasma. The fourth is the H_2 annealed result previously presented in Figure 20 for comparison. All samples were treated for 20 mins at 200 °C on both sides, results are depicted in Figure 23.

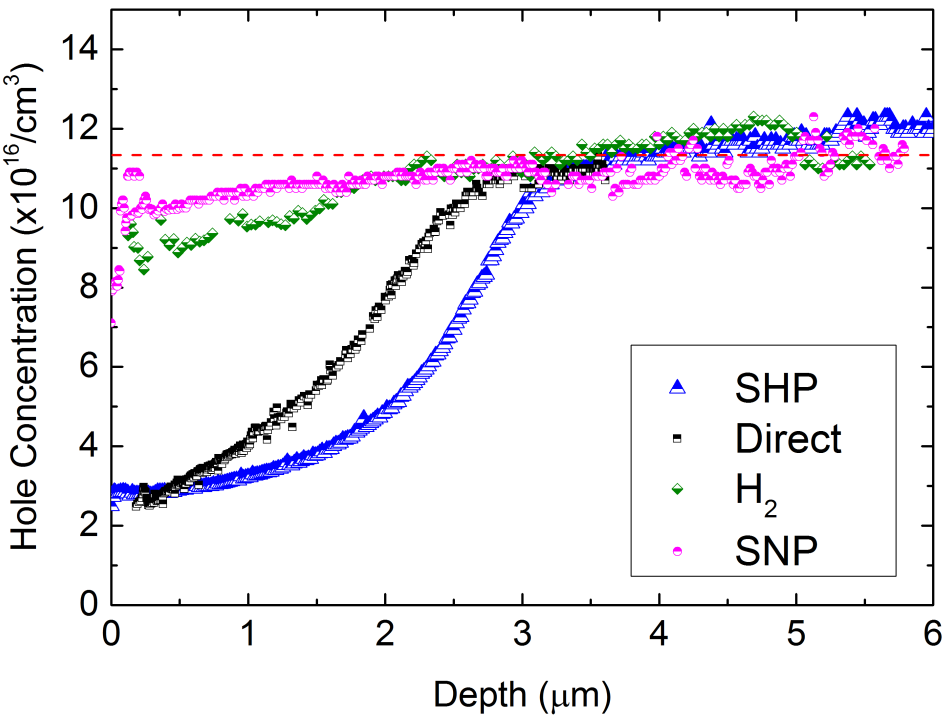


Figure 23 Active B concentration versus etch depth measured using eCV. Bare Si samples exposed to SHP (blue triangles), direct plasma (black squares), and shielded nitrogen plasma (SNP) (pink circles) all at 200 °C for 20 mins. H_2 annealed samples at 200 °C for 20 mins included for comparison as well as background B doping (red dashed line)

Figure 23 clearly demonstrates that using SHP leads to a large number of B atoms being deactivated up to a depth of 3 μm. Using the manufacturer's supplied background B concentration of 1.17 x10^{17}/cm^3, it is possible to use trapezoidal

integration to calculate the area between the background concentration line and the depth profile of the SHP exposed sample. This area corresponds to the amount of deactivated B atoms, and thus how many H atoms were needed to form the H-B pairs. This gives a lower-bound estimate of the total amount of H introduced into Si. It is a lower-bound because, although B is very effective at trapping H, some H atoms will have been trapped by other impurities, surface states or may not have been trapped and instead diffused through the sample. A summary of the calculated H-B pairs for each sample is shown in Table VII.

Table VII Summary of calculated H-B pairs

Sample process, 200 °C, 20 mins	[H-B] / cm^2
SHP	$2.35 \pm 0.2 \times 10^{13}$
Direct plasma (no shield)	$1.28 \pm 0.2 \times 10^{13}$
SNP (no H in plasma)	$0.092 \pm 0.005 \times 10^{13}$
H_2 anneal	$0.36 \pm 0.02 \times 10^{13}$

It is clear from Table VII that in the absence of H in the PECVD plasma, such as the SNP sample, a negligible amount of atomic H is introduced into the Si. Conversely, the presence of atomic H in the SHP sample provides strong evidence that atomic H is being released from the underside of the Pd shield. Combining this with the result of the H_2 anneal, which showed very little H introduction to Si at 200 °C, thus demonstrating negligible H_2 dissociation on the surface of Si at 200 °C, is compelling evidence of the release of atomic H from Pd.

The unfortunate limitation of the B deactivation technique for measuring levels of atomic H is the temperature at which the dissociation of the H-B complex occurs. Indeed, at temperatures above 250 °C, atomic H bound to a substitutional B atom has enough energy to rapidly decouple from the complex and travel further into Si, deactivating another B atom until it decouples again, and the

process is repeated [45]. This decoupling makes it impossible to accurately measure atomic H concentrations using the B deactivation methods at temperatures above 250 °C. This was a severe limitation for this work, as it was later seen, that the passivation quality using SHP improved with temperature. As such, a more in-depth study of the temperature dependence of SHP as well as the H-B complex is shown in Section 4.3.4.

4.3.3 Damage-Free Passivation

The second test to judge the efficacy of SHP as a hydrogenation technique was to measure its damage-free quality. As shown in Figure 24, direct, unshielded, exposure to the H containing plasma caused considerable surface damage which manifested as surface traps for H. This was evident from the reduced H available to passivate B atoms, resulting in the passivation of fewer B atoms. SHP allowed 1.83 times more H to passivate B atoms than the direct plasma exposure method. The surface damage was also seen in Figure 24 B) represented by the sharp decrease in minority-carrier lifetime after exposure.

The damage-free quality of SHP can be demonstrated by using 1 Ω.cm n-type single crystal FZ Si samples with 100 nm thermal SiO_2 and exposing them to a NH_3 plasma, shielded by a Pd leaf. The first sample was subjected to SHP at 200 °C and the second at 350 °C both for 40 minutes. To differentiate the lifetime improvements caused by H introduction from any temperature effects, another set of samples of the same batch was exposed to an anneal under the Pd leaf with the plasma turned off but all other conditions remaining the same. The third sample batch was exposed to the NH_3 plasma without a shield.

In order to obtain the optimal field effect passivation and therefore detect any decrease in the bulk lifetime, the samples were corona-charged post-SHP as described by Bonilla in [79], [143]. In Figure 24 the maximum injection-level

dependent lifetime is shown for each sample, as well as the extracted J_0 as a function of surface potential [150].

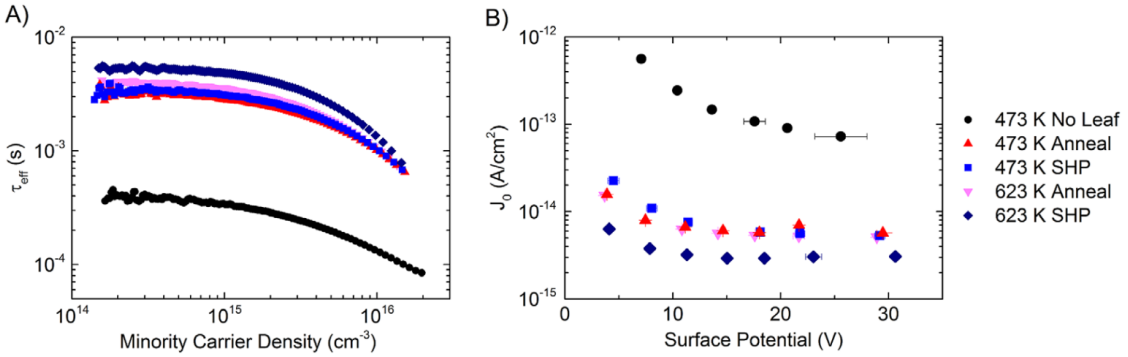


Figure 24 A)Maximum effective lifetime of n-type Si with 100 nm SiO_2 after corona charging as a function of minority carrier density for wafers processed for 40 min on each side, with direct plasma exposure (No leaf), SHP and thermal annealing (leaf in place, no plasma) at temperatures of 473 and 623 K. B) Extracted J_0 as a function of surface potential for each set of conditions.

It is clear from Figure 24 A) that when no leaf is present the interface between the Si and the thermal SiO_2 is significantly degraded, as the lifetime is below 400 µs at 10^{15} cm^{-3} injection level and only shows a slight improvement with corona-applied surface charge. This is likely caused by a dielectric breakdown due to UV exposure and charged ions.

The sample exposed to H plasma at 200 °C whilst being protected by the Pd leaf, has a comparable effective lifetime to the wafer that only received 200 °C thermal anneal in the same conditions, in the range of 500 µs at 10^{15} cm^{-3} injection level. This indicates that there has been no degradation of the Si/SiO_2 interface in the protected sample.

When the temperature is increased to 350 °C in Figure 24 B), the J_0 of the sample subjected to SHP reached a minimum of 2.9 fA, compared to 4.7 fA for the sample exposed to the thermal treatment alone. This corresponded to effective lifetimes of 4.8 and 3.6ms respectively at a minority carrier density of 1 x 10^{15} cm^{-3}. This

result suggests that at 350 °C H-passivation at the Si/SiO_2 interface reduces the number of active interface traps, while still avoiding the introduction of any damage. It is important to note that higher minority carrier lifetimes have been achieved on this material in this doctorate by optimising the SHP technique. This is presented in Chapter 5 Section 5.1.1.

A second experiment was conducted to obtain further evidence that SHP causes no damage to the Si/SiO_2 interface, as well as to apply SHP to a thinner more commercially relevant thickness of SiO_2. Samples in this case only had a standard 10 nm SiO_2 layer, as per the parameters shown in Chapter 3 Section 3.2 . SHP was performed for 45 mins at 380 ˚C on both sides on the sample, using a prepared Pd leaf and 1 Ω.cm n-type FZ Si passivated with a 10 nm thermal oxide. The sample is then corona charged to obtain maximum minority carrier lifetime. The control sample only received the corona charge in order to differentiate between H effects and field-effect passivation (FEP) effects. This is shown in Figure 25.

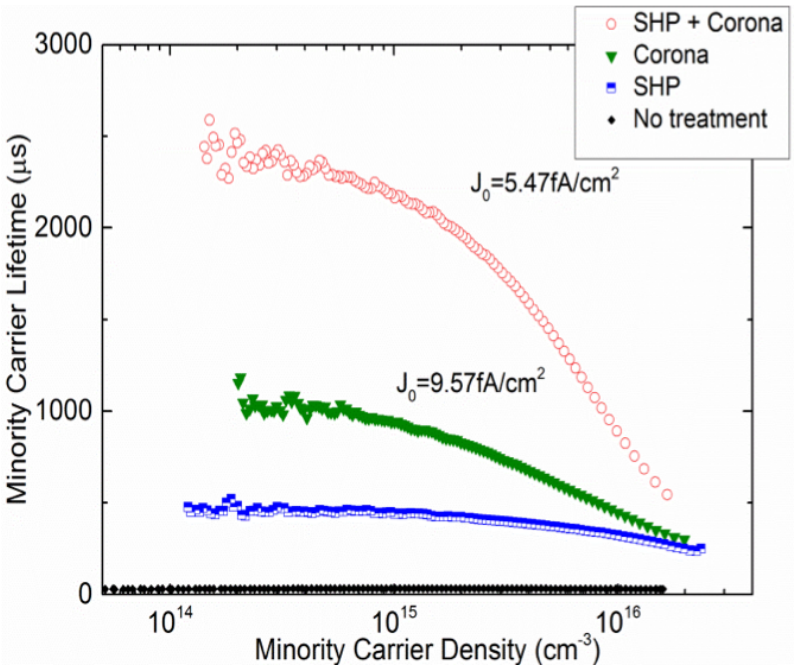


Figure 25 Effective minority carrier lifetimes as a function of minority carrier density for a 1 Ωcm 200 µm n-type FZ Si sample with a 10 nm thermal oxide. The SHP exposure was performed at 380 ˚C for 45 minutes each side. The J_0 values were extracted using the Kane-Swanson method [150]

It is observed that after SHP treatment, the surface passivation has been markedly improved as the minority carrier lifetime increased from 10 μs to 475 μs at 10^{15} cm^{-3} minority carrier injection level, shown as half-filled blue squares. Once extrinsic (FEP) was applied via corona discharge, the lifetime improved to 2.2 ms at 10^{15} cm^{-3} injection level, shown as the empty red circles. The sample that had not seen any SHP prior to corona, shown as the green triangles, only reached a lifetime of 1 ms at the 10^{15} cm^{-3} injection level.

This is an important result as it demonstrates the potential of using SHP as a means of achieving excellent surface passivation at moderately low temperatures and on thin oxides. This also confirms that the potential damage caused by exposure to direct plasma was effectively avoided by the use of the leaf.

4.3.4 Temperature Dependence

One of the advantages of SHP over alternative processes is the ability to perform hydrogenation at low temperatures (below 400 °C). In this experiment, the temperature dependence of atomic H introduction into Si was investigated. Figure 26 presents the active B concentration as a function of depth for p-type single crystal Si wafers subjected to 20 minutes of SHP, performed with a prepared Pd leaf, at temperatures between 150 °C and 250 °C. The other conditions are the standard parameters shown in Chapter 3 Section 3.5 . It is observed that, at 150 °C, B acceptors trap large quantities of atomic H but at a very shallow depth. As the temperature is increased the near surface H concentration is reduced but the depth over which it is trapped increases so that the overall quantity of H present increases. This is in agreement with previous results published by Raman *et al* [91].

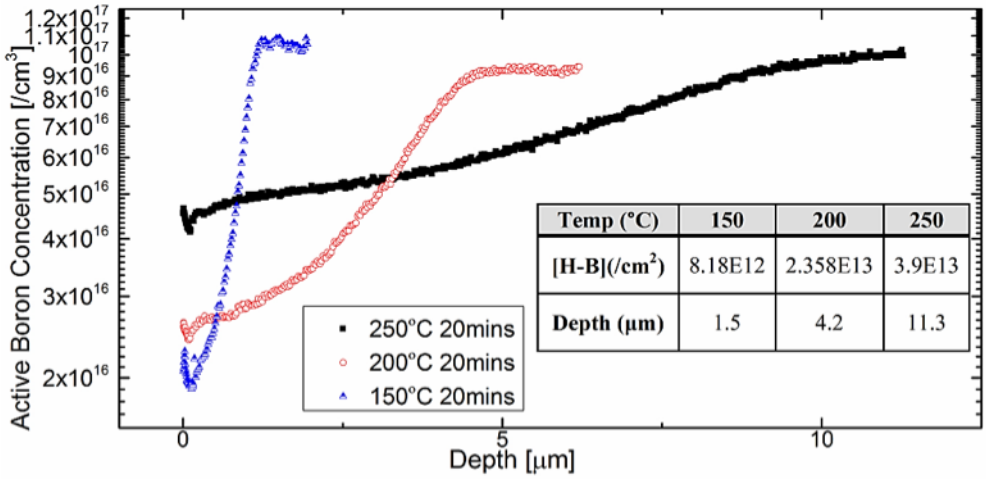


Figure 26 Depth profile of active B concentration as measured using ECV after exposure to SHP at temperatures between 150 °C and 250 °C. Inset: table with integrated [H-B] and corresponding penetration depth.

The shape of the curves seen in Figure 26, especially at 250 °C, could be due to the increased thermal energy available to break the bond between H and B acceptors, thus causing de-trapping and re-trapping processes. More interestingly, Figure 26 shows that the total amount of H bound to B is increasing strongly with temperature in this range. It is unlikely that this increase could be caused by faster transport of atomic H through the Pd leaf bulk, as this process is not expected to be rate limited in this temperature range [134], [137], [169], [170]. A possible hypothesis for the increased deactivation of B acceptors at higher temperatures is due to the interaction of atomic H and Si. Indeed, it is likely that with increased energy, the rate of atomic H transitioning from the surface to the Si bulk is increased. Since the energy barrier for H release from the surface of Pd is around 2.2 eV [177], it is unlikely that a small increase in temperature would result in a large increase in atomic H release from Pd leaf. This makes interactions at the surface of Si more likely to be affected by the temperature change.

4.3.5 Time, Plasma Power and Chamber pressure Dependence

It was seen that the introduction of H into Si to form H-B pairs using SHP was temperature dependent in Section 4.3.4. As such, the optimisation of SHP for H

passivation began by operating the PECVD at its maximum temperature of 380 °C. This showed, across all SHP experiments in this doctorate, the best H-passivation results. It is unclear which rate limiting step is affected by this increase in temperature. Different hypotheses are discussed at the end of this chapter.

The next step in optimising the SHP process was to change other PECVD variables such as exposure time, plasma power and chamber pressure dependence. The results from these experiments are presented in this Section 4.3.5.

First, the sample exposure time to the shielded H-containing plasma was varied. As a means of distinguishing between H-related effects and temperature effects, a control sample was annealed for the same amount of time, without exposure to the plasma, at the same temperature. The experiments were conducted on the standard n-type 1 Ω.cm, 100 nm SiO_2 samples described in Section 3.1 . The PECVD parameters were also the standard ones described in 3.5 and the exposure time was changed from 5 minutes to 60 minutes on each side of the Si sample. Both the SHP and annealed samples were then corona charged, with the standard parameters, in order to obtain the highest passivation quality and minority carrier lifetime possible. The minority carrier lifetime of the samples before and after corona was measured using Sinton Lifetime Tool [176]. These results are presented in Figure 27.

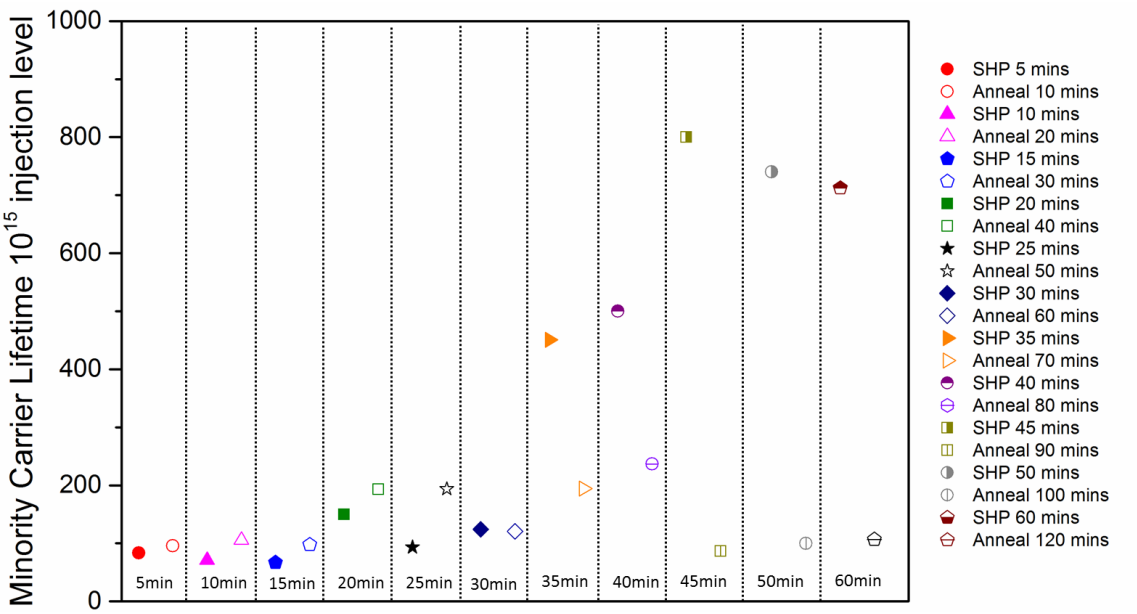


Figure 27 Minority carrier lifetime at 10^{15} / cm³ injection level for varying exposure times. Filled in icons represent the SHP samples, empty icons the control annealed sample (no H).

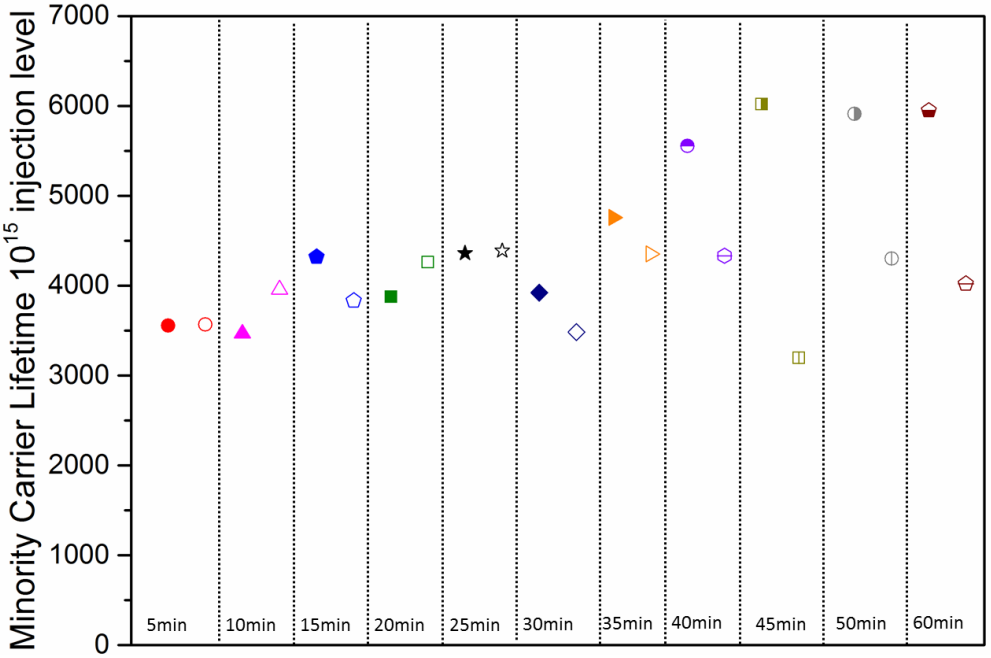


Figure 28 Minority carrier lifetime at 10^{15} / cm³ injection level for varying exposure times after corona charging. Filled in icons represent the SHP samples, empty icons the control annealed sample (no H).

The SHP samples before corona charging show an interesting minority carrier lifetime trend with increasing shielded exposure time, as seen in Figure 27. When the shielded plasma exposure times are below 25 minutes, the samples show a

lower lifetime than the annealed samples that have not received any H exposure. However, when the time is over 25 minutes the SHP samples systematically show a higher lifetime than the annealed samples. Additionally, after 40 minutes the minority carrier lifetime peaks at 800 μs and then slowly decreases and plateaus at around 700 μs for an injection level of 10^{15} cm^{-3} compared to the annealed samples which have lifetimes between 100 and 200 μs for all anneal times.

Once corona charge is applied to both the SHP and annealed samples a similar trend is seen. Below 25 mins of exposure, which corresponds to 50 mins of anneal time, the SHP samples have a similar minority carrier lifetime to the control annealed samples, generally increasing with exposure time from 3.5 ms to 4.2 ms at an injection level of 10^{15} cm^{-2}. After 30 minutes, however, the lifetimes of the SHP exposed samples are considerably higher than the control samples, peaking at approximately 6 ms whilst the control samples' lifetimes remain around 4 ms. After 40 minutes, the lifetime decreases slightly to plateau at 5.8 ms.

The effect of varying the power used in the PECVD to generate the NH_3 plasma was investigated next. The SHP conditions remained the same as the standard recipe: (100 sccm NH_3, 650 mTorr, 350 °C), but the RF plasma power was altered from 25 W to 100 W during the 30 min exposure. The lifetime was measured pre and post corona charging on the Sinton tool. The effect of this power change on the minority carrier lifetime of n-type FZ Si with 100 nm SiO_2 is shown in Figure 29.

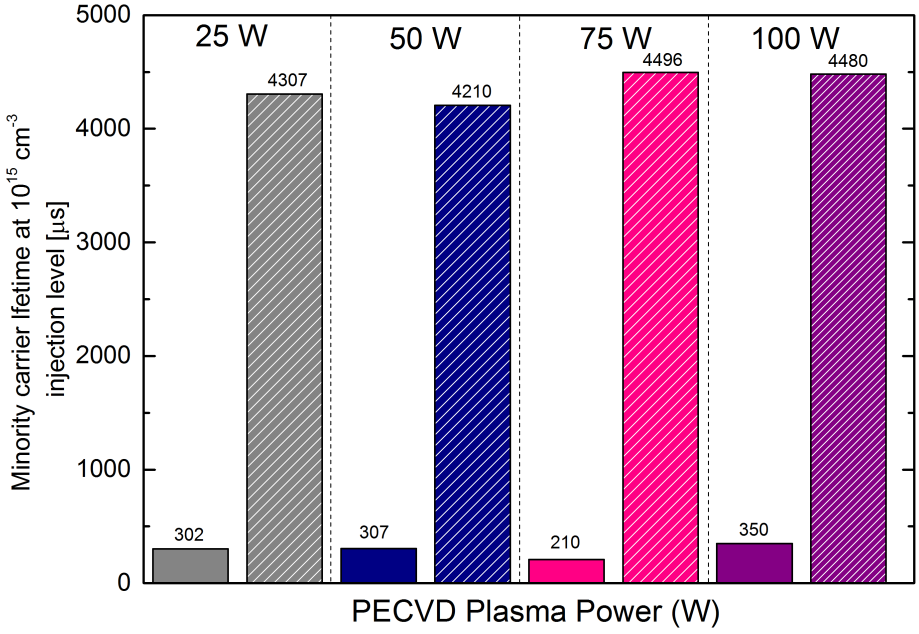


Figure 29 Minority carrier lifetime at 10^{15} / cm^3 injection level for varying RF plasma power before corona charge, and after corona charging (dashed).

As seen in Figure 29, varying the RF plasma power from 25 W up to 100 W did not seem to have a large effect on the H-passivation quality of the SiO_2/Si interface as the minority carrier lifetime is not seen to improve with increasing power. It is important to note that the lifetime of the standard recipe sample at 100 W power, shown in blue, has a lifetime of 4.5 ms after corona charging. This is a lower lifetime than will be shown later on the same Si structure. This is likely caused by the exposure time being 30 mins instead of the optimised 45 mins.

Lastly the effect of varying the chamber pressure was tested. The standard recipe was used for an exposure time of 30 mins and a pressure range between 250 mTorr and 1800 mTorr compared to the standard 650 mTorr. The effect of the chamber pressure change on the minority carrier lifetime of n-type FZ Si with 100 nm SiO_2 is shown in Figure 30.

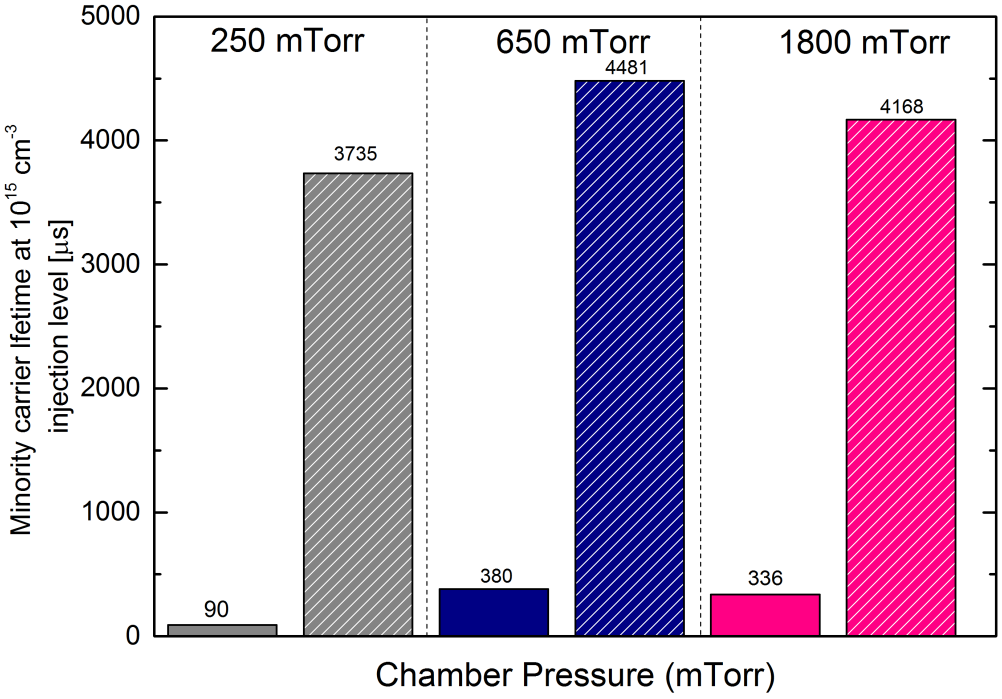


Figure 30 Minority carrier lifetime at 10^{15} / cm^3 injection level for varying chamber pressure power before corona charge, and after corona charging (dashed).

It can be seen in Figure 30, that increasing the pressure from 650 mTorr to 1800 mTorr does not improve the minority carrier lifetime before or after corona charging as the lifetime slightly decreases from 4.5 ms at 650 mTorr to 4.2 ms at 1800 mTorr 10^{15} cm^{-3} injection level. The effective minority carrier lifetime difference is not very significant compared to the change in pressure. At the lower pressure of 250 mTorr however, the lifetime of the sample that underwent SHP, without corona, is much lower than the other pressures with 90 µs instead of an average of 360 µs. This difference is also seen after 60 s of corona charging with a maximum lifetime of 3.7 ms compared to 4.5 ms. This discrepancy is thought to be caused by the very low pressure affecting the plasma. Indeed, it was noted that during the exposure at 250 mTorr the plasma regularly turned on and off over the 30 mins of exposure time because gas pressure was too low to maintain a plasma. This will affect the total amount of H introduced into Si and therefore reduce the H-passivation benefit on the minority carrier lifetime which is seen in the other samples. It is likely that by setting the pressure to lower than 650 mTorr but still high enough to maintain a constant plasma for 30 mins, the lifetime would remain unaffected, as is seen with the 1800 mTorr pressure.

4.3.6 Variability in SHP Efficiency

4.3.6.1 Surface preparation

The results presented in the previous sections all portray the suitable behaviour of the Pd leaf, as well as experimental reproducibility. However, during initial SHP tests some SHP exposures showed more atomic H deactivating B acceptors than other exposures. This occurred when conditions such as time and temperature remained constant. The only variable was the length of time the Pd leaf had been exposed to the H containing plasma. Indeed, some experiments used a 'fresh' leaf that had never been exposed to the H containing plasma, whilst other experiments, later in the day, used a leaf that had been exposed to the plasma for at least 1 hour. The effect of "preparation time" was investigated, and the results are shown in Figure 31.

In the "prep leaf" samples, the 100 nm Pd leaf has been pre-exposed, in its holder, to the NH_3 plasma at 250 ˚C for 30 minutes. The "new leaf" indicates a Pd leaf that has not been exposed to any plasma. The "no leaf" samples are exposed to direct plasma without a shield. All the samples are exposed at 200 ˚C for 5, 10 and 20 minutes.

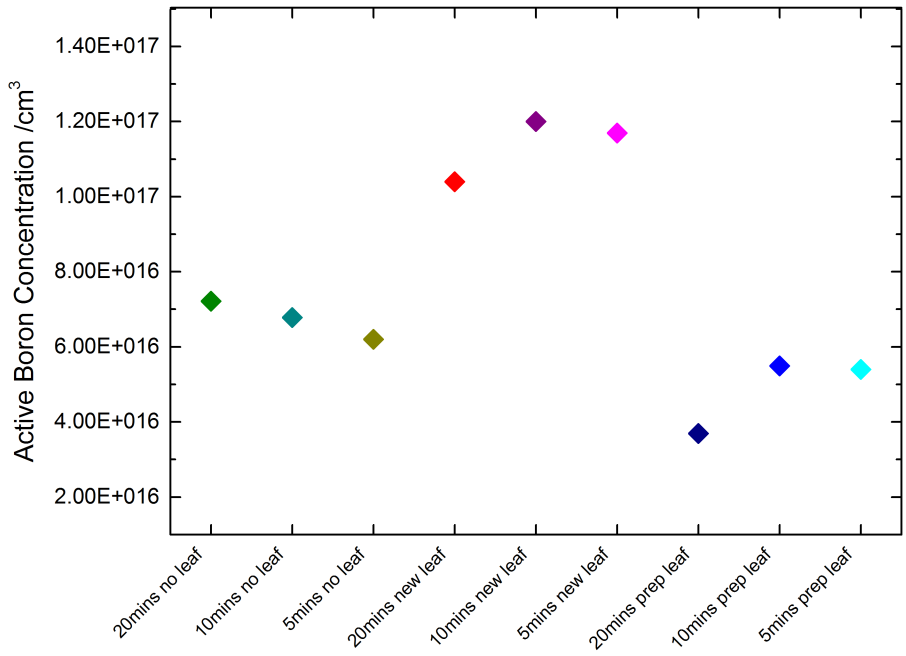


Figure 31 Active B-Concentration /cm³ using three different conditions. Direct plasma (no leaf), untreated leaf (new leaf), prepared leaf for 30mins 250 ˚C. Samples exposed to plasma for 5, 10 and 20 mins all at 200 °C.

Figure 31 shows the maximum level of B deactivated in each B doped sample. These results were obtained using CV equipment which can only record changes up to a depth of 1 μm. Since this technique cannot provide the full depth profile the eCV equipment provides, the maximum level of deactivated B is recorded instead. This maximum B deactivation level is consistently seen to be within 1 μm of the sample's surface on the eCV samples. This is a good indication of how much H was introduced in each sample and can therefore give an indication as to whether or not preparing the leaf has an effect on H introduction in Si.

As can be seen in Figure 31 the used (prep) leaf samples result in a reduced background B concentration from 1.17 x 10^{17} cm^{-3} to 0.37 and 0.47 x10^{17} cm^{-3} active B atoms. When a new, unprepared, leaf is used then 1 to 1.17 x10^{17} cm^{-3} active B atoms are recorded.

Different hypotheses were devised at this point. The first entailed pinholes developing in the Pd leaf which would allow more H to reach the sample. This

theory was dispelled through a visual inspection, where no pinholes were seen in leaves that had produced high levels of atomic H in Si.

If unseen pinholes were indeed the reason for a higher level of H in prepared leaves, then a reduction in lifetime would be seen in exposed samples, similar to an exposure to a direct plasma. This is not the case as seen in Figure 24. Unseen pinholes would allow charged H ions to reach the sample, potentially increasing the surface charge of the dielectric. KP measurements showed that this was not the case in any samples processed using SHP and a prepared leaf because they were all seen to have negligible surface charge.

The second and more promising hypothesis entails the presence of a native oxide on both surfaces of the Pd leaf, which would pose an initial barrier to H diffusion through the Pd leaf. The first, top, surface oxide would be removed upon exposure to H from the plasma, and the second would be etched off by the atomic H leaving the underside of the leaf. Different experiments were devised to test the presence of this native oxide and its effect on initial H incorporation into the Pd.

Figure 32 presents results from samples subjected to SHP treatment under five different leaf conditions:

1. The leaf as received, directly from the manufacturer without any treatment
2. "Prepared" leaf: one side of the leaf exposed to H plasma for 90 minutes in the SHP holder at 250 ˚C
3. Re-oxidised leaf: after "preparation" the leaf is subjected to 5 mins of O_2 ashing on both sides in a Reactive Ion Etcher (RIE), to form a thin PdOx layer on both surfaces. Using the PlasmaLabs 80+, under conditions 100 sccm O_2, 200 W, 30 mTorr at room temperature
4. Poisoned leaf: surface of the leaf is contaminated with S by exposure to very small concentrations of H_2S gas. This is discussed in 4.3.6.2.
5. No leaf: sample is directly exposed to the plasma

Figure 32 presents the minimum B concentrations in the first 1 μm of the Si wafer with different surface preparations, clearly demonstrating significant de-activation of the B acceptor. The background B concentration level for all samples is 1.17 x 10^{17}/cm^3. The levels of active B atoms are recorded in Table VIII.

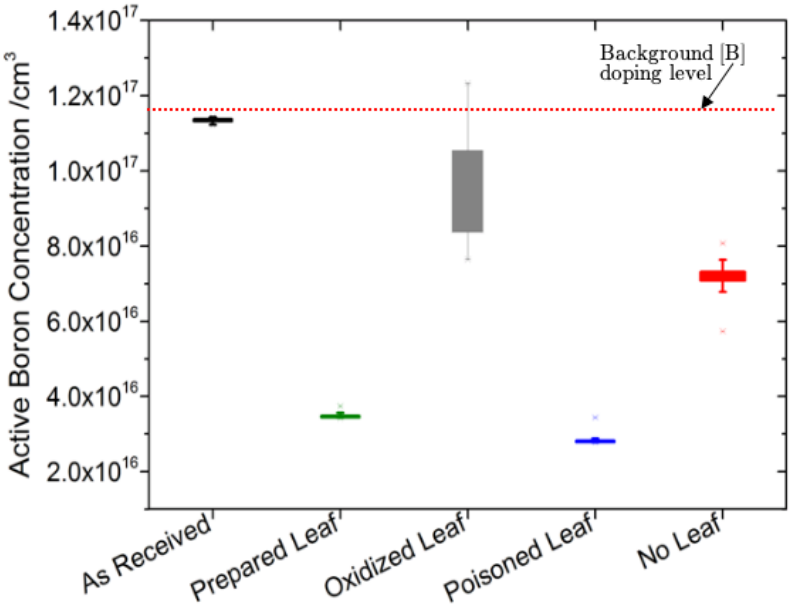


Figure 32 Measured minimum active B concentration in the first 1 μm of Si samples with a uniform doping concentration of 1.17×10^{17} cm^{-3} after exposure to an NH_3 plasma for 20 minutes at 200 °C. Smaller values of active B indicate a larger concentration of atomic H in the Si. Samples were exposed under the following Pd leaf conditions: as received, prepared, re-oxidised, poisoned and under direct plasma without a leaf.

Table VIII Summary of calculated H-B pairs

Sample process, 200 °C, 20 mins	Active B concentration / cm^3
As received	1.17 ± 0.2 x 10^{17}
Prepared leaf	0.34 ± 0.2 x 10^{17}
Oxidised leaf	0.92 to 1 x10^{17}
Poisoined leaf	0.32 ± 0.4 x 10^{17}
No leaf (direct plasna)	0.61 ± 1.0 x 10^{17}

The lower quantity of atomic H released by the "as-received", ie no treatment, leaf is attributed to the presence of a surface oxide that acts as an effective initial barrier to atomic H. It is suggested in the literature that the native oxide on Pd acts as an initial barrier for H diffusion [169], [177] but that prolonged exposure to atomic H would cause its reduction, leaving the surface of the Pd bare [178]. PdO_x posing an initial barrier to H-incorporation into Pd bulk is confirmed by the low level of B-deactivation observed when the re-oxidised leaf is used as an SHP shield.

It is interesting to note the level of B deactivation when no leaf was used, one could expect similar, if not higher, levels of atomic H to be present in the Si sample since there is no shield to slow down diffusion, or encourage recombination. However, the level of B deactivated is less than using the oxide free, prepared, Pd leaf. This is believed to be caused by the creation of additional traps from plasma induced ionic bombardment or an increased surface charge which would repel some H atoms. Both cases would reduce the creation of H-B pairs. Figure 32 also records the result obtained using a poisoned leaf. This poisoning was done using sulphur gas and is explained in greater detail in 4.3.6.2.

4.3.6.2 Sulphur Poisoning

As introduced in Chapter 2 Section 2.3 , Pd has the particular capability of catalytically splitting H_2 into H before its transition from surface to bulk Pd. This effect is mirrored on the underside of the leaf where H is thought to recombine into H_2 before desorbing from the surface. However, as seen in Section 4.3.2, in this thesis, atomic H is released from the Pd leaf. As such, it is hypothesized that there is a parallel transport mechanism whereby atomic H is released directly from the Pd without undergoing recombinative desorption, which is discussed further in Section 4.4

As this is a parallel mechanism, there is still potentially a large fraction of H that recombines into H_2 on the under-side of the leaf. H_2 would not improve the H-

passivation quality of the SHP exposed sample. It is therefore of interest to reduce the fraction of H_2 from the lower surface of Pd. Since the catalytic property of Pd is not required in the atomic H source SHP process, there is a possibility that supressing this quality would also reduce the fraction of H being released as H_2 from the leaf.

S poisoning of Pd has been widely published as a concern for H purification using Pd membranes [165], [179]–[181]. S has been shown to suppress the catalytic properties of Pd for splitting H_2 molecules, this impedes H_2 from passing through the Pd membrane, therefore making it impossible to purify H_2 from other gasses. For atomic H however, Livshits *et al* have published that the activation energy required for the absorption of atomic H into bulk Pd is so low (0.2-0.4 eV) that S contamination does not affect it. As such, S poisoning of the SHP Pd leaf should not impede atomic H transport through the shield. In order to test the effect of S poisoning, the Pd leaf was placed in its holder and prepared via plasma exposure as per the Chapter 3 Section 3.5 standard parameters. The entire leaf and holder apparatus was then placed in a large trough to be exposed to a small quantity of H_2S gas, as explained in more detail in Section 3.5.3.

SHP was conducted using the poisoned Pd leaf to introduce H into highly B-doped Si samples at 200 °C for 20 mins. An unpoisoned, but prepared leaf, was also used on the same types of samples for comparison. eCV was then conducted on these samples to measure the depth profile of H-B pairs. The results are shown in Figure 33.

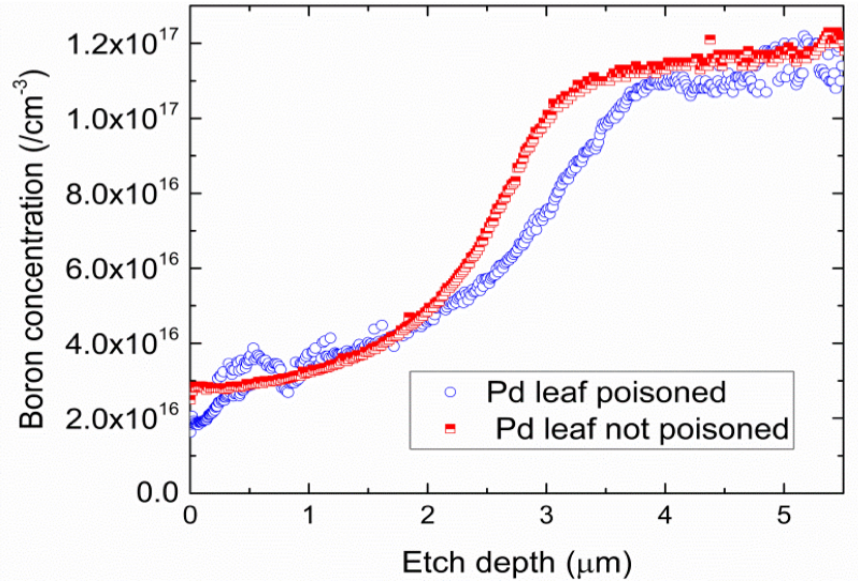


Figure 33 B concentration cm^{-3} versus depth measured using ECV. Samples exposed to NH_3 plasma for 20 mins at 200 ℃, plasma power of 100 W. Samples were processed using a prepared Pd leaf (red squares) and a prepared and poisoned Pd leaf (blue circles) Background doping concentration is ~ 1.1 x 10^{17} cm^{-3}.

It can be seen in Figure 33 that the samples exposed to plasma under a poisoned leaf appear to have slightly fewer active B atoms with a total H-B pairs level (calculated using trapezoidal integration) of 2.6 ± 0.1 x 10^{13} cm^{-3} compared to 2.35 ± 0.15 x 10^{13} cm^{-3} when a non-poisoned prepared leaf is used. The error was calculated using three measurements on three separate samples of each condition. Only one sample of each is shown in Figure 33. This is, however, a small difference which may not be worth the extra processing steps of poisoning the Pd leaf with S as described in the experimental methods. It would be interesting to perform XPS on the surface of the poisoned shield to confirm that it was poisoned successfully.

4.3.6.3 Surface preparation summary

Through the results presented in the previous sub-sections, methods of increasing levels of atomic H introduced in samples using SHP are investigated. It was found that surface preparation, in the form of a pre-exposure of Pd to the H-containing plasma, plays a critical role when using Pd leaves as shields. This is because the

native oxide, PdOx, poses an initial barrier to H diffusion through bulk Pd. The effect of purposeful S poisoning was also observed as a potential way of increasing atomic H released from Pd surfaces by reducing the likelihood of recombinative desorption.

4.4 DISCUSSION

The results presented in this Chapter demonstrate that atomic H is being released from the underside of oxide-free Pd leaf and that this atomic H is introduced into Si and can passivate SiO_2/Si interfaces. Atomic H being released from Pd is of particular significance as it seems to be in contradiction with the accepted literature on the permeation of H in Pd membranes as discussed in Chapter 2 Section 2.3 . The H-purification has further advanced the knowledge of H in Pd membranes. The reported understanding of the permeation of H through Pd is that it consists of a 7 step process [137].

1. Diffusion of H_2 to the surface of the Pd membrane
2. Dissociative adsorption of H_2 into H onto the surface of Pd.
3. Transition of H from the surface into the bulk of Pd
4. Diffusion of H through the bulk of Pd
5. Transition of H from the bulk onto the surface of Pd
6. Recombinative desorption of H into H_2
7. Diffusion of H_2 away from the Pd surface [138]

The 6th step, 'total' recombinative desorption, does not allow for the release of atomic H, as seen in Section 4.3.2. Instead, a modified H transport through Pd is suggested in this thesis.

In a PECVD atomic H source, a small fraction, typically under 5%, of the NH_3 molecules will dissociate into H_2 [182]. As such, the accepted method for H transport through Pd involving the catalytic dissociation from H_2 to H may still occur. For the ionised H atoms however, the postulated transport mechanism is

slightly different, as shown in Figure 34. Atomic H no longer requires the catalytic property of Pd to dissociate H_2 on its surface. The transport mechanism is hypothesised to comprise of two parallel paths, both no longer requiring step (2) and one process not exhibiting step (6), as shown in Figure 34.

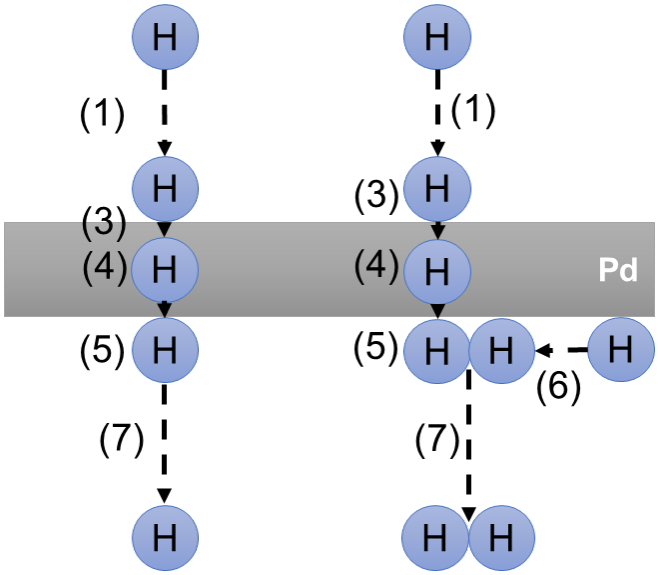


Figure 34 Schematic representation of H transport through Pd with an atomic H source

Results presented in this chapter have made it clear that atomic H is being released from the underside of the Pd leaf. The theory that H_2 is always being released from Pd, as per the accepted H transport mechanism, and could then dissociate on the surface of Si to allow for the passivation of B atoms was dispelled in Section 4.3.1. This was done through an atmospheric H_2 gas anneal, showing negligible H-B pairs, and thus very low levels of H_2 dissociation on the Si surface at 200 °C. It was also shown that atomic H could not have reached the sample by other means than transport through the Pd leaf, as this would have caused surface damage of the Si sample, which was not observed. As such, different transport mechanisms must take place, as postulated in Figure 34. It is believed that under low pressure conditions, atomic H is being released from Pd without recombining first. This contradicts the assumption of a purely recombinative desorption process reported in the literature and must be considered a surprising result. Figure 34 depicts the two parallel transport mechanisms believed to take place in this case. The proportion of atomic H that is being released from the

underside of the Pd leaf without recombining first is not yet known. Both recombinative and non recombinative desorption from the Pd leaf are shown.

It is unclear why the many published work on H diffusion through Pd did not see any atomic H being released. A possible reason is simply that the authors were not looking for it. Indeed, a vast majority of the published work on H transport through Pd originates from the H purification industry, where H concentration is measured compared to other impurity gasses, these works do not differentiate between the atomic and molecular form. This ties into the second reason why atomic H may not have been detected in those experiments: their experimental set-up does not allow for atomic H detection. As discussed in Chapter 2 Section 2.1.3, atomic H is notoriously difficult to detect and it is likely that unless the experimental set-up was designed with atomic H detection in mind, none would have been recorded.

There are some published works on the release of atomic H from Pd but all have specific conditions: either during a Pd-hydride decomposition [138] or under bombardment by electrons with energies in excess of 2 keV [139].

Lisowski *et al* introduced atomic H to a thin Pd film to form Pd hydride. They have shown that once the Pd has become a Pd hydride (with up to 0.8 volume fraction H), atomic H can be released by increasing the temperature of the Pd film. This increase causes the thin Pd hydride film to decompose and release atomic H which they detected using a gold film and TMDS (thermal desorption mass spectrometry). The level of atomic H detected in their experiment is small, 0.01%.

The second relevant paper detecting atomic H is by Tyurin *et al* where they use ionic bombardment to radiate a H saturated Pd film. They postulated that the bombardment provided sufficient energy to excite the H atoms on the surface of Pd and stimulate non-equilibrium emission of positive ions.

The conditions of the work presented in this chapter however, are different from these two cases. As described in Section 4.2 the Pd leaf used in this work was only exposed to ions with energies of several hundred eV [23] compared to the several keV Tyurin used in his experiments. There is a possibility that the UV from the plasma increases the energy of atomic H within the Pd leaf, but not to reach the values shown by Tyurin and Gahan *et al* [183][184]. Additionally, the 100 nm leaf is relatively thick when considering movements of atoms through a lattice, and as such it is inconceivable for any H atoms to not have neutralised and fully thermalised once they have diffused across the Pd shield.

What is possible however, is that the atomic H species are found in higher concentration on the underside surface of the Pd leaf. This higher concentration translates to a higher chemical activity in that region which, for H atoms, means higher Fermi energy. This higher energy may increase the number of H atoms leaving the leaf. The second part of the hypothesis explaining why atomic H is seen in SHP processes, is the low pressure and low temperature quality of the experiment. A high-pressure environment, as is the case for most of the published H-Pd literature, would make it hard to maintain high concentrations of atomic H in the gas phase, as it would be likely for it to recombine in the time it takes to diffuse from the source to the upper surface of the Pd shield. Additionally, the higher temperature used in the other H-Pd systems may encourage the recombination action of H into H_2. These two parameters may be one of the reasons why other works have not identified this parallel H transport mechanism through Pd.

Finally, the SHP set-up in the experiments presented in this chapter has the vital difference of using an atomic H supply compared to the H_2 supply used in a lot of the literature. Livshits *et al* used a similar atomic H source for their experiment but only noted an abnormally high level of H penetration through a 20 μm Pd membrane, without making the distinction between molecular and atomic H [25].

The results presented in this chapter have brought strong evidence for the hypotheses discussed above. SHP is presented in section 4.3.3 as a means to provide damage free H passivation as well as a damage-free source of atomic H. Figure 22 shows the effectiveness of SHP on thin oxides, achieving minority carrier lifetimes of 2.2 ms 10^{15} cm^{-3} injection level. The effect of temperature is also discussed in this chapter over a small range, where more atomic H is observed to deactivate B acceptors as the temperature increases. This process is thought to be related to the higher release of atomic H from the underside of the Pd leaf rather than from faster transport through bulk Pd.

Although the catalytic property of Pd is no longer required for the fraction of ionised H atoms, it will still be necessary for any H_2 molecules that are to be transported across the Pd shield. As such, this property may still be beneficial in increasing the level of H released from the underside of the leaf. As presented in 4.3.6.2, S poisoning can be used to remove the catalytic property of Pd to split H_2 into H and conversely to recombine H into H_2 before it is released from the surface of Pd. This is particularly relevant for the underside of the Pd shield, as it is beneficial for passivation purposes to have the highest concentration of H present between the leaf and the sample. It may not be beneficial however, to supress this property for the upper surface of the Pd leaf as it would prevent any H_2 from diffusing through the shield. A future experiment which might show higher levels of H-B than those currently seen with S poisoning, would be to only poison the lower surface of the Pd shield, allowing for H_2 to dissociate and diffuse through Pd, but then minimising the recombinative desorption rate and encouraging H to be released from the lower, poisoned, surface.

One of the key benefits of SHP over alternative techniques such as FGA and dielectric films, is its ability to introduce atomic H at low temperatures as shown in Figure 25. This is of particular relevance for future solar cell structure which may be subject to degradation at high temperatures, such as heterojunctions and amorphous Si layers, and, of course, relevant to reduce the thermal budget of solar cell production. Further comparison of SHP with alternative techniques, the

application of SHP to different oxide thickness and the possibility of making SHP an in-line process is investigated in Chapter 5.

CHAPTER 5 SHP APPLICATION TO STRUCTURES

Chapter 4 presented Shielded Hydrogen Plasma (SHP) as a method to introduce atomic H to Si samples at a wide range of temperatures, at a low cost and without causing any surface damage. Chapter 5 aims to explore the applications of SHP to different Si structures, test the possibility of using different metals as a shield, and compare SHP to other hydrogenation techniques.

5.1 SHP APPLICATIONS

In this Section, SHP is used to passivate the interface of 100 nm thick SiO_2-Si, as these samples had better initial lifetimes. The aim was to try to obtain an interface with the fewest possible active defect states.

5.1.1 THICK OXIDE PASSIVATION

SHP was performed on 200 μm thick, 1 Ω.cm, n-type float zone Si samples with a 100 nm thermally-grown SiO_2 coating, at 950 °C in a quartz tube with dichloroethane (DCE) and O_2, sourced from Fraunhofer ISE.

Figure 35 shows SHP results on samples exposed to the shielded NH_3 plasma under a prepared and poisoned Pd leaf at 380 °C for 45 minutes on both surfaces using the standard SHP recipe. The samples were lifetime tested before and after each process using the PCD Sinton lifetime tester. In order to achieve the best possible lifetime, field effect passivation was performed post-SHP using the corona charging method described by Bonilla et al [185].

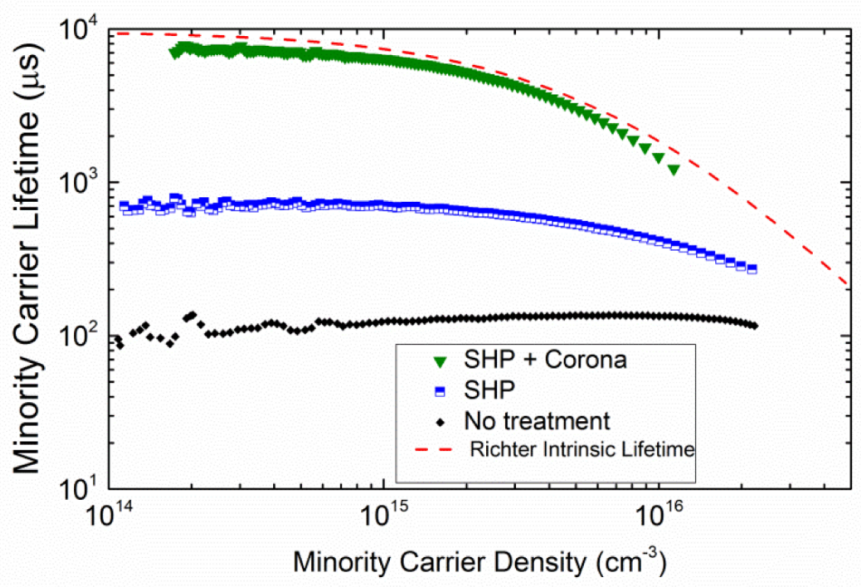


Figure 35 Minority carrier lifetime versus minority carrier density. Initial lifetime shown as black dots. SHP performed using a prepared, poisoned Pd leaf for 45 mins at 380 °C on both sides (blue squares). Corona charging was used to achieve maximum lifetime (green triangles). The Richter intrinsic lifetime limit is shown as a red dashed line for comparison [34].

It can be seen in Figure 35 that the sample treated with SHP using a prepared poisoned leaf alone increased the effective minority carrier lifetime from 12 μs to 1050 μs, and after corona charging to 6.3 ms, very close to the Richter intrinsic lifetime limit. Using the methodology developed by Bonilla [186] this is equivalent to an SRV ≤ 0.17 cm/s, a J_{0e} of 0.47 fA/cm² and an iV_{oc} of 740.1 mV. This was at the time, the world's best chemical surface passivation ever achieved with a single oxide layer. Since then Collett *et al* has achieved a lower SRV using the enhanced alneal methodology [187].

It is interesting to compare these results, obtained with a poisoned leaf, to those done without poisoning as shown Figure 33. There is a 1.3 ms difference between the result in Figure 33 and the one shown in Figure 35. The seemingly increased effect of S poisoning on the lifetime of the samples shown in Figure 35 compared to the level of H-B pairs recorded in Figure 33 may be due to the different temperatures at which the SHP was performed for these two tests. The B deactivation samples, shown in Figure 33 were processed with SHP at 200 ˚C,

whereas the lifetime samples Figure 35, were processed at 380 ˚C. This increase in temperature could alter the kinetics of the catalytic surface properties of the Pd. It is thought that there is an energy barrier to atomic H pairing on the Pd surface before its release as H_2 [134]. Thus, at higher temperatures the conversion of atomic to H_2 on the Pd surface will be faster than at lower temperatures. This might explain why S poisoning, which is expected to largely stop the recombination process at any temperature, would result in a bigger effect on atomic H emission at high temperatures compared to low temperatures [180].

5.1.2 P-TYPE SI

The SHP process was repeated on p-type, 1 Ωcm FZ Si coated with 100 nm of SiO_2. The samples were exposed to H from SHP using a prepared and poisoned Pd-Ag foil, for 45 minutes at 350 ˚C. The samples were corona charged, for 60 s after SHP to obtain a maximum minority carrier lifetime. Lifetime measurements were taken before and after each process as shown in Figure 36.

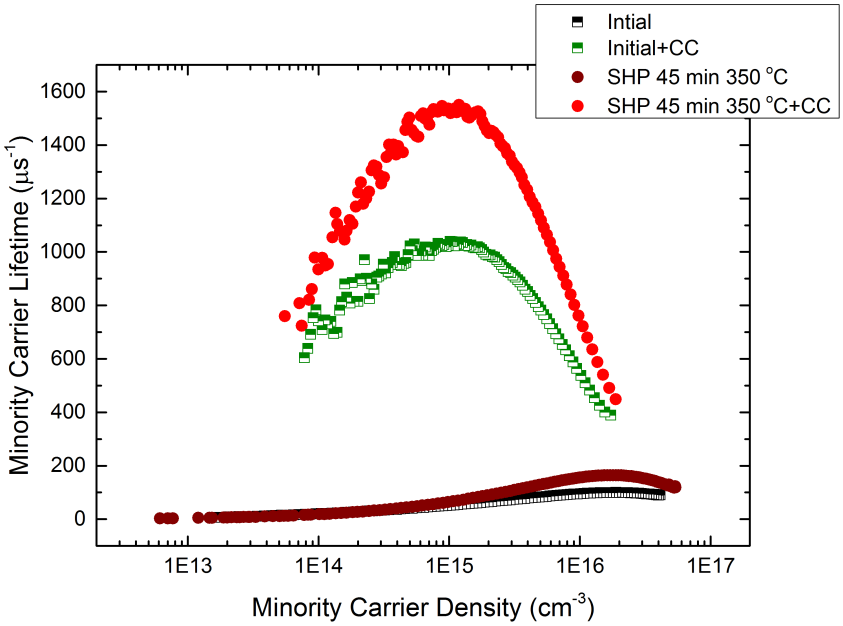


Figure 36 Minority carrier lifetime versus minority carrier density. Initial lifetime (black squares) and after corona charging (green squares). SHP with prepared, poisoned Pd leaf for 45 mins at 350 °C on p-type FZ Si (brown circles) and after corona (red circles).

The J_0 values were also extracted from the Sinton Lifetime software as per 3.6.1.1. The samples without SHP had a J_0 of 100 fA/cm^2 before corona and 250 fA/cm^2 after corona. The SHP samples has a J_0 of 17 fA/cm^2 before corona charging and 15 fA/cm^2 after. It is clear from Figure 36 and the lower J_0 values in the SHP samples compared to the non-hydrogenated samples, that the SHP process had a beneficial effect on the minority carrier lifetime after corona charging of the p-type sample, shown in red, compared to the sample without any H-introduction, shown in green. The maximum lifetime of the SHP plus corona is 1.5 ms at 10^{15} cm^{-3} injection level, compared to 1 ms for a sample with only FEP from corona charging.

The lifetime difference in this p-type FZ Si sample is much less pronounced than in the n-type FZ samples in Figure 33. This difference in SHP efficacy could be due to a few reasons. The main one is that the base p-type material available in the Semiconductor Group at Oxford has a lower starting lifetime than the n-type material [188]. This is indicated by the shape of the lifetime curves which suggest a bulk-limited lifetime after SHP treatment. Secondly, it is known [189], that H-passivation is more effective on n-type surfaces compared to p-type due to the charge of H at the interface being H^+. Indeed, H^+ will passivate certain defects which affect holes more than electrons. This would cause the electron minority carrier lifetime to remain below that of holes in n-type.

5.2 Investigating Different Metallic Shields

This section presents the SHP efficacy when metallic shields other than 100 nm Pd leaf are used.

5.2.1 Motivation

While Pd is an excellent test material and has demonstrated exceptional permeability to H, making it an excellent material for SHP, from an industrial perspective a less expensive, more durable material would be favourable. Chapter 4 Section 4.3.6.2, has shown that removing the catalytic property of Pd via S-poisoning was beneficial for the introduction of atomic H. As such, this catalytic property is not a requirement for an SHP shield candidate. Thus, it is likely that other metals may also be viable options for the shield.

It is widely known that batch processes requiring samples to be processed in a vacuum are unfavourable to large-scale PV manufacturing as they do not deliver high wafer throughput. This is because a vacuum must be created for each batch. Being able to only process a few wafers per vacuum pump down, such as processes in a PECVD is not cost effective, which is one of the reasons why remote plasma hydrogenation is not a widely used industrial technique. SHP however, has the potential to be developed into an in-line process as is shown in the schematic of Figure 37.

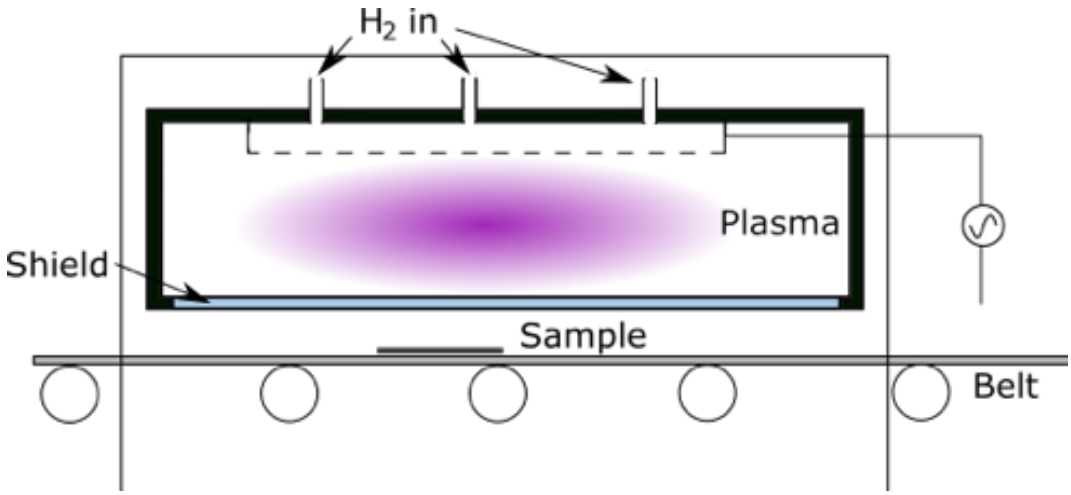


Figure 37 Schematic representation of SHP apparatus adapted for in line processing

Although SHP already has great potential in a research laboratory environment, its greatest advantage in an industrial setting would be the ability to completely separate the plasma chamber from the environment of the sample, as shown in Figure 37. In this version of the SHP process, only the plasma is in a vacuum

chamber. The plasma is generated via the upper shower electrode, which lets a H-containing gas in, while the shield acts as the lower electrode. The sample is placed a short distance below the shield, and is moved along with a belt system. In this in-line system, neutral atomic H is released from the shield and can passivate the moving sample underneath it.

There are two main concerns in the practical realisation of this system. The first is that the pressure difference between the vacuum containing the plasma and the conveyor belt could be up to 1 atm. This amounts to considerable force on the shield. The 100 nm Pd leaf used thus far would not sustain such pressure difference, and therefore an alternative shield must be found, which would also not undergo a phase change in order to maintain durability. The second concern is whether the H will cross the inert gas environment and reach the sample surface without having recombined into H_2. This has not been a concern in the laboratory SHP experiments, as they have been conducted in a low pressure environment (650 mTorr), meaning that the atomic H released from the underside of the Pd leaf had statistically less chance of recombining than in a high pressure environment.

The mean free path, λ, is the average distance a particle of an ideal gas will travel before colliding with another member of the gas. If the separation between the shield and the sample is of the order of a mean free path, then some fraction of the H is expected to cross this distance without interacting with other H and recombining to H_2. This would lead to atomic H reaching the Si sample surface. Assuming H behaves as an ideal gas, the mean free path, λ, can be calculated as [190][84]:

$$\lambda = \frac{kT}{\sqrt{2}\,\pi d^2 p} \tag{5.1}$$

Where k is the Boltzmann constant: k = 1.38 x 10^{-23} J / K, T is temperature in Kelvin, d is the diameter of the gas particle, and p is the pressure of the gas.

Using a H diameter of 240 pm, a temperature of 623 K and typical partial pressure of H released from Pd in SHP of 0.001 atm we obtain a mean free path of 0.33 mm. Modern engineering techniques are routinely capable of operating with a separation this small [191]–[193]. Additionally, the sample could be placed in an inert gas atmosphere, making it possible for the partial pressure of H released to be lowered further, thereby increasing the mean free path distance, allowing for the sample to be placed further away from the shield.

The maximum pressure around the conveyor belt will be dependent on the material used for the shield, and how much pressure this shield can sustain. It is interesting to calculate the minimum foil thickness required to sustain at least 1 atm of pressure difference for a given size of grid support.

If the metal shield is considered as a plate with fixed supports on all sides, under uniform load (applied pressure) then the maximum pressure for any given thickness can be expressed by [194], [195]:

$$\sigma_c = k\frac{\pi^2 E}{12(1-\nu^2)(\frac{b}{t})^2} \tag{5.2}$$

Where σ_c is the critical (maximum) load before failure, k is a geometrical plate failure coefficient, which is 6.97 for fixed supported plates on all sides, E is the elastic modulus for the plate's material and ν is the Poisson's ratio. b/t is the widest length over the thickness.

For plates with a thickness less than 10 % the width of the plate however, this equation must be subbed into the equation for modulus of rupture, which will occur at a smaller load than the critical load calculated. The modulus of rupture is the ultimate tensile strength of the plate and is defined by [196]:

$$W_{UTS} = \beta\sigma_c t^2 \tag{5.3}$$

where β is a dimensional constant depending on the area of the plate and has a value of 5.48 from [197]

Combining (5.2) and (5.3) and solving for the thickness of the plate t we obtain:

$$t = \sqrt[4]{\frac{12b^2 W_{UTS}(1-\upsilon^2)}{\beta k \pi^2 E}} \tag{5.4}$$

If Pd leaf or foil is considered for the plate which is supported by a grid with a separation of 5 mm the values are as follows: E = 137 GPa = 137000 N/mm^2 , $\nu = 0.37$, k = 6.97, Area = a x b = 25 mm^2.

Therefore the minimum thickness of Pd required to sustain a modulus of rupture of 1 atm is 26.6 μm. It is likely however, that the pressure difference across the shield would be less than 1 atm due to the sample being in a low pressure environment through the use of differential pumps. Reducing the pressure to 0.5 atm and reducing the separation between the supporting grid to 3 mm we obtain a minimum shield thickness of 11 μm.

As it can be seen, the minimum thickness will depend on the materials used and their respective Young's Modulus. For Al for example the minimum thickness required to sustain 1 atm with 5 mm spaced grid supports would be 18 μm.

Pd was an obvious material to choose for initial SHP proof of principle experiments due to its high permeability of H, demonstrated in many papers relating to the H purification industry [134], [169], [170], [198]. However, there are other metals with high permeability and solubility of H, which may be cheaper than Pd to be used in larger quantity in industry. Figure 38 shows the permeability of atomic H in different metals with respect to temperature.

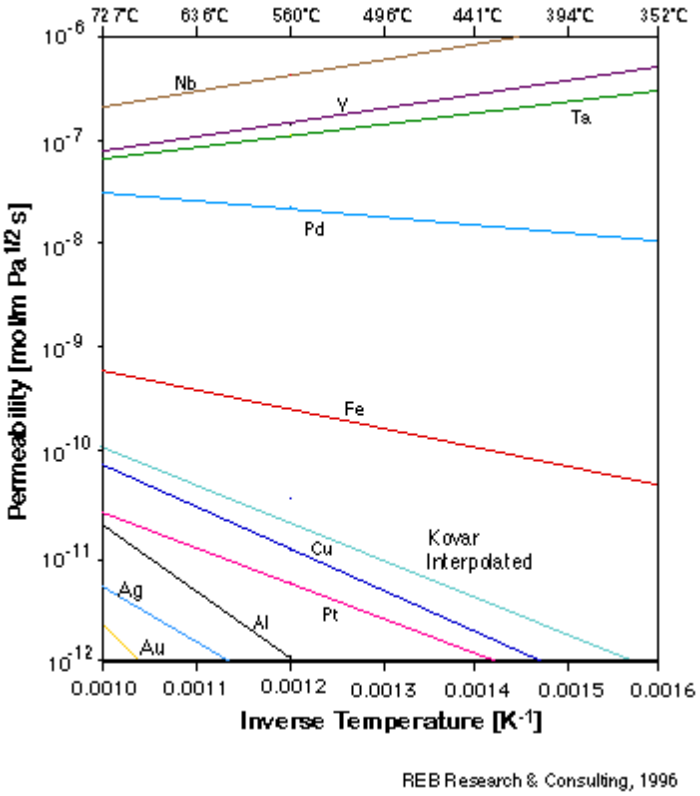


Figure 38 Permeability of H in different metals as a function of temperature [174]

It can be seen that niobium, vanadium, tantalum and palladium have the highest permeability of H, whilst copper, platinum, aluminium and gold have lower but non-negligible permeability of H. The permeability of a material is the product of the diffusivity and solubility of another chemical species within the material. For SHP application, it is unclear whether it is desirable to have a shield material with both high solubility and diffusivity to H or perhaps just one of the two. Indeed, a high diffusivity will allow H to travel rapidly through the bulk of the shield, relatively unaffected by temperature changes [199]. This is thought to be an advantage. A high solubility, however, may have a negative effect on the concentration of H released from the shield. A high bulk solubility for H translates to a lower energy state of H in the bulk, which may lead to less H transitioning from the bulk to the surface of the shield [135], [200]–[202]. Contamination probability into bulk Si was also considered, and metals known to be strong recombination centres such as Fe were not considered as potential shields.

Since Figure 38 and [174], [199], [203] suggest that other metals may indeed be effective as shields, different metallic leaves were sourced and tests conducted. This is presented in Section 5.2.2.

5.2.2 Metallic Shields

As introduced in Figure 38, metals than Pd are permeable to atomic H. Contamination considerations for Si combined with the ease and cost by which metallic leaves or foils are acquired led to the following metals being investigated as shown in Table IX.

Table IX List of metals tested for usage as SHP shields

Metal	Composition	Thickness
Pd-Ag foil	75% Pd 25% Ag	10 μm
Al leaf	99.9% Al	100 nm
Al foil	99% Al	25 μm
Ni foil	99% Ni	10 μm
Pt leaf	99% Pt	100 nm

In order to test the efficacy of each metal as a shield, the level of H introduced into p-type Si from SHP deactivating B dopants was measured. The level of H-B pairs formed was considered to be proportional to the level of atomic H released from the metallic shields. Sections 5.2.3, 5.2.5, 5.2.6, 5.2.7, and 5.2.8 present the results obtained.

5.2.3 Pd-Ag

5.2.3.1 Pd-Ag Alloy

It has been reported in the literature [135], [177], [204], [205] that Pd leaf membranes have durability issues when exposed to high quantity of H. Grashoff

et al [204] reported that under 300 °C and 20 atm pressure, an increasing level of H present in pure Pd leads to a β-Pd hydride phase which coexists with the α phase. This is illustrated in Figure 39.

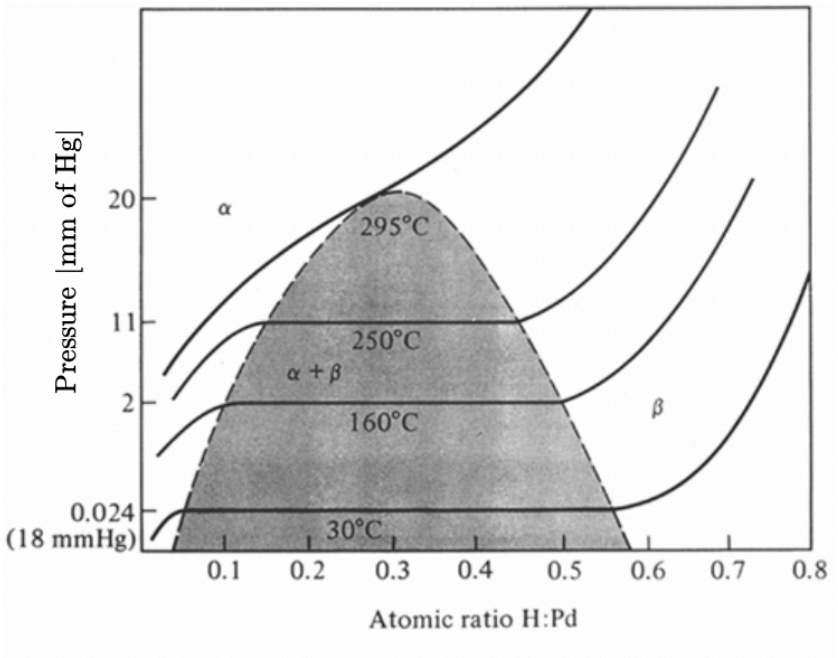


Figure 39 Phase diagram showing typical absorption relationship in Pd-H system. The α→β transformation occurs below 300 °C and below 20 atm pressure, causing lattice distortion. Figure from Bruning and Sieverts [206].

It is known that the β phase has a larger lattice structure than the α phase, and an expansion of 10 % in volume is seen when H is introduced to Pd with an atomic ratio (H:Pd) of 0.5 [183]. If Pd is exposed to repeated hydrogenation and dehydrogenation cycles, it has been reported that β phase growth results in dislocation hardening caused by severe strains in the material. This can cause the premature rupture of the Pd membrane. The effect of the phase change was observed on the Pd leaf used as an SHP shield as in Figure 40.

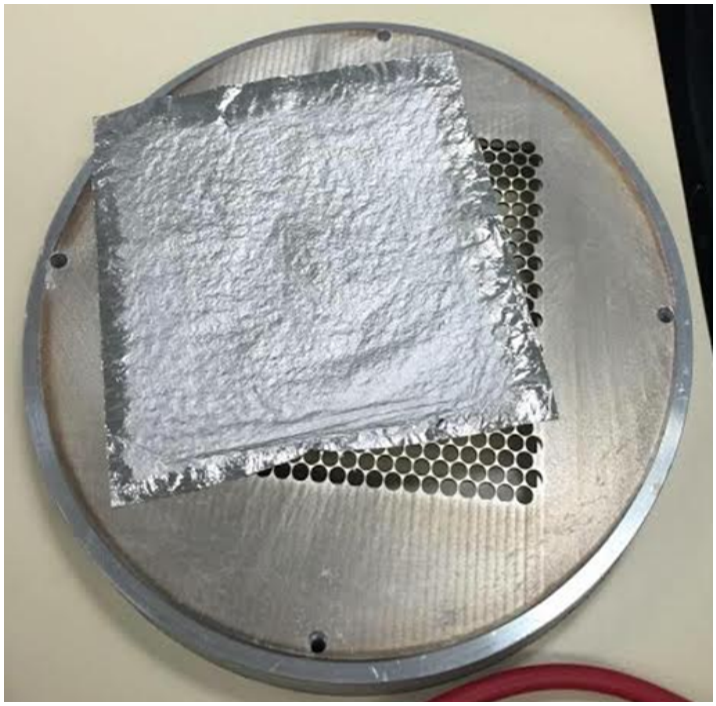


Figure 40 Photograph of SHP set-up in Oxford. Seen is the Pd leaf having been exposed to a few cycles of hydrogenation. The part of the leaf exposed to the H-containing plasma appears less reflective.

The Pd leaf shown in Figure 40 has been exposed to more than 3 hydrogenation cycles. The area that is held in place by the Al grid can be seen to be of a different finish than the edges of the leaf which were hidden from the plasma by the occulting edges of the holder. The area exposed to the plasma is matte which could indicate internal strain causing the material to deform and be work hardened. It has been observed during SHP experiments that once a Pd leaf has become matte like the one pictured here, it can no longer be used as an SHP shield as another exposure to the H containing plasma will typically result in its rupture.

An obvious method to avoid the phase change is to operate SHP experiments above 300 °C. This is restrictive however, and negates a key benefit of SHP - its low temperature passivation ability. As such, it is necessary to suppress the phase change seen at 300 °C to a temperature well below the temperature to be used for SHP. Hunter *et al* filed a patent in 1956 [207] showing the dimensional stability of the Pd-Ag alloy when exposed to H. At silver levels above 20% the

Pd-Ag alloy's phase transformation is supressed to below room temperature which makes it dimensionally stable within SHP's operating temperatures. It is interesting to note that the literature also reports a higher permeability of H through 25:75 Ag-Pd than pure Pd. Grashoff *et al* report a 12% increase permeability with 25% Ag [204].

When the Pd-Ag foil was used in SHP experiments, no rupture was recorded even after more than 100 hydrogenation cycles. The Pd-Ag foil did not exhibit the matte surface change that the Pd leaf did and was used for over 2 years without rupturing.

5.2.4 Using Pd-Ag for SHP

It was favourable for SHP experiments to investigate the possibility of using a more durable shield material which would not rupture due to the phase change described in 5.2.3. It was also interesting to investigate how a different thickness would affect the transport of H through the shield.

Pd-Ag foil (10 μm thickness, 75% Pd, 25% Ag), sourced from Fischer Scientific, was used as the metal shield for SHP on 0.175 Ω.cm, B-doped, p-type Si. The samples were exposed to the H containing plasma under the prepared and poisoned Pd-Ag foil for 30 mins at 200 ℃. Figure 41 shows the resulting ionised B concentration using Pd-Ag foil and Pd (100 nm thick), as a function of depth measured using eCV

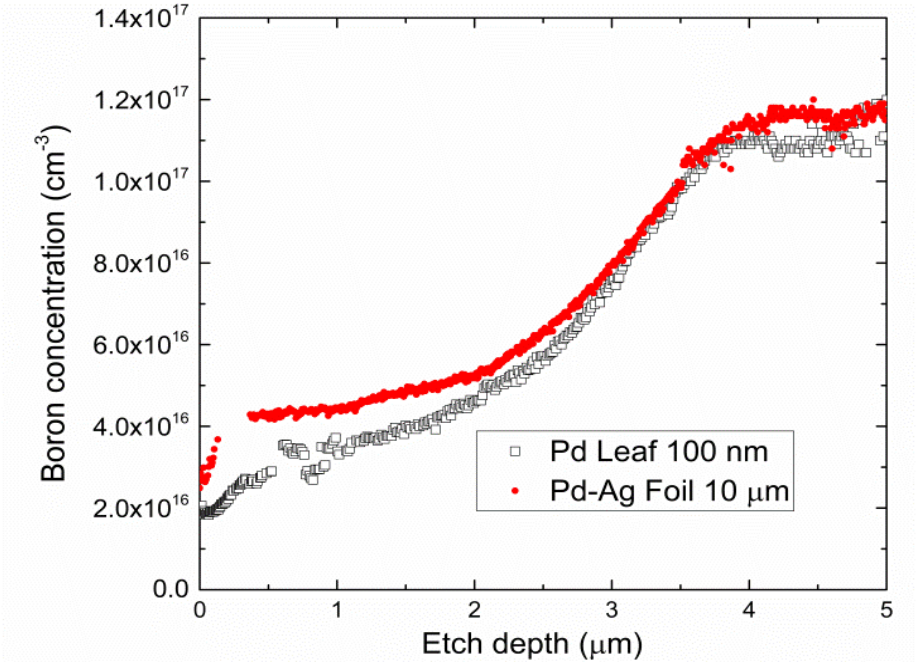


Figure 41 Ionised B concentration as a function of depth measured using eCV. Samples were exposed to NH_3 plasma under SHP shield for 30 mins at 200 ℃, with a plasma power of 100W. Pd leaf shield is shown as empty black squares. Pd-Ag foil shield is shown as red dots.

It can be seen that under the same conditions, the Pd leaf and 100 times thicker Pd-Ag foil behave similarly as SHP shields. Both samples were exposed under a poisoned shield and show comparable levels of atomic H introduced. Using trapezoidal integration methods, the total B deactivated can be calculated: using the Pd-Ag foil gives $1.98 \pm 0.2 \times 10^{13}$ /cm^2 compared to $2.35 \pm 0.2 \times 10^{13}$ /cm^2 using the leaf. Since the foil is 100 times thicker, this is an excellent result. This corroborates observations on superpermeability where the thickness of the membrane had a negligible impact on the permeation of H [183]. It also provides some evidence for the identity of the rate limiting step in the release of atomic H from Pd in SHP. Indeed, the increased thickness not having a drastic effect on the levels of H released suggests that the rate limiting step of the process is not diffusion through the bulk of Pd but instead its release from the Pd surface or introduction into the Si. This is expanded upon in Section 5.4 .

5.2.5 Aluminium Leaf

Section 4.3.2 has shown that the catalytic property of Pd was not necessary for atomic H introduction into Si, as such Al leaf seems a good alternative material. Highly B-doped Si, standard sample listed in Chapter 2, was exposed to a H-containing plasma, generated in the PECVD with NH_3 gas by RF power. The background B-doping concentration is 1.17 x 10^{17} cm^{-3}. The Al leaf used as a SHP shield was 100 nm thick, with a native AlOx on both surfaces. It is unlikely that the H plasma could etch off AlOx, as it is extremely unreactive. Since AlOx is extremely fast to form on the surface of Al, even if it had been etched by the plasma it would have immediately reformed during the sample placement under the shield after preparation. As such, one sample was exposed to H plasma under Al leaf for 20 minutes and another for 50 minutes in order to have similar total exposure times on the Al leaf to the Pd leaf. For reference the results of 5 and 30 mins SHP with a prepared Pd leaf is also shown in Figure 42.

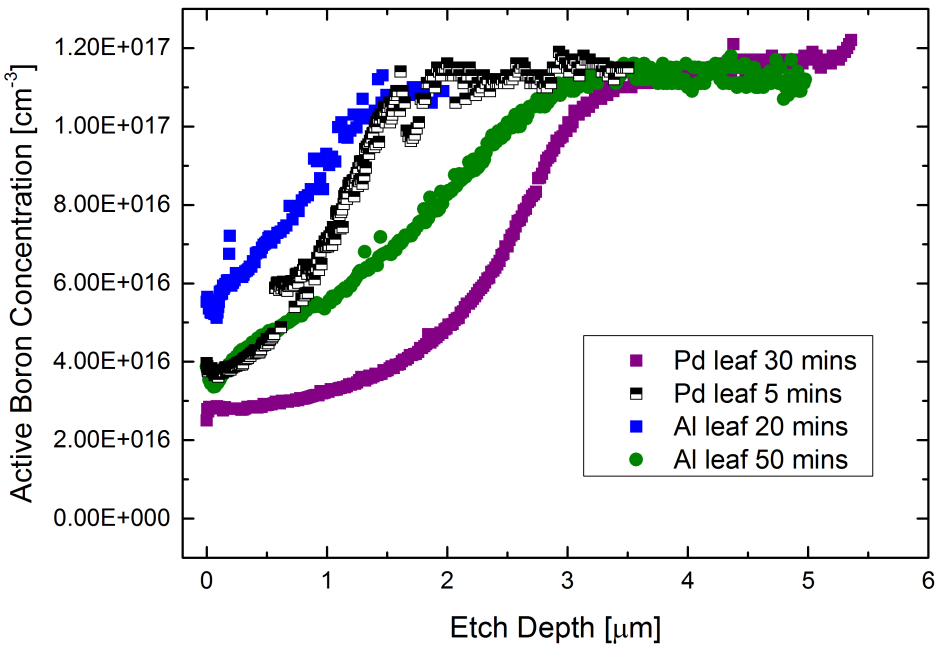


Figure 42 Active B concentration against etch depth measured with eCV. Four samples exposed to shielded H containing plasma at 200 °C for varying times and using different shields.

Standard prepared Pd leaf for 30 mins and 5 mins shown as purple squares and half black squares. Al leaf for 20 and 50 mins shown as blue squares and green circles.

Table X Total level of H deactivating B with Pd leaf and Al leaf

Shield material	Exposure time	[H-B] / cm^2
Pd leaf - prepared	5 mins	$0.91 \pm 0.03 \times 10^{13}$
Pd leaf - prepared	30 mins	$2.35 \pm 0.2 \times 10^{13}$
Al leaf	20 mins	$0.55 \pm 0.03 \times 10^{13}$
Al leaf	50 mins	$1.37 \pm 0.2 \times 10^{13}$

It can be seen from Figure 42 that the 100 nm Al leaf allowed the release of atomic H as a decrease in the level of active B concentration in both the 20 min and 50 min sample is seen. The total level of B deactivated, and therefore a lower limit for the amount of H introduced in the samples, is shown in Table X. It can be seen that exposing the Si sample to a H containing plasma protected by an Al leaf for 50 mins results in 2.5 times more B deactivated than exposing the sample under Al leaf for 20 mins. Compared to the result obtained using a prepared Pd leaf, there are 1.7 times fewer B deactivated in the 50 min Al leaf compared to 30 min exposed (plus 20 mins prepared) Pd leaf. The Al leaf is 100 nm which was calculated as unable to sustain the potential 1 atm pressure difference in the in-line SHP design. A thicker Al shield was tried next.

5.2.6 Aluminium Foil

A 25 μm thick Al was used as the shield in the results presented in Figure 43. The foil was standard "kitchen foil" which is 99% pure Al. It is 250 times thicker than the Al leaf used in Figure 42. Unlike Pd leaf, the Al foil was not prepared by exposing it to the H containing plasma prior to the SHP experiment.

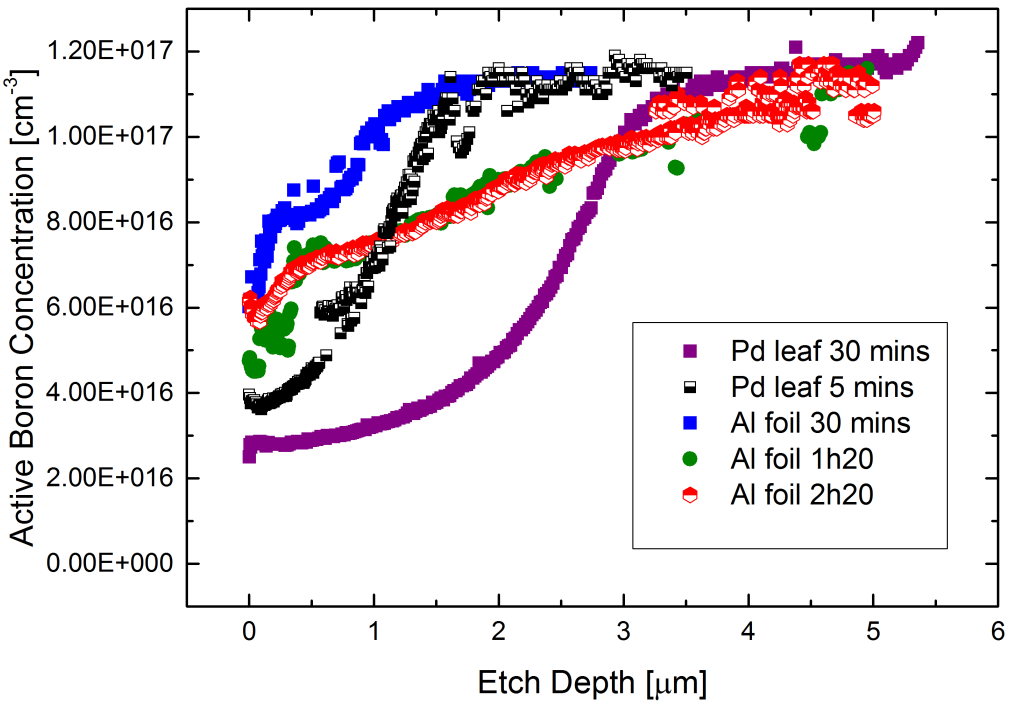


Figure 43 Active B concentration against etch depth measured with eCV. Five samples exposed to shielded H containing plasma at 200 °C for varying times and using different shields. Standard prepared Pd leaf for 30 mins and 5 mins shown as purple squares and half black squares. Al foil for 30 min 1h20 and 2h20 blue squares, green circles and half red circles.

Figure 43 demonstrates that 25 μm thick Al foil allows atomic H introduction into B-doped Si, as the B concentration of all H-exposed samples decreased after SHP treatment. Trapezoidal integration was performed on the eCV results using a background B concentration of 1.17 x 10^{17} /cm^3, to calculate the total level of B-H, this is displayed in Table XI.

Table XI Total level of H deactivating B with Pd leaf and Al foil

Shield material	Exposure time	[H-B] / cm^2
Pd leaf - prepared	5 mins	0.91 ± 0.03 x 10^{13}
Pd leaf - prepared	30 mins	2.35 ± 0.2 x 10^{13}
Al foil	30 mins	0.41 ± 0.03 x10^{13}
Al foil	80 mins	0.96 ± 0.03 x 10^{13}
Al foil	140 mins	0.98 ± 0.02 x 10^{13}

It can be seen that an 80 mins exposure to the H containing plasma using Al foil as the shield is roughly equivalent to a 5 mins exposure using a prepared Pd leaf, meaning that Al foil introduces H into Si at a rate 16 times slower. The amount of H bonded to B after 80 mins using Al foil is 2.35 times greater than after 30 mins.

It is interesting to observe that after 80 mins of exposure time, the H-B level seems to plateau and not much more B is deactivated even if the sample is exposed for 140 mins instead of 80. This saturation effect is also seen using Pd leaf after 45 mins of exposure time. This can be explained by what is considered the rate limiting step. It seems that H transport through the shields is not limiting the introduction of H into Si. Instead, it may be the release of H from the lower surface of the shields, or the introduction of H into bulk Si from the surface. These processes would reach a maximum rate of H-introduction. If this is paired with a competing process such as the dissociation of H-B pairs, or the formation of H-dimers after a certain concentration is reached, the overall level of H-B pairs recorded would be independent of exposure time.

5.2.7 Nickel Foil

It was shown in Figure 38 that many transition metals had high enough permeability and diffusivity to H to be considered as candidates for SHP shields. Ni is about 3000 times cheaper than Pd but has a H diffusivity of $5.6 \pm 0.5 \times 10^{-10}$ cm^2/s [208][3] compared to $2.83 \pm 0.05 \times 10^{-3}$ cm^2/s for Pd. Although this diffusivity is much less than H in Pd, the diffusion rate of H in the shield's bulk is not thought to be the rate limiting step. As such, Ni foil was considered, the results are shown in Figure 44. The Ni foil was 10 μm thick and was prepared and S poisoned as per Section 3.5.3.

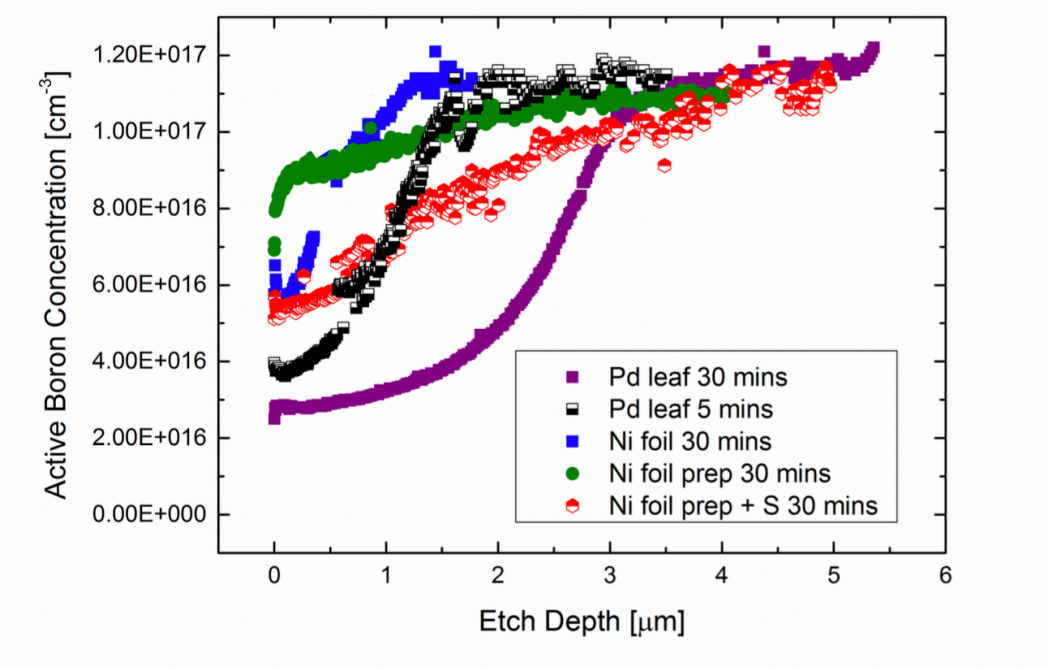


Figure 44 Active B concentration against etch depth measured with eCV. Five samples exposed to shielded H-containing plasma at 200 °C for varying times and using different shields.

Standard prepared Pd leaf for 30 mins and 5 mins shown as purple squares and half black squares. Ni foil for 30 mins not prep, prep and S poisoned shown as blue squares, green circles and half red circles.

Table XII Total level of H deactivating B with Pd leaf and Ni foil

Shield material	Exposure time	[H-B] / cm²
Pd leaf - prepared	5 mins	$0.91 \pm 0.03 \times 10^{13}$
Pd leaf - prepared	30 mins	$2.35 \pm 0.2 \times 10^{13}$
Ni foil	30 mins	$0.34 \pm 0.02 \times 10^{13}$
Ni foil – prepared 20 mins	30 mins	$0.70 \pm 0.02 \times 10^{13}$
Ni foil – prep + S poison	30 mins	$0.96 \pm 0.02 \times 10^{13}$

It can be seen that H is introduced into Si using another metal than Pd as a shield, in this case Ni, shown in Figure 44. The samples chosen for this set of experiments investigated surface preparation rather than time. Pre-exposure of the Ni foil to the plasma increases the level of H in Si by 50% whilst preparation with S poisoning increased it by 64%. Compared to the standard Pd leaf 30 mins level of H, the best Ni result is 59% less effective at introducing H than Pd. There

are some concerns regarding Ni contamination in Si however, as the solubility and diffusivity of Ni in Si reaches a concerning level with temperatures above 600 °C [209]. Ni is known to be a harmful contaminant in Si, and as such should its use should be questioned if the SHP process is to be conducted at higher temperatures.

5.2.8 Platinum Leaf

The last metal that was tested as a SHP shield was Pt. Although it is an expensive metal it is half the price of Pd (April 2019 stock market prices). The results are shown in Figure 45, similarly to Ni foil, the 100 nm Pt leaf is tested as is, prepared via a 30 min plasma exposure, and S-poisoned.

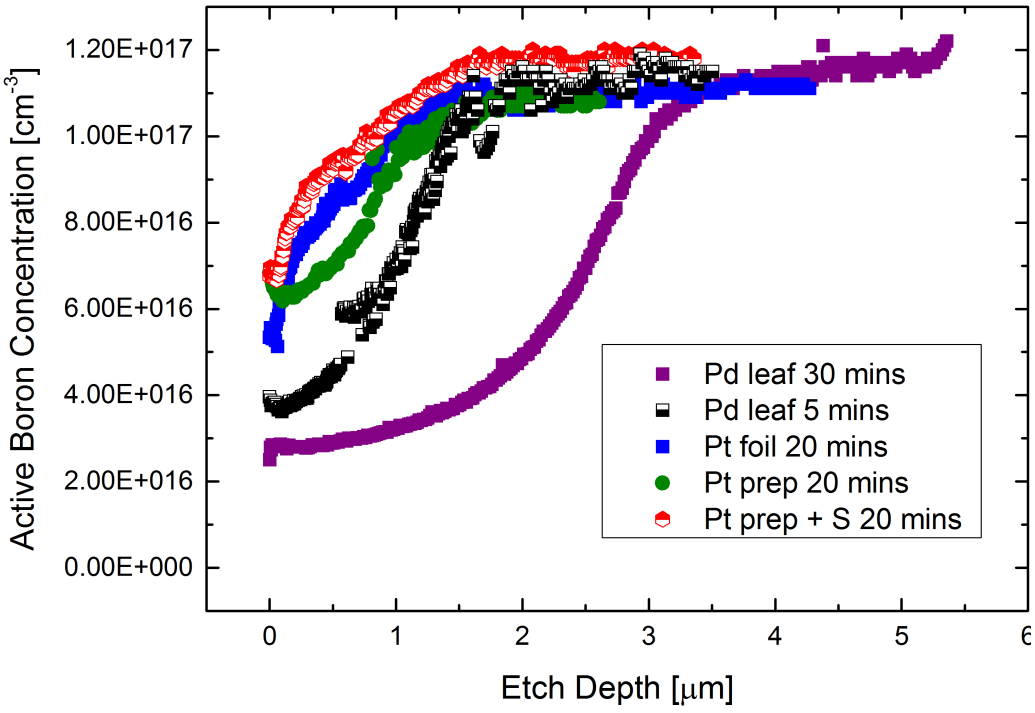


Figure 45 Active B concentration against etch depth measured with eCV. Samples exposed to shielded H-containing plasma at 200 °C for varying times and using different shields. Standard prepared Pd leaf for 30 mins and 5 mins shown as purple squares and half black squares. Pt leaf for 30 mins not prep, prep and S poisoned shown as blue squares, green circles and half red hexagons respectively

Table XIII Total level of H deactivating B with Pd leaf and Pt leaf

Shield material	Exposure time	[H-B] / cm²
Pd leaf - prepared	5 mins	$0.91 \pm 0.03 \times 10^{13}$
Pd leaf - prepared	30 mins	$2.35 \pm 0.2 \times 10^{13}$
Pt leaf	30 mins	$0.41 \pm 0.05 \times 10^{13}$
Pt leaf – prepared 20 mins	30 mins	$0.56 \pm 0.03 \times 10^{13}$
Pt leaf – prep + S poison	30 mins	$0.3 \pm 0.02 \times 10^{13}$

Pt leaf is shown to allow atomic H through and into B doped Si. The quantities observed to deactivate B through eCV are in line with the Al and Ni shields. Indeed, the non-prepared 30 mins exposure using Pt introduced 19% more H than Ni and approximately the same level as Al foil. These results are to be expected as the room temperature diffusivity of H in Pt is similar to that of Ni and Al at $2.3 \pm 0.3 \times 10^{-9}$ cm²/s compared to $5.6 \pm 0.5 \times 10^{-10}$ cm²/s for Ni and $1.7 \pm 0.45 \times 10^{-10}$ cm² /s for Al [210].[4]. When the Pt foil is prepared for the standard 20 mins, the level of H deactivating B increases by 38%. When the leaf is S poisoned however, the level decreases by 27% compared to the unprepared leaf. This was unexpected.

5.2.9 Summary of Different Metallic Shields

As shown in the previous sections, Pd is not the only potential metal for use as a plasma shield for SHP. Many metals [136], [170], [203] have non negligible permeability and diffusivity to H and a few of the more accessible ones were tested in these experiments. A summary of the results is shown in Table XIV.

Table XIV Summary of total level of H deactivating B

Shield material	Exposure time	[H-B] / cm²
Pd leaf - prepared	5 mins	$0.91 \pm 0.03 \times 10^{13}$
Pd leaf - prepared	30 mins	$2.35 \pm 0.2 \times 10^{13}$
Al leaf	20 mins	$0.55 \pm 0.03 \times 10^{13}$
Al leaf	50 mins	$1.37 \pm 0.2 \times 10^{13}$
Al foil	20 mins	$0.41 \pm 0.03 \times 10^{13}$
Al foil	80 mins	$0.96 \pm 0.03 \times 10^{13}$
Al foil	140 mins	$0.98 \pm 0.02 \times 10^{13}$
Ni foil	30 mins	$0.34 \pm 0.02 \times 10^{13}$
Ni foil – prepared 20 mins	30 mins	$0.70 \pm 0.02 \times 10^{13}$
Ni foil – prep + S poison	30 mins	$0.96 \pm 0.02 \times 10^{13}$
Pt leaf	30 mins	$0.41 \pm 0.05 \times 10^{13}$
Pt leaf – prepared 20 mins	30 mins	$0.56 \pm 0.03 \times 10^{13}$
Pt leaf – prep + S poison	30 mins	$0.3 \pm 0.02 \times 10^{13}$

Although none of the metals tested have shown B-deactivation levels of more than half the figures reported with a prepared Pd leaf, the levels are encouraging. Optimisation of the SHP process using these different metals would lead to greater levels of H introduced into Si than the levels reported in this thesis. The price advantage, sometimes 3000 times cheaper for Ni, is crucial for industrial application, and as such positive results from materials such as Al foil is extremely promising. Additionally, as Chapter 6 will introduce, overly high concentrations of H such as those introduced using Pd-SHP can sometimes cause H-related defects in Si. As such, metals that limit the concentration of H introduced at temperatures below 400 °C may offer more control than a highly diffusive metal such as Pd.

5.3 SHP Compared to Common Hydrogenation techniques

The efficacy of SHP using Pd and other metals has been shown in Chapter 4 and the previous sections. It is interesting to compare SHP with other known hydrogenation techniques, namely direct plasma, H_2 anneal, wet hydrogenation, fired SiN_x and remote plasma.

5.3.1 Direct Plasma

One of the key advantages of SHP is its ability to introduce atomic H for passivation without causing any surface damage. Direct plasma on the other hand, causes a lot of surface damage as explained in Chapter 2 Section 2.1.4.4.2. These two processes are interesting to compare from a passivation quality point of view. To do this, n-type 1 Ω.cm Fz Si with 10 nm and 100 nm SiO_2 dielectric layers, as per the standard sample shown in Chapter 3 Section 3.5 , were exposed to a shielded H-containing plasma in the PECVD chamber. The lifetimes of the samples were measured prior to any plasma exposure using the Sinton Lifetime measurement tool. The samples were either exposed to the plasma directly or exposed under a Pd-Ag foil shield using standard SHP parameters at 350 °C for 45 mins on each side. The results are depicted in Figure 46.

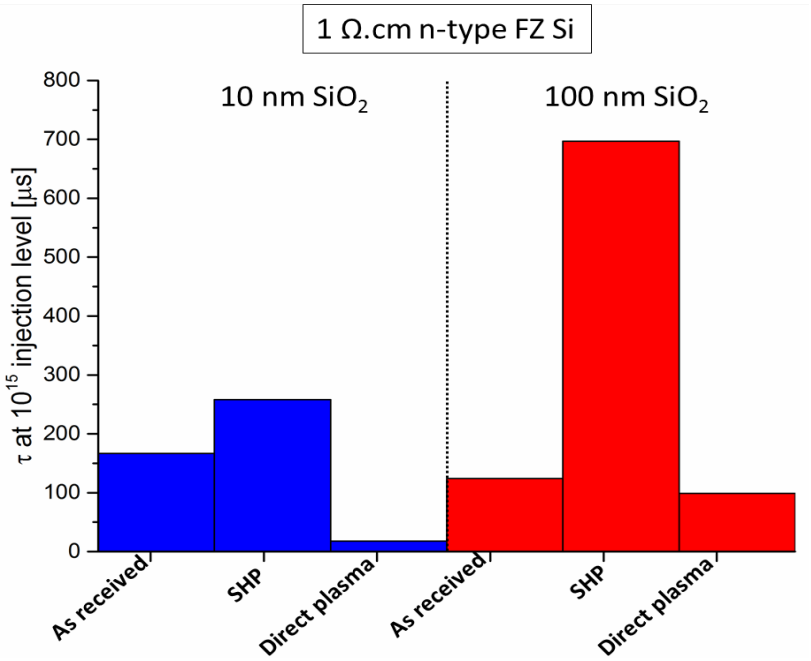


Figure 46 Minority carrier lifetime at 10^{15}/cm³ injection level for 10 nm and 100 nm SiO_2.

Figure 46 shows the difference in lifetime on both 10 and 100 nm SiO_2 when exposed to a direct plasma compared to a shielded plasma. For the 10 nm oxide, the lifetime measured prior to any process was 160 µs at 10^{15} cm^{-3} injection level, but when it was exposed to a H-containing plasma shielded by a prepared Pd leaf for 45 mins at 350 °C the lifetime rose to 260 µs at 10^{15} cm^{-3} injection level. When another 10 nm SiO_2-Si sample was instead exposed to the plasma directly the lifetime decreased from 160 to 15 µs at 10^{15} cm^{-3} injection level. Similarly, with the 100 nm SiO_2 coated sample, the lifetime rose from 140 µs to 710 µs at 10^{15} cm^{-3} injection level with SHP but decreased to 100 µs when exposed to the direct plasma. This constitutes strong evidence that the damage-free quality of the SHP process is much higher than the direct plasma approach. Additionally, as is shown in Figure 47, the lifetime of a direct plasma exposed sample does not improve considerably after corona charge.

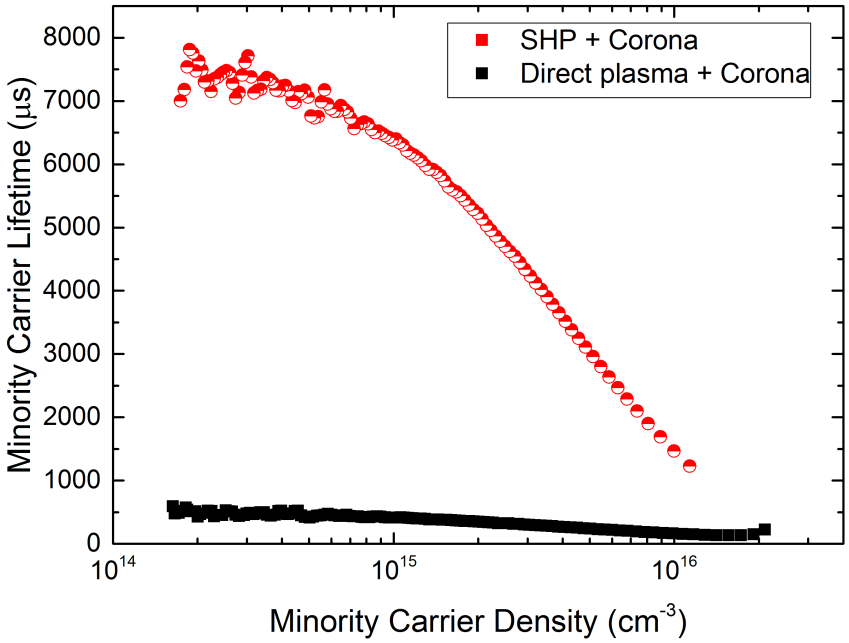


Figure 47 Minority carrier lifetime versus injection level for n-type 1 Ω.cm Fz Si with 100 nm SiO_2. Sample exposed to SHP at 350 °C for 45 minutes under prepared Pd-Ag foil is shown as red squares. Sample exposed to direct plasma at 350 °C for 45 minutes is shown as black squares. Both samples were corona charged for 60 s at 30 kV.

This indicates that the lifetime improvement that is seen with SHP is not due to any deposited charge on the surface, which was corroborated by the absence of charge at the interface directly after SHP exposure using KP equipment. Indeed, if surface charge alone improved the interface passivation quality, it would also do so on the direct plasma sample, which is not the case. The low lifetime of the direct plasma sample of just 550 µs at 10^{15} cm^{-3} injection level compared to the SHP sample with a 6.3 ms lifetime, also shows the extent of the damage caused by the plasma.

5.3.2 H_2 Anneal

Another common method of introducing atomic H into Si for the extrinsic passivation is a forming gas anneal [96]. Typically, a forming gas is a mixture of H_2 and N_2 gas, in the ratio N_2:H_2, 96:4, and this technique is performed at a high temperature of above 400 °C [211]. As previously discussed, many Si solar architectures such as silicon heterojunctions and organic solar cells cannot sustain

such high temperature processes [212], [213], so an alternative low-temperature hydrogenation technique was needed; such as SHP. Highly B-doped p-type single crystal Si was used to compare the efficacy of forming gas anneals to SHP. The first batch of samples were exposed to pure H_2 gas in a tube furnace at 200 °C for 30 minutes. The second batch of samples were exposed to an NH_3 plasma in the PECVD at 200 °C for 30 minutes, protected by a prepared Pd leaf using SHP. The eCV results are shown in Chapter 3 when testing if H_2 would dissociate on the surface of bare Si at 200 °C, the total H-B pairs calculated using trapezoidal integration are shown in Table XV.

Table XV Total level of H deactivating B using SHP Pd leaf and H2 anneal

Shield material	Exposure time	[H-B] / cm^3
Pd leaf - prepared	30 mins	$2.35 \pm 0.2 \times 10^{13}$
H_2 anneal	30 mins	$0.36 \pm 0.02 \times 10^{13}$

As is shown in Table XV, SHP at 200 °C is much more effective than an anneal in pure H_2. SHP introduces 6.5 times more H than the H_2 anneal under these conditions.

5.3.3 HF Dip

It is known from the literature that acidic solutions, particularly those involving HF, can passivate Si though the introduction of atomic H [214]–[216]. As such, when SHP was first being tested at the start of this doctorate it was thought that the H recorded in the Si samples using CV measurements could be from the HF and RCA treatments used to clean the wafers prior to exposure. It was therefore interesting to evaluate HF dips as an atomic H source in Si as well as differentiate between HF-H and plasma-H from SHP. In order to differentiate between hydrogenation from HF or H_2O and SHP, a B-doped Si sample was dipped in 49% HF solution for 5 seconds, then RCA 1 and RCA 2 cleaned before being HF

dipped for a further 5 mins. This process is the standard cleaning process for the B-doped samples used for eCV throughout this thesis. The sample was then placed in the PECVD chamber on a clean wafer, under the Pd shield at 200 °C for 30 mins with the plasma turned off. The second sample was cleaned and HF dipped in the same manner before being SHP treated as usual under the same conditions.

Table XVI Total level of H deactivating B using SHP Pd leaf and HF dip

Shield material	Exposure time	[H-B] / cm²
Pd leaf - prepared	30 mins	$2.35 \pm 0.2 \times 10^{13}$
HF dip + anneal	5 + 30 mins	$0.15 \pm 0.08 \times 10^{13}$

It can be seen that the level of H introduced via wet hydrogenation techniques is negligible compared to SHP which introduces more than one order of magnitude more H.

5.3.4 Remote Plasma

The hydrogenation technique most similar in set-up to SHP is remote plasma as described in Chapter 1. It also uses a plasma source to generate atomic H. Remote plasma avoids surface damage to the Si sample via UV rays by placing the sample in a separate chamber to where the plasma is generated. Atomic H is generated in a separate chamber and then travels down a tube with an L-shaped bend to stop the Si sample from having any direct line of sight with the plasma. In this experiment, samples were exposed to a remote plasma at the University of Manchester, in order to compare to SHP results. The remote plasma was operated at the equipment's maximum power, 70 W and under the following parameters: 625 mTorr with 100 sccm H_2 for 30 minutes at 380 °C. The samples exposed to the remote hydrogenation process were the standard n-type samples with 100 nm SiO_2. The sample was lifetime tested prior hydrogenation and after the remote plasma process. The sample was then corona charged to increase the surface

passivation quality of the oxide and allow for the investigation of any surface or bulk damage. In order to compare this result to one obtained with the SHP technique, a sample from the same Si wafer was exposed to SHP under similar conditions to the remote plasma: 70 W, 625 mTorr with 100 sccm NH_3 for 30 minutes at 380 °C. The PECVD at the Materials Department's cleanroom at Begbroke Science Park is unable to operate with H_2 gas, as such NH_3 had to be used. The extracted lifetime results at 10^{15} cm^{-3} injection level of both samples as well as a control sample which had not treatment are shown in Figure 48.

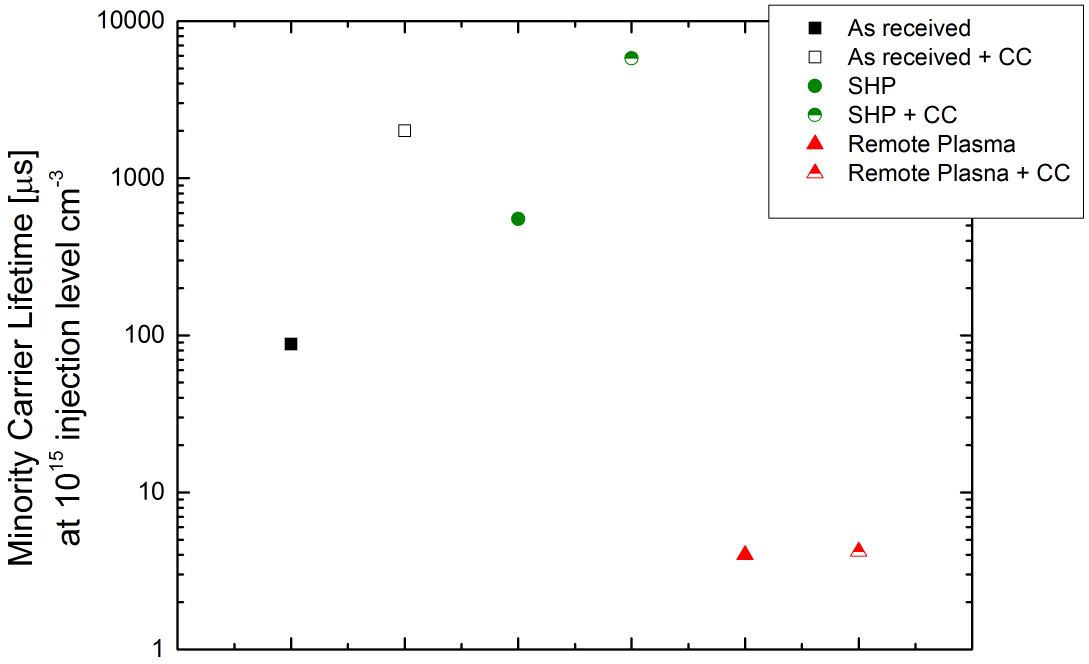


Figure 48 Extracted minority carrier lifetime at 10^{15} cm^{-3} injection level for three sample batches. As received (no H exposure) shown as black square and empty black square post corona charging (CC). SHP for 30 mins at 380 °C with prepared Pd leaf (green circles) and after corona charging (half green circle). Remote plasma 30 mins at 380 °C (red triangle) and after corona charging (half red triangle).

It can be seen in Figure 48 that the lifetime of the remote plasma exposed sample was subjected to a dramatic lifetime decrease from the original 102 µs to 4 µs at 10^{15} cm^{-3} injection level after exposure. Even after corona charging the lifetime of the sample did not increase significantly. KP measurements were taken to ensure the corona charge had applied an expected amount of surface potential. The SHP sample was observed to have -18 V of surface charge after a 60 s standard corona

process. The remote plasma sample only showed -1.2 V. The corona charging was repeated in incremental steps on the remote plasma sample but no higher values of surface charge were obtained. It is believed that the oxide was destroyed during the remote plasma hydrogenation, making it unable to sustain any surface charge and therefore preventing field effect passivation. A broken down oxide could also explain the low lifetime exhibited by the remote plasma sample as the surface passivation would be extremely poor. An alternative hypothesis is that the level of H introduced using remote plasma was high enough to create H-related defects at the interface and in the near surface region.

There are many possible reasons for the break-down of the oxide from remote plasma hydrogenation. Since this technique, unlike SHP, does not contain a metallic membrane allowing for H atoms to be thermalised and neutralised, it is possible that the dissociated H from the H_2 plasma remained highly charged during the remote plasma hydrogenation. An excess charge on the SiO_2 layer could have caused dielectric breakdown as explained in Chapter 2. This is a surprising result as remote plasma hydrogenation has been shown to effectively passivate Si in the literature [117]. Unfortunately, since the equipment was not readily available on site in the laboratory of The University of Oxford, this experiment was not repeated as part of this Doctorate.

For this thesis B-doped samples were also treated with a remote-plasma hydrogenation at Manchester and sent to UNSW for eCV characterization. However, the preliminary results were inconclusive and are being repeated, but obtaining results from this new batch was unfortunately impossible in the time-frame of this doctorate. Instead, remote-plasma effectivity comparison to SHP can be achieved with results from the literature. Hamer published remote-plasma results in his thesis [105], using the industrial, Remote In-line Passivation (RIPA) tool [217], [218]. This remote-plasma operates at high power, of the order of 1 kV to generate H from a plasma. Hamer uses highly B-doped Si and records the level of B deactivated post RIPA process. The p-type Si samples used had a resistivity of 0.05 Ωcm corresponding to a doping concentration of 9.3×10^{17} cm^{-3}. Hamer

reported a level of H-B pairs of the order of 10^{14} cm^{-2} for an 30 mins remote-plasma exposure at 290 °C, which is more than the 2.35 ± 0.2 x 10^{13} cm^{-2} reported using SHP and a prepared Pd leaf. This comparison is not ideal however as the RIPA power was an order of magnitude higher, the process was done at a higher temperature and the p-type sample used also had nearly an order of magnitude more B-atoms than in the SHP experiment. What can be said despite these differences is that the level of H introduced in both techniques is relatively similar considering the differences in B-concentration and thus available H traps.

5.3.5 Fired Silicon Nitride For Hydrogen Release

A common method of introducing H into Si for passivation involves using a H-rich SiN_x dielectric layer on top of Si. The SiN_x contains up to 20 at. % H and also acts as an antireflection coating, and field effect passivation, making it an attractive hydrogenation technique [4-8]. In order to release H into Si from SiN_x, a postdeposition anneal with temperatures above 600 °C is required [219]. The concentration of H that is released from the SiN_x, transitions into Si and able to hydrogenate defects in the bulk of Si is known to be small compared to the concentration of H in SiN_x. This makes H in Si from SiN_x hard to quantify and detect [87]. As such, the mechanisms of fired SiN_x for bulk hydrogenation of defects are not well understood.

Boehme and Lucovsky [220] have hypothesized that bulk hydrogenation does not occur at all using SiN_x layers, whilst Sopori *et al* have calculated from models that the H concentrations near the Si surface could be close to 5 x 10^{16} cm^{-3} [57].

The most comparable set of experiments to SHP, however, were conducted by Stavola *et al,* as they used Pt-doped Si to effectively trap any H released from the annealed SiN_x even at temperatures close to 600 °C [87]. They reported a value for H concentration that lies in the middle of Boehme and Sopori's work

with a H-Pt concentration of 6 x 10^{12} cm^{-2} when the SiN_x was fired at 750 °C for 10 minutes. Seeing as the 80 nm SiN_x layer used in their work contained an estimated H concentration of 1 x 10^{22} cm^{-3}, which corresponds to an areal density of released H of 4 x10^{15} cm^{-3} [221], the H introduced into Si amounts to only 0.15 % of the H released from SiN_x.

Comparing these values to the concentration of H introduced into bulk Si using SHP, it can be seen that even the 5 minutes exposed SHP sample under Pd-Ag foil at 200 °C outperforms the SiN_x sample with a level of H-B pairs of 9.14 ± 0.1 x 10^{12} cm^{-2}. Comparing this with 10 minutes of fired SiN_x (6 x 10^{12} cm^{-2}) [221][52], SHP introduces 1.56 times more H in half of the time and at a much lower temperature. As was shown in the experiments demonstrating the positive relation between H introduction and increasing temperature in Chapter 4 Section 4.3.4, it is expected that SHP would perform better in terms of H introduction at higher temperatures. It is also expected that there exists a maximum H introduction rate which will be dependent upon H desorption and absorption kinetics on the underside of the shield and into Si. This should result in H incorporation into Si reaching a plateau rate with increasing temperature. This work does not address higher temperature SHP processes as the PECVD equipment at Oxford is only rated up to 380 °C.

Another interesting finding from both Stavola and Sopori was the presence of damage caused by PECVD SiN_x deposition [51], [57], [96]. Although the Si surface is only exposed to the direct silane plasma for less than 5 seconds during initial SiN_x deposition, it is enough to cause substantial surface damage which is then subsequently passivated by the H released from the nitride. This is an effect that is completely avoided using SHP and may be a reason why more H is seen deeper in the Si using SHP, as less H is trapped by the surface damage. In industry however, a remote plasma is often used to deposit nitrides to avoid this effect, and using SHP would not make considerable differences to the level of damage.

5.4 DISCUSSION

Chapter 5 has demonstrated that SHP is extremely effective at passivating the interface between SiO_2 and Si on n-type FZ samples. Bonilla *et al* published a review paper in 2017 on the efficacy of different dielectrics for surface passivation, this paper showed the efficacy of SHP compared to many other techniques [186]. Figures from this paper are shown in Figure 49 (a) and (b). The SHP result is highlighted by a blue arrow for clarity.

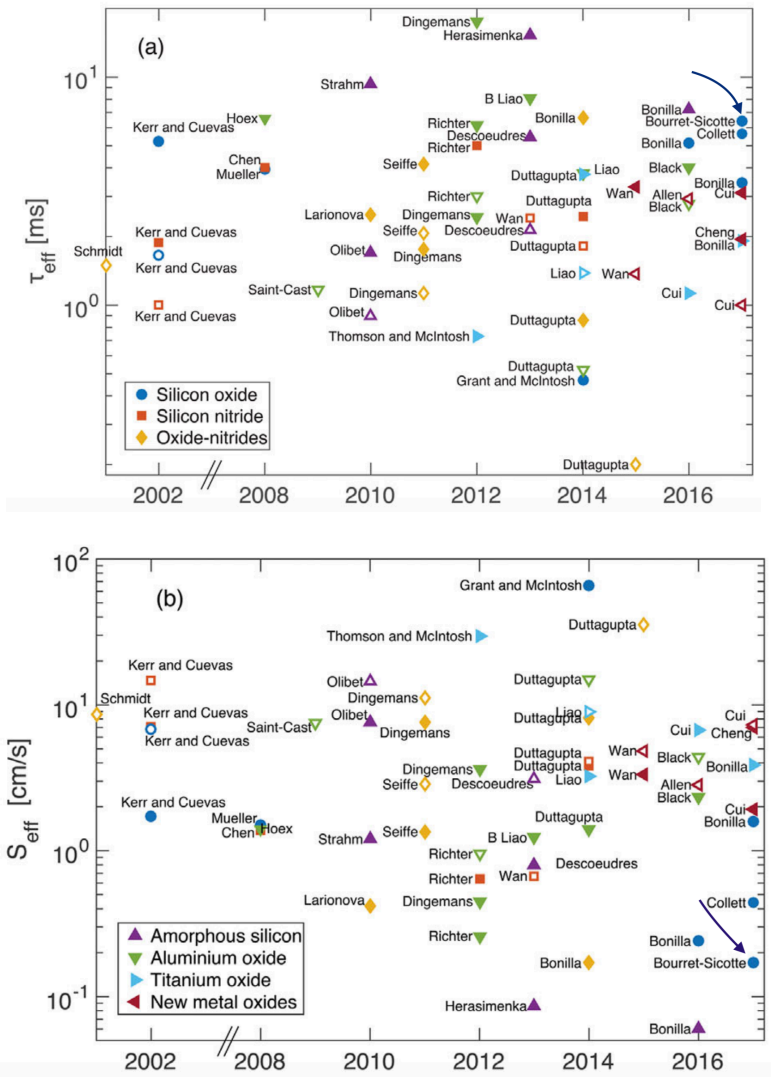


Figure 49 Surface passivation metrics for dielectric coatings developed over the past two decades, for n-type (closed symbols) and p-type (open symbols) Si surfaces. (a) effective lifetime and (b) shows effective SRV. All values of S_{eff} and τ_{eff} are given at $\Delta n = 10^{15}$ cm^{-3},and calculated directly from reported PC τ_{eff} (Δn) measurements [186].

It can be seen from Figure 49 that on single layer SiO_x (closed blue circles), "Bourret-Sicotte" (ie SHP), obtained the highest lifetime of 6.3 ms, as well as the lowest surface recombination velocity with $S_{eff} = 0.24$ cms^{-1}, in 2017. This was an extremely encouraging result as it confirmed the relevancy of SHP as a hydrogenation technique and established a strong argument to convince other research labs to adopt the technique. SHP so far was seen to be low cost, damage-free, easy to implement over a wide range of temperatures, and now an extremely effective passivation technique. One of its drawbacks, however, is the fragile quality of the Pd leaf.

This fragility is of particular importance when the conversion of the current batch process PECVD SHP system to an atmospheric, in-line, system is considered. It was shown that the shield needed to be 11 μm in order to withstand a pressure differential of 0.5 atm in Section 5.2.1.

To remedy this problem, experiments involving other metals as well as a 100 times thicker Pd-Ag foil (10 μm) were demonstrated in Section 5.2 . Results showed that the thicker Pd-Ag worked exceptionally well compared to the 0.1 μm Pd leaf. The Pd-Ag foil showed a level of B-deactivation corresponding to 1.98×10^{13} cm^{-2} compared to 2.35×10^{13} cm^{-2} for the Pd leaf. This corresponds to a H introduction decrease of 18 % between the two shields. The fact that the increased thickness of the Pd shield did not proportionally impede the diffusion of H through the bulk is in line with reported studies of the transport of H through Pd, and specifically an effect known as "superpermeability" [166], [179], [183], [222].

Many published works have reported the phenomenon of Pd superpermeability, which is observed in experimental studies using an atomic H source through a Pd membrane. Superpermeation was investigated in detail by Livshits *et al* in 1975. They coined the term "superpermeability" for systems that have a high diffusivity

for H and are exposed to an atomic H source. The result of superpermeation is a drastically enhanced permeation rate compared to a H_2 source. H_2 coming in contact with the surface of Pd usually undergoes dissociative chemisorption, which has a high activation energy and presents a high energy barrier for molecules [199]. When the Pd membrane, or in the case of SHP, leaf or foil, is exposed to an atomic H source, the activation energy for non-dissociative adsorption is much lower which results in much higher concentration of H in the bulk Pd. Since this superpermeation results in bulk saturation of H in Pd, and since the transport of H through Pd is extremely fast [166], [179], [183], the rate limiting step is the desorption on the lower surface. As such the thickness of the Pd does not largely affect the concentration of H desorbing from its lower surface and nor the level of H-B seen using the foil compared to the leaf when an atomic H source is used.

The efficacy of different metals such as Ni, Pt and Al foil/leaf is also presented in Section 5.2.2. These metals were chosen for their relatively high diffusivity to H as well as their ease of accessibility and cost. The different metals behaved as expected for the most part, with the most H diffusive ones showing highest levels of H-B pairs in the tested Si samples on the eCV instrument. Al foil behaved slightly surprisingly, as despite its low diffusivity rate of $1.7 \pm 0.45 \times 10^{-10}$ cm^2 /s [1] compared to H in Pd at $2.83 \pm 0.05 \times 10^{-3}$ cm^2/s, it showed levels of H introduction into Si which were 16 times slower than using Pd foil. Although this is much slower than Pd it is surprisingly large, given the 7 orders of magnitude difference in their diffusivity rates. This once again suggests the rate limiting step of the H transport system in SHP is not the diffusion through the bulk of the shield.

Although only a select few metals were tested during this doctorate, there are many more suitable candidates for use as an SHP shield. Since the S-poisoning experiment in Chapter 4 Section 4.3.6.2, showed that the catalytic property of Pd was not a requirement for effective introduction of H into Si, many metals

would indeed be suitable. There is extensive literature available on the diffusivity of H through different metals, as well as their permeability. Vanadium, Niobium and other group V metals have shown extremely high permeability to atomic H but are typically not used for H purification membranes. The reason for this is the phase change they undergo upon exposure to H, which is similar to the one seen in Pd, and become excessively brittle [222]. Nishimuri *et al* have demonstrated, however, that alloying V-Ni allows for the phase change to be suppressed in a similar manner to Pd-Ag [223]. This has enabled experiments, such as ones conducted by Amano *et al,* on the characterisation of H permeation through Pd plated V-Ni-Y alloys (composition 15: 84.95: 0.05) [224]. They have found permeation values in the range of 2 to 8 x 10^7 mol/msPa$^{1/2}$, which is similar to that of Pd (8.11 x 10^7 mol/msPa$^{1/2}$) but these alloys have the added benefit of being much cheaper as they are composed mostly of Ni.

Since an in-line process would require large areas of metallic shield, cost will be considered of great importance, making cheaper V-Ni-Y alloys very interesting. These metals were either too expensive or hard to obtain, and thus were considered beyond the scope of this doctorate.

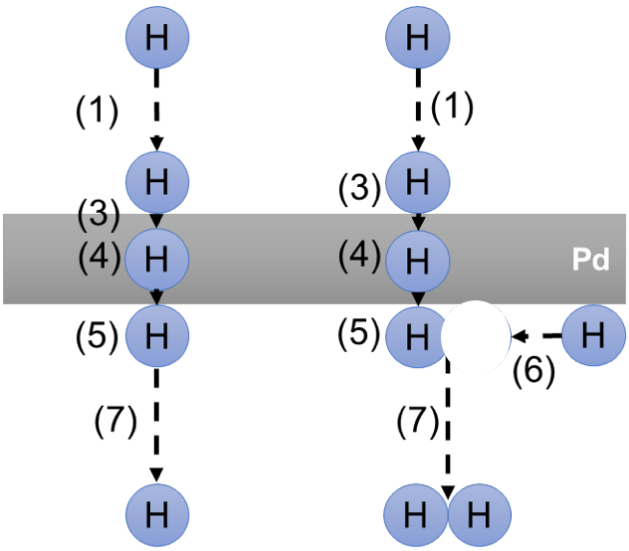
Section 5.3 evaluated SHP's efficacy as a passivation technique compared to other common hydrogenation techniques. Levels of atomic H introduced into B-doped Si were used to compare the techniques. SHP was compared to a pure H_2 anneal, direct plasma exposure, HF dips and fired SiN_x dielectrics. On all accounts, higher concentration of atomic H was recorded at 200 °C using Pd-Ag foil SHP and an NH_3 plasma generating atomic H. The comparison of SHP to remote plasma hydrogenation was conducted using surface passivation improvements on minority carrier lifetimes. The remote plasma sample hydrogenated at the University of Manchester was seen to have a much poorer lifetime than the SHP sample. A more in depth study using eCV characterization is expected to give more comparative results. This is expected to occur as part of the further work of this doctorate.

It is interesting to compare SHP's levels of H-B pairs of 2.35 x 10^{13} cm^{-2} with Stavola's results using fired SiN_x layers [87]. By using Pt-doped Si they were able to effectively capture atomic H forming Pt-H complexes which are stable at temperatures up to 650 °C. This is an interesting finding for SHP's future, as using Pt-doped Si would allow for H concentration tests to be conducted at above the 200 °C limit of H-B pairs. Stavola *et al* concluded that only 0.15 % of the H contained in the H-rich SiN_x layer was actually incorporated into the bulk of Si. This resulted in a H-Pt concentration of 5 x 10^{12} cm^{-2} which is almost 5 times less H than what was seen with SHP and Pd leaf. The difference could be attributed to the different capture efficacy of Pt compared to B. However, both dopants are said to effectively trap most if not all H at their respective temperatures of 600 °C and 200 °C [87]. As such, it seems that most of the H contained in SiN_x out-diffuses back into the atmosphere. This is likely since the energy barrier between SiN_x-Si is higher than SiN_x-air as observed by Boehme *et al* [225].

It is also possible that the H released from dielectrics does not transition to the bulk as it may be trapped at the interface by defects. Indeed, Sopori *et al* have published multiple papers observing the damage associated with PECVD deposition of nitrides. Since the bare Si sample is exposed to a direct plasma, albeit for a few seconds, before the first layer of SiN_x can be deposited, substantial surface damage is observed. This was consistent with the surface damage seen with a direct plasma hydrogenation technique and included surface pitting and hard UV damage. Both of these processes are known to create surface traps which will capture a fraction of the H released by the dielectric [226], [227]. This fraction, however, is expected to be small as the damaged layer was reported to only be of the order of 0.1 μm [228]. This plasma induced surface damage is, of course, not seen using Shielded Hydrogen Plasma Passivation, but the difference in surface-trapped H is nowhere near enough to make up the five-fold difference seen between the two techniques. As such, it can be said that SHP introduces considerably more atomic H into Si than most other common techniques, even at

the low temperature of 200 °C. Furthermore, a post SHP high temperature anneal may increase the rate of H-incorporation from the interface to the bulk. This may increase the bulk-passivation quality of the SHP process.

The results presented in this Chapter have shown that for most shields, H-diffusion through the bulk of the metal was not the rate limiting step. This brings to question the system's rate limiting step and how to increase the concentration of H in Si further. The H-transport mechanism introduced in Chapter 4 is considered once more, and the schematic is included in oppoFigure 50 for clarity.



oppoFigure 50 Schematic of H transport through Pd shield using atomic H source

Results presented in Chapters 4 and 5 have given a strong indication as to which step may be rate limiting. If we consider step (1) and (3), which are the diffusion of H into the Pd leaf and its transition from surface to bulk Pd, the concentration of atomic H reaching the upper surface of the Pd leaf is governed by plasma parameters such as chamber pressure and RF power. Chapter 4 Section 4.3.5 has shown that varying these parameters does not result in considerable improvements in either H-B pairs or lifetime improvements, suggesting steps (1) and (3) are not rate limiting. The transport of H across bulk Pd, shown as step (4) in oppoFigure 50, is unlikely to be rate limiting as shown by the similar level of H-B obtained using the 100 times thicker Pd-Ag foil compared to Pd leaf in Figure 41. Step (6) only occurs when H undergoes recombinative desorption

leaving Pd as H_2. It is known from the literature and the H_2 anneal result, that H_2 does not dissociate on the surface of Si at 200 °C. As such, step (6) on its own will not be a rate limiting step as the H_2 released would not be introduced into Si.

Increasing the temperature is shown, in Chapter 4 Section 4.3.4, to increase the level of detected H-B pairs. Temperature increase could affect many steps when considering the entire system of H introduction into bulk Si - incorporation into the oxide, diffusion through oxide, movement across the oxide-Si interface, and diffusion through the bulk Si. However, if the H-Pd system is first considered in isolation, temperature change would affect step (5). It is postulated that once H has transitioned from bulk to the lower surface of the Pd shield, it can either leave the surface as H or recombine. It is likely that an increase in temperature would increase the energy of H at the lower Pd surface and increase the probability of it leaving the leaf in its atomic form, thus increasing the concentration of atomic H available to enter Si. Another method to increase the concentration of H underneath the Pd leaf, which would also be a good test to confirm whether or not step (5) is rate limiting, would be to increase the surface area of the Pd shield. Surface roughening would increase the surface area by at least two-fold, which would increase the number of sites available for H to occupy when it transitions from bulk to surface Pd. This test was not done in this thesis, but it is something the group at Oxford University is planning for future work.

Considering the rate limiting steps for the entire H-Pd-SiO_2-Si system is far more complex. One step that is of particular interest, however, is the transition of H across the interface of the SiO_2 dielectric and the bulk of Si. This is considered in detail in Chapter 6.

CHAPTER 6 The use of SHP to Study H-related Defects

Chapters 4 and 5 have introduced the use of a Shielded Hydrogen Plasma (SHP) as a successful method for the passivation of Si. SHP introduces atomic H at low temperatures with no observable surface damage. In Chapter 5, SHP was compared to other hydrogenation techniques, such as post-deposition annealed SiN_x, FGA anneals and Remote Plasma. The possibility of adapting the current batch-design SHP to an in-line process was considered in Chapter 5. To this end, more durable and less costly alternative shields were tested. This Chapter applies SHP as an effective H-introduction tool to study H-related defects in Si, and the movement of H in SiO_2-Si and across that interface.

6.1 Effect of SHP on Bare and Ionic FEP Si

The results presented in Chapter 6 show the effect of hydrogenation using SHP on bare Si samples, as well as samples which have undergone an ionic field effect passivation (FEP) process. Initially unexpectedly, the minority carrier lifetime of the bare Si samples and the ionic FEP samples exposed to SHP dramatically decreases. This goes against the positive passivation effects seen in Chapters 4 and 5. The following Section 6.1.1 presents the results obtained.

6.1.1 Hydrogen Related Defects in Bare Si

In order to investigate the effect of H in Si, with minimal complications due to other crystal defects, n- and p-type float zone Si was used, wafers were 200 μm thick with a resistivity of 1 Ω·cm. For bare Si samples, any oxide was removed using a hydrofluoric acid, HF, dip. The samples were then RCA cleaned followed

by a second HF dip to minimize any oxide present immediately prior to hydrogenation.

The process flow for the samples is shown in Figure 51. The SHP treatment was conducted by exposing the samples for 30 mins at 350 °C in a PECVD, Oxford Instruments Plasmalab Plus 80, with an NH_3 plasma at the following conditions: 100W RF power, 650 mTorr chamber pressure, 100sccm NH_3 gas and with Pd/Ag foil with a composition of 75:25 and prepared as per Chapter 3 Section 3.5.2.

Specimens were also made under identical experimental conditions except with N_2 being used as the process gas (Shielded N_2 Plasma SNP). The difference between these two sets of specimens is simply that atomic H is produced for the first but not for the second. As-received material (after the oxide strip but with no SHP) was also characterized for comparison.

In order to measure the lifetimes of all bare-Si samples which would otherwise be too low to measure, a SiN_X passivating layer was subsequently deposited using PECVD at 380 °C. The SiN_x recipe was as follows: 380 °C table temperature, 400 mTorr chamber pressure, 20W RF power, 400sccm SiH_4, 20 sccm NH_3 600 sccm N_2. The samples were deposited for 4 mins on either side to obtain a SiN_x thickness of 80 nm ± 5 nm.

The specimens were then corona charged to improve the quality of surface passivation by applying field effect passivation so that bulk effects could be more easily observed [143]. The corona charge was applied in a point-to-plane set-up with a 30 kV bias and 60 s intervals of charge deposition. The resulting surface potentials were measured using a Kelvin Probe and were on the order of 5 V. Effective minority carrier lifetime measurements were carried out with a Sinton Instruments WCT120, with intrinsic recombination calculated using the Richter model [34]. The process flow chart is shown in Figure 51.

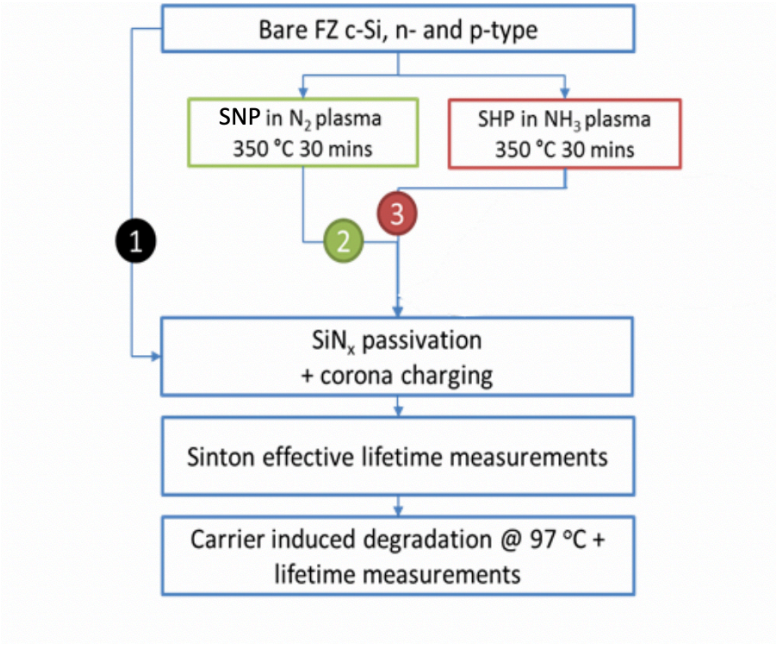


Figure 51 Process flow chart for both n- and p-type FZ Si.

6.1.2 Effects on Bare Si

The results of photoconductance lifetime (Sinton) measurements on bare n-type Si after the processes shown in Figure 51 and before light soaking are shown in Figure 52. The shielded N_2 plasma treatment has very little effect on material lifetime compared to the as-received material. This indicates that at 350 °C, plasma processing and associated UV damage make little or no difference to the sample lifetime when the shield is present. Somewhat unexpectedly however, the lifetime of the n-type sample exposed atomic H using SHP decreased dramatically indicating that the atomic H produced is introducing recombination centres into the Si.

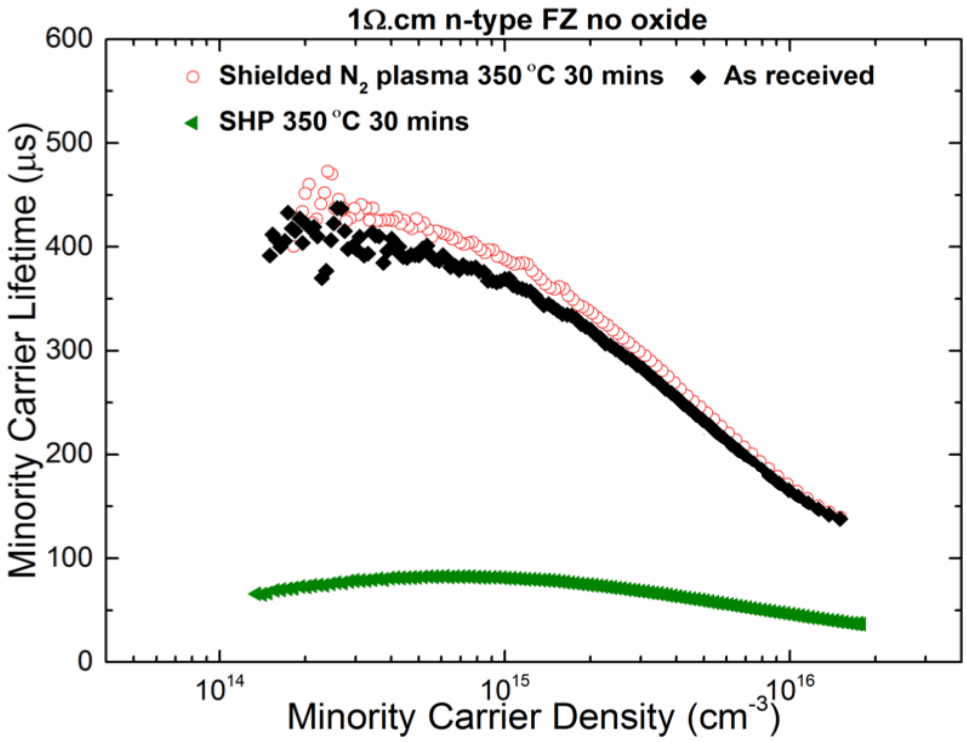


Figure 52 Minority carrier lifetime in µs versus injection level for n-type FZ Si with 50 nm SiN_x coating. As received (black diamonds) is HF dipped with SiN_x. SNP (empty red circles) is HF dipped, SNP 30 mins 350 °C with SiN_x. SHP (green triangles) is HF dipped, SHP 30 mins 350 °C with SiN_x. All samples are corona charged as per [143].

As can be seen in Figure 52, both control samples have very similar lifetimes after SiN_x and corona charging of approximately 380 µs at 10^{15} cm^{-3} injection level. The H-exposed via SHP sample however, has a much lower lifetime of 100 µs even after corona charging. This is a dramatic reduction in lifetime, which is interesting to study.

This experiment was repeated on p-type, using the same conditions as in Figure 51. The J_0 values were extracted from the Sinton Lifetime software as per 3.6.1.1. This is shown in Figure 53.

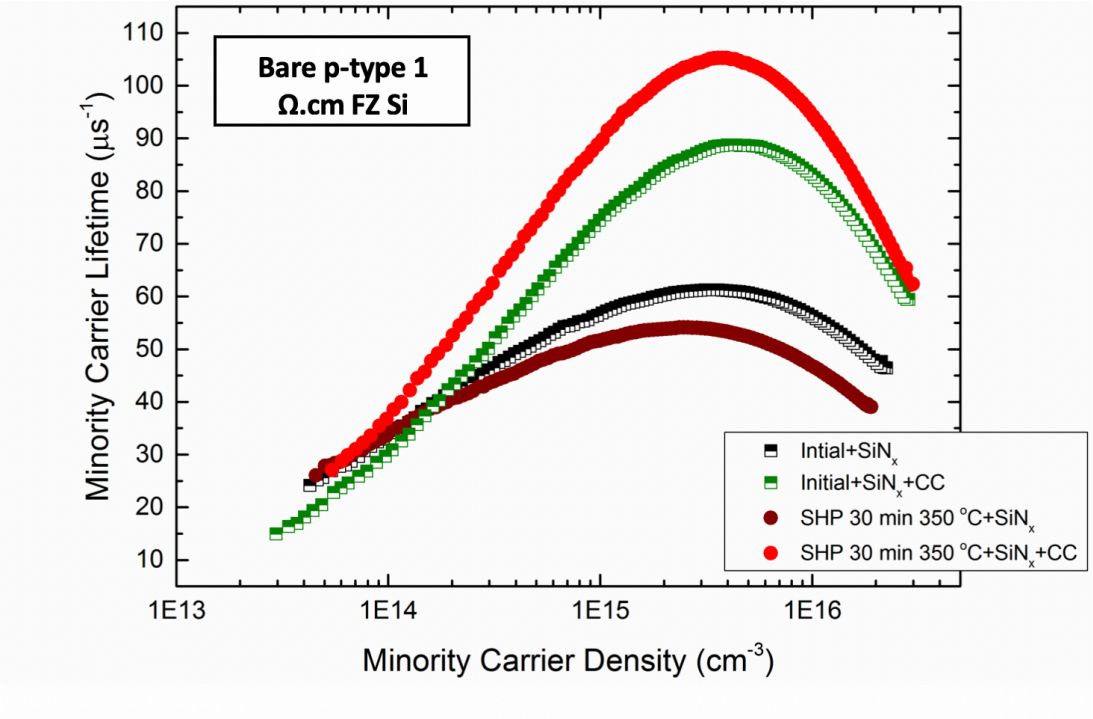


Figure 53 Minority Carrier Lifetime in µs over injection level for p-type FZ Si with a 50 nm SiN_x coating. As-received (black half-filled squares.). As-received with SiN_x and corona charge (CC) (green half-filled squares). SHP 30 mins 350 °C with SiN_x (dark red circles). SHP 30 mins 350 °C with SiN_x and corona charge (red circles). All samples are corona charged (CC) [143].

The J_0 values for the non-SHP samples were 63 fA/cm^{-2} before corona charging and 41 fA/cm^{-2}. The SHP samples had J_0 values of 106 fA/cm^{-2} before corona charging and 48 fA/cm^2 after. As can be seen from Figure 53, the p-type sample does not exhibit the same lifetime reduction behaviour as the n-type sample. The p-type sample had the same HF oxide strip as the n-type sample, however instead of undergoing a dramatic minority carrier lifetime reduction, the sample exposed to SHP has a lifetime of 105 µs which is slightly higher than the control sample's lifetime of 90 µs. However, this is not a very significant difference considering sample-to-sample lifetime variations of ± 20 µs. The J_0 values of both the SHP sample and the control sample show a reduction in recombination at the surface post corona charging as they decrease to 48 fA/cm^2 and 41 fA/cm^2 respectively. These similar J_0 values reflect the similar minority carrier lifetimes recorded. As

such, the improvements in lifetimes seen in both samples can be said to be due to a lower surface recombination level.

6.1.3 Effects on SiO_2 with Ionic FEP

Experiments were also conducted where SHP was performed on n-type Si with 100 nm SiO_2 that had received an ionic FEP treatment. The motivation for these experiments stemmed from other work in the Oxford Semiconductor and Photovoltaic Materials group. Collett and Bonilla have investigated ionic field effect passivation of SiO_2-Si interfaces [83], [144]. In their experiments, they purposefully introduce charged ionic species, such as K^+, at the interface by driving them through the oxide using corona charge and a short anneal. These charged species cause band bending which reduces recombination rates as previously explained in Chapter 2. Collett *et al* have obtained the extremely low surface recombination velocity of 3.3 cm/s using a spin coating technique on 1 Ωcm n-type Si. More details of the experiments can be found in reference [26].

Since ionic FEP has shown extremely promising results as an industrially compatible technique to introduce stable FEP, combining it with SHP to add chemical passivation was an interesting approach to see if even better passivation could be achieved. Ionic FEP was introduced using spin coating as the ionic precursor deposition technique. A solution of KCl and IPA, as per Chapter 3 Section 3.4.1, was used to deposit a uniform layer of KCl ions. For one batch of samples the K^+ ions were driven to the interface by a corona charge deposition of 1.9×10^{12} q/cm^2 followed by a hot plate anneal at 450 °C for 15 seconds. Kelvin Probe (KP) was used between all steps to record surface charge and determine whether the K^+ ions had indeed passed through to the interface. The absence of surface charge after the post corona anneal indicates this as the Cl^- ions dissociate from K^+ and neutralise the corona deposited charge, thus removing the surface charge as shown in [83]. Some samples were then exposed to H under a prepared Pd-Ag foil using standard SHP at a range of temperatures for 40 minutes. Other samples which were used as control samples were exposed to an N_2 plasma under

Pd-Ag foil using the same conditions. The order in which these steps were conducted was varied from sample to sample, as per the process details in Table XVIII. The results are displayed in Figure 54.

Table XVII Summary of Process Steps

Sample number:	Process
1	As-received samples, no processing
2	Spin coating of KCl (not driven to interface) + SHP at 200 °C for 40 minutes on each side + corona charged + 450 °C anneal to drive K^+ to interface + corona charge for max FEP
3	Spin coating of KCl + corona charge + 450 °C to drive K^+ to interface + SHP at 100 °C (blue)
4	Spin coating of KCl + corona charge + 450 °C to drive K^+ to interface + SHP at 150 °C (green).
5	Spin coating of KCl + corona charge + 450 °C to drive K^+ to interface + SHP at 200 °C (orange).
6	Spin coating of KCl + corona charge + 450 °C to drive K^+ to interface + exposure to N_2 plasma (SNP) at 200 °C for 40 minutes on each side + corona charge.

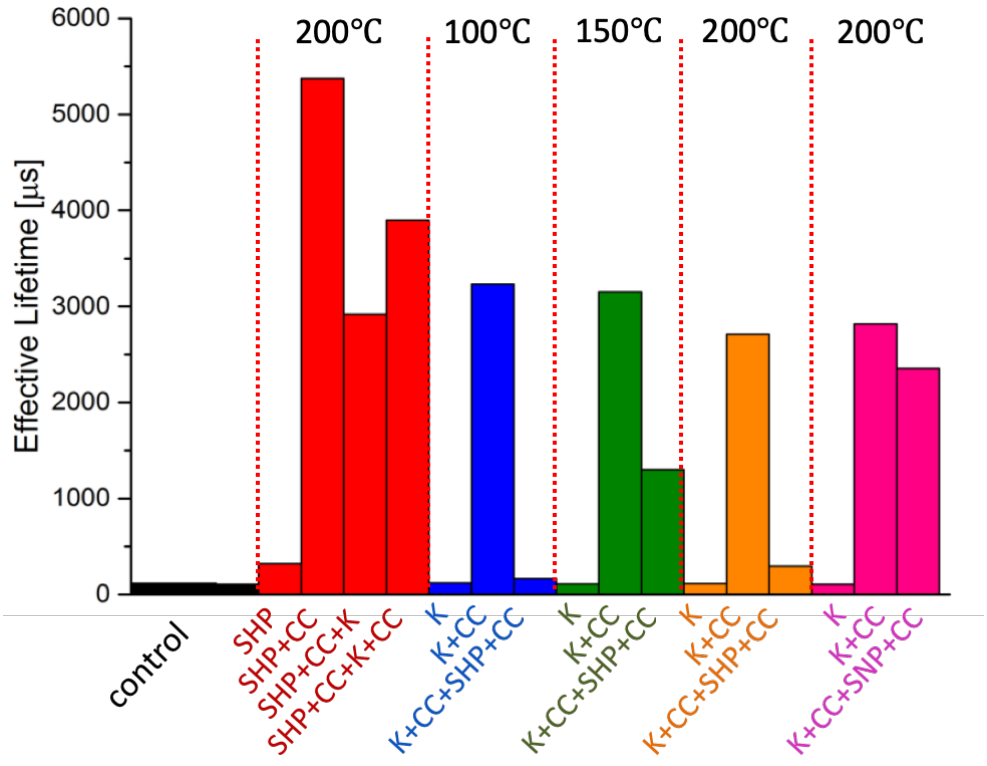


Figure 54 Effective minority carrier lifetime for each sample batch. Control (black), SHP prior to K FEP (red), K FEP prior to SHP at 100, 150, 200 °C (blue, green, orange), K FEP prior to SNP at 200 °C (pink). SHP and SNP were processed under PECVD plasmas for 40 minutes on either side.

The lifetime results seen in Figure 54 were unexpected and interesting. It can be seen that when ions are present at the n-type Si/SiO_2 interface, an exposure to SHP decreases the lifetime in a similar manner to that when SHP is applied on a bare n-type Si surface. When SHP is performed after ionic drift, a drastic lifetime decrease is observed. However, when SHP is performed before ionic drift, the lifetime decrease is much reduced. Indeed, in the samples 3,4 and 5, which have K^+ ions at the interface, SHP treatment at any temperature decreases the maximum FEP lifetime from 3 ms to below 50 μs. When SHP is conducted before the K^+ ions are at the interface, however, as seen in red, the lifetime remains much higher at 4 ms. Although this is indeed a high lifetime, it is still lower than the SHP + CC lifetime of 5.2 ms. This small reduction is thought to be caused by the presence of ions at the interface introducing a small number of defect states, and the interface quality, as shown in [83]. The reduction in chemical passivation limits the achievable lifetime when charge is maximised.

There are several possible causes for the lifetime reduction of the samples with ions at the interface and SHP exposure.

It could be hypothesised that the 80 minutes anneal during SHP is the cause of reduced FEP efficacy due to K^+ migration from the interface by thermal diffusion. However, the SNP sample which has undergone the same temperature treatment with K ions at the interface does not exhibit such a dramatic lifetime decrease with a final value of 2.5 ms. As such the lifetime decrease is not thought to be a temperature effect.

Another possible explanation is that the introduced H from SHP is bonding with the K^+ ions and therefore removing interface charge. If H was passivating K^+ ions, or the thermal process was driving the ions away from the interface we would expect to observe a reduction in interface charge. This was not the case as shown in Figure 55. The final explanation could be that the introduced H is inducing some defect in the Si near the surface.

Interface charge measurements were then taken on an Hg-CV probe to record any change in interface charge post H introduction using SHP. These measurements were taken by Katherine Collett and are shown in Figure 55. In Figure 55, the n-type 100 nm SiO_2 sample was spin coated with KCl, K^+ ions were drifted to the interface using corona and hot plate before being treated under SHP for 30 mins at 200 °C.

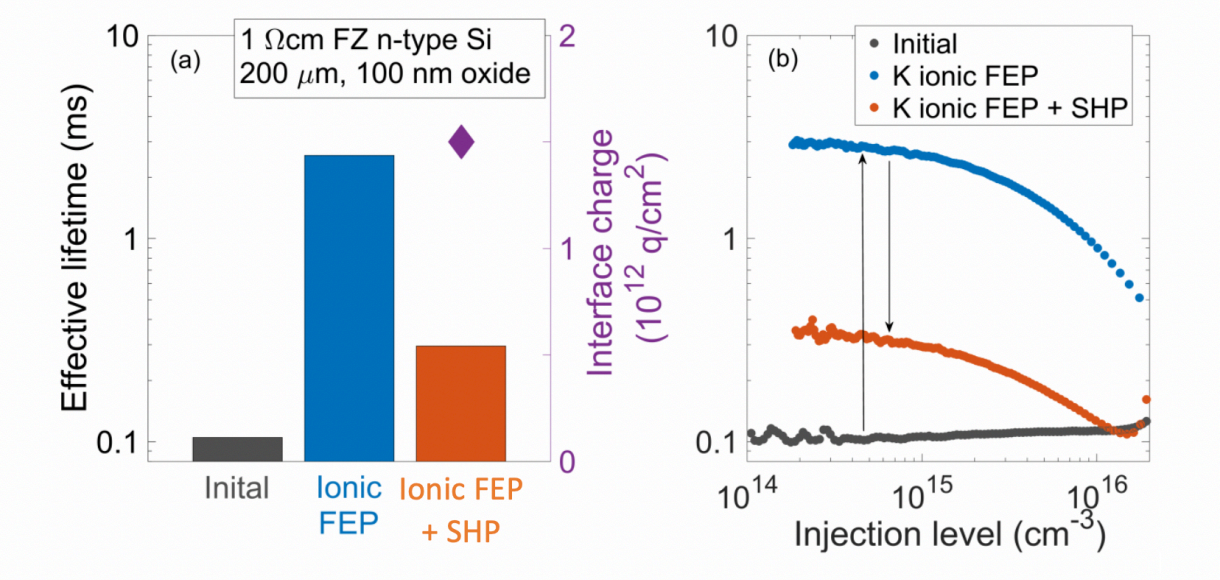


Figure 55 Ionic FEP introduction followed by SHP showing (a) the effective lifetimes at an injection level of 10^{15} cm^{-3} after each processing step along with the final interface charge concentration and (b) the injection dependent effective lifetime curves after each step [26].

The purple diamond in Figure 55 (a) denotes the interface charge after SHP is applied to a sample that had K^+ ions already present at the interface. From Collett [65], it is known that a typical interface charge for charged K^+ ions at the interface of 100 nm SiO_2-Si is 1.7 x 10^{12} q/cm^2, this generally corresponds to a lifetime of ˜2.2 ms. The sample with ionic drift and SHP exposure in Figure 55 has an interface charge of 1.5 x 10^{12} q/cm^2 with a lifetime of 40 µs. This provides strong evidence that the K^+ ions are still charged and at the interface and indicates that the lifetime decrease is not caused by H bonding with K^+ ions and therefore removing the interface charge.

Such a high interface charge however, has been shown to result in a lifetime of 2 ms when using ionic FEP alone. The high interface charge and low lifetime particularly of the post-ionic FEP + SHP sample shown in Figure 55 indicates that another defect mechanism must therefore be present in the Si, and this is discussed in Section 6.1.4.

The ionic FEP combined with subsequent H exposure using SHP was also tested on p-type Si. K^+ ions were deposited and drifted to the interface, as per the conditions in Figure 51, on 100 nm SiO_2 p-type FZ Si. A control without any ions was also used. Both samples were exposed to SHP under Pd-Ag foil for 30 mins at 350 °C. The results are shown in Figure 56.

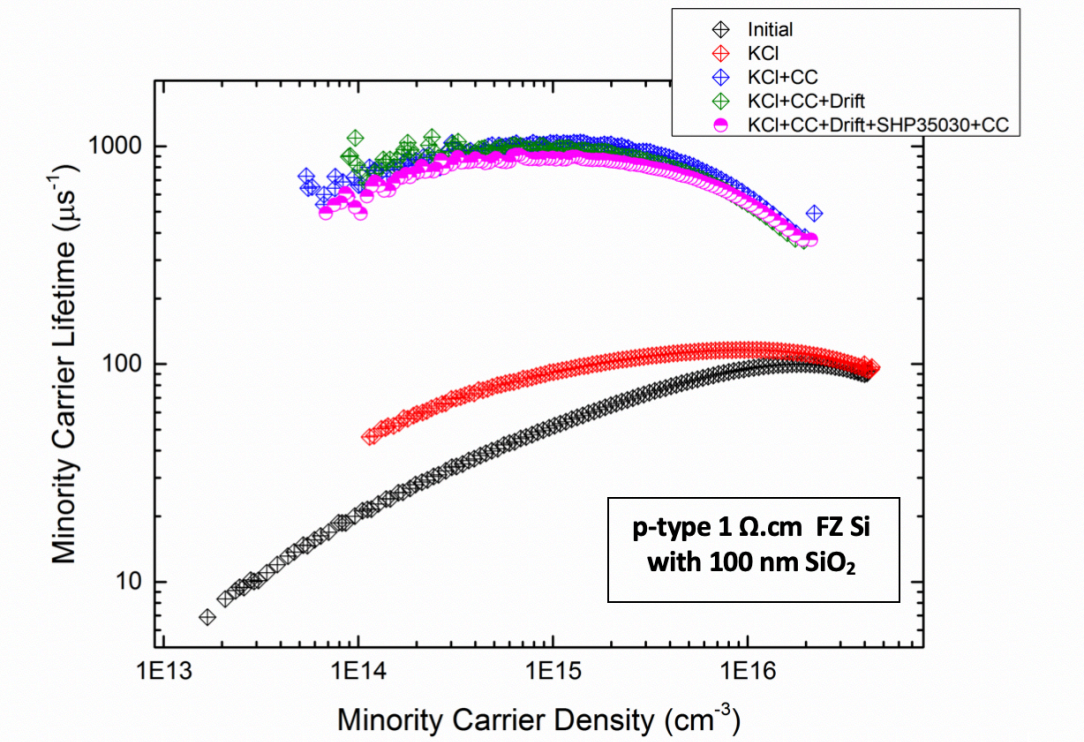


Figure 56 Minority carrier lifetime in µs over injection level for p-type FZ Si with 100 nm SiO_2 coating. As-received (black diamond). KCl spin coated (red rhombus). KCl + corona charge (blue rhombus). KCl spin-coated + drifted through with corona and 450 °C anneal (green rhombus). KCl spin-coated and drift with SHP exposure under Pd-Ag foil, 350 °C 30 minutes with corona. All samples are corona charged as per [143].

As in Section 6.1.2, p-type Si behaves differently to n-type Si under the same H exposure conditions. In Figure 56, the p-type sample does not exhibit the

dramatic reduction in lifetime when it is exposed to H using SHP post ionic drift. Instead, the minority carrier lifetime after SHP exposure remains the same as post K^+ drift, at a value of 880 μs at 10^{15} injection level.

6.1.4 Discussion on the Effect of SHP on Bare and Ionic FEP Samples

The results presented in 6.1.2 and 6.1.3 showed that introducing atomic H into n-type Si which was not covered by a dielectric seems to have a negative effect on the minority carrier lifetime. This is represented by a dramatic lifetime reduction that is not observed when the bare Si sample is exposed to a shielded plasma that does not contain H, such as an N_2 plasma. It is important to note that both the bare n-type Si sample and the dielectric-coated sample with ions present at the interface have a similar lifetime decrease, and as such it is likely that the same defect is forming in both cases. Furthermore, the lack of decrease of lifetime when p-type samples are used in both cases is strong indication that the damage is H-related. This will be explored in greater depth in subsequent discussions. Lastly, although only a small sample size is shown in this Section, the experiment was repeated more than 10 times and always showed the dramatic decrease in lifetime upon H introduction.

In order to understand the processes leading to a lifetime decrease, this thesis considers movement of H in Si, first at a low temperature and without an oxide present. It is widely known that the diffusivity of H in Si has a strong dependence on temperature. The earliest quantitative measurements of the diffusivity of H in Si were performed by Van Wieringen and Warmoltz [229] in 1956. They used mass spectrometry to record the permeation of H_2 through a Si cell wall over a temperature range of $970 - 1200$ °C. They then used the permeation (F) equation:

$$F = -AD_H \frac{\delta[H]}{\delta r} molecules\ s^{-1} \tag{6.1}$$

Here, A is the cell area and $\frac{\delta[H]}{\delta r}$ is the concentration gradient in molecules cm^{-3} over the thickness of the wall. From this they calculated the diffusion coefficient D_H as [229]:

$$D_{H,VWW} = 9.4 \times 10^{-3} \exp\left[\frac{-0.48eV}{kT}\right] cm^2 s^{-1} \tag{6.2}$$

Ichimiya *et al* in 1968 performed a similar experiment, which used high resistivity, p-type FZ Si and measured concentrations of tritium over a similar temperature range of 900 – 1200 °C. Their experiments led to a different D_H of [230]:

$$D_{H,IF} = 4.2 \times 10^{-5} \exp\left[\frac{-0.56eV}{kT}\right] cm^2 s^{-1} \tag{6.3}$$

However, Ichimiya et al used a thin oxide (5 nm), which they believe reduced out-diffusion of H, which is how they explain their rather different pre-exponential factor. For low-temperature H diffusion at 300 °C, Pearton *et al* report widely different values for observed introduced H concentration in bulk Si than what would be expected from both of the reported D_H coefficients [231]. Indeed, Pearton *et al* reported, as shown in Figure 57, that the concentration of deuterium or H seen in Si when introduced from a plasma at temperatures is up to two orders of magnitudes less than what would be expected when the diffusion process is described using D_H values extrapolated from high temperature. They hypothesize that this is due to the substantial fraction of H being trapped by B acceptors and thus forming [H-B] pairs. These pairs are only stable up to 250 °C and would disscotiate at higher temperatures until H has diffused through the wafer. This would explain why at higher temperatures, the concentration of H measured to have gone through the Si wafer is closer to that extrapolated from the D_H values. It is also important to note that many published papers [85], [231]–[233], have observed that H diffusion in n-type is slower than in p-type Si. Although the interstitial diffusivity of H remains unaffected, the majority of H diffusion at low temperature is done through the capture and release of H at traps, and as such, the effective diffusivity is affected by the amount and nature

of traps present [234]. In p-type Si the main trap is B, but in n-type it is thought that there are many more traps, a lot of which are unknown. This would explain why the effective diffusivity of H is slower in n-type. This is of particular interest for the defect formation seen after SHP since the defects formed must act as traps for H in n-type and may contribute to the lower effective diffusivity observed.

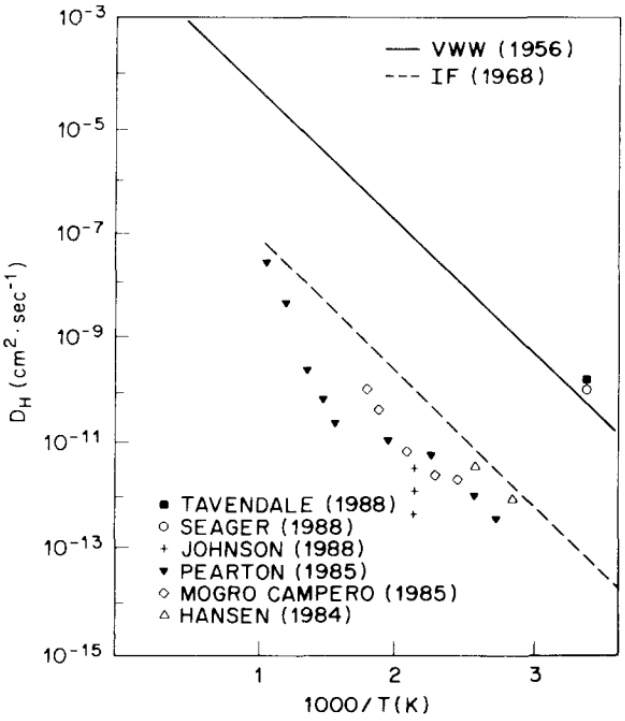


Figure 57 Compilation of experimental data, diffusivities of H in Si, together with lines representing the Van Wieringen and Warmoltz and Ichimiya and Furuichi data. (After ref.[231].)

Regardless of which D_H value is used, the diffusivity of H is exponentially related to a change in temperature. As temperature increases, the diffusivity of H in Si also increases. Using the equation calculated by Ichimiya *et al* for $D_{H.IF}$, it is possible to calculate the diffusion coefficient for H in Si at SHP operating temperatures of 200 °C, and a typical SiN_x post deposition anneal temperature of 800 °C.

$$D_{H,IF}(200°C) = 4.53 \times 10^{-11} cm^2 s^{-1}$$
$$D_{H,IF}(800°C) = 9.83 \times 10^{-8} cm^2 s^{-1}$$

These two values for diffusivity are far larger than the expected effective, trap limited, diffusivity. However, an upper estimate of the characteristic diffusion lengthscale can be made using these coefficients, as shown below.

Using Ichimiya's coefficient evaluated at 200 °C, and for the SHP exposure time: t = 30 minutes, as well as the equation for diffusion length: $D_L=\sqrt{D_{H,IF}t}$, it is calculated that the H introduced would not have diffused through more than approximately 2 μm compared to 133 μm at 800 °C for the same time. This enables the following postulate to be drawn: the relatively low effective diffusivity of H in Si at 200 °C leads to a high concentration of H in the near surface region (within 3 μm) which causes a recombination active defect to be formed. It is not clear at this stage whether the effective diffusivity is limited by trapping of H at the defect generated itself or if H is trapped by another, recombination inactive, defect. This is explained schematically in Figure 58.

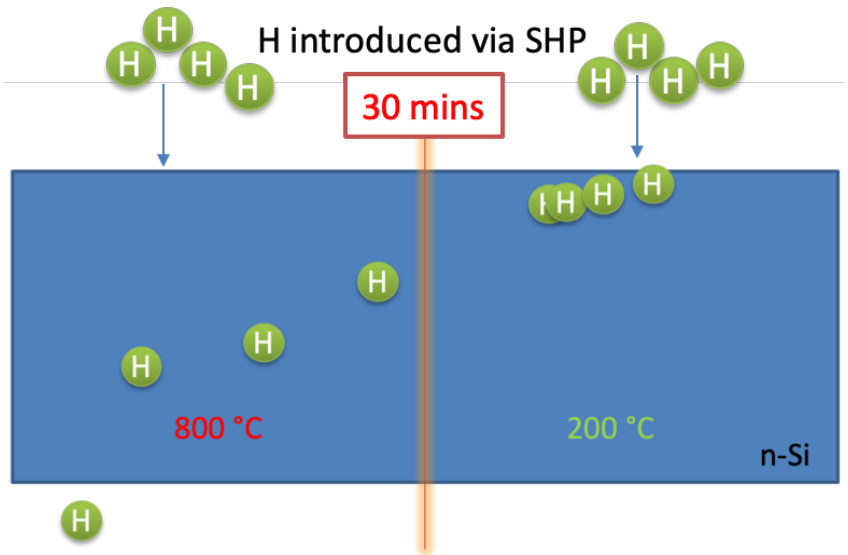


Figure 58 Schematic of atomic H transport at 200 °C and 800 °C in n-type Si

The schematic in Figure 58 explains a hypothesis as to why exposing atomic H, using SHP, to bare n-type Si results in a dramatic reduction in minority carrier lifetime. The low diffusivity of H at that temperature allows for a highly localised concentration of H to be reached near the boundary, which is above a threshold

concentration, thus producing some H-related defect which acts as a recombination centre and ultimately reducing minority carrier lifetime. At 800 °C the effective diffusivity is high enough for H to diffuse a greater distance into the depth of the Si wafer without reaching the required concentration for significant amounts of the recombination active defect to form. It is likely that the defect formed is unstable at high temperatures. This implies that even if the defect seen at low temperatures is formed at higher temperatures, it would not be stable and instead break up quickly, leading to no observable damage. This breaking-up effect might be observable for a short, high temperature anneal on samples that have exhibited H-related damage from bare SHP exposure. This would imply that additionally to the H concentration threshold required to form the H-related defect, there is also a temperature threshold for the stable formation of this defect.

The H-related damage seen on bare Si at 200 °C was not observed in Chapters 3 and 4 when H was introduced using SHP on a dielectric coated n-type Si. The potential reason for this is illustrated in Figure 59.

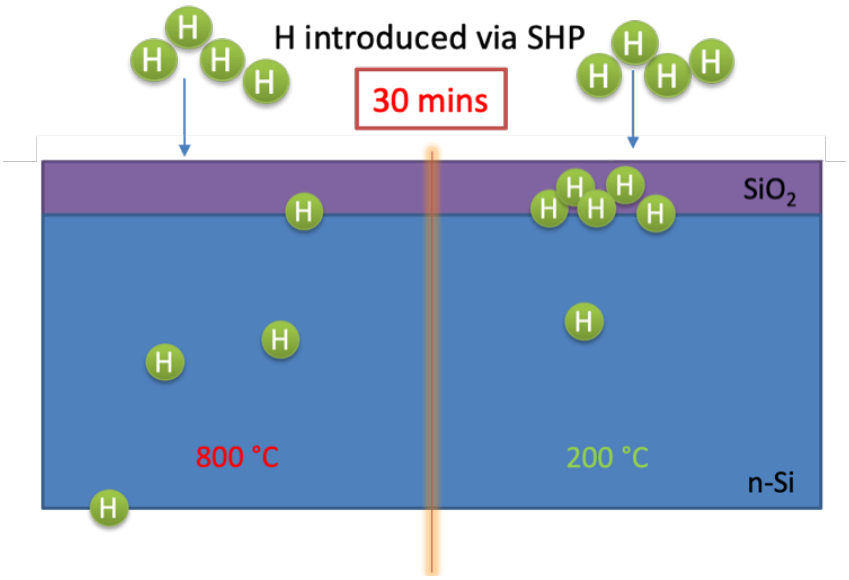


Figure 59 Schematic of atomic H transport at 200 °C (SHP) and 800 °C (theoretical) in 100 nm SiO_2-Si n-type Si

As shown in Figure 59, it is hypothesized that when a dielectric layer is present, such as 100 nm of SiO_2, the H introduced via SHP at 200 °C does not reach the

threshold concentration to cause H-related damage. It is postulated that SiO_2 acts as a barrier to H incorporation into Si, which slows down the passage of H into bulk Si, allowing the threshold concentration of H at the near surface to be avoided, thus preventing defect formation. The reduction in H flux across a dielectric coated Si sample has been reported in the literature by Nickel *et al* [84]. In their work, they observe H-flux being reduced by four orders of magnitude by the SiO_2 layer, which is independent of the thickness of the oxide. However, they propose an alternative explanation to the one proposed in this thesis, which is that the "decrease of the D flux is primarily caused by a reflection of monatomic H at the oxide surface" [84].

K^+ ions located on the surface of SiO_2 are now considered. This situation arises in the context of FEP processing of dielectric layers when SHP exposure is conducted prior to ionic drift. It has been shown in Figure 55 that ionic spin coating had very little effect on the lifetime of the tested samples. As such, it is unlikely that the ions at the surface will have any effect on H-transport, as postulated in Figure 60.

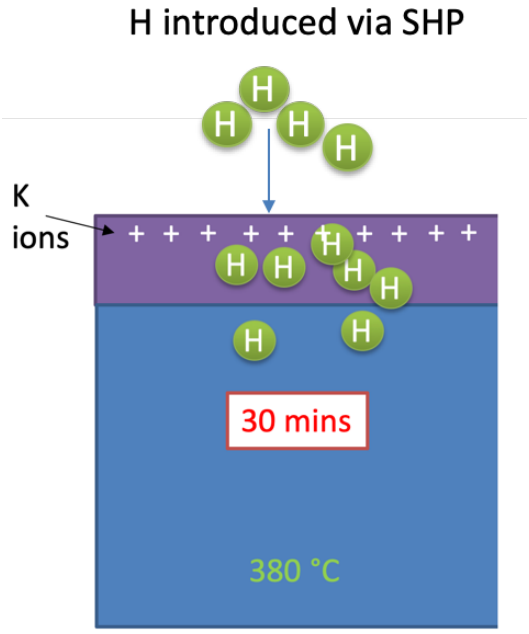


Figure 60 Schematic of atomic H transport at 380 °C with K ions deposited on 100 nm SiO_2-Si n-type Si. No drift.

In the case shown in Figure 60 the K^+ ions at the surface have little to no effect on H introduction. The atomic H introduced via SHP behaves much like in Figure 59, and no damage layer is seen. Additionally, it is likely that the 450 °C anneal required to drift the K^+ ions to the interface allow for the H atoms to diffuse further into the Si bulk, thus decreasing the concentration of H near the surface.

When the K^+ ions are drifted through using corona charge and an anneal however, a different scenario is hypothesised as shown in Figure 61. It was seen in Figure 55, that a post ionic drift SHP exposure led to a substantial minority carrier lifetime decrease. CV measurements showed no decrease in interface charge, indicating that FEP was still present at the interface despite H-introduction. Possible reasons for this decrease are discussed here.

The deposited K^+ ions are drifted through to the interface during the 15 second anneal and induce negative charge in the adjacent bulk Si. This juxtaposition of positive ionic charge at the interface and negative electronic charge in the Si produces a dipole at the interface. This has been studied by Deru [235] and Kealey who find a dipole length of ~4nm with a typical charge of ~5 x 10^{12} e/cm^2. This gives rise to an electrostatic field of 1.15 x 10^7 Vcm^{-1} across the interface.

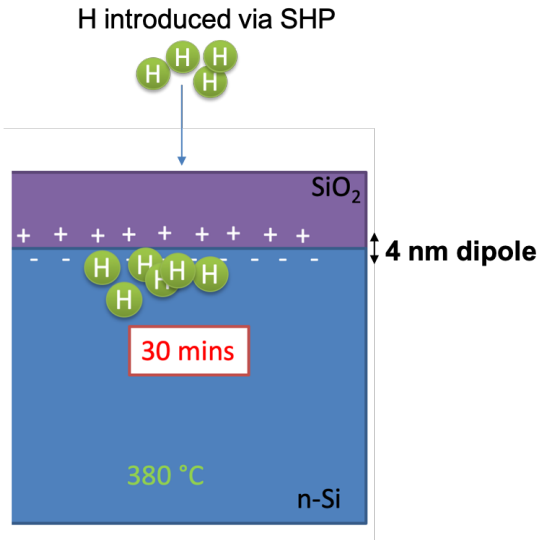


Figure 61 Schematic of atomic H transport at 380 °C with K^+ ions drifted using CC and 450 °C anneal. K^+ ions at the interface between 100 nm SiO_2 and n-type Si.

As can be seen in Figure 61, the drifted K^+ ions at the oxide Si interface created a dipole through the attraction of negative mobile charge in the near-surface Si bulk (electrons). It is known that H in SiO_2 migrates predominantly as a neutral atom and as a positive ion [236], [237] . The field generated across the interface attracts and subsequently pulls the H atoms across the SiO_2-Si interface. It is proposed that the very strong field across the interface has the effect of increasing the rate of introduction of positively charged H ions from the oxide into the Si. This then greatly increases the flux of H into the Si such that a much higher concentration of atomic H is found in the near surface region of the Si. This concentration surpasses the damage-inducing threshold and the minority carrier lifetime is seen to decrease dramatically, as in Figure 55.

This model would suggest that the transport of H across the bulk of SiO_2 is in fact very fast, and that the reason SiO_2 coated Si is accepted to be a diffusion barrier to H is not because of slow transport of H through the oxide but rather because of slow transport across the SiO_2-Si interface. The addition of an electric field directed into the Si at this interface allows the interface barrier to be overcome and for high concentrations of H to pass freely into the Si.

Only a few published papers have experimentally measured the diffusivity of atomic H in SiO_2 to date. Griscom and Shkrob [238], [239] calculate the diffusion coefficient of H in SiO_2 to be:

$$D_{H,IF} = 10^{-4} \exp\left[\frac{-0.17 \pm 0.02eV}{kT}\right] cm^2 s^{-1} \tag{6.4}$$

This lies between the two diffusion coefficients reported for H in Si as presented earlier in this Section 6.1.4 [229], [230]. Thus, this high diffusivity in oxide does not correspond with the reported effect of transport across SiO_2 as being the rate limiting step for the incorporation of H into Si [84]. Thus, this data also supports the hypothesis that transport across the oxide Si interface is the rate limiting step for incorporation of H into Si through an oxide layer.

The above discussion of H introduction into Si both with and without an oxide layer present, and as described in Figure 59, Figure 60 and Figure 61 can be summarised as follows:

1. At low temperatures (less than 350 °C) there exists a threshold concentration of atomic H that causes electrically active H-related defects to form in n-type Si. Note however that at higher temperatures this threshold may not exist due to the H-related defects then not being stable.
2. Atomic H introduced at low temperature into bare n-type Si has low diffusivity and, provided the H is introduced quickly enough, reaches the defect-inducing threshold concentration.
3. High temperature ($\geqslant$600 °C) introduction of H from SiN_x or other dielectrics does not allow this threshold concentration to be reached due to increased diffusivity of H at higher temperature and/or insufficient H being introduced.
4. The presence of an oxide reduces the rate of H incorporation into Si and thus the threshold concentration is not reached even if atomic H is introduced at 200 °C.
5. The presence of positively charged ions at the interface between SiO_2-Si generates a strong field which allows H to cross the SiO_2-Si interface more rapidly. This allows large concentrations of H to form in the near-surface Si, reaching the threshold concentration and causing H-related defects. This also shows that the rate limiting step for H incorporation into Si through an oxide is not passage through the oxide but across the interface.
6. The K^+ ion drift to the interface of SiO_2/Si, post SHP, using a 450 °C anneal potentially allows for the atomic H to diffuse further into the Si bulk. This reduces the concentration of H at the near-surface and the threshold concentration is not reached.
7. The H-related defect concentration is highest at the Si surface and becomes insignificant within about 4 μm.

8. The H-related defects don't form in p-type Si, or are electrically inactive.

This description of H incorporation into Si includes a number of new proposals, and further experiments were carried out to provide evidence for their veracity, and to use the SHP incorporation of H into Si to study other effects related to H in Si. These experiments are described below.

6.1.5 Investigation of the cause of SHP-induced lifetime reduction in n-type Si.

6.1.5.1 Evidence for H-concentration and damaged layer

The first experiment was conducted to gather evidence on the identity of the lifetime-limiting defect produced by SHP applied to bare Si. It is known that H has a diffusivity several orders of magnitude higher than most other elements in Si at the relatively low temperature of 350 °C, and it is faster than any other species likely to be present in the SHP process [104], [121], [240]. Since the bare n- and p-type wafers were exposed to a H-containing plasma under a Pd-Ag foil, there is a strong likelihood that this large lifetime reduction was indeed caused by the introduction of H. Another piece of evidence which would increase the validity of this hypothesis would be to observe a concentration gradient of defects from the H exposed surface. Indeed, a concentration gradient from the surface would imply that the defect was caused from H introduction from the upper surface. The defect concentration would then reduce as it travels deeper into the wafer.

In order to observe a potential defect layer as well as a concentration gradient, n-type 1 Ωcm, FZ Si with no oxide was exposed to H from SHP for 30 mins at 350 °C. The sample was then coated with 50 nm of SiN_x, as per the standard recipe in Chapter 3 Section 3.2.2, to enable lifetime measurements. A dramatic

lifetime decrease was observed as in Figure 55. The SiN_x layer was then etched off using HF. Once the surface was bare, tetramethylammonium hydroxide (TMAH) was used to etch off incremental layers of Si. TMAH was used in 20 wt.% in water at 80 °C which had an etch rate of 0.1 ± 0.02 µm/min [241], [242]. The Si sample was then coated with standard SiN_x and lifetime tested using Sinton. The new process step is denoted by the number four and the results are presented in Figure 63.

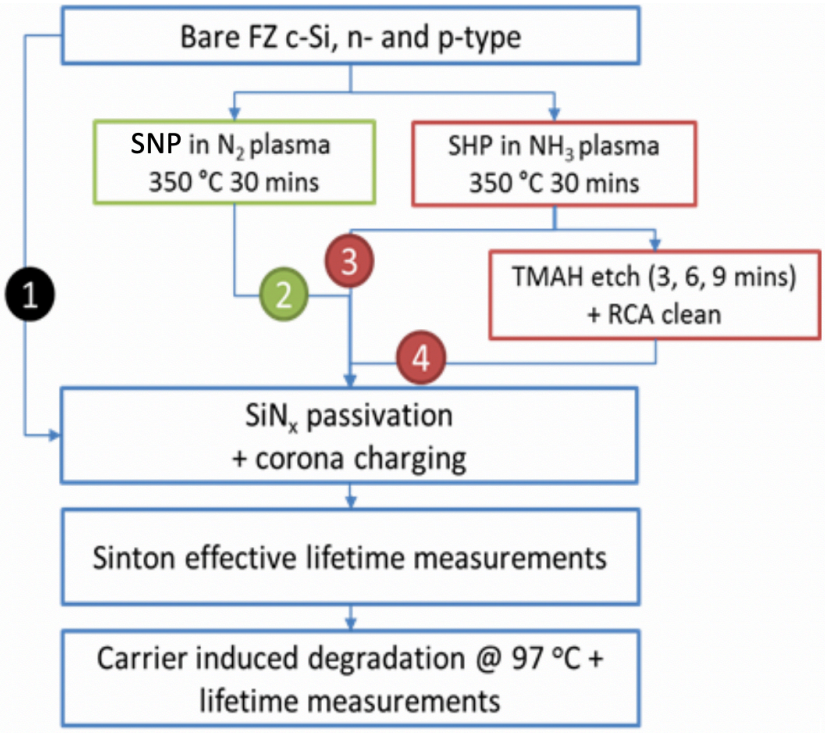


Figure 62 Process flow chart for both n- and p-type FZ Si, with added batch (4) which receives a TMAH etch

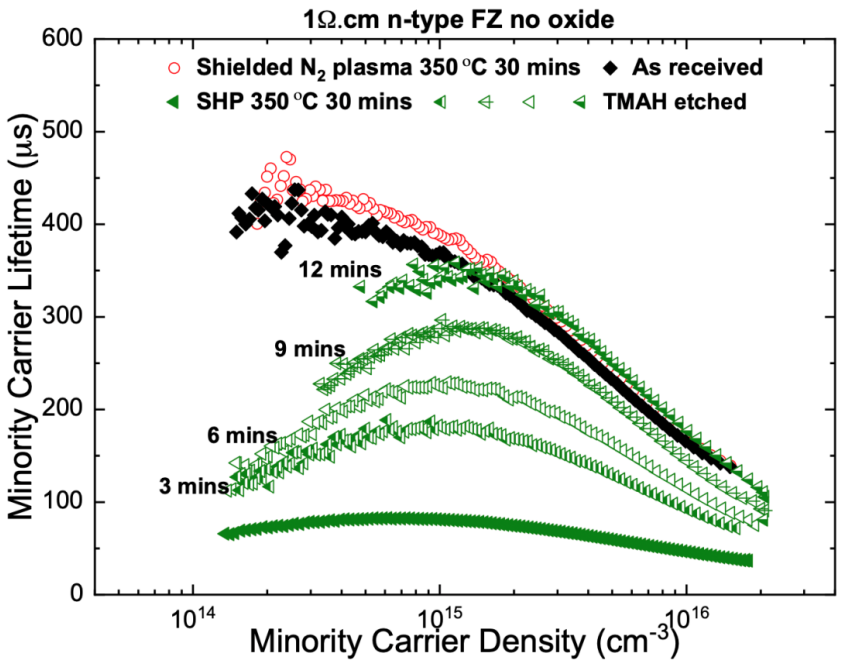


Figure 63 Minority carrier lifetime in µs versus injection level for 200 µm n-type FZ Si with 50 nm SiN_x coating. As-received (bare Si + SiN_x) (black diamonds). SNP (empty red circles) (bare Si + SiN_x). SHP (green filled triangles), HF+ SHP 30 mins 350 °C + SiN_x. TMAH samples (empty green triangles) are the SHP sample + TMAH for 3 mins each time. All samples are corona charged as per [143].

In Figure 63 the SHP 'damaged' sample was TMAH etched incrementally. The first 3 min etch, corresponding to 0.4 ± 0.08 µm, showed a lifetime increase from 70 µs to 175 µs at 10^{15} injection level. The subsequent 3 min etch, total time 6 min and 0.8 ± 0.16 µm of material removed, improved the minority carrier lifetime further to 230 µs at 10^{15} injection level. The 9 min TMAH etch, removing 1.20 ± 0.24 µm of Si, showed a lifetime of 300 µs at 10^{15} injection level. The last TMAH etch with a total time of 12 mins and 1.60 ± 0.32 µm of Si removed, showed an almost completely recovered lifetime level of 350 µs at 10^{15} injection level. All these results have been corona charged as per [143] in order to achieve the best surface passivation so that the underlying trends in bulk lifetime can better be seen. Subsequent TMAH etches did not improve the lifetime further.

The minority carrier lifetime increases with the amount of Si material, and therefore the concentration of defects, removed. This constitutes strong evidence for the defect having a concentration gradient profile. This is consistent with the H concentration profile seen to deactivate B acceptors in Chapter 4 Section 4.3.4. It also represents strong evidence that this defect is produced in the near-surface region by the introduction of atomic H from SHP at low temperature.

In addition to the TMAH etching experiment, PEDOT:PSS was used to observe the surface recombination as a function of surface carrier population of a Si sample that exhibited a dramatic lifetime decrease. This aimed to determine the location of the damaged region within the Si. The sample chosen was n-type FZ Si with 100 nm SiO_2. It had K^+ ions drifted to the interface before a standard SHP process. The initial minority carrier lifetime was 106 μs and after ionic drift and SHP the lifetime degraded to 30 μs, all at a 10^{15} cm^{-3} injection level.

PEDOT:PSS was applied to the sample in the method described in Chapter 3 Section 3.6.6. It allowed for the lifetime to be recorded with a constant applied bias and very precise voltage intervals. The voltage applied ranged from -18 V to 18 V using an SMU. A control sample which had not received any ions or SHP was also tested under the same conditions.

The extracted lifetime for the post ionic drift and SHP exposed n-type FZ 100 nm SiO2-Si sample at a range of injection levels for different applied voltages is shown in Figure 64.

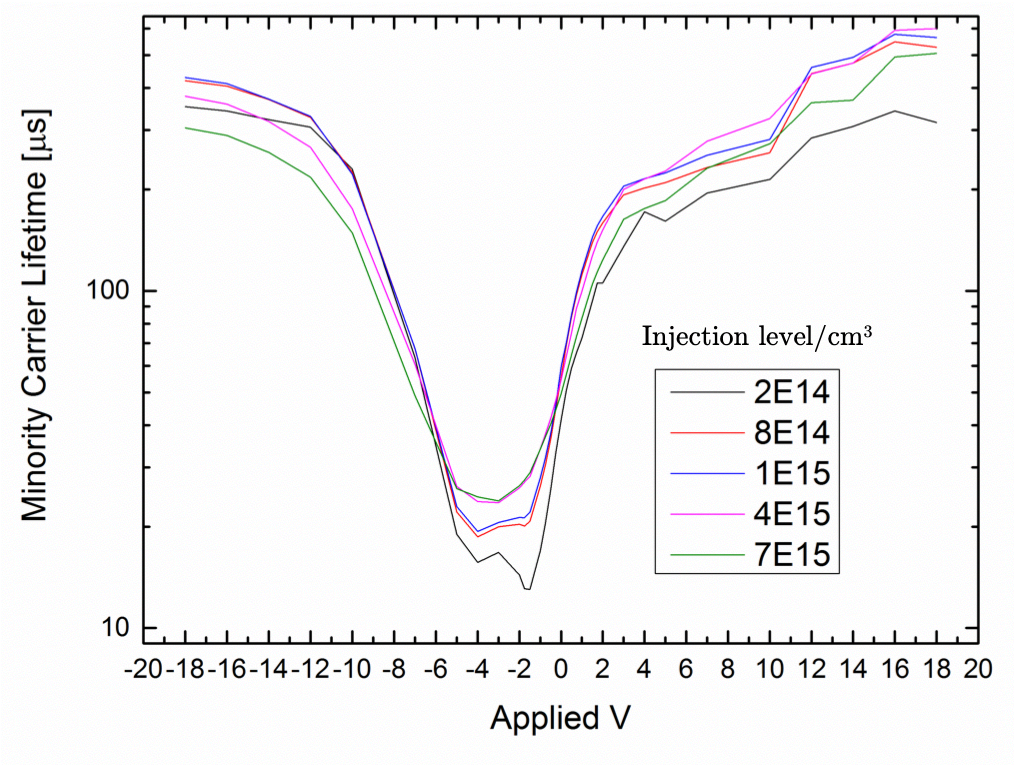


Figure 64 Minority Carrier Lifetime (µs) against Applied Voltage (V) (from SMU) for different injection levels in cm^{-3}. Sample received K^+ ion, drifted using CC and hot plate, SHP exposure for 30 mins at 350 °C. PEDOT PSS applied on front surface.

It can be seen in Figure 64 that at all injection levels there is a broad minimum between -0.75 V and -5 V which corresponds to the n-type FZ Si sample being in deep depletion. Bonilla *et al* published a similar figure on an n-type sample without any near-surface damage which showed a much narrower dip. The figure published in [161] is reported in Figure 65, for ease of comparison.

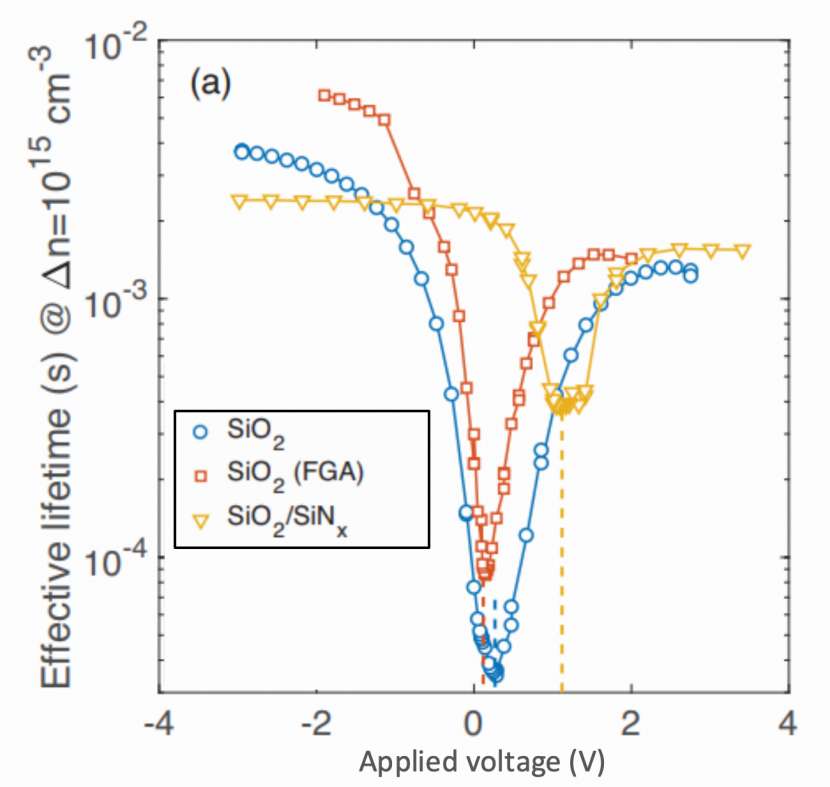


Figure 65 Effective lifetime as a function of gate bias on the surface of the dielectric for n-type 1 Ωcm FZ Si passivated with SiO_2, SiO_2/SiN_x and SiO_2 with an FGA treatment.

It can be seen in Figure 65, that the minimum lifetime when the Si sample is in deep depletion occurs around 0 V and is less than 1 V wide. The same sample structure, (n-type 1 Ωcm FZ Si passivated with 100 nm SiO_2), exposed to SHP with K^+ ions at the interface in Figure 64, has a minimal lifetime dip which spans over 4 V. This is evidence that the lifetime limiting defect is in the near surface region and is in the form of a damaged layer. Indeed, a larger applied voltage is required to recover the lifetime, and the sample is in deep depletion across a larger voltage as there is a higher density of defects in the near-surface region. The lifetime of the sample in Figure 64 does not, however, recover to the level seen in Figure 65. The maximum lifetime in the K^+ and SHP sample is 430 μs at the 10^{15} cm^{-3} injection level compared to 4 ms at 10^{15} cm^{-3}, reported by Bonilla in Figure 65 and [161].

This effect can also be seen from the lifetime curves associated with the applied voltage using PEDOT:PSS on the drifted K^+ and SHP exposed n-type sample as shown in Figure 66 and Figure 67.

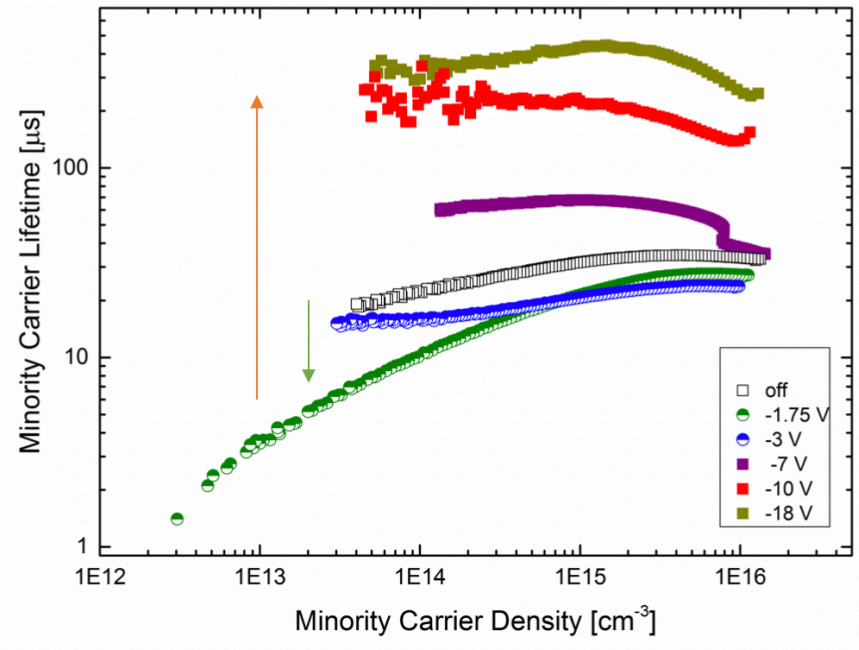


Figure 66 Minority carrier lifetime (µs) versus injection level (cm^{-3}) for negative applied V on n-type Si with K^+ driften at interface and exposed to SHP at 350 °C for 30 mins.

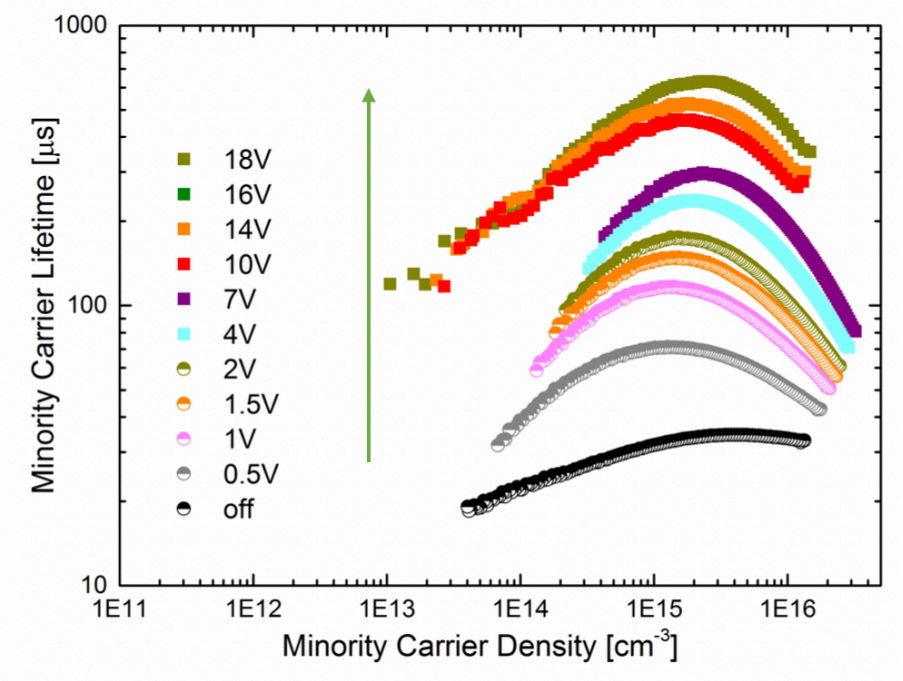


Figure 67 Minority carrier lifetime (µs) versus injection level (cm^{-3}) for positive applied V on n-type Si with K^+ drifted at interface and exposed to SHP at 350 °C for 30 mins.

The lifetime curves seen in Figure 66 and Figure 67 indicate the presence of a near-surface damage region. Indeed, it is seen that the lifetime of the sample is strongly influenced by the surface charge applied. This indicates that the defect generated is not evenly distributed throughout the bulk, as this would lead to no lifetime improvements seen with applied potential. Moreover, there is a significant and indicative lifetime dip at low injection levels (10^{15} cm^{-3}) when positive voltage is applied. Steingruber suggests this indicates a near-surface damage region [243], but not one purely located at the interface.

6.1.5.2 Degradation in n-type FZ Si under Light Soaking

The experiments on bare Si have demonstrated that atomic H introduced at 350 °C immediately produces recombination active defects in n-type Si which is a new result. In order to investigate this effect further, SHP processed samples were illuminated under a halogen lamp at 97 °C ± 2 °C at 0.6 W/ cm^2. Both n- and p-type samples were selected for hot light-soaking.

This technique is used to observe a H-related defect named Light and elevated Temperature Induced Defect (LeTiD). Illuminating a Si sample, or cell, at approximately 1 sun illumination and 90 °C for a prolonged time is a well-known technique to activate and reduce defects caused by H [53], [56], [122], [244], [245], as introduced in Chapter 2 Section 2.2 .

In Figure 68, the previously named 'normalized defect density' (NDD) [245] of n-type samples exposed to SHP are compared with the n-type control sample. This thesis proposes that NDD is not an accurate name for the data used to calculate it, as it is a normalised change in lifetime calculation, rather than a discrete measurement of defect density. This thesis instead refers to it as Normalised Lifetime Reduction (NLR). The NLR is calculated as follows:

$$NLR = \frac{1}{\tau_{eff}} - \frac{1}{\tau_{eff,initial}} \tag{6.5}$$

The control sample received an oxide strip before applying a SiN_x coating. For the SHP n-type samples, one was not TMAH etched and the others were TMAH etched for 6, 12 and 18 mins respectively. These samples were a different batch to those shown in Figure 4 but were processed as shown in Figure 3.

The non-etched sample shows a much higher NLR level than the control sample and the etched samples. The etched samples show different levels of NLR. The 6 min etch shows a higher level of NLR compared to the longer etch times of 12 and 18 mins. Figure 68 also includes fiducial marker lines.

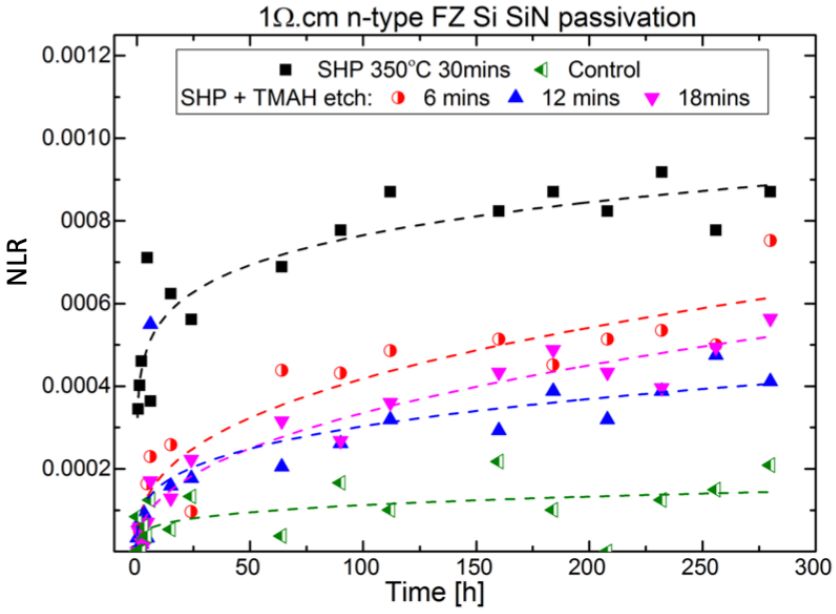


Figure 68 Normalised Lifetime Reduction (NLR) vs hot illumination time (97 °C ± 2 °C at 0.6 W/ cm²). N-type SHP with SiN_x passivation with TMAH etch (0 mins, 6 mins, 12 mins and 18 mins) and control (oxide strip and SiN_x passivation)

To differentiate between bulk degradation and surface degradation of the n-type samples, lifetime curves were analysed as shown in Figure 69. The sample was exposed to atomic H using SHP at 350 °C for 30 mins on both sides. It was then

light-soaked (97 °C ± 2 °C at 0.6 W/ cm²) up to 280 h. The lifetime curves for 20 mins, 18 h and 280 h are shown.

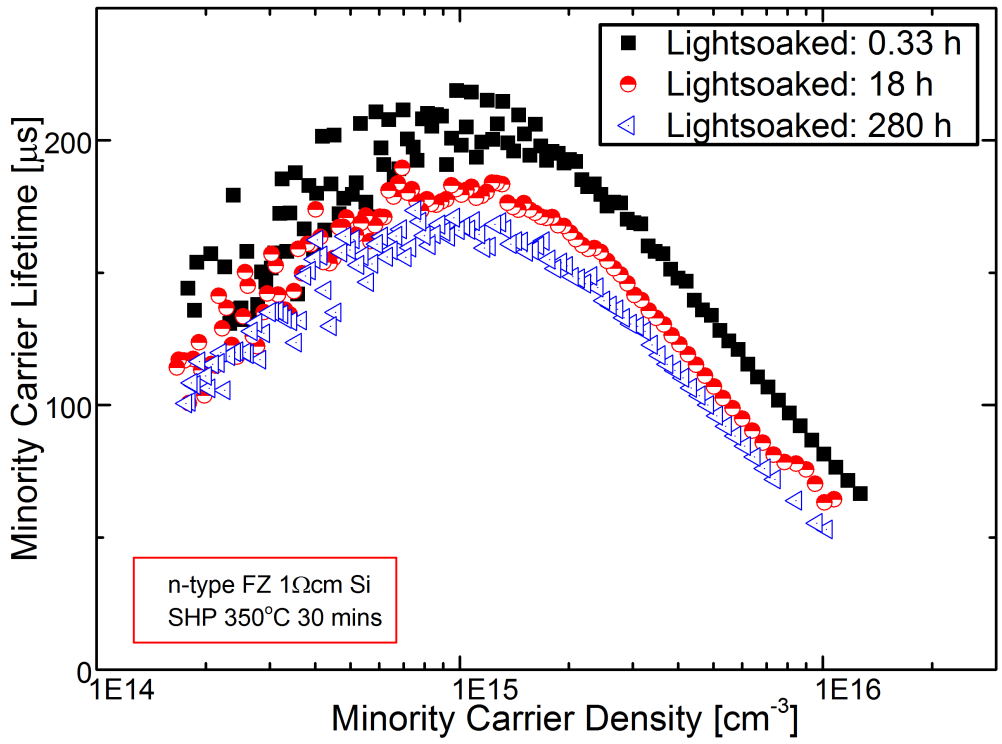


Figure 69 Minority carrier lifetime vs minority carrier density. n-type SHP for 350 °C for 30 mins both sides and SiN_x passivation. Degradation time 0.33 h (black squares), 18 h (red circles) and 280 h (blue empty triangles).

There is a distinctive dip in lifetime at low injection levels on all three curves similar to the observations made by Steinegrube [243]. This dip is indicative of near-surface recombination, which in previous reports on p-type has been suggested to be a result of H-induced defects [243], [246], rather than degradation in surface passivation quality which would instead affect the interface. Moreover, the similarity of the shapes of all three curves as the lifetime degrades through light-soaking is consistent with an increase in the concentration of the lifetime-limiting defect rather than a change in surface passivation. This is further supported by the lack of decay in the sample with identical SiN_x passivation which has not been exposed to SHP as shown as the control sample in Figure 68.

6.1.5.3 Evidence for Dipole-Aided H-introduction across the SiO2/Si Interface

It was seen in Figure 55 that exposing an n-type FZ 1 Ωcm FZ Si passivated with 100 nm SiO_2 to H using SHP caused a dramatic reduction in lifetime, but only if K^+ ions were located at the interface between SiO_2 and Si. The reason for this is postulated in Section 6.1.4 as being caused by K^+ ions generating a dipole at the interface, allowing a higher rate of H introduction into Si. This higher rate of introduction combined with the low-temperature H introduction via SHP is thought to enable a threshold concentration of H to be reached in the near-surface region, thereby creating a H-related damage layer. This would imply that the concentration of H in bulk Si in a sample with K^+ ions at the interface is higher than in a sample without any ions at the interface.

In order to gather evidence for this postulated dipole-aided transport mechanism of H across the SiO_2/Si interface, the following experiment was conducted.

Two p-type 1 Ωcm FZ Si passivated with 100 nm SiO_2 with a B-doping concentration of 1.1×10^{16} cm^{-3} were used for capacitance-voltage (C-V) measurements. One of the samples received ionic FEP and had K^+ ions drifted at the SiO_2/Si interface, while the other sample had no ions. Both samples were exposed to H from SHP at 200 °C for 30 mins. C-V characterization was then used to calculate the doping profile of each sample. The result is shown in Figure 70.

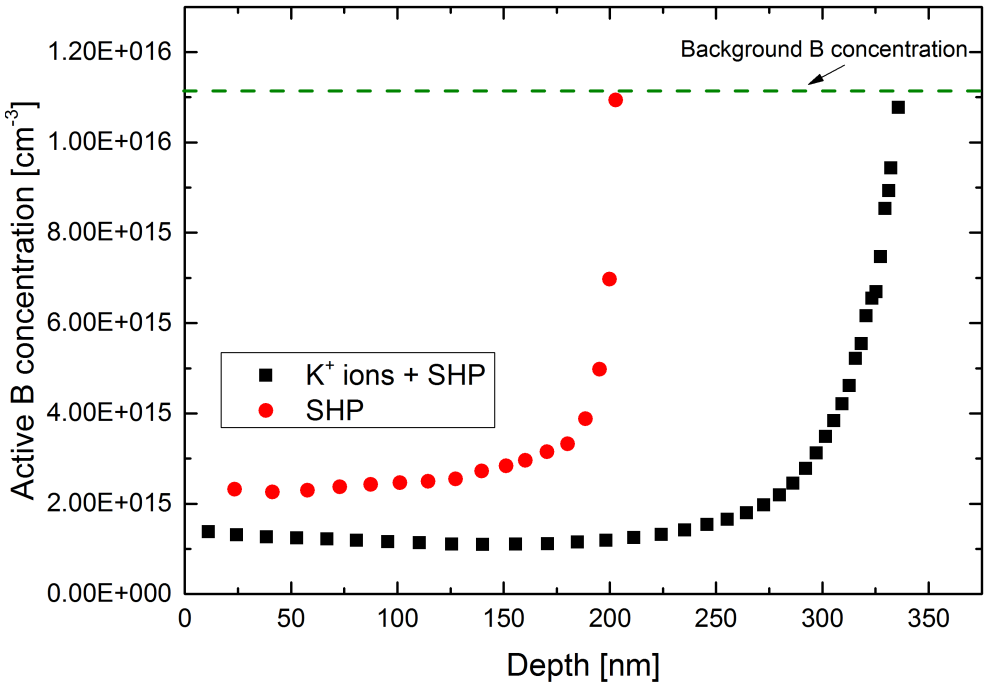


Figure 70 Active B concentration versus depth characterised using C-V technique on 1 Ωcm p-type Si. Red dot sample was exposed to SHP for 30 mins at 200 °C. Black square sample has had K^+ ions drifted to interface followed by SHP for 30 mins at 200 °C.

As shown in Figure 70, the sample with K^+ at the interface has less active B atoms after SHP exposure than the sample without any ions present. This would suggest that the dipole generated by the ions at the interface do indeed increase the concentration of H in Si. The total amount of H-B pairs, and therefore a lower-bound value for the total depth-integrated concentration of H introduced into Si is 1.6 x 10^{11} cm^{-2} for the SHP sample compared to 3.1 x 10^{11} cm^{-2} for the ionic FEP + SHP samples. This two-fold difference is a strong indication that the postulated dipole-aided H-transport mechanism theory in Section 6.1.4 is indeed correct. Section 6.1.5.4 will discuss evidence for the damage-inducing threshold concentration of H.

6.1.5.4 Evidence for Threshold Concentration

The results presented in Figure 54 and Figure 55 as well as the H transport model shown in Figure 61 have postulated that the introduction of K^+ ions at the interface between SiO_2-Si allows H atoms to overcome the interface barrier to

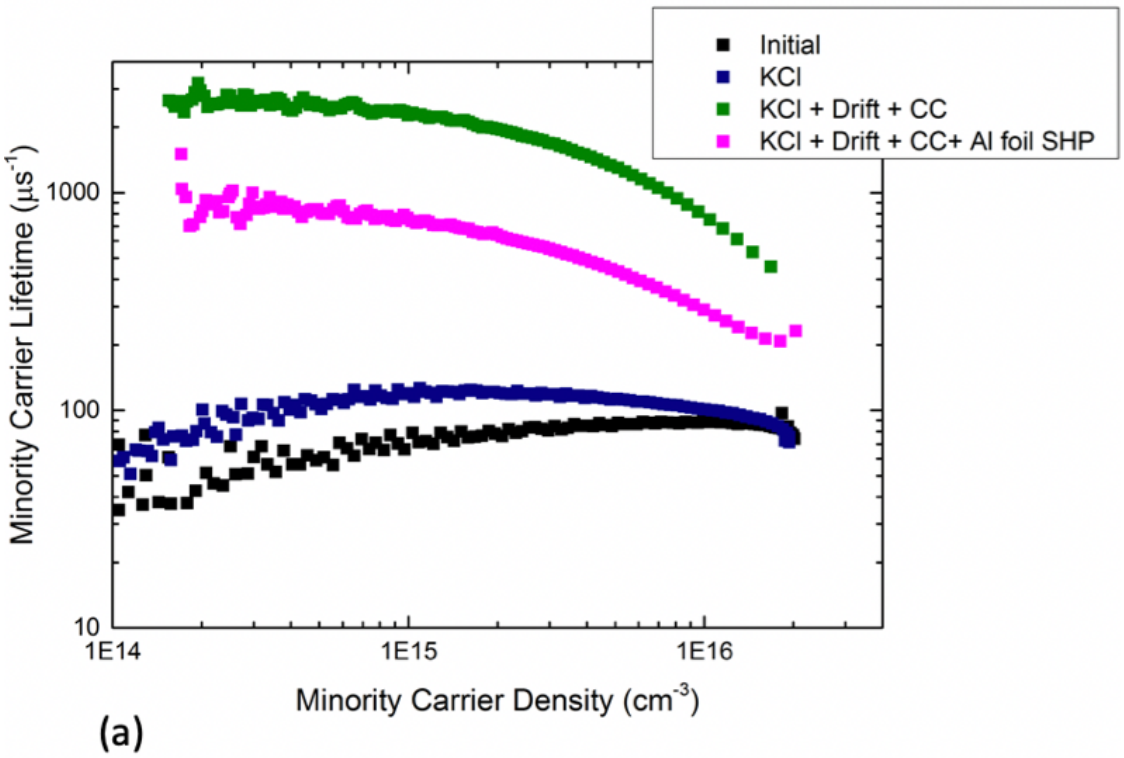
cross into bulk Si from SiO_2. This causes H to be in high concentration in the near-surface region of Si, which causes damage in n-type. The models presented agree with the proposed hypothesis by Nickel *et al* and Johnson *et al* that the concentration of H required to cause a lifetime-limiting defect has a certain threshold [133], [247]. The published literature however, has never seen the generation of this defect on Si samples with a dielectric layer. The existence of this required threshold is investigated in the experiments that follow.

The concentration in the near-surface Si will be dependent upon two main variables: the rate at which H enters into the Si and the rate at which H diffuses away from the Si surface. At low temperatures, 380 °C or less, the diffusivity of H through Si is relatively low, which enables a concentration build-up of H. When K^+ ions are present the rate of introduction of H into Si is thought to be extremely fast. One method to provide evidence for the existence of a threshold concentration is to carry out experiments that purposefully avoid its creation. One obvious method would be to increase the temperature at which H is introduced during SHP in order to increase the diffusivity of H. This was not possible during this work however, due to equipment limitations. An alternative method was then to reduce the rate of H introduction into Si. The rate of H introduction into Si was reduced by using Al foil instead of Pd-Ag foil for the SHP shield.

As presented in Chapter 5 Section 5.2.6, Al foil deactivated a similar level of B, $9.8 \pm 0.2 \times 10^{12}\,cm^{-2}$, in 140 minutes to Pd-Ag foil in 5 minutes, making the H introduction rate into Si 16 times slower with Al foil than with Pd-Ag foil. As such, it is hypothesised that when using Al foil, the peak concentration of H in the near surface region of Si should be lower since there is a longer time for the H to diffuse away from the surface and the production of the lifetime-reducing H-related defect will be reduced.

The experiment used the standard 200 µm n-type FZ Si, 1 Ωcm coated with thermally grown 100 nm SiO_2. K^+ ions were spin coated using KCl and drifted through using corona charge as per Section 3.4.2. The ions were required at the interface to allow for an increased H-incorporation into Si from the dielectric across the interface. The Si samples were then exposed to H-containing plasma using SHP and an Al foil for 40 minutes, before being lifetime tested as shown in Figure 71 (a). The interface charge was also recorded using C-V, a charge concentration of 1.6 x 10^{12} q/cm^2 was observed. This is similar to the interface charge recorded in the initial K^+ drift and SHP experiments, with a value of 1.5 x 10^{12} q/cm^2.

The second batch of samples from the same n-type material was exposed to H from SHP using a prepared Pd-Ag foil, but for a 16 times shorter time period of 2.5 mins, as shown in Figure 71 b). All samples were exposed at 380 °C.



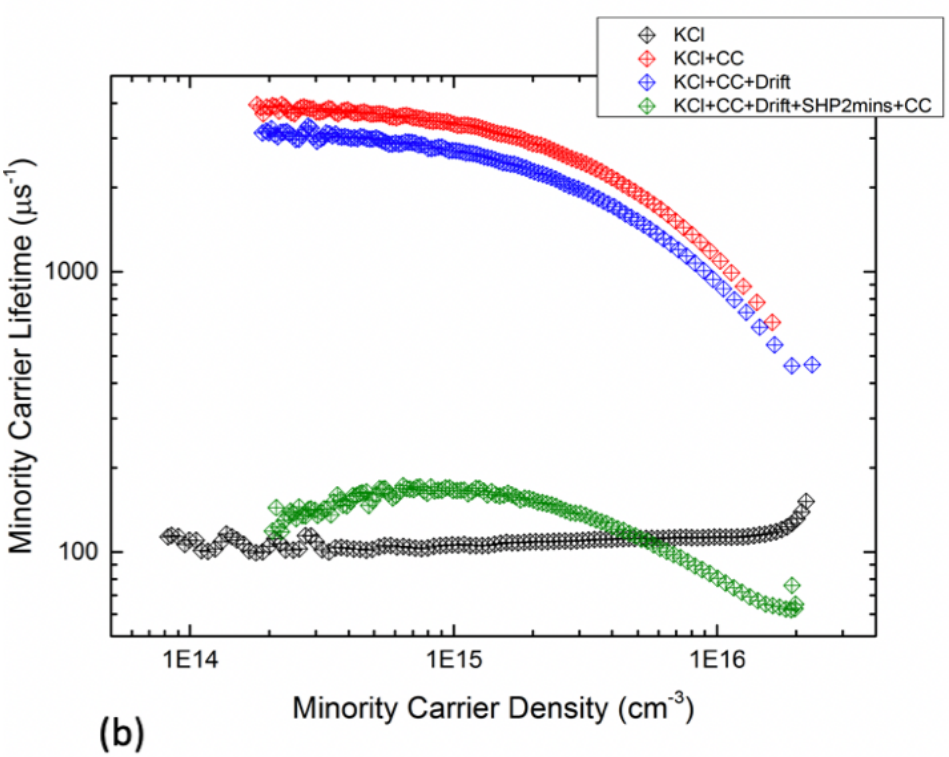


Figure 71 Minority carrier lifetime vs minority carrier density for n-type FZ Si 100 nm SiO_2. a) Control sample (black), KCl spin-coated (blue) K drift with corona and hot plate (green), SHP - Al foil at 380 °C for 40 mins both sides (pink). b) As received sample (black), KCl spin-coated and corona (red) K^+ drift with corona and hot plate (blue), SHP with Pd-Ag foil at 380 °C for 2.5 mins both sides (green)

The difference in minority carrier lifetime between H-exposed samples using Al foil compared to Pd-Ag with a field present at the interface is large. It can be seen in Figure 71 (a) that the Al foil, which introduces H at a rate 16 times slower, severely mitigates the lifetime decrease that is otherwise seen using Pd-Ag foil and ions shown in Figure 71 (b). The minority carrier lifetimes at 10^{15} cm^{-3} for the different samples before ions, after drift, and after H exposure are summarised in Table XVIII.

Table XVIII Minority carrier lifetimes for samples exposed to H-containing plasma using SHP and Al foil or Pd-Ag foil.

Lifetimes at 10^{15}/cm^2 injection level	Al Foil – 40 minutes	Pd-Ag Foil – 2.5 minutes
Starting lifetimes	105 µs	98 µs
After K^+ ions + Corona	2.2 ms	2.5 ms
After K^+ ions + SHP + Corona	700 µs	15 µs

For the same total level of introduced H, using Al foil causes the lifetime to decrease from 2.2 ms to 700 μs, whilst using Pd-Ag foil caused the minority carrier lifetime to decrease from 2.5 ms to 15 μs.

It is thus concluded that using an Al foil shield to introduce H into Si at 380 °C 16 times slower than when using a Pd-Ag shield results in a lower peak concentration of H in the material. This in turn produces a substantially lower concentration of H related defects. This finding strongly supports the postulate that the H defect formation occurs more when the H concentration exceeds a certain value.

6.2 Transport of H in Si through an Oxide layer: Discussion and Conclusions

It has been demonstrated in Chapter 4 that SHP is an effective plasma-induced damage-free method, even at low temperatures, for introducing H into Si. It is thus an attractive technique for studying H-related defects in both n- and p-type FZ Si as is presented in this Chapter.

The first results Section 6.1 , demonstrated the effect of SHP on bare n- and p-type Si as well as its effect after ionic FEP introduction. It was observed, and subsequently discussed in Section 6.1.4, that using SHP at 350 °C to introduce H into n-type material that has no dielectric surface layer generates defects which greatly degrade lifetime as demonstrated in Figure 52. There, the lifetime decreased from 380 μs to less than 100 μs even after corona charging. When p-type samples were tested under the same conditions, the lifetime decrease effect was not observed. This difference between n- and p-type samples was also observed when K^+ ions were drifted to the interface of SiO_2-Si. When ions were

present at the n-type interface, a lifetime decrease was recorded, but this was not observed in p-type Si.

Models were developed and discussed in Section 6.1.4 in an attempt to explain the cause of the lifetime decrease in n-type. The models had four main postulates:

1. The damage generated in n-type is H-related.
2. H-damage is only significant when the introduced H reaches a certain concentration level
3. Ions at the SiO_2-Si interface induce a dipole which generates a field large enough to allow H to overcome the interface barrier.
4. H-transport through SiO_2 is in fact extremely fast, and the barrier to passage of H into the Si is the interface.

In order to gather evidence for these postulates, the experiments presented in Section 6.1.5 were devised. It is very likely for the damage to be H-related due to the different behaviour exhibited by n-type and p-type samples under the same conditions. This different behaviour could be caused by the charge state of atomic H in p-type compared to n-type Si. In p-type Si, H exists almost exclusively as H^+ [240], [248] which is not conducive to the formation of these extended recombination active defects, as the charged species repel each other. On the other hand, H in n-type Si can exist as H^0 and H^- thus increasing the probability of formation of these H induced defects., as these species do not repel each other. Moreover, the hot light-soaking performed in Figure 68 showed the normalised lifetime to degrade more with increasing time. This suggests that the defect is activated with light and temperature which coincides with H-related damage [122], [244], [249]. Lastly, H-related damage introduced via H-exposure is likely to demonstrate a concentration gradient behaviour related to its diffusion coefficient. This is in contrast to defects caused by impurities already present in the bulk, activated by temperature, which would be present and cause damage throughout the depth of the wafer.

Figure 63 demonstrates that the TMAH etch of the n-type sample largely removed the H-related defect region as seen by the recovered lifetime after each 3 minute etch, which corresponded to approximately 1.6 μm removed from both surfaces of Si after 12 minutes. This amount of material removed to recover lifetime is concurrent with the calculations for H-diffusion through n-type Si in Section 6.1.4. Using the equations in Section 6.1.4 to calculate the intrinsic diffusion length of H in Si at 350 °C, D_L is found to be in the range of 23 μm. However, the effective diffusivity of H is expected to be much slower, especially in n-type Si, [234], and a certain level of H is needed to create the observed H-related defect. As such, a damaged layer with a width of approximately 2 μm is well within the expected H-diffusivity.

Even after this lifetime-recovering etching process, all of the TMAH etched n-type samples still showed some defect complex being activated through the hot light-soaking. This indicates that some of these defects are produced deeper than the 2 μm of material removed by the 12 min TMAH etch and only become recombination active upon light and elevated temperature exposure. It was seen that a longer etch time resulted in a lower concentration of defects being activated after hot light-soaking n-type FZ Si samples. This is consistent with the hypothesis that SHP causes a concentration of H-induced recombination centers towards the wafer surface, and is therefore in the form of a damaged layer, as postulated by the models in Section 6.1.4. In contrast to the n-type material, introduction of H by SHP into p-type FZ Si without a surface dielectric does not produce defects which are immediately electrically active. This is likely to be caused by the type of H species present in n-type compared to p-type material as previously discussed. It is likely that the p-type samples would exhibit a lifetime decrease after light-soaking, as previously shown in the literature [245].

The results using PEDOT:PSS on n-type Si with 100 nm SiO_2 and K^+ ions drifted at the interface showed a significant decrease in lifetime. It was seen in Figure 66 and Figure 67, that the shape of the lifetime curves had an indicative dip at low

injection level. This dip has been reported to predominantly occur in the presence of near-surface damage by Steingrube [250], which corroborates the models presented in Section 6.1.4.

The models postulated in Section 6.1.4 include a new theory of dipole-aided H transport across the SiO_2-Si interface. This theory states that the dielectric layer does indeed act as a diffusion barrier to H, as the literature suggests, but that it is the interface that hinders the introduction rate of H into Si from the oxide rather than the diffusion of H across this oxide. When charged ions are located at this interface, the strong field generated is enough to aid the transport of H across the interface, thereby increasing the concentration of H in the near-surface region of Si. The results observed in Figure 70 lend strong support to this claim. Two p-type Si samples with the same 100 nm SiO_2 were used. One had K^+ ions at the interface, and therefore had a strong field across the interface, whilst the other had no ions. Both samples were exposed to the same SHP treatment. Using C-V characterisation, it was possible to record the concentration of H-B pairs in the first 300 nm of the samples. The sample with ions at the interface showed a two-fold increase in H-B pairs than the sample without any ions. Although C-V characterisation is not as indicative as an eCV characterization, due to the measurement being limited to a shallower depth (300 nm compared to 10 μm), this result gives strong indication that the dipole at the interface does indeed increase the flux of H into Si.

Since H introduction with ionic FEP remained a low-temperature process, the diffusivity of H in Si was low, leading to a high concentration of H in the near-surface region. It is believed that this caused H concentration to reach the defect production threshold, explaining the reduction in lifetime seen in Figure 55. In order to investigate the presence of this concentration threshold, Al foil was used for SHP H exposure. Al foil was shown in Chapter 5 Section 5.2.6 to introduce H at a rate 16 times slower than Pd-Ag foil. Figure 71 a) and b) show that introducing the same level of H at a slower rate using Al foil mitigated the lifetime

decrease. This is strong evidence for the existence of a threshold concentration, since a slower, less concentrated, incorporation of H is less defect-inducing.

Although the results presented in this chapter provide compelling evidence for H being the cause of the lifetime-limiting defects, the exact nature of the defect remains unclear. It has been reported that in high concentrations and at low temperatures H can lead to the formation of recombination active complexes [131]. The formation of H stabilized platelets (or micro-cracks) within the first 100 nm of the exposed Si surface has been observed by a number of authors [131]–[133] using transmission electron microscopy (TEM). However, these authors observe these defects when atomic H is introduced at 150 °C and they are seen to decrease in density during a 350 °C 60 min anneal. In this thesis, the introduction of H at 350 °C using SHP is shown to still cause H-related defects, therefore it is unlikely for platelets or microcracks to be responsible for the damaged region seen in this thesis. Additionally, the defect created is much deeper than 100 nm as it is still present after a 9 minute etch which approximates to 1 μm of material removed.

The results presented and the subsequent analysis in this chapter are strong evidence in support of the models proposed. The damage seen is indeed H-related and occurs much more when a certain concentration threshold is reached, and at low temperature in n-type Si. The data presented suggest that it is the transport across the SiO_2/Si interface that is the rate limiting step for incorporation of H into Si through an oxide layer. This limiting step can be overcome through K^+ introduction at the interface generating a field which increases the rate at which H is incorporated into Si from SiO_2.

6.2.1 Further Work

Although the results presented in Chapter 5 were compelling towards validating the H-transport models, some questions remain unanswered. The lifetime-limiting

defect was confirmed to be H-related and likely not to be in the form platelets nor microcracks and certainly not the very near (100 nm) surface platelets observed by others to form at 150 °C. However, the exact form of the H-related defect remains unknown.

The necessity of a certain H concentration for immediate H-damage in n-type Si was seen, however the value of this concentration remains unknown. The following three experiments would allow for the quantification of it, but were deemed outside the scope of this thesis:

1. High temperature SHP exposure: introducing H above 400 °C would allow for the diffusivity of H to be increased, thus observing the point at which the concentration threshold is not reached.
2. Using TEM to investigate the identity of the H-related defects induced via SHP on bare Si as well as K^+ drifted samples. This would provide additional evidence that the defect observed in this thesis is not platelets or microcracks.
3. Conducting eCV characterisation of B-doped wafers with thin and thick oxides and with and without K^+ ions at the interface. This would provide more evidence that H-transport through the oxide is extremely fast, and as such is thickness independence. It would also allow for the quantification of the H-concentration increase when ions are present through a deeper depth than in Figure 70.

CHAPTER 7 SUMMARY & FURTHER WORK

The work in this thesis focused on devising methods to improve the efficiency of Si solar cells, namely through H passivation.

Hydrogen in semiconductors has been extensively researched for the past 30 years, primarily due to its ability to passivate both deep-level defects and shallow-level dopants [48], [51], [121]. Passivation is a phenomenon whereby fast diffusing interstitial H binds to crystallographic defects or impurities resulting in a reduction in their electrical activity. As such, the introduction of H into Si is commonly perceived as a performance enhancing process, and is standard in the vast majority of commercial Si solar cells.

H passivation is routinely done in the manufacturing of solar cells. The most common method involves the deposition of H rich dielectrics such as SiN_x:H and a post deposition fire to release H into Si. However, this vacuum based batch-process technique requires a high temperature firing step which can be unfavorable for new generation solar cells, such as organic cells and heterojunctions. A low temperature alternative exists: Remote Plasma Hydrogenation, but the machinery required is very specialist and remains a batch process.

In this thesis, a novel technique of damage-free, direct H passivation, developed during this doctorate, and dubbed Shielded Hydrogen Plasma (SHP), is used to introduce atomic H into Si wafer. This method allows for the excellent passivation of SiO_2-Si interfaces as well as the investigation of purely H induced defects without the need for a high temperature dielectric firing step.

The aims of this thesis were as follows:

1. Demonstrate atomic H being released from Pd,
2. Establish SHP as a damage free, low temperature, hydrogenation technique,
3. Observe the efficacy of SHP on different structures,
4. Analyse the possibility of converting SHP to an in-line process with the use of different metallic shields,
5. Introduce SHP as a tool to study H-movement in SiO_2,
6. Attempt to understand H-related damage in n-type FZ Si.

These aims were addressed in the three different results and discussion Chapters. The first results Chapter 4, introduced SHP as a hydrogenation technique and went on to show atomic H release as well as its damage-free quality. Chapter 5, followed by displaying the efficacy of SHP on different thicknesses oxides as well as on p-type Si. Chapter 5 also considered and tested different metals to use as a shield in SHP and their potential for an in-line conversion. Lastly, Chapter 6 showed the effect of SHP on bare n-type Si and on SiO_2 with ions at the interface, and the damage associated with those exposures. The summary of these findings as well as areas for further work are reviewed below.

7.1 Shielded Hydrogen Plasma – A novel Hydrogenation Technique

In Chapter 4 it was hypothesised that atomic H was released from the underside of the Pd leaf. This postulate went against most of the published literature on H movement through Pd. Experiments were devised to gather evidence for that hypothesis as well as discount any other possible explanation of the observed H in n-type Si.

It was seen that a anneal in pure H_2 gas at 200 °C did not lead to any B deactivation in the Si sample, suggesting that H_2 is incapable of dissociating on

the surface of Si at those low temperatures. This leads to the conclusion that the H-B pairs seen in the Si sample exposed to H from SHP must originate from atomic H present on the underside of the leaf. Additionally, a comparison with a direct plasma exposed sample was conducted and lower levels of H-B pairs were recorded than in the shielded sample. This suggests that the direct plasma causes surface damage which traps a fraction of the introduced atomic H. This leads to the conclusion that SHP is indeed damage free as more H-B pairs are recorded.

The somewhat unexpected observation of atomic H being released from a Pd film opens up a number of exciting new possibilities. SHP is both an effective source of atomic H and is damage free. This Chapter has demonstrated the importance of leaf preparation and the effectiveness of SHP on thin Si oxides, achieving minority carrier lifetimes of 2.2 ms at 10^{15} cm^{-3} injection level. The effect of temperature was also observed over a small range, where more atomic H is seen to deactivate B acceptors as the temperature increases.

SHP has the potential to be an alternative to forming gas anneals and remote plasma exposures by performing efficient H passivation at low temperatures, with no damage and with minimal equipment needed. Furthermore, this technique could allow the samples to be located in a separate chamber from the plasma itself, opening up the possibility for in-line processing as explored in Chapter 5. In order to realize this, shields will need to be demonstrated that are capable of withstanding pressure differences of up to 1 atm, while also maintaining sufficient atomic H fluxes at the sample surface.

For this reason, Chapter 4 focused on analysing the effect of shield thickness and shield material on levels of H introduced, as well as applying SHP to different Si material.

7.2 SHP: Applications and Metallic Shield Investigation

In this second results chapter, two main topics were discussed. The first was the application of SHP to different Si structures and materials. This included exposing 100 nm SiO_2-Si and p-type material to H from SHP. The result on 100 nm SiO_2-Si n-type material was exceptional, achieving a minority carrier lifetime of 6.3 ms at 10^{15} cm^{-3} injection level which was, at the time of publication, the highest lifetime achieved on this structure. Dr Collett, surpassed this lifetime using intrinsic ionic field effect passivation in 2019.

The possibility of converting the current, batch PECVD process SHP, to an in-line system was discussed in Chapter 5. In the in-line design the plasma chamber remains in a vacuum whilst the samples are separated from the vacuum by the metallic shield. The samples are processed in a low-pressure environment via a conveyor belt. In order for this system to be possible, the shield must sustain a pressure differential of at least 1 atm. Calculations were made in Chapter 4, that showed that a Pd shield must be around 2 μm in thickness to sustain this pressure without failure. This led to the test of thicker Pd-Ag foils as well as other metals such as Al, Ni and Pt. The results showed that the Pd-Ag foil, which was 100 times thicker than the leaf used in Chapter 4, introduced similar levels of H into the Si sample. This result was evidence for the H-transport through bulk Pd not being a rate limiting step in H introduction into Si from SHP. The other metals tested had expected results which correlated with their H-diffusivities. It was found that using Al foil as a shield introduced H into B doped Si 16 times slower than Pd-Ag foil, which was then a useful property in Chapter 5.

SHP was then compared to other common hydrogenation techniques. Somewhat unexpectedly, more H-B pairs were observed in the shielded plasma sample than in the direct plasma sample. This is thought to be caused by the additional H traps created with the associated plasma damage in the directly exposed sample.

When comparing lifetime n-type FZ samples exposed to H from SHP and direct plasma, SHP greatly outperforms the direct plasma sample whose lifetime remains extremely low, even post corona charging. SHP was then compared with a technique similar to a forming gas anneal (FGA). Instead of using a mixture of N_2 and H_2, pure H_2 gas was used to increase the possible level of H-B pairs. SHP introduced almost 7 times more H than the H_2 anneal at 200 °C. The next technique compared was wet or acidic hydrogenation. HF dips are known to improve interfaces through hydrogenation, but it was unclear how much H would be introduced from HF after a 200 °C anneal post HF dip. The levels of H-B pair observed using HF and an anneal were negligible compared to SHP which introduced more than an order of magnitude more H into the Si sample. The most common hydrogenation technique in solar cells remains fired H-rich SiN_x dielectrics, which made it an obvious technique to compare to SHP. Since the experiments in this thesis were constrained to a low temperature due to equipment restrictions, it was impossible to obtain SHP results at the normal firing temperatures above 600 °C. As such, the comparison was done through experimental results published in the literature. Somewhat unexpectedly, SHP performed at 200 °C introduced nearly two-fold more H than a fired SiN_x at 600 °C. The authors [87] showed that although the SiN_x layer is deposited with a high concentration of H (1×10^{22} cm^{-3}), only 0.15% is introduced into bulk Si. The remaining is either trapped or effuses out of the SiN_x. As such, SHP introduces almost two-fold more H at 200 °C than the fired SiN_x at 600 °C.

Lastly, the technique most direct comparable to SHP was tested: Remote Plasma Hydrogenation. Lifetime tests were conducted on a remote-plasma hydrogenated sample, which was treated at Manchester University. The lifetime of this sample is seen to be much lower than a typical SHP sample under similar conditions, 4 μs compared to 6.3 ms at the 10^{15} cm^{-2} injection level. The low lifetime of the remote plasma was attributed to a potentially broken-down oxide. Experiments

reported in the literature [105] have observed concentrations of H-B pairs using an industrial remote-plasma tool (RIPA) of the order of 10^{14} cm^{-2}, which is an order of magnitude more than the level seen with SHP. This comparison is not ideal however, as the RIPA power used was 1 kW compared to 100 W in SHP. More experiments would be required to compare the techniques further.

The discussion from Chapter 4, introduced the question of which step was rate limiting for the introduction of H into Si from SHP, this question was addressed more in depth in Chapter 5.

7.3 SHP to Study H-Related Defects

Chapters 3 and 4 have introduced Shielded Hydrogen Plasma as a successful H passivation technique for Si. SHP introduces atomic H at low temperatures without any surface damage. Chapter 5 introduced SHP as an effective H introduction tool to study H-related defects in Si and the movement of H in SiO_2-Si and across that interface.

The results presented in this last chapter showed that introducing H from SHP into dielectric free n-type causes a dramatic lifetime crash caused by a damaged layer in the near surface region. This damage layer was, surprisingly at first, also observed on n-type 100 nm SiO_2-Si but only with the presence of K^+ ions at the interface.

These results led to a questioning and finally a new understanding of H-transport through SiO_2 and across the SiO_2-Si interface.

It was postulated that the transport through SiO_2 is in fact extremely fast, and it is the interface energy barrier that impedes the diffusion of H into bulk Si. When ions are drifted to this interface, they carry a considerable charge, generating a dipole across the interface. This dipole induces a field which allows

H to overcome the energy barrier and diffuse, at high rate, into Si reaching a certain threshold concentration.

This threshold concentration was the other main postulate from Chapter 5. H must be present in a high concentration in order to form the observed defect layer. This would explain why at high temperatures H-related damage is not seen in bare n-type Si, due to the increased diffusion rate of H through the bulk. The identification of the damage being H-related was also investigated and gathered strong evidence. Since the damage is not seen in p-type, both using the bare Si introduction and the field aided introduction, it is very likely that H is responsible for the damage as it is in a different species in p-type, which is not conducive to damage. Additionally, H is known to be in high concentrations from SHP and the damage density is seen to increase under light and elevated temperature, all indications that H is indeed the cause of the minority carrier lifetime reduction.

7.4 Conclusions and Further Work

This thesis has investigated many aspects of H introduction into Si: from its beneficial effect via the novel technique of Shielded Hydrogen Plasma, to the H-related damage seen in n-type FZ Si. Two main postulates have contradicted the accepted literature: atomic H can be released from the surface of Pd, and the transport of H from SiO_2 is interface limited rather than diffusion limited. Results have been presented throughout this thesis that have gathered compelling evidence for these postulates, however there are more key experiments to be done to concretise these theories.

A major limitation of this doctorate was the inability to perform high temperature SHP. This would be feasible in a high temperature PECVD machine, which is quite common but unavailable at the University of Oxford. High temperature SHP would allow to test different metals at high temperatures which may not allow H to permeate at lower temperatures, it would also allow to test in another

way the presence (or absence at high temperature) of a damage-inducing concentration threshold by increasing the diffusivity of H in Si.

Along with the additional experiments suggested in Chapter 5, it would be interesting to build an in-line SHP system prototype. Indeed, SHP is currently an excellent laboratory technique, but an in-line version of it would enable the technique to be adopted by industry.

To conclude, I have high hopes that SHP will remain a popular technique in the years to come, certainly at the University of Oxford and the group's research partners: Manchester University, Warwick and Southampton as well as its international partners UNSW. It is my belief that SHP will begin to gain real traction when next generation solar cells gain market share as it is the only effective low temperature hydrogenation technique that has been shown to have in-line production potential.

REFERENCES

[1] IPCC, "SPECIAL REPORT: GLOBAL WARMING OF 1.5 °C," 2018. Chapter 3, pp. 1-143.

[2] K. Northon, "Long-Term Warming Trend Continued in 2017: NASA, NOAA," *NOAA*, 2018. Web Page. https://climate.nasa.gov/.

[3] "Climate Change 2014 Synthesis Report Summary for Policymakers," *Intergov. Panel Clim. Chang.*, 2014. Report vol. 1, pp. 1-143.

[4] A. Shepherd and D. Wingham, "Recent sea-level contributions of the Antarctic and Greenland ice sheets," *Science*, vol. 315, no. 5818. pp. 1529–1532, 2007.

[5] A. Shepherd, "Antarctica unravelled," *Physics World*, vol. 19, no. 5. pp. 21–26, 2006.

[6] H. Konrad *et al.*, "Net retreat of Antarctic glacier grounding lines," *Nat. Geosci.*, vol. 11, no. 4, pp. 258–262, 2018.

[7] WWF, *Living Blue Planet Report*. Online Report, vol, 1. 2015.

[8] B. S. R. of W. Energy, "67 th edition - BP Statistical Review of World Energy," 2018. Report, vol. 67.

[9] M. A. Green, "Photovoltaics: Technology overview," *Energy Policy*, vol. 28, no. 14, pp. 989–998, 2000.

[10] IEA, International Energy Agency. *Renewables 2018*. [Online Report] 2018.

[11] S. Heck, K. Aanesen, and D. Pinner, "Solar power: Darkest before dawn," *McKinsey Co.*, no. May, pp. 1–16, 2012.

[12] International Energy Agency, "2018 Snapshot of Global Photovoltaic Markets - IEA PVPS," *Rep. IEA PVPS T1-332018*, pp. 1–16, 2018.

[13] Perfomance Measure British Petroleum, "Bp Technology Outlook," no. November, pp. 43, 2015. Online Presentation.

[14] Shell International B.V., "Meeting the goals of the Paris agreement (Sky scenario)," pp. 72, 2018.

[15] International Technology Roadmap for Photovoltaic, "ITRPV Ninth Edition 2018 including maturity report," 2018.

[16] C. Battaglia, A. Cuevas, S. De Wolf, "High-efficiency crystalline silicon solar cells: Status and perspectives." Energy and Environmental Science. 9 (2016), pp. 1552–1576.

[17] R. Fu, D. Feldman, and R. Margolis, "U . S . Solar Photovoltaic System Cost Benchmark : Q1 2018," 2018.

[18] M. Green, "Solar Cells- Operating Principles, Technology and System Applications," *Englewood Cliffs, NJ, Prentice-Hall, Inc., 1982. 28*. pp. 1–39, 1982.

[19] M. A. Green, *Silicon Solar Cells: Advanced Principles & Practice*. Centre for Photovoltaic Devices and Systems, University of New South Wales, pp. 199, 1995.

[20] ENF, "ENF List of Solar Companies and Products - Including Solar Panel and Inverter PV Manufacturers," *ENF*, 2019. [Online]. Available: https://www.enfsolar.com/.

[21] K. Masuko *et al.*, "Achievement of more than 25% conversion efficiency with crystalline silicon heterojunction solar cell," *IEEE J. Photovoltaics*, 2014.

[22] C. T. Sah, R. N. Noyce, and W. Shockley, "Carrier Generation and Recombination in P-N Junctions and P-N Junction Characteristics," *Proc. IRE*, vol. 45, no. 9, pp. 1228–1243, 1957.

[23] S. M. Sze and K. K. Ng, *Physics of Semiconductor Devices*. 2007. Print.

[24] S, R, Bonilla, "Surface passivation for silicon solar cells," University of Oxford, DPhil Thesis, 2015.

[25] W. Shockley and W. T. Read, "Statistics of the Recombination of Holes and Electrons,"

Phys. Rev., vol. 87, no. 46, pp. 835–842, 1952.

[26] K. Collett, "Surface Passivation for Silicon Solar Cells using Stable Extrinsic Field Effect Passivation" Department of Materials Science Literature Review, University of Oxford, September, 2015.

[27] A. Metz *et al.*, "International Technology Roadmap for Photovoltaic (ITRPV) 2014," 2015 6th edition.

[28] Y. P. Varshni and Y. P. Varshni, "Temperature dependence of the energy gap in semiconductors," *Physica*, vol. 34, pp. 149–154, 1967.

[29] M. A. Green, "Third generation photovoltaics: Ultra-high conversion efficiency at low cost," *Prog. Photovoltaics Res. Appl.*, vol. 9, no. 2, pp. 123–135, 2001.

[30] J. Dziewior and W. Schmid, "Auger coefficient for highly doped and highly excited silicon," *Appl. Phys. Lett.*, vol. 31, pp. 346–348, 1977.

[31] A. Hangleiter and R. Hocker, "Enhancement of band-to-band Auger recombination by electron-hole correlations," *Phys. Rev. Lett.*, vol. 65, no. 2, pp. 215–218, 1990.

[32] S. W. Glunz, D. Biro, S. Rein, and W. Warta, "Field-effect passivation of the SiO_2Si interface," *J. Appl. Phys.*, vol. 86, no. 1, p. 683, 1999.

[33] P. P. Altermatt, F. Geelhaar, T. Trupke, X. Dai, A. Neisser, and E. Daub, "Injection dependence of spontaneous radiative recombination in crystalline silicon: Experimental verification and theoretical analysis," *Appl. Phys. Lett.*, vol. 88, no. 26, 2006.

[34] A. Richter, S. W. Glunz, F. Werner, J. Schmidt, and A. Cuevas, "Improved quantitative description of Auger recombination in crystalline silicon," *Phys. Rev. B - Condens. Matter Mater. Phys.*, vol. 86, no. 16, 2012.

[35] R. N. Hall, "Electron-hole recombination in germanium" *Physical Review*. 87 (1952), pp. 387.

[36] N. E. Grant, F. E. Rougieux, D. MacDonald, J. Bullock, and Y. Wan, "Grown-in defects mlimiting the bulk lifetime of p -type float-zone silicon wafers," *J. Appl. Phys.*, vol. 117, no. 5, 2015.

[37] E. C. Shaw, P. Hamer, K. A. Collett, G. Bourrett-Sicotte, R. S. Bonilla, and P. R. Wilshaw, "Saw Damage Gettering for industrially relevant mc-Si feedstock," *Phys. Status Solidi Appl. Mater. Sci.*, vol. 214, no. 7, 2017.

[38] D. Chen *et al.*, "Hydrogen Induced Degradation: A Possible Mechanism for Light- and Elevated Temperature-induced Degradation in n-type Silicon," *Sol. Energy Mater. Sol. Cells*, 2017.vol. 185, pp. 174-182

[39] M. Kim *et al.*, "Impact of thermal processes on multi-crystalline silicon," *Front. Energy*, 2017. vol 11, no. 1, pp. 32–41.

[40] G. Bauer, "Absolutwerte der optischen Absorptionskonstanten von Alkalihalogenidkristallen im Gebiet ihrer ultravioletten Eigenfrequenzen," *Ann. Phys.*, 1934. vol. 411, no. 4, pp. 434-464

[41] M. A. Green and M. J. Keevers, "Optical properties of intrinsic silicon at 300 K," *Prog. Photovoltaics Res. Appl.*, 1995. vol. 3, pp. 189-192.

[42] A. G. Aberle, "Crystalline Silicon Solar Cells: advanced surface passivation and analysis." Sydney, Australia: UNSW, pp. 335, 2009 [Print].

[43] E. Mollwo and D. Zwingel, "ESR and luminescence of trapped hole centers in ZnO and SnO_2," *J. Lumin.*, vol. 12–13, no. C, pp. 441–445, 1976.

[44] E. . Haller, B. Joos, and L. M. Falicov, "Acceptor complexes in germanium: Systems with tunneling hydrogen," *J. Chem. Inf. Model.*, vol. 53, no. 4798, pp. 160, 1989.

[45] C. T. Sah, J. Y. C. Sun, and J. J. T. Tzou, "Deactivation of the boron acceptor in silicon by hydrogen," *Appl. Phys. Lett.*, vol. 43, no. 2, pp. 204–206, 1983.

[46] J. I. Pankove and M. L. Tarng, "Amorphous silicon as a passivant for crystalline silicon," *Appl. Phys. Lett.*, vol. 34, no. 2, pp. 156–157, 1979.

[47] N. M. Johnson and S. K. Hahn, "Hydrogen passivation of the oxygen-related thermal-

donor defect in silicon," *Appl. Phys. Lett.*, vol. 48, no. 11, pp. 709–711, 1986.

[48] C. G. Van de Walle and J. Neugebauer, "Hydrogen in semiconductors," *Bull. Mater. Sci.*, vol. 19, no. 1, pp. 39–50, 1996.

[49] S. J. Pearton, J. W. Corbett, and T. S. Shi, "Hydrogen in crystalline semiconductors," *Appl. Phys. A Solids Surfaces*, vol. 43, no. 3, pp. 153–195, 1987.

[50] R. Lüdemann, "Hydrogen passivation of multicrystalline silicon solar cells," *Mater. Sci. Eng. B*, vol. 58, pp. 86–90, 1999.

[51] B. L. Sopori *et al.*, "Hydrogen in silicon: A discussion of diffusion and passivation mechanisms," *Sol. Energy Mater. Sol. Cells*, vol. 41–42, pp. 159–169, 1996.

[52] M. Stavola *et al.*, "IR characterization of hydrogen in crystalline silicon solar cells," *Phys. B Condens. Matter*, vol. 404, no. 23–24, pp. 5066–5070, 2009.

[53] P. Hamer, B. Hallam, S. Wenham, and M. Abbott, "Manipulation of Hydrogen Charge States for Passivation of P-Type Wafers in Photovoltaics," *IEEE J. Photovoltaics*, vol. 4, no. 5, pp. 1252–1260, 2014.

[54] N. M. Johnson, C. Herring, and C. G. Van De Walle, "Inverted order of acceptor and donor levels of monatomic hydrogen in silicon," *Phys. Rev. Lett.*, vol. 73, no. 1, pp. 130–133, 1994.

[55] C. Herring, N. Johnson, and C. Van de Walle, "Energy levels of isolated interstitial hydrogen in silicon," *Phys. Rev. B*, vol. 64, no. 12, pp. 1–27, 2001.

[56] B. J. Hallam *et al.*, "Hydrogen passivation of B-O defects in Czochralski silicon," in *Energy Procedia*, 2013, vol. 38, pp. 561–570.

[57] B. L. Sopori, Y. Zhang, and R. Reedy, "H diffusion for impurity and defect passivation: A physical model for solar cell processing," *Conf. Rec. 29th IEEE Photovolt. Spec. Conf. 2002*, May, pp. 222–226, 2002.

[58] S. Lindekugel, H. Lautenschlager, T. Ruof, and S. Reber, "Plasma Hydrogen Passivation For Crystalline Silicon Thin-Films," *Sol. Energy*, no. 1 September, pp. 2232–2235, 2008.

[59] J. Schmidt, M. Kerr, and A. Cuevas, "Surface passivation of silicon solar cells using plasma-enhanced chemical-vapour-deposited SiN films and thin thermal SiO 2 plasma SiN stacks," *Semicond. Sci. Technol.*, vol. 16, no. 3, p. 164, 2001.

[60] Z. Zhuo *et al.*, "Interface properties of SiOxNy layer on Si prepared by atmospheric-pressure plasma oxidation-nitridation," *Nanoscale Res. Lett.*, vol. 8, no. 1, p. 201, 2013.

[61] A. Aberle, S. Glunz, and W. Warta, "Field effect passivation of high efficiency silicon solar cells," *Sol. Energy Mater. Sol. Cells*, vol. 29, no. 2, pp. 175–182, Mar. 1993.

[62] N. M. Terlinden, G. Dingemans, M. C. M. van de Sanden, and W. M. M. Kessels, "Role of field-effect on c-Si surface passivation by ultrathin (2–20 nm) atomic layer deposited Al2O3," *Appl. Phys. Lett.*, vol. 96, no. 11, pp. 112101, Mar. 2010.

[63] S. W. Glunz, D. Biro, S. Rein, and W. Warta, "Field-effect passivation of the SiO2-Si interface," *J. Appl. Phys.*, vol. 86, no. 1, pp. 683, 1999.

[64] J. Mandelkorn and J. H. Lamneck, "Simplified fabrication of back surface electric field silicon cells and novel characteristics of such cells," *Sol. Cells*, vol. 29, no. 2-3 pp. 121-130, 1990.

[65] K. Collett, "Surface Passivation for Silicon Solar Cells using Stable Extrinsic Field Effect Passivation," University of Oxford, DPhil Thesis 2018.

[66] R. S. Bonilla, F. Woodcock, and P. R. Wilshaw, "Very low surface recombination velocity in n-type c-Si using extrinsic field effect passivation," *J. Appl. Phys.*, vol. 116, no. 5, pp. 054102, 2014.

[67] A. G. Aberle, S. Glunz, and W. Warta, "Impact of illumination level and oxide parameters on Shockley-Read-Hall recombination at the Si-SiO2 interface," *J. Appl. Phys.*, vol. 71, no. 9, pp. 4422–4431, 1992.

[68] S. Dauwe, J. Schmidt, A. Metz, and R. Hezel, "Fixed charge density in silicon nitride films

on crystalline silicon surfaces under illumination," *Conference Record of the IEEE Photovoltaic Specialists Conference* 2003, pp. 162–165.

[69] J. Schmidt *et al.*, "Advances in the Surface Passivation of Silicon Solar Cells," *Energy Procedia*, vol. 15, pp. 30–39, Jan. 2012.

[70] B. Hoex, J. J. H. Gielis, M. C. M. van de Sanden, and W. M. M. Kessels, "On the c-Si surface passivation mechanism by the negative-charge-dielectric Al_2O_3," *J. Appl. Phys.*, vol. 104, no. 11, pp. 113, 2008.

[71] A. G. Aberle, S. Glunz, and W. Warta, "Impact of illumination level and oxide parameters on Shockley-Read-Hall recombination at the Si-SiO_2 interface," *J. Appl. Phys.*, vol. 71, no. 9, pp. 4422-4431, 1992.

[72] D. Suh, W. Liang, and K. Weber, "The study of Al_2O_3 Passivation by corona charge," *27th Eur. Photovolt. Sol. Energy Conf. Exhib.*, Proceedings, 2012.

[73] S. Mack *et al.*, "Silicon surface passivation by thin thermal Oxide/PECVD layer stack systems," *IEEE J. Photovoltaics*, vol. 1, no. 2, pp. 135–145, Oct. 2011.

[74] Y. Larionova, V. Mertens, N.-P. Harder, and R. Brendel, "Surface passivation of n-type Czochralski silicon substrates by thermal-SiO2/plasma-enhanced chemical vapor deposition SiN stacks," *Appl. Phys. Lett.*, vol. 96, no. 3, pp. 032105, Jan. 2010.

[75] M. Goldman, A. Goldman, and R. S. Sigmond, "The corona discharge, its properties and specific uses," *Pure Appl. Chem.*, vol. 67, no. 9, pp. 1353-1362, 1985.

[76] D. K. Schroder, M. S. Fung, R. L. Verkuil, S. Pandey, W. H. Howland, and M. Kleefstra, "Corona-oxide-semiconductor device characterization," Third Edition (2005) pp. 1-779, Published by John Wiley and Sons

[77] T. C. Kho, S. C. Baker-Finch, and K. R. McIntosh, "The study of thermal silicon dioxide electrets formed by corona discharge and rapid-thermal annealing," *J. Appl. Phys.*, vol. 109, no. 5, pp. 6, 2011.

[78] R. S. Bonilla, C. Reichel, M. Hermle, S. Senkader, and P. R. Wilshaw, "Controlled field effect surface passivation of crystalline n-type silicon and its application to back-contact silicon solar cells," in *2014 IEEE 40th Photovoltaic Specialist Conference (PVSC)*, pp. 571–576, 2014.

[79] R. S. Bonilla and P. R. Wilshaw, "Stable field effect surface passivation of n-type Cz silicon," in *Energy Procedia - Proceedings of the 3rd Silicon PV Conference*, vol. 38, pp. 816–822, 2013.

[80] H. Amjadi, "Investigations on charge storage and transport in plasma-deposited inorganic electrets," *Dielectr. Electr. Insul. IEEE Trans.*, vol. 6, no. 2, pp. 236–241, Apr, 1999.

[81] R. S. Bonilla and P. R. Wilshaw, "A technique for field effect surface passivation for silicon solar cells," *Appl. Phys. Lett.*, vol. 104, no. 23, 2014.

[82] R. S. Bonilla and P. R. Wilshaw, "A technique for field effect surface passivation for silicon solar cells," *Appl. Phys. Lett.*, vol. 104, no. 23, 2014.

[83] R. S. Bonilla, K. Collett, L. Rands, G. Martins, R. Lobo, and P. R. Wilshaw, "Stable, Extrinsic, Field Effect Passivation for Back Contact Silicon Solar Cells," *Solid State Phenom.*, vol. 242, pp. 67–72, Oct. 2015.

[84] N. H. Nickel, "Hydrogen diffusion through silicon/silicon dioxide interfaces Hydrogen diffusion through silicon-silicon dioxide interfaces," *J. Vac. Sci. Technol. B*, vol. 18, 2000.

[85] R. Rizk, P. De Mierry, D. Ballutaud, M. Aucouturier, and D. Mathiot, "Hydrogen diffusion and passivation processes in p- and n-type crystalline silicon," *Phys. Rev. B*, vol. 44, no. 12, pp. 6141–6151, 1991.

[86] B. J. Hallam *et al.*, "Advanced Bulk Defect Passivation for Silicon Solar Cells," *IEEE J. Photovoltaics*, vol. 4, no. 1, pp. 88–95, Jan. 2014.

[87] M. Stavola *et al.*, "Hydrogenation of Si from SiNx : H films: How much hydrogen is really in the Si?," *Proc. 3rd World Conf. Photovolt. Energy Conversion, Vols a-C*, pp. 909–912, 2003.

[88] B. Hallam, B. Tjahjono, and S. Wenham, "Effect of PECVD silicon oxynitride film composition on the surface passivation of silicon wafers," *Sol. Energy Mater. Sol. Cells*, vol. 96, no. 1, pp. 173–179, 2012.

[89] S. Wilking, A. Herguth, and G. Hahn, "Influence of hydrogen on the regeneration of boron-oxygen related defects in crystalline silicon," *J. Appl. Phys.*, vol. 113, no. 19, 2013.

[90] M. Blech *et al.*, "Detailed Study of PECVD Silicon Nitride and Correlation of Various Characterization Techniques," *24th Eur. Photovolt. Sol. Energy Conf. Exhib.*, pp. 507–511, 2009.

[91] M. Stutzmann, "Hydrogen passivation of boron acceptors in silicon: Raman studies," *Phys. Rev. B*, vol. 35, no. 11, pp. 5921–5924, 1987.

[92] P. C. Srivastava and U. P. Singh, "Hydrogen in semiconductors," *Bull. Mater. Sci.*, vol. 19, no. 1, pp. 39–50, 1996.

[93] S. Watanabe, N. Nakayama, and T. Ito, "Homogeneous hydrogen-terminated Si(111) surface formed using aqueous HF solution and water," *Appl. Phys. Lett.*, vol. 59, no. 12, pp. 1458-1460, 1991.

[94] U. Römer *et al.*, "Recombination behavior and contact resistance of n+ and p+ poly-crystalline Si/mono-crystalline Si junctions," *Sol. Energy Mater. Sol. Cells*, vol. 131, pp. 85–91, 2014.

[95] R. Choi, C. S. Kang, H.-J. Cho, Y.-H. Kim, M. S. Akbar, and J. C. Lee, "Effects of high temperature forming gas anneal on the characteristics of metal-oxide-semiconductor field-effect transistor with HFO_2 gate stack," *Appl. Phys. Lett.*, vol. 84, no. 24, pp. 4839–4841, 2004.

[96] B. Sopori, M. I. Symko, R. Reedy, K. Jones, and R. Matson, "Mechanism(s) of hydrogen diffusion in silicon solar cells during forming gas anneal," in *Conference Record of the Twenty Sixth IEEE Photovoltaic Specialists Conference* , 1997, pp. 25–30.

[97] B. Sopori, Y. Zhang, and N. M. Ravindra, "Silicon device processing in H-ambients: H-diffusion mechanisms and influence on electronic properties," *J. Electron. Mater.*, vol. 30, no. 12, pp. 1616-1627, 2001.

[98] M. Symko, "Dissociation of molecular hydrogen into atomic hydrogen," PhD Thesis, University of Denver, 1998.

[99] E. Galeazzo, W. J. Salcedo, H. E. Maldonado Peres, and F. J. Ramirez-Fernandez, "Porous silicon patterned by hydrogen ion implantation," *Sensors Actuators, B Chem.*, vool. 76, no. 3, pp. 3430346, 2001.

[100] D. J. Mazey, R. S. Nelson, and R. S. Barnes, "Observation of ion bombardment damage in silicon," *Philos. Mag.*, vol. 17, no. 150, pp. 1145–1161, 1968.

[101] S. J. Jeng, G. S. Oehrlein, and G. J. Scilla, "Hydrogen plasma induced defects in silicon," *Appl. Phys. Lett.*, vol. 53, no. 18, pp. 1735–1737, 1988.

[102] A. G. Aberle, "Overview on SiN surface passivation of crystalline silicon solar cells," *Sol. Energy Mater. Sol. Cells*, vol. 65, no. 1, pp. 239–248, 2001.

[103] C. Boehme and G. Lucovsky, "H loss mechanism during anneal of silicon nitride: Chemical dissociation," *J. Appl. Phys.*, vol. 88, no. 10, pp. 6055–6059, 2000.

[104] M. Sheoran *et al.*, "Hydrogen diffusion in silicon from plasma-enhanced chemical vapor deposited silicon nitride film at high temperature," *Appl. Phys. Lett.*, vol. 92, no. 17, pp. 1–4, 2008.

[105] P. G. Hamer, "Hydrogen Charge States and Dopant Interactions in Crystalline Silicon Solar Cells," PhD Thesis, University of New South Wales, August, 2014.

[106] M. Sheoran *et al.*, "Hydrogen diffusion in silicon from plasma-enhanced chemical vapor deposited silicon nitride film at high temperature," *Appl. Phys. Lett.*, vol. 92, no. 17, 2008.

[107] F. Duerinckx and J. Szlufcik, "Defect passivation of industrial multicrystalline solar cells based on PECVD silicon nitride," *Sol. Energy Mater. Sol. Cells*, vol. 72, no. 1–4, pp. 231–246, 2002.

[108] G. Dingemans and E. Kessels, "Status and prospects of Al_2O_3 - based surface passivation schemes for silicon solar cells," *J. Vac. Sci. Technol. A Vacuum, Surfaces Film.*, vol. 30, no. 4, pp. 1–27, Jul. 2012.

[109] S. De Wolf and M. Kondo, "Nature of doped a-Si:H/c-Si interface recombination," *J. Appl. Phys.*, vol. 105, no. 10, p. 103707, May 2009.

[110] T. Tatsumi, S. Fukuda, and S. Kadomura, "Etch Rate Acceleration Of sio2During Wet Treatment After Gate Etching," *Jpn. J. Appl. Phys.*, vol. 32, no. 12 S, pp. 6114–6118, 1993.

[111] T. Tatsumi, S. Fukuda, and S. Kadomura, "Radiation Damage of S i O2Surface Induced by Vacuum Ultraviolet Photons of High-Density Plasma," *Jpn. J. Appl. Phys.*, vol. 33, no. 4S, p. 2175, 1994.

[112] G. S. Oehrlein, R. M. Tromp, Y. H. Lee, and E. J. Petrillo, "Study of silicon contamination and near-surface damage caused by CF_4/H_2 reactive ion etching," *Appl. Phys. Lett.*, vol. 45, no. 4, pp. 420–422, 1984.

[113] T. Yunogami, T. Mizutani, K. Suzuki, and S. Nishimatsu, "Radiation damage in SiO_2/Si induced by vuv photons," *Jpn. J. Appl. Phys.*, vol. 28, no. 10 R, pp. 2172–2176, 1989.

[114] D. B. Graves, "Plasma Processing," *IEEE Trans. Plasma Sci.*, vol. 22, no. 1, pp. 31–42, 1994.

[115] H. C. Shin and C. Hu, "Thin gate oxide damage due to plasma processing," *Semicond. Sci. Technol.*, vol. 11, no. 4, pp. 463–473, 1996.

[116] L. M. Ephrath, "Parameter Dependence of RIE Induced Radiation Damage in Silicon Dioxide," *J. Electrochem. Soc.*, vol. 128, no. 11, p. 2415, 2006.

[117] M. Keevers, A. Turner, U. Schubert, P. A. Basore, and M. A. Green, "Remarkable effective hydrogenation of crystalline silicon on glass modules," *20th Eur. Photovolt. Sol. Energy Conf.*, no. January 2005, pp. 1305–1308, 2005.

[118] S. C. Kim *et al.*, "Hydrogenated Silicon Films Prepared by Remote Plasma CVD," *MRS Proc.*, Symposium, vol. 192, 2011.

[119] A. M. Wróbel, I. Błaszczyk-Łężak, A. Walkiewicz-Pietrzykowska, D. M. Bieliński, T. Aoki, and Y. Hatanaka, "Silicon Carbonitride Films by Remote Hydrogen-Nitrogen Plasma CVD from a Tetramethyldisilazane Source," *J. Electrochem. Soc.*, vol. 13, no. 4, pp. 731-737, 2004.

[120] S. Kar, J. I. Pankove, and Y. S. Tsuo, "Remote plasma hydrogenation of ion beam amorphized silicon," *Appl. Phys. Lett.*, vol. 59, no. 6, pp. 126-129, 1991.

[121] S. J. Pearton, "Hydrogen in Crystalline Semiconductors: Part I - Silicon," *Int. J. Mod. Phys. B*, vol. 8, no. 9, pp. 1093–1158, 1994.

[122] C. E. Chan *et al.*, "Rapid Stabilization of High-Performance Multicrystalline P-type Silicon PERC Cells," *IEEE J. Photovoltaics*, vol. 6, no. 6, pp. 1473–1479, 2016.

[123] K. Nakayashiki *et al.*, "Engineering Solutions and Root-Cause Analysis for Light-Induced Degradation in p-Type Multicrystalline Silicon PERC Modules," *IEEE J. Photovoltaics*, vol. 6, no. 4, pp. 860–868, 2016.

[124] K. Ramspeck *et al.*, "Light Induced Degradation of Rear Passivated mc-Si Solar Cells," *Proc. 27th Eur. Photovolt. Sol. Energy Conf.*, pp. 861–865, 2012.

[125] D. Bredemeier *et al.*, "Lifetime degradation and regeneration in multicrystalline silicon under illumination at elevated temperature," *AIP Adv.*, vol. 035119, no. 2016, 2017.

[126] D. Bredemeier, D. Walter, S. Herlufsen, and J. Schmidt, "Understanding the Light-induced Lifetime Degradation and Regeneration in Multicrystalline Silicon," *Energy Procedia*, vol. 92, pp. 773–778, 2016.

[127] T. Niewelt, M. Selinger, N. E. Grant, W. Kwapil, J. D. Murphy, and M. C. Schubert, "Light-induced activation and deactivation of bulk defects in boron-doped float-zone silicon," *J. Appl. Phys.*, vol. 121, no. 18, 2017.

[128] D. Sperber, A. Graf, A. Heilemann, A. Herguth, and G. Hahn, "Bulk and surface

instabilities in boron doped float-zone samples during light induced degradation treatments," *Energy Procedia*, vol. 124, pp. 794–798, 2017.

[129] C. Renevier, E. Fourmond, M. Forster, S. Parola, M. Le Coz, and E. Picard, "Lifetime degradation on n-type wafers with boron-diffused and SiO_2/SiN-passivated surface," *Energy Procedia*, vol. 55, pp. 280–286, 2014.

[130] D. Chen *et al.*, "Hydrogen Induced Degradation: A Possible Mechanism for Light- and Elevated Temperature- Induced Degradation in n-type Silicon," *Sol. Energy Mater. Sol. Cells*, vol. 185, pp. 174-182, 2018.

[131] N. M. Johnson, F. Ponce, R. Street, and R. Nemanich, "Defects in single-crystal silicon induced by hydrogenation," *Phys. Rev. B*, vol. 35, no. 8, 1987.

[132] S. K. Estreicher, "Hydrogen-related defects in crystalline semiconductors: a theorist's perspective," *Mater. Sci. Eng. R*, vol. 14, no. 7–8, pp. 319–412, 1995.

[133] N. H. Nickel, G. B. Anderson, and J. Walker, "Hydrogen-induced platelets in disordered silicon," *Solid State Commun.*, vol 99, no. 9, pp. 427-431, 1996.

[134] F. A. Lewis, "The Hydrides of Palladium and Palladium Alloys," *Platin. Met. Rev.*, no. 4, pp. 132–137, 1960.

[135] G. Holleck, "Diffusion and Solubility of Hydrogen in Palladium and Palladium-Silver Alloys," *J. Phys. Chem.*, vol. 74, pp. 503–511, 1970.

[136] M. A. Pick and K. Sonnenberg, "A model for atomic hydrogen-metal interactions - application to recycling, recombination and permeation," *J. Nucl. Mater.*, vol. 131, no. 2–3, pp. 208–220, 1985.

[137] T. L. Ward and T. Dao, "Model of hydrogen permeation behavior in palladium membranes," *J. Memb. Sci.*, vol. 153, no. January 1998, pp. 211–231, 1999.

[138] W. Lisowski, E. Nowicka, Z. Wolfram, and R. Dus, "Atomic Hydrogen Desorption from Thin Palladium Hydride Films," vol. 31, pp. 157–162, 1988.

[139] Y. Tyurin and I. Chernov, "Non-equilibrium release of atomic hydrogen from metals under irradiation," *Int. J. Hydrogen Energy*, vol. 27, no. 7–8, pp. 829–837, 2002.

[140] L. Rands, "Passivation of silicon surfaces through the introduction of charge into insulating layers," Masters Thesis, University of Oxford, 2015.

[141] "Film Sense Elipsometer Applications." [WWW Document], https://film-sense.com/ n.d. 2015

[142] A. Beyer, M. Rennau, and G. Ebest, "Corona Charging of Insulated Surfaces and the Application in the Photovoltaic," in *13th European photovoltaic solar energy conference*, 1995, pp. 1254–1257.

[143] R. S. Bonilla, N. Jennison, D. Clayton-Warwick, K. A. Collett, L. Rands, and P. R. Wilshaw, "Corona charge in SiO2: kinetics and surface passivation for high efficiency silicon solar cells," *Energy Procedia*, vol. 92, pp. 326–335, 2016.

[144] K. A. Collett *et al.*, "Scalable Techniques for Producing Field-Effect Passivation in High-Efficiency Silicon Solar Cells," *IEEE J. Photovoltaics*, vol. 9, no. 1, pp. 26–33, 2019.

[145] S. Du, "Ionic Field Effect Surface Passivation of Silicon Solar Cells.," University of Oxford, Department of Materials Science, Masters Thesis, 2018.

[146] R. A. Sinton and A. Cuevas, "Contactless determination of current–voltage characteristics and minority-carrier lifetimes in semiconductors from quasi-steady-state photoconductance data," *Appl. Phys. Lett.*, vol. 69, no. 17, p. 2510, Oct. 1996.

[147] R. S. Bonilla, G. Martins, and P. R. Wilshaw, "Investigation of Parasitic Edge Recombination in High-Lifetime Oxidized n-Si," *Solid State Phenom.*, vol. 242, pp. 73–79, 2015.

[148] A. L. Blum *et al.*, "Inter-laboratory study of eddy-current measurement of excess-carrier recombination lifetime," in *Conference Record of the IEEE Photovoltaic Specialists Conference*, 2013, pp. 1396–1401.

[149] K. R. McIntosh and L. E. Black, "On effective surface recombination parameters," *J. Appl. Phys.*, vol. 116, no. 1, pp. 014503, Jul. 2014.

[150] D. E. Kane and R. M. Swanson, "Measurement of the emitter saturation current by a contactless photoconductivity decay method," in *IEEE photovoltaic specialists conference 18*, 1985, vol. 69, pp. 578–583.

[151] A. L. Blum, J. S. Swirhun, R. A. Sinton, and A. Kimmerle, "An updated analysis to the WCT-120 QSSPC measurement system using advanced device physics," in *28th European Photovoltaic Solar Energy Conference and Exhibition*, pp. 1521-1523, 2013.

[152] P. Hamer *et al.*, "Boron-Oxygen Defect Formation Rates and Activity at Elevated Temperatures," in *Energy Procedia*, vol. 92, pp. 791-800, 2016.

[153] W. C. Johnson, W. C. Johnson, and P. T. Panousis, "The Influence of Debye Length on the C-V Measurement of Doping Profiles," *IEEE Trans. Electron Devices*, vol. 18, no. 10, pp. 965–973, 1971.

[154] P. Blood, "Capacitance-voltage profiling and the characterisation of III-V semiconductors using electrolyte barriers," *Semicond. Sci. Technol.*, vol. 1, no. 1, pp. 7–27, 1986.

[155] D. K. Schroder, "*Semiconductor materials and device characterization*," Print. vol. 44, no. 4. 2006.

[156] Probion Analysis, "ECV Profiling." [Online]. Available: https://www.probion.fr/en/tutorials/ecvp/ecvprofiling.html. [Accessed: 05-Nov-2018].

[157] E. Peiner, "Doping Profile Analysis in Si by Electrochemical Capacitance-Voltage Measurements," *J. Electrochem. Soc.*, vol. 142, no. 2, p. 576, 2006.

[158] C. P. Herrero, M. Stutzmann, and A. Breitschwerdt, "Hydrogen Diffusion in Boron-Doped Silicon," *MRS Proc.*, vol. 163, 2011.

[159] C. P. Herrero, M. Stutzmann, and A. Breitschwerdt, "Boron-hydrogen complexes in crystalline silicon," *Phys. Rev. B*, vol. 43, no. 2, pp. 1555–1575, 1991.

[160] R. B. M. Girisch, R. P. Mertens, R. F. Dekeersmaecker, and R. F. De Keersmaecker, "Determination of Si-SiO2 Interface Recombination Parameters using a Gate-Controlled Point-Junction Diode under Illumination," *IEEE Trans. Electron Devices*, vol. 35, no. 2, pp. 203–222, 1988.

[161] R. S. Bonilla, "Controlling Surface Carrier Density via a PEDOT:PSS Gate: An Application to the Study of Silicon-Dielectric Interface Recombination," *Sol. RRL*, vol. 2, no. 10, pp. 1800172, 2018.

[162] B. Nemeth *et al.*, "Polycrystalline silicon passivated tunneling contacts for high efficiency silicon solar cells," *J. Mater. Res.*, vol. 31, no. 06, pp. 671–681, 2016.

[163] J. Schmidt and M. Kerr, "Highest-quality surface passivation of low-resistivity p-type silicon using stoichiometric PECVD silicon nitride," *Sol. Energy Mater. Sol. Cells*, vol. 65, no. 1, pp. 585–591, 2001.

[164] F. Feldmann, M. Bivour, C. Reichel, M. Hermle, and S. W. Glunz, "Passivated rear contacts for high-efficiency n-type Si solar cells providing high interface passivation quality and excellent transport characteristics," *Sol. Energy Mater. Sol. Cells*, vol. 120, no. Part A, pp. 270–274, 2014.

[165] J. F. Gabitto and C. Tsouris, "Sulfur Poisoning of Metal Membranes for Hydrogen Separation," *Int. Rev. Chem. Eng.*, vol. 1, September, pp. 394–411, 2009.

[166] A. I. Livshitz, M. E. Notkin, Y. Pustovoit, and A. A. Samartsev, "Superpermeability of solid membranes and gas evacuation Part II Permeation of hydrogen through a palladium membrane under different gas and membrane boundary conditions," *Vacuum*, vol. 29, no. 3, pp. 113–124, Jan. 1979.

[167] B. Mccool, G. Xomeritakis, and Y. S. Lin, "Composition control and hydrogen permeation characteristics of sputter deposited palladium ffi silver membranes," vol. 161, 1999.

[168] F. a. Lewis, "The Palladium-Hydrogen System - A Survey of Hydride Formation and the Effects," *Platin. Met. Rev.*, vol. 26, no. 1, pp. 20–27, 1982.

[169] A. G. Knapton, "Palladium Alloys for Hydrogen Diffusion Membranes," *Platin. Met. Rev.*, no. 6, pp. 44–50, 1977.

[170] B. D. Morreale *et al.*, "The permeability of hydrogen in bulk palladium at elevated temperatures and pressures," vol. 212, pp. 87–97, 2003.

[171] S. Uemiya, N. Sato, H. Ando, Y. Kude, T. Matsuda, and E. Kikuchi, "Separation of hydrogen through palladium thin film supported on a porous glass tube," *J. Memb. Sci.*, vol. 56, no. 3, pp. 303–313, 1991.

[172] S. N. Paglieri and J. D. Way, "Innovations in Palladium Membrane Research," *Sep. Purif. Rev.*, vol. 31, no. 1, pp. 1–169, 2002.

[173] W. Kern, "The Evolution of Silicon Wafer Cleaning Technology," *J. Electrochem. Soc.*, vol. 137, no. 6, p. 1887, 2006.

[174] R. E. Buxbaum and A. B. Kinney, "Hydrogen transport through tubular membranes of palladium-coated tantalum and niobium," *Ind. Eng. Chem. Res.*, vol. 35, no. 2, pp. 530–537, 1996.

[175] B. L. Sopori *et al.*, "Hydrogen in silicon: A discussion of diffusion and passivation mechanisms," *Sol. Energy Mater. Sol. Cells*, vol. 41-42, pp. 159-169, 1996.

[176] R. A. Sinton, A. Cuevas, and M. Stuckings, "Quasi-steady-state photoconductance, a new method for solar cell material and device characterization," in *Photovoltaic Specialists Conference, 1996., Conference Record of the Twenty Fifth IEEE*, 1996, pp. 457–460.

[177] D. N. Jewett and A. C. Makrides, "Diffusion of hydrogen through palladium and palladium-silver alloys," *Trans. Faraday Soc.*, vol. 61, pp. 932–939, 1965.

[178] K. J. Jeon *et al.*, "Hydrogen gas sensing properties of PdO thin films with nano-sized cracks." *Nanotechnology*, vol. 21, issue 16, 2010.

[179] A. I. Livshits, M. E. Notkin, and A. A. Samartsev, "Physico-chemical origin of superpermeability - Large-scale effects of surface chemistry on 'hot' hydrogen permeation and absorption in metals," *J. Nucl. Mater.*, vol. 170, no. 1, pp. 79–94, 1990.

[180] A. B. Antoniazzi, A. A. Haasz, and P. C. Stangeby, "The effect of adsorbed carbon and sulphur on hydrogen permeation through palladium," *J. Nucl. Mater.*, vol. 162–164, pp. 1065–1070, Apr. 1989.

[181] F. J. Castro, G. Meyer, and G. Zampieri, "Effects of sulfur poisoning on hydrogen desorption from palladium," *J. Alloys Compd.*, vol. 332, pp. 612–616, 2002.

[182] H. F. Sterling and R. C. G. Swann, "Chemical vapour deposition promoted by r.f. discharge," *Solid State Electron.*, vol. 8, no. 8, pp. 653–654, 1965.

[183] M. Bacal, A. M. Bruneteau, A. I. Livshits, V. N. Alimov, and M. E. Notkin, "Hydrogen superpermeable membrane operation under plasma conditions," *Fusion Eng. Des.*, vol. 65, no. 3 SPEC., pp. 423–427, 2003.

[184] D. Gahan, S. Daniels, C. Hayden, D. O. O'Sullivan, and M. B. Hopkins, "Characterization of an asymmetric parallel plate radio-frequency discharge using a retarding field energy analyzer," *Plasma Sources Sci. Technol.*, vol. 21, no. 1, 2012.

[185] R. S. Bonilla, P. G. Hamer, and P. R. Wilshaw, "Lowest surface recombination in n-type oxidised crystalline silicon by means of extrinsic field effect passivation," in *EUPVSEC*, pp. 707–710, 2016.

[186] R. S. Bonilla, B. Hoex, K. A. Collett, G. Bourret-Sicotte, and P. R. Wilshaw, "Surface passivation mechanisms in dielectric coatings for silicon solar cells: A review," *Phys. status solidi.* vol. 214, no. 7, 2017.

[187] K. A. Collett *et al.*, "An enhanced alneal process to produce SRV less than 1 cm/s in 1 Ω cm n-type Si," *Sol. Energy Mater. Sol. Cells*, vol. 173, pp. 50-58, 2017.

[188] N. Jennison, "Improving Extrinsic Surface Passivation for P-Type Silicon in Solar Cells," Department of Materials Science, Masters Thesis, University of Oxford, 2017.

[189] J. E. Cotter, J. H. Guo, P. J. Cousins, M. D. Abbott, F. W. Chen, and K. C. Fisher, "P-type versus n-type silicon wafers: Prospects for high-efficiency commercial silicon solar

cells," *IEEE Trans. Electron Devices*, vol. 53, no. 8, pp. 1893-1901, 2006.

[190] S. J. Blundell and K. M. Blundell, "*Concepts in Thermal Physics*.", pp. 1-512, Published by Oxford University Press 2010.

[191] A. Arnaud, "Industrial production of coated glass: Future trend for expanding needs," *J. Non. Cryst. Solids*, vol. 218, pp. 12–18, 1997.

[192] G. Ward, L, "United States Patent Office," *J. Am. Soc. Nav. Eng.*, vol. 39, no. 4, pp. 620–622, 2009.

[193] D. Riggs, O, "Precision Moving Platform," 1976. U.S. Patent Agency. [Online]

[194] R. J. Knops and E. W. Wilkes, "Theory of Elastic Stability," in *Mechanics of Solids*, pp. 125-302 Published by Springer Berlin Heidelberg, 1973.

[195] D. O. Brush, B. O. Almroth, and J. W. Hutchinson, "Buckling of Bars, Plates, and Shells," *J. Appl. Mech.*, vol. 42, no. 4, p. 911, 1975.

[196] R. J. Roark, W. C. Young, and R. Plunkett, "Formulas for Stress and Strain," *J. Appl. Mech.*, vol. 43, no. 3, p. 522, 1976.

[197] H. E. Shull and L. W. Hu, "Load-Carrying Capacities of Simply Supported Rectangular Plates," *J. Appl. Mech.*, vol. 30, issue 4 pp. 617-621, 1960.

[198] B. D. Kay, C. H. F. Peden, and D. W. Goodman, "Kinetics of hydrogen absorption by Pd(110)," *Phys. Rev. B*, vol. 34, no. 2, pp. 817–822, 1986.

[199] S. BAYKARA, "Theoretical evaluation of diffusivity of hydrogen in palladium and rhodium," *Int. J. Hydrogen Energy*, vol. 29, no. 15, pp. 1631–1636, Dec. 2004.

[200] J. R. Scully, G. A. Young Jr., and S. W. Smith, "Hydrogen Solubility, Diffusion and Trapping in High Purity Aluminum and Selected Al-Base Alloys," *Mater. Sci. Forum*, vol. 331–337, pp. 1583–1600, 2009.

[201] E. R. Weber, "Transition metals in silicon," *Appl. Phys. A Solids Surfaces*, vol. 30, no. 1, pp. 1–22, 1983.

[202] C. G. Van De Walle, "Energies of various configurations of hydrogen in silicon," *Phys. Rev. B*, vol. 49, no. 7, pp. 4579–4585, 1994.

[203] J. P. Muscat and D. M. Newns, "Chemisorption on metals," *Prog. Surf. Sci.*, vol. 9, no. 1, pp. 1–43, 1978.

[204] B. G. J. Grashoff, C. E. Pilkington, and C. W. Corti, "The Purification of Hydrogen," *Platin. Met. Rev.*, no. 4, pp. 157–169, 1983.

[205] D. Fort, J. P. G. Farr, and I. R. Harris, "A comparison of palladium-silver and palladium-yttrium alloys as hydrogen separation membranes," vol. 39, pp. 293–308, 1975.

[206] A. Sieverts and H. Brüning, "Über die Fällung von Platinmohr," *Zeitschrift für Anorg. und Allg. Chemie*, vol. 201, no. 1, pp. 113–121, 1931.

[207] J. B. Hunter, "Platinum membrane," US Patent no. 2,773,561, 1956.

[208] J. Li, A. Oudriss, A. Metsue, J. Bouhattate, and X. Feaugas, "Anisotropy of hydrogen diffusion in nickel single crystals: The effects of self-stress and hydrogen concentration on diffusion," *Sci. Rep.*, vol. 7, 2017.

[209] F. H. M. Spit, D. Gupta, and K. N. Tu, "Diffusivity and solubility of Ni (63Ni) in monocrystalline Si," *Phys. Rev. B*, vol. 39, no. 2, pp. 1255-1260, 1989.

[210] O. W. Richardson, J. Nicol, and T. Parnell, " I. The diffusion of hydrogen through hot platinum ," *London, Edinburgh, Dublin Philos. Mag. J. Sci.*, vol. 8, no. 43, pp. 1–29, 2009.

[211] M. J. Kerr, J. Schmidt, A. Cuevas, and J. H. Bultman, "Surface recombination velocity of phosphorus-diffused silicon solar cell emitters passivated with plasma enhanced chemical vapor deposited silicon nitride and thermal silicon oxide," *J. Appl. Phys.*, vol. 89, no. 7, pp. 3821–3826, 2001.

[212] F. Feldmann, M. Bivour, C. Reichel, H. Steinkemper, M. Hermle, and S. W. Glunz, "Tunnel oxide passivated contacts as an alternative to partial rear contacts," *Sol. Energy Mater. Sol. Cells*, vol. 131, pp. 46–50, 2014.

[213] P. Hamer *et al.*, "Hydrogen induced contact resistance in PERC solar cells," *Sol. Energy Mater. Sol. Cells*, vol. 184, pp. 91–97, 2018.

[214] Y. J. C. G. W. Trucks, Krishnan Raghavachari, G. S. Higashi, "Mechanism of HF etching of silicon surfaces: A theoretical understanding of hydrogen passivation," *Phys. Rev. Lett.*, vol. 66, no. 12, p. 1647, 1991.

[215] S. Rivillon, Y. J. Chabal, F. Amy, and A. Kahn, "Hydrogen passivation of germanium (100) surface using wet chemical preparation," *Appl. Phys. Lett.*, vol. 87, no. 25, pp. 1–3, 2005.

[216] D. B. Fenner, D. K. Biegelsen, and R. D. Bringans, "Silicon surface passivation by hydrogen termination: A comparative study of preparation methods," *J. Appl. Phys.*, vol. 66, no. 1, pp. 419–424, 1989.

[217] M. Keevers and A. Turner, "Method and Apparatus For Hydrogenation of Thin Film Silicon on Glass," US Patent, no. 8039051B2, 2006.

[218] P. A. Basore, "CSG-1: Manufacturing a new polycrystalline silicon PV technology," in *Conference Record of the 2006 IEEE 4th World Conference on Photovoltaic Energy Conversion, WCPEC-4*, 2007.

[219] A. G. Aberle, "Overview on SiN surface passivation of crystalline silicon solar cells," *Sol. Energy Mater. Sol. Cells*, vol. 65, no. 1–4, pp. 239–248, 2001.

[220] C. Boehme and G. Lucovsky, "Dissociation reactions of hydrogen in remote plasma-enhanced chemical-vapor-deposition silicon nitride," *J. Vac. Sci. Technol. A Vacuum, Surfaces, Film.*, vol. 19, no. 5, p. 2622, 2001.

[221] W. A. Lanford and M. J. Rand, "The hydrogen content of plasma-deposited silicon nitride," *J. Appl. Phys.*, vol. 49, no. 4, pp. 2473–2477, 1978.

[222] A. I. Livshits, F. Sube, M. N. Solovyev, M. E. Notkin, and M. Bacal, "Plasma driven superpermeation of hydrogen through group Va metals," *J. Appl. Phys.*, vol. 84, no. 5, pp. 2558–2564, 1998.

[223] C. Nishimura, M. Komaki, S. Hwang, and M. Amano, "V-Ni alloy membranes for hydrogen purification," *J. Alloys Compd.*, vol. 330, no. 332, pp. 902–906, 2002.

[224] M. Amano, M. Komaki, and C. Nishimura, "Hydrogen permeation characteristics of palladium-plated VNi alloy membranes," *J. Less-Common Met.*, vol. 172–174, no. Part B, pp. 727–731, 1991.

[225] C. Boehme and G. Lucovsky, "Origins of silicon solar cell passivation by SiNx:H anneal," *J. Non. Cryst. Solids*, vol. 299–302, no. PART 2, pp. 1157–1161, 2002.

[226] B. Sopori *et al.*, "Damage-layer-mediated H diffusion during SiN:H processing: A comprehensive model," in *Conference Record of the 2006 IEEE 4th World Conference on Photovoltaic Energy Conversion, WCPEC-4*, 2007, vol. 1, pp. 1028–1031.

[227] B. L. Sopori *et al.*, "On the Mechanism of Hydrogen Diffusion in Si Solar Cells Using PECVD SiN:H," *MRS Proc.*, vol. 813, 2011.

[228] B. Sopori *et al.*, "A comprehensive model of hydrogen transport into a solar cell during silicon nitride processing for fire-through metallization," Conference Record of the IEEE Photovoltaic Specialists Conference 2005, pp. 1039–1042.

[229] A. Van Wieringen and N. Warmoltz, "On the permeation of hydrogen and helium in single crystal silicon and germanium at elevated temperatures," *Physica*, vol. 22, no. 6–12, pp. 849–865, 1956.

[230] T. Ichimiya and A. Furuichi, "On the solubility and diffusion coefficient of tritium in single crystals of silicon," *Int. J. Appl. Radiat. Isot.*, vol. 19, no. 7, pp. 573–578, 1968.

[231] S. J. Pearton, J. W. Corbett, and J. T. Borenstein, "Hydrogen diffusion in crystalline semiconductors," *Phys. B Phys. Condens. Matter*, vol. 170, no. 1–4, pp. 85–97, 1991.

[232] R. Rizk, P. de Mierry, D. Ballutaud, M. Aucouturier, and D. Mathiot, "On the modeling of hydrogen diffusion processes and complex formation in p-type crystalline silicon," *Phys. B Phys. Condens. Matter*, vol. 170, no. 1–4, pp. 129–134, 1991.

[233] R. Rizk, P. De Mierry, D. Ballutaud, M. Aucouturier, and D. Mathiot, "Hydrogen Diffusion in N-Type Silicon.Comparison With P-Type Silicon," *MRS Proc.*, vol. 209, 2011.

[234] D. Mathiot, "Modeling of hydrogen diffusion in n- and p-type silicon," *Phys. Rev. B*, vol. 40, no. 8, pp. 5867-5870, 1989.

[235] J. Deru, "Extrinsic Surface Passication of Si," Department of Materials Science, Masters Thesis, University of Oxford, 2019.

[236] F. J. Feigl, R. Gale, H. Chew, C. W. Magee, and D. R. Young, "Current-induced hydrogen migration and interface trap generation in aluminum-silicon dioxide-silicon capacitors," *Nucl. Inst. Methods Phys. Res. B*, vol. 1, no. 2–3, pp. 348–354, 1984.

[237] S. T. Pantelides, S. N. Rashkeev, R. Buczko, D. M. Fleetwood, and R. D. Schrimpf, "Reactions of hydrogen with Si-SiO 2 interfaces," in *IEEE Transactions on Nuclear Science*, 2000, vol. 47, no. 6 III, pp. 2262–2268.

[238] D. L. Griscom, "Diffusion of radiolytic molecular hydrogen as a mechanism for the post-irradiation buildup of interface states in SiO2-on-Si structures," *J. Appl. Phys.*, vol. 58, no. 7, pp. 2524–2533, 1985.

[239] I. Shkrob and A. Trifunac, "Time-resolved EPR of spin-polarized mobile H atoms in amorphous silica: The involvement of small polarons," *Phys. Rev. B - Condens. Matter Mater. Phys.*, vol. 54, no. 21, pp. 15073–15078, 1996.

[240] D. Mathiot, "Modeling of hydrogen diffusion in n-and p-type silicon," *Phys. Rev. B*, vol. 40, no. 8, pp. 5867–5870, 1989.

[241] J. S. You, D. Kim, J. Y. Huh, H. J. Park, J. J. Pak, and C. S. Kang, "Experiments on anisotropic etching of Si in TMAH," *Sol. Energy Mater. Sol. Cells*, vol. 66, no. 1–4, pp. 37–44, 2001.

[242] J. T. L. Thong, W. K. Choi, and C. W. Chong, "TMAH etching of silicon and the interaction of etching parameters," *Sensors Actuators, A Phys.*, vol. 63, no. 3, pp. 243–249, 1997.

[243] S. Steingrube, P. P. Altermatt, D. S. Steingrube, J. Schmidt, and R. Brendel, "Interpretation of recombination at c-Si/SiNx interfaces by surface damage," *J. Appl. Phys.*, vol. 108, no. 1, p. 014506, 2010.

[244] D. Chen *et al.*, "Hydrogen induced degradation: A possible mechanism for light- and elevated temperature- induced degradation in n-type silicon," *Sol. Energy Mater. Sol. Cells*, vol. 185, pp. 174–182, 2018.

[245] D. Chen *et al.*, "Evidence of an identical firing-activated carrier-induced defect in monocrystalline and multicrystalline silicon," *Sol. Energy Mater. Sol. Cells*, vol. 172, no. August, pp. 293–300, 2017.

[246] A. C. N. Wenham *et al.*, "Hydrogen-Induced Degradation," in *2018 IEEE 7th World Conference on Photovoltaic Energy Conversion, WCPEC 2018 - A Joint Conference of 45th IEEE PVSC, 28th PVSEC and 34th EU PVSEC*, 2018.

[247] N. P. Johnson, F. Ponce, R. Street, and R. Nemanich, "Defects in single-crystal silicon induced by hydrogenation," *Phys. Rev. B*, vol. 35, no. 8, pp. 4166–4169, Mar. 1987.

[248] N. M. Johnson and C. Herring, "Charge States of Hydrogen in p-Type and n-Type Silicon," *Mater. Sci. Forum*, vol. 38–41, pp. 961–966, Jan. 1991.

[249] C. Chan *et al.*, "Instability of Increased Contact Resistance in Silicon Solar Cells Following Post-Firing Thermal Processes," *Sol. RRL*, vol. 1, no. 11, p. 1700129, Oct. 2017.

[250] S. Steingrube, P. P. Altermatt, D. S. Steingrube, J. Schmidt, and R. Brendel, "Interpretation of recombination at c-Si/SiN_x interfaces by surface damage," *J. Appl. Phys.*, vol. 108, no. 1, p. 014506, Jul. 2010.